

**Ph.D. Program in Civil, Chemical and Environmental Engineering
Curriculum in Structural and Geotechnical Engineering,
Mechanics and Materials**

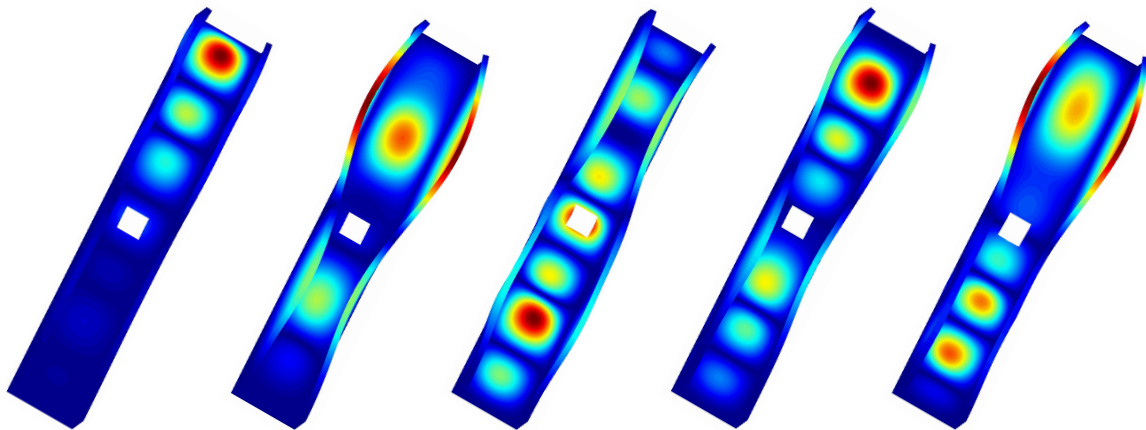


Department of Civil, Chemical and Environmental Engineering
Polytechnic School, University of Genoa, Italy.

Doctor of Philosophy in Engineering (Cotutelle)



School of Civil Engineering
Faculty of Engineering and Information Technologies
The University of Sydney, NSW, Australia.



**New approaches for linear and nonlinear analyses
of thin-walled members in the framework of the
Generalized Beam Theory**

Alberto Ferrarotti

NEW APPROACHES FOR LINEAR AND NONLINEAR ANALYSES
OF THIN-WALLED MEMBERS IN THE FRAMEWORK OF THE
GENERALIZED BEAM THEORY

BY

ALBERTO FERRAROTTI

*Dissertation discussed in partial fulfillment of
the requirements for the Degree of*

DOCTOR OF PHILOSOPHY (COTUTELLE)

*Civil, Chemical and Environmental Engineering
curriculum in Structural and Geotechnical Engineering, Mechanics and Materials,
Department of Civil, Chemical and Environmental Engineering, University of Genoa, Italy*

*School of Civil Engineering, Faculty of Engineering and Information Technologies,
The University of Sydney, NSW, Australia*



April, 2018

Advisers:

Prof. Giuseppe Piccardo - University of Genoa, Italy

Prof. Gianluca Ranzi - The University of Sydney, NSW, Australia

External Reviewers:

Prof. Nicola Luigi Rizzi - University of Roma Tre, Italy

Dr. Jurgen Becque - The University of Sheffield, UK

Examination Committee:

Prof. Riccardo Zandonini - University of Trento, Italy

Prof. Marco Paggi - IMT School for Advanced Studies, Lucca, Italy

Prof. Ivo Calì - University of Catania, Italy

Prof. Antonio Brencich - University of Genoa, Italy

Final Exam

10th May 2018

Ph.D. Program in Civil, Chemical and Environmental Engineering

Curriculum in Structural and Geotechnical Engineering, Mechanics and Materials

Cycle XXX

Coordinator of the Program:

Prof. Guido Busca - University of Genoa, Italy

Coordinator of the Curriculum:

Prof. Roberta Massabò - University of Genoa, Italy

to my grandfather Giovanni

PREFACE

The research presented in this Thesis was carried out at the Department of Civil, Chemical and Environmental Engineering (DICCA) of the University of Genova under the supervision of Professor Giuseppe Piccardo, and at the School of Civil Engineering of the University of Sydney under the supervision of Professor Gianluca Ranzi.

First of all I want to thank my supervisors Professor Giuseppe Piccardo and Professor Gianluca Ranzi for their guidance, help and valuable comments throughout the process of this work.

I would also like to thank Gerard Taig for his help and valuable discussions concerning the use of ABAQUS and the development of a FE-based GBT solver within Matlab.

To my family, to my mother Daniela and my father Giuseppe, my brother Stefano and my grandmother Ida, for their unbounded love and encouragement.

To Mariasole, very soon my wife, for her encouragement, for her support and confidence, for letting me go and waiting me back home. Your love had walked through the distance and had made all possible.

Many thanks to my new Australian friends, particularly to Daniele and Terri, that made me feel at home.

Finally, to all my friends, thank you.

Genoa, April 2018.

Alberto Ferrarotti

ABSTRACT

The Generalized Beam Theory (GBT) is a reliable and efficient tool for the linear and non-linear analysis of thin-walled members (TWMs). The theory is based on a semi-variational (Kantorovich-Vlasov) approach in which the displacement field is expressed as a linear combination of *assumed* deformation fields (i.e., *trial functions*) related to the cross-section, and *unknown* amplitude functions (i.e., *linear coordinates*) defined on the sole beam longitudinal abscissa. The use of the GBT relies on two fundamental steps to be performed: (a) selection of the deformation fields for the cross-section (usually referred to as *cross-section analysis*); and (b) solution of the obtained equivalent 1D problem (named *member analysis*).

This thesis proposes new approaches for the elastic linear and nonlinear analysis of TWMs within the framework of the GBT. The main contributions are represented by: (a) a novel straightforward dynamic approach for the cross-section analysis, (b) a GBT formulation for the partial interaction analysis of multi-component TWMs, (c) a displacement - based GBT formulation for the linear elastic analysis of composite TWMs with large web penetrations, and (d) a nonlinear GBT approach for the analysis of arbitrary open, closed and partially-closed TWMs.

The novel and straightforward approach for the cross-section analysis is based on the so-called dynamic approach (GBT-D), where the GBT trial functions are identified from the dynamic analysis of a linear elastic planar frame representing the cross-section. The method relies on the solution of a very limited number of constrained eigenvalue problems. It is much simpler to use than the classic static approach for the cross-section analysis, in addition to provide even better results from the point of view of accuracy and symmetry of obtained displacement fields.

The proposed cross-section analysis is suited for developing a GBT-based formulation for the study of the linear-elastic behavior of multi-component TWMs. The novelty of the approach consists on its ability to accurately model the partial interaction between the different components forming the cross-section in both longitudinal and transverse directions. The ease of use of the model is outlined by two application performed on multi-component members subjected to eccentric loads. Values calculated with ABAQUS finite element models are used to validate the proposed method.

A displacement-based GBT formulation for the partial interaction analysis of composite TWMs with large web penetrations is then proposed. It is based on the definition of a variable transform which allows to express the unknown linear coordinates in terms of cross-section nodal degrees-of-freedom (DOFs). The proposed approach leads to a beam-like finite element that is equivalent to an assembly of flat quadrilateral shell elements, making possible to deal straightforwardly with penetrations, local constraints and localized longitudinal stiffeners. A numerical example is presented to highlight the capabilities and accuracy of the proposed approach.

Finally, a nonlinear GBT approach is developed according to the nonlinear Galerkin method, which calls for the evaluation of nonlinear (passive) trial functions, to be used in conjunction with linear (active) ones, in describing the displacement field. Since nonlinear trial functions do not increase the number of the unknowns, the GBT spirit, as a reduction method, is preserved. Two promising examples are discussed, showing how equilibrium paths can be determined by using few linear trial functions in conjunction with the corresponding nonlinear trial functions, supplying good results when compared with burdensome finite-element solutions.

SOMMARIO

La “Teoria di Trave Generalizzata” (GBT) è uno strumento affidabile ed efficiente per l’analisi lineare e nonlineare di travi a parete sottili (TWMs). La teoria si basa su un approccio semi-variazionale alla Kantorovich-Vlasov, in cui il campo di spostamenti è espresso come combinazione lineare di campi deformativi *noti* (i.e., *funzioni di forma*) dipendenti dalla sezione trasversale, e ampiezze *incognite* (i.e., *coordinate lineari*) definite sul solo asse longitudinale. GBT richiede le seguenti due analisi: (a) selezione dei campi deformativi per la sezione trasversale (comunemente chiamata *analisi sezionale*); e (b) soluzione del risultante problema 1D equivalente (denominata *analisi dell’elemento*).

Questa tesi propone nuovi approcci per l’analisi elastica lineare e nonlineare di TWMs nell’ambito della GBT. I principali contributi riguardano: (a) una nuova procedura dinamica diretta per l’analisi sezionale, (b) una formulazione GBT per l’analisi della interazione parziale di TWMs multi-componenti, (c) una GBT formulata in termini di spostamenti per l’analisi elastica lineare di TWMs composite con grandi perforazioni d’anima, e (d) un approccio GBT nonlineare per l’analisi di TWMs arbitrariamente aperte, chiuse o parzialmente chiuse.

La nuova procedura diretta per l’analisi sezionale è basata sul cosiddetto approccio dinamico (GBT-D), in cui le funzioni di forma GBT sono identificate a partire dall’analisi dinamica di un telaio piano elastico lineare rappresentante la sezione trasversale. Il metodo si basa sulla soluzione di un numero molto limitato di problemi agli autovalori vincolati. Il metodo è molto più semplice del corrispondente statico ed è in grado di fornire risultati migliori da un punto di vista di accuratezza e rispetto delle simmetrie dei campi deformativi ottenuti.

L’analisi sezionale proposta è utilizzata per lo sviluppo di una formulazione GBT per lo studio elastico lineare di TWMs multi-componenti. La novità dell’approccio risiede nella sua capacità di modellare la interazione parziale fra le differenti componenti sia in direzione longitudinale che trasversale. La facilità di utilizzo del metodo proposto è evidenziata attraverso due applicazioni su travi multi-componenti caricate eccentricamente. I risultati ottenuti con modelli agli elementi finiti sviluppati con ABAQUS sono stati usati a fini validativi.

Viene in seguito proposta una GBT formulata in termini di spostamenti per l’analisi della interazione parziale di TWMs composite con grandi perforazioni d’anima. Essa si fonda su un cambio di variabili che consente di esprimere le coordinate lineari incognite in termini di gradi di libertà nodali della sezione. Questo conduce a elementi finiti di tipo trave equivalenti ad un assemblaggio di elementi finiti di tipo piastra, consentendo un approccio diretto per l’analisi di elementi con fori, vincoli puntuali e irrigidenti longitudinali locali. Le capacità e facilità di utilizzo del metodo sono illustrate per mezzo di un esempio numerico.

Infine, viene sviluppato un approccio GBT nonlineare basato sul metodo di Galerkin nonlineare, che richiede la valutazione di funzioni di forma nonlineari (passive) da utilizzarsi congiuntamente a quelle lineari (attive). Poichè le funzioni di forma nonlineari non incrementano il numero di gradi di libertà, lo spirito GBT quale metodo di riduzione è preservato. Due promettenti applicazioni vengono proposte, che evidenziano come i percorsi di equilibrio possano essere ottenuti usando poche funzioni di forma lineari di concerto con le corrispondenti nonlineari, ottenendo buoni risultati rispetto a soluzioni ottenute con laboriosi modelli agli elementi finiti.

PREFACE

As part of the candidature, and in support of this thesis, the following papers have been submitted for consideration, accepted or published in international journals and conferences.

Journal Papers

1. Piccardo, G., Ferrarotti, A. and Luongo, A. (2017). Nonlinear Generalized Beam Theory for open thin-walled members, *Mathematics and Mechanics of Solids* **22**(10): 1907-1921, doi: 10.1177/1081286516649990
2. Ferrarotti, A., Piccardo, G. and Luongo, A. (2017). A novel straightforward dynamic approach for the evaluation of extensional modes within GBT ‘cross-section analysis’, *Thin-Walled Structures* **114**: 52-69, doi: 10.1016/j.tws.2017.01.001
3. Ferrarotti, A., Ranzi, G., Taig, G. and Piccardo, G. (2017). Partial interaction analysis of multi-component members within the GBT, *Steel and Composite Structures*, **25**(5): 625-638, doi: 10.12989/scs.2017.25.5.625

Conference Papers

1. Ferrarotti, A., Piccardo, G. and Luongo, A. (2016). Dynamic approaches to ‘cross-section analysis’ within the GBT formulation, *Proceedings of the 14th International Symposium On Structural Engineering ISSE, Beijing, China, October 12-15, 2016*.
2. Ferrarotti, A., Ranzi, G., Taig, G., Piccardo, G. and Luongo, A. (2016). Partial interaction analysis of multi-component members in the framework of the GBT, *Proceedings of the 7th International Conference on Coupled Instabilities in Metal Structures, Baltimore, Maryland, USA, November 7-8, 2016*.
3. Ferrarotti, A., Ranzi and Piccardo, G. (2017). Partial interaction analysis of multi-component members with the D-GBT approach, *Proceedings of the 16th International Symposium on tubular structures ISTS16, Melbourne, Victoria, Australia, December 4-6, 2017*.

INDEX

Abstract	ix
Sommario	xi
Preface	xiii
Index	xvii
Chapter 1. Introduction	1
1.1. Formulations for the analysis of thin-walled members: general overview	1
1.2. Generalized Beam Theory (GBT)	2
1.3. Aims and scope of the thesis	4
1.4. General layout of the thesis	4
Chapter 2. Overview on the Generalized Beam Theory	7
2.1. Introduction	7
2.2. Literature review	8
2.3. Linear GBT formulation	17
Chapter 3. Novel straightforward dynamic approach for the GBT cross-section analysis	23
3.1. Overview on the GBT-D approach	25
3.1.1. Planar Eigenvalue Problem (PEP)	26
3.1.2. Warping Eigenvalue Problem	32
3.2. Novel straightforward dynamic approach for the evalua- tion of extension trial functions	34
3.3. Conventional and non-conventional trial functions within the GBT-D approach	43
3.4. On the influence of the polynomial order in the FE-based GBT cross-section analysis	44

Chapter 4. Partial interaction analysis of multi-component TWMs within the GBT framework	49
4.1. Basis of the GBT approach for the partial interaction analysis of multi-component TWMs	51
4.2. GBT-D cross-section analysis for multi-component TWMs ..	55
4.2.1. Conventional and extensional trial functions for multi-component members: an unconstrained approach	58
4.2.2. Enhanced GBT-D approach to evaluate conventional and extension trial functions for multi-component members	61
4.3. Applications	64
Chapter 5. Displacement-based GBT for composite TWMs with large web penetrations	79
5.1. Displacement-based GBT: formulation	81
5.2. Displacement-based GBT for composite TWMs	89
Chapter 6. Nonlinear Generalized Beam Theory for arbitrary open and closed TWMs	111
6.1. Nonlinear cross-section analysis	112
6.1.1. First-order (active) fields	114
6.1.2. Second-order (passive) fields	115
6.2. A formal analogy for the calculation of nonlinear fields	117
6.2.1. Equivalent thermal problem for arbitrary TWM cross-sections	118
6.2.2. Kinematic procedure for open TWM cross-sections	124
6.3. Member analysis	131
6.4. Applications	134
Chapter 7. Conclusions and perspectives	143
7.1. Conclusions	143
7.2. Further research	144

Appendix A. Stiffness and Mass Element Matrices for cross-section Finite Elements	147
A.1. Beam Finite Elements for linear cross-section analysis	147
A.1.1. In-plane 6 DOF, out-of-plane 2 DOF finite element (FE ₁)	147
A.1.2. In-plane 7 DOF, out-of-plane 3 DOF finite element (FE ₂)	148
A.1.3. In-plane 11 DOF, out-of-plane 5 DOF finite element (FE ₃)	149
A.2. Beam Finite Elements for nonlinear cross-section analysis ...	154
A.2.1. In-plane 10 DOF, out-of-plane 7 DOF finite element (FE ₄)	154
Appendix B. The planar Euler-Bernoulli beam as an equivalent Generalized Spring	157
Appendix C. Constrained algebraic eigenvalue problems	161
Appendix D. Displacement-based GBT equations and relevant bound- ary conditions	163
References	168

Chapter 1

Introduction

1.1 Formulations for the analysis of thin-walled members: general overview

Thin-walled members (TWMs) are locally deformable beams behaving in a substantially different way from compact ones, since their response is strongly influenced by changes in shape of the cross-section, both in-plane (i.e., distortion) and out-of-plane (i.e., warping). These deformations, commonly negligible for beams with compact cross-sections, represent instead the characteristic feature of TWMs and remarkably affect their mechanical behavior. Well-known examples of such mechanisms are the following: (a) warping induced by non-uniform torsion on open TWMs, leading to a greater torsional stiffness than the one associated to the de Saint-Venant theory; (b) flattening in bent tubular members, leading to a progressive decay of the bending stiffness with increasing deflection; and (c) local/distorsional buckling, which strongly reduce the load-bearing capacity of the member, in addition to cause dangerous effects in case of interaction with global (Eulerian or flexural-torsional) modes.

The first mathematical model for the analysis of TWMs was developed by the Russian mathematician V.Z. Vlasov (Vlasov, 1961). The theory, developed for open cross-sections under the hypothesis of small displacements (i.e., linearized kinematics), is founded on the following two basic hypothesis: (i) the *beam cross-section is not deformable in its own plane*, and (b) *shear deformation on the middle surface is negligible*. As a consequence of the first hypothesis, the in-plane motion is described according to the rigid-body kinematic laws. The second hypothesis allows to express the warping as function of the in-plane motion, to within a rigid longitudinal displacement. Therefore, the generic configuration of the system is identified by the position of points belonging to the beam longitudinal axis as well as by the (rigid) rotation of the cross-section around the same axis.

Since then, several beam models have been developed in the Literature to investigate the behavior of TWMs. They can be classified according to the following two philosophies:

- (a) direct formulations as a one-dimensional (1D) continuum;
- (b) derivations from a three-dimensional (3D) Cauchy continuum.

Direct formulations are based on the so called *polar continuum* (also known as Cosserat's continuum or structured continuum). It is richer than the classic Cauchy's one, since material particles composing it are endowed with orientation (i.e., they can translate and, in addition, can rotate). In this context, the beam is considered as a 1D object, geometrically described by its axis made up of orientable body-points, each of them possessing six degrees of freedom (i.e., as in the 3D beam made of rigid cross-sections). It is noteworthy that cross-sections disappear in direct models. However, their attitude is described by points' orientation, thus regaining the information lost. When dealing with TWMs, the key point is how to include the cross-section

distortions, in order to keep the model one-dimensional. Warping is commonly introduced by means of suitable internal constraints among the kinematic descriptors (e.g., Rizzi and Tatone, 1996; Ruta et al., 2006), while additional kinematic descriptors, usually referred to as *distorsional variables*, may be included in the structured continuum to describe in-plane distortions (e.g., Luongo and Zulli, 2013, 2014).

Formulations derived from the 3D Cauchy continuum consist in “approximate” models that exploit the geometric peculiarity of the beam, in particular its slenderness, in order to obtain equivalent 1D descriptions, where all variables involved depend on only one coordinate, commonly the beam axis. The main aim is to obtain reduced models which are simpler and computationally more efficient to solve than the 3D elasticity problem. As a matter of fact, while the latter may in principle be solved for TWMs, e.g. by means of a numerical shell-based Finite Element (FE) approximation, such an approach is burdensome and very time consuming, due to the difficulty in solving governing (partial differential) equations, as well as to the large number of degrees of freedom involved in the analysis. Contrariwise, reduced approaches derived from the 3D Cauchy continuum are elegant and powerful tool for the linear and nonlinear analysis of TWMs. Among the others, semi-variational approaches, such as the Finite Strip Method (FSM) and the Generalized Beam Theory (GBT), have attracted the attention of several researchers (e.g., Silvestre and Camotim, 2002a,b; Ádány and Schafer, 2006a,b).

1.2 Generalized Beam Theory (GBT)

The present thesis is focused on the GBT. Within its framework, the TWM is considered as an assembly of (generally, but not necessarily) flat thin plates, free to bend in the plane orthogonal to the member axis according to the Kirchhoff model. The original proposal extends the Vlasov theory (Vlasov, 1961) accounting for deformable cross-sections. The basic idea of the method consists in representing the displacement field as a linear combination of *assumed* cross-section *deformation fields* (commonly referred to in the Literature as *deformation modes*) and *unknown amplitude functions*. While the former are relied on the sole curvilinear abscissa lying on the TWM mid-line profile, the latter depend on the single beam abscissa. A variational principle, as the Principle of Virtual Works, provides the weak formulation of the problem, leading to a system of (coupled) ordinary differential equations, commonly referred to as *GBT equations*, in the unknown amplitude functions, with the relevant boundary conditions. These equations, equal in number to the the deformation fields considered, generalize the classical Vlasov beam theory, the latter accounting for rigid cross-sections and thus described by four amplitude functions, each one associated to a rigid motion of the cross-section, namely three translations (two bendings and one axial extension) and one rotation (torsion) around the shear center. The GBT approach falls within Kantorovich’s semi-variational method (e.g., Kantorovich and Krylov, 1958), where the dimensionality of a problem is reduced through a technique of partially-assumed modes. In the case of the GBT, the three-dimensional continuous problem is transformed into a vector-valued one-dimensional one. In particular, the GBT consists of two phases: (i) the choice of the deformation modes, referred to as *cross-sectional analysis*, and (ii) the solution of the amplitude equations, denoted as *member analysis*.

In the last decades, GBT has had a large diffusion in the scientific community thanks to the

strong impulse given to it by Camotim and co-workers. They generalized the method to include new aspects, not present in the original formulation, and combined it with a FE approach, so that GBT is now applicable to a wide range of fields, from orthotropic TWMs (e.g., Silva et al., 2006) to thin-walled frames (e.g., Camotim et al., 2010), from buckling interaction phenomena (e.g., Gonçalves and Camotim, 2004; Dinis and Camotim, 2011) to the elasto-plastic analysis of TWMs (e.g., Abambres, Camotim and Silvestre, 2014), from linear dynamic problems (e.g., Bebiano, Camotim and Silvestre, 2013) to TWMs with curved circular axis (e.g., Peres et al., 2016). The key feature of the GBT approach relies on its modal nature. In fact, the use of known deformation fields allows to give a clear physical interpretation to the mechanical behavior experienced by the TWM, particularly referred to the buckling nature (i.e., flexural-torsional, local, distortional). Moreover, providing a suitable choice of known of deformation fields, the TWM behavior can be accurately described by using a very limited number of degrees of freedoms, increasing considerably the numeric efficiency of the approach.

In spite of advantages previously outlined, however, some aspects of the GBT framework are still involved and time-consuming, in particular: (a) cross-section analysis, (b) analysis of structural systems, and (c) geometrically nonlinear analysis. The classic procedure for the cross-section analysis (e.g., Bebiano et al., 2015) is based on the preliminary identification of a set of elementary (physically meaningless) deformation fields, defined as the solution of as many linear static structural analyses as the number of fields themselves. The final set of (physically meaningful) functions is then achieved by means of a sequence of eigenproblems, defined through stiffness matrices arising from the member analysis. Therefore, the procedure is not based on pure kinematic concepts, but it is, in some sense, mixed and recursive. Very recently, a different approach for the GBT cross-section analysis has been proposed, namely GBT-D, with the aim to provide a suitable set of fields for arbitrary simple and composite TWMs by means of a very limited number of eigenproblems (e.g., Piccardo et al., 2014a; Taig and Ranzi, 2015). The procedure is based on the dynamic analysis of an equivalent frame having the shape of the cross-section. Despite the procedure is less involved than the corresponding static one, obtained fields seems to be slightly imprecise. The GBT-based analysis of structural systems, such as thin-walled frames or locally stiffened and perforated elements, which can be treated as an assembly of TWMs with constant cross-section, is also quite involved. As a matter of facts, due to the modal nature of the approach, continuity of displacement fields on interfaces between composing members can't be enforced automatically (as it would be possible using a FE method), but must be enforced through constraint equations depending on deformation fields. Finally, the GBT-based geometrically nonlinear analysis (e.g., Silvestre and Camotim, 2003b) is based on the use of (linear) deformation fields stemming from the classic cross-section analysis. The latter may not be entirely suitable to capture nonlinear effects, such as the approaching of cross-section natural nodes as a consequence of large in-plane inflection. As a consequence, it may take a large number of linear fields to approximate a typical nonlinear effect, losing the spirit of the GBT as reduction method and, not at least, leading to a very time consuming procedure.

1.3 Aims and scope of the thesis

The scope of the Thesis is to provide new approaches to improve the reliability and numerical efficiency of the GBT framework in dealing with linear and nonlinear analysis of TWMs. The main aims can be summarized as follows:

- to develop a novel straightforward dynamic approach for the GBT cross-section analysis, able to provide very clean and precise deformation fields for arbitrary open, closed and partially-closed cross-sections by using a very limited number of (non recursive) analyses;
- to provide a GBT-based approach for the analysis of composite and multi-component TWMs, which includes the shear deformability of connections placed at interfaces between components in a rational and automatic fashion;
- to develop a direct and efficient displacement-based GBT formulation which allows the analysis of composite TWMs with large penetrations as a structural system. The approach should benefit of assembly procedures commonly adopted in standard FE models, which allows to avoid the use of constraint equations to enforce continuity between elements forming the structural system;
- to introduce an innovative nonlinear GBT formulation where linear deformation fields stemming from cross-section analysis are supplied, according to the nonlinear Galerkin method, with nonlinear fields, accounting from nonlinear effects. The formulation should be able to capture the essence of the TWM nonlinear behavior by using a very reduced number of fields, thus constituting a very reliable and computationally efficient approach.

1.4 General layout of the thesis

This Thesis is organized in seven chapters, with the first and final ones being the introduction and conclusions, respectively.

Chapter 2 is aimed to provide a general overview on the GBT. A detailed Literature review of the research work related to the thesis topic is first presented. The linear elastic (first-order) GBT formulation is then illustrated to clarify the procedure and to describe the main hypotheses and assumptions.

The novel straightforward dynamic approach for the GBT cross-section analysis illustrated in Chapter 3. The procedure is based on the formulation of a very limited number of constrained eigenvalue problems which allow to obtain the full set of displacement fields in a straightforward and non-recursive way. The Chapter is structured in order to highlight differences and similarities with others GBT-D based approaches available in the Literature. For this reason, the latter are first presented, while the new formulation is introduced subsequently. An illustrative example follows each step of the illustrated procedures, in order to highlight criticisms and improvements provided by the novel approach, while three additional examples present its versatility and ease-to-use. The set of deformation fields obtained by using the dynamic approach

are then summarized, while the influence of polynomial order of shape functions adopted in a FE-based cross-section analysis is finally discussed.

Chapter 4 presents a GBT-based approach for the longitudinal and transverse partial interaction analysis of multi-component TWMs. The model generalizes the GBT approach for the partial interaction analysis of composite steel-concrete members recently proposed in Taig et al. (2016). The partial interaction is included in the analysis by means of shear deformable linear elastic springs placed at the interface between adjacent components and assumed to be uniformly distributed along the member length. Two dynamic procedures for the cross-section analysis are then proposed. The first stems from the so-called unconstrained approach available in the Literature (e.g., Taig et al., 2016), while the second constitutes the generalization of the novel dynamic procedure presented in Chapter 3. An illustrative example of multi-component TWM taken from the Literature is presented in order to highlight the differences, in terms of obtained trial functions, between the two proposals. Finally, the proposed GBT approach is validated using the numerical results determined with a refined finite element model developed in ABAQUS/Standard (Simulia, 2010) as reference. To this end, the linear elastic analysis of two real multi-component TWMs taken from the Literature is presented.

The displacement-based GBT formulation for the analysis of composite TWMs with large web penetrations is proposed in Chapter 5. The method is based on a variable transformation which allows to express unknown coordinates in terms of unknown nodal displacements and rotations. In this way, the GBT-based beam-like FE is transformed into an assembly of GBT-based shell-like FEs, which benefit of assembly procedures commonly adopted in standard FE models. Therefore, structural systems can be obtained by simply assembling the contribution of each member, with no need to resort to constraint equations to restore compatibility conditions between adjacent elements. In the Chapter, the basis of the displacement-based GBT formulation are first outlined, based on as very recently formalized in Gonçalves and Camotim (2017a,b). The model for composite steel-concrete members is then proposed, based on the GBT formulation for the partial interaction analysis of multi-component TWM proposed in Chapter 4. An application on a large-span composite beam with multiple web-perforations taken from Mills (2001) is then proposed, and results are compared with the ones obtained by means of a refined shell-based FE model developed with ABAQUS/Standard (Simulia, 2010) for validation purposes.

The nonlinear GBT approach is illustrated in Chapter 6. The methodology is valid for arbitrary open, closed and partially-closed cross-sections. The core of the formulation is represented by a nonlinear cross-section analysis, which is outlined at first in the Chapter. It allows to identify a set of passive fields, resulting slave of linear ones and able to describe the nonlinear geometrical effects induced on the cross-section by linear fields themselves. A formal analogy with a thermal problem is then suited to develop a direct and computationally efficient approach for the evaluation of passive fields within a FE-based (discrete) description. Finally, the (non-linear) member analysis is briefly addressed, while the accuracy and efficiency of the proposed NGBT is pointed out by means of two examples, whose results are validated against the ones obtained with traditional finite-element solutions obtained with ABAQUS/Standard (Simulia, 2010).

Finally, Chapter 7 discusses the main results and draws conclusions from the thesis. Some perspectives for future researches are suggested as well. Four Appendices provides details and

general purpose procedures which make proposed approaches fully operational.

Chapter 2

Overview on the Generalized Beam Theory

2.1 Introduction

In this Chapter, an extended Literature review on the GBT is provided. A very short description concerning reduced approaches for the linear and nonlinear analysis of TWMs which are alternative to GBT is here proposed. They all assume the thin-walled beam as an assembly of folded plates. One of the most reliable and efficient approaches for the TWM analysis is the shell-based Finite Element Analysis (FEA - e.g., Reddy, 2005; Bathe, 2014). Although the approach has been established as one of the most powerful and versatile tool, it is generally very demanding, from a computational viewpoint, and may not be suitable for design purposes, due to the large number of degrees-of-freedom (DOF) required.

A very efficient alternative is represented by the so-called Finite Strip Method (FSM). First introduced by Professor Cheung (Cheung, 1976), it belongs to the family of semi-variational approaches. It is based on subdividing plates forming the TWM into longitudinal strips by means of fictitious lines. The ends of such strips always constitute a part of the boundary. Strips are reciprocally connected along a discrete number of nodal lines, which coincide with the longitudinal boundaries of strips themselves. The displacement field is assumed, in the spirit of semi-variational (Kantorovich) method, as a linear combination of simple polynomials within the cross-section and continuously differentiable smooth series in the longitudinal direction, whose functions should satisfy *a priori* the end boundary conditions. Thus for a strip, the two-dimensional problem is reduced to a one-dimensional one. Different choices can be made as regards longitudinal shape functions. The original proposal calls for trigonometric functions or exponentials, however different families of functions have been introduced later on, leading to different variants of the method. Among the others, the so-called spline finite strip method (sFSM), making use of spline longitudinal series functions, is worth of mentioning due to its large diffusion in the scientific community (e.g., Lau and Hancock, 1986; Vrcelj and Bradford, 2008; Eccher et al., 2009; Pham, 2017).

When compared to other alternative approaches, the modal nature of the GBT approach presents two many advantages, related to its capability to give a clear and straightforward physical interpretation of the TWM behavior:

1. GBT allows to clarify the distinction between local and global buckling as well as in identifying and analyzing buckling interaction phenomena.
2. The TWM behavior can generally be fully described within the GBT by a subset of modes, whose selection is made based on their mechanical interpretation, allowing to significantly reduce the number of DOF.

The capability in distinguishing between local and global buckling has been recently included in both FSM and FEA. The goal has been achieved by suitably introducing internal constraints

to be applied on displacement fields, leading to the so-called constrained finite strip method (cFSM, e.g. Ádány and Schafer, 2008; Ádány et al., 2009) and constrained finite element method (e.g., Ádány, 2017; Ádány et al., 2017). On the other hand, the modal selection allowed by the GBT approach and its related efficiency in reducing the problem dimension are unique and constitute, in some sense, a GBT privilege.

2.2 Literature review

The development of the GBT has been pioneered by Professor R. Schardt and co-workers at the University of Darmstadt, Germany. The definitive reference of their work is a book by Schardt (1989), written in German. The work has extended over more than 30 years, but only little has been published in English (e.g., Schardt, 1983, 1994). The dissemination in English is mainly due to Davies and co-workers. Their first contribution is mainly descriptive and illustrates the use of the GBT approach for the first- and second-order analysis by means of realistic examples (Davies and Leach, 1992). The theory has been then fully detailed in Davies and Leach (1994); Davies et al. (1994); Leach (1994), while further extensions have been later proposed in terms of validation with experimental results (Leach and Davies, 1996) and design of perforated cold-formed steel sections and thin-walled purlins (Davies et al., 1997; Jiang and Davies, 1997).

The large diffusion in the scientific community of the GBT approach is due to the strong impulse given to it in the last two decades by Professor D. Camotim and co-workers at the University of Lisbon, Portugal. Their first contributions (Silvestre and Camotim, 2002a,b) deal with first-order and second-order GBT for orthotropic materials. Nevertheless these contributions represent an extension of previous works by Schardt and Davies, they are considered as main references since they detail and formalize the cross-section analysis and buckling analysis in the framework of GBT. The procedure for the cross-section analysis is presented in Silvestre and Camotim (2002a). The formulation is limited to open cross-sections and is based on the fundamental Vlasov hypothesis of (V1) in-plane (tangential) inextensibility, and (V2) membrane zero-shear deformation. Deformation modes are classified into (a) rigid-body modes, (b) distortional modes, and (c) local (bending) modes. Rigid-body modes are those referred to the Vlasov beam theory (i.e., three translations and one rotation around the shear center). Distortional modes involve in- and out-of-plane displacements of natural nodes (i.e., the ends of plate segments composing the cross-section) together with transverse bending of plates themselves, and are based on the so-called *elementary warping functions*. They are achieved by first discretizing the cross-section in plate segments by means of nodes inserted at their ends, then unitary warping displacements are applied at one natural node at a time, while keeping all the remaining ones at rest. A set of linearly independent *warping modes* is obtained, in number equal to the number of natural nodes, consisting of piece-wise linear warping fields. The corresponding in-plane tangential displacement is sought, for each one of those modes, based on the zero-shear Vlasov condition and leading to step-wise constant distributions. The in-plane transverse displacement is finally achieved by restoring the compatibility of displacement and rotations at natural nodes: the force method is adopted for this purpose. Local modes depict transverse bending of plates composing the cross-section and negligible displacements of the

natural nodes. They are obtained as the solution of the elastic problem where unit displacements are assigned, orthogonal to the plate segment, at intermediate nodes (i.e., not at corners). Except for rigid-body modes, the set of obtained fields is *local-type* in nature, since they involve nontrivial displacement only in a few adjacent nodes. The use of such modes leads to highly coupled differential equations and complicates the task of finding a solution. Additionally, the physical meaning of the various modes is by no means obvious, even in the case of the most trivial and well known phenomena, such as plate bending. Therefore, a change of basis is performed to obtain *global-type* deformation modes. The latter are obtained as the eigenvectors of a properly defined eigenvalue problem aimed to simultaneously diagonalize the warping (axial) and transverse bending stiffness matrices. Deformation modes obtained in Silvestre and Camotim (2002a) are used for the second-order (buckling) analysis in Silvestre and Camotim (2002b). Since obtained deformation modes obey the Vlasov hypothesis, the relevant geometric nonlinear effects can be included by modifying the sole membrane longitudinal strain expression. In particular, only nonlinear terms relevant to the cross-section displacement in its own plane are considered in the analysis. The paper also includes a comparison between GBT and the theory proposed by Bauld and Tzeng (1984), while the physical meaning of cross-section stiffness terms obtained using GBT is pointed out. The approach for the buckling analysis proposed in Silvestre and Camotim (2002b) is valid limited to open cross-section and has been adopted for the analysis of pultruded FRP lipped channels in Silvestre and Camotim (2003a). Analytical formulas have been obtained for the distortional buckling of steel C and Z-section members in Silvestre and Camotim (2004a), and validation with experimental results has been proposed in Silvestre and Camotim (2004b). The proposed cross-section and buckling analyses have been then extended in Dinis et al. (2006) for TWMs with arbitrary branched open cross-sections and then applied for the buckling analysis of members subjected to non-uniform bending in Bebiano et al. (2007). Nonlinear membrane shear strains terms inherent to the in-plane bending of cross-section plates have been considered in the latter work, pointing out the effect on the final results of shear stresses induced by bending moment gradients.

The set of deformation modes provided by Silvestre and Camotim (2002a) obeys the Vlasov hypothesis. As previously illustrated, such a set can be suited in a wide range of problems dealing with open cross-section TWMs, nevertheless it is not exhaustive in describing all deformation configurations the cross-section can depict. The need of additional deformation modes violating the Vlasov hypothesis has been firstly pointed out in Silvestre and Camotim (2003b). In this contribution, a set of so called *shear* modes (i.e., in-plane transverse extension modes and out-of-plane shear-deformable modes) have been introduced in addition to the *fundamental* ones (i.e., modes obeying Vlasov hypothesis) to account for geometric non-linearities. Simão and Simões da Silva (2004) proposed a unified energy formulation for the stability analysis of open and closed thin-walled members within the GBT, discussing the importance of including the effect of shear flow on closed cross-sections and membrane shear distortions. A shear-deformable mode accounting for the classic Bredt torsion (e.g., Oden and Ripperger, 1981) has been included in Gonçalves and Camotim (2004) for the analysis of closed sections, while the importance in including the (Bredt-like) torsion mode and the axisymmetric (in-plane radial-extension) mode for the buckling analysis of circular shells and tubes has been evidenced in Silvestre (2007). Shear modes were included in Silva et al. (2006) for the analysis of FRP composite beams with open branched cross-section, pointing out their fundamental role in case

of orthotropic behavior. Finally, the need of in-plane extensible non-warpable modes has been shown in Silvestre (2008) for the analysis of elliptical cylindrical TWMs. In order to generalize the capabilities of GBT in modeling arbitrary TWMs, the cross-section analysis has been extended. A unified procedure for the cross-section analysis for arbitrary cross-section, including shear modes, was first proposed in Gonçalves et al. (2009). The formulation proposed in Gonçalves et al. (2010) represents a fundamental reference concerning the cross-section analysis since it constitutes a general approach, valid for arbitrary polygonal cross-section (with open and closed branches), for the calculation of a complete set of deformation modes to be used within the GBT framework. The classification of deformation modes based on kinematic consideration represents a fundamental contribution of the work. In particular, three classes of deformation modes have been identified: (i) *conventional modes* are the ones obtained with the procedure originally proposed by Schardt (Schardt, 1989; Silvestre and Camotim, 2002a) and include: (i-a) rigid-body modes, (i-b) distortional modes, (i-c) local (bending) modes and, in case of closed branches, (i-d) the pure torsion shear mode stemming from the Bredt theory; (ii) *shear modes* violate the Vlasov hypothesis V2 and are characterized by nil in-plane deformation and non-nil warping distribution; (iii) *transverse extension modes* are in-plane deformation fields violating the hypothesis V1 and associated with nil warping. Extension and shear modes are commonly referred to as *non-conventional modes*. A different classification was proposed in Silvestre et al. (2011), aimed to provide a physical characterization of deformation modes more suitable for comparison between GBT and cFSM. An improved procedure for determining shear modes for complex multi-cell cross-sections has been proposed in Gonçalves et al. (2014). It is worth to be noted that shear modes described above involve non-nil warping distributions on the plate mid-line. Thus, they introduce membrane shear deformations on the sole mid-plane of the beam, while plates forming the cross-section remain unshearable within their thickness. de Miranda et al. (2013) introduced for the first time an additional set of (non-conventional) shear-deformable fields involving variability of the warping displacement along the plate thickness beside that along the plate mid-line. In this way, the full set of shear fields is able to completely recover the classical Timoshenko beam theory. The contribution in Bebiano et al. (2015) represent a general unified approach for the cross-section analysis, developed with the aim to rationalize and automate the GBT-based analyses. It relies on the definition of eleven eigenvalue problems involving proper-defined stiffness matrices to obtain the final set of GBT (global-type) deformation modes from the (local-type) elementary ones. Finally, a cross-section analysis for curved thin-walled cross-sections has been proposed in Gonçalves and Camotim (2016), where the use of a polygonal approximation of the cross-section mid-line improves the efficiency of the method and allows to handle polygonal sections with rounded corners.

The procedure for the cross-section analysis described so far stems, from a conceptual viewpoint, from the original proposal advanced by Schardt (1989) and consists on two phases. At first, a set of local-type elementary modes is obtained by solving a series of *static* analyses, one for each mode, on an elastic frame having the shape of the cross-section mid-line. Secondly, the final set of global-type deformation modes is achieved by solving a series of eigenproblems, aimed to simultaneously diagonalize some proper defined stiffness matrices. This procedure is usually referred to as *static approach* for the cross-section analysis, due to the static nature of analyses adopted for calculating elementary modes. Recently, a completely different methodology has been proposed in Ranzi and Luongo (2011) limited to conventional modes. In the work,

the set of deformation modes is directly achieved as the eigenvectors of a positive semi-definite eigenvalue problem. The approach is referred to as *dynamic approach* for the cross-section analysis (GBT-D) since the free dynamics of the unconstrained planar frame, represented by the mid-lines of plate segments forming the cross-section, is chosen as the eigenvalue problem. The approach completely reverses the classic procedure for the cross-section analysis. As a matter of fact, the static approach first calls for elementary warping functions, while the in-plane distributions are subsequently evaluated by enforcing the Vlasov V2 hypothesis. On the contrary, the in-plane deformation modes are evaluated at first in the dynamic approach through a planar eigenvalue problem and the warping distributions are achieved afterwards by enforcing the unshearability condition V2. Moreover, transverse inextensibility condition V1 is automatically enforced in the static approach by choosing step-wise linear warping functions, inducing step-wise constant transverse displacements (i.e., plates composing the cross-section are inextensible). Instead, the hypothesis V1 is incorporated in the dynamic approach by means of internal inextensibility constraints to be enforced within the planar eigenvalue problem on each plate element composing the cross-section. The dynamic approach has been then condensed in a one-step procedure in Piccardo et al. (2014b) thanks to the definition of a quadratic functional, whose steady conditions leads to an eigenvalue problem generating the full set of conventional modes. A further extension of the dynamic approach for the calculation of non-conventional fields is available in Piccardo et al. (2014a). In particular, the set of extension modes is chosen as the orthogonal supplement of the in-plane conventional distributions, while shear modes stem from a warping eigenvalue problem. A slightly different procedure has been identified in Taig et al. (2015), where the dynamic analysis of an unconstrained planar frame has been chosen as reference eigenvalue problem. Conventional and extension modes are further separated by means of an orthogonalization procedure very similar to as proposed in Silvestre and Camotim (2002a). The dynamic approach for the cross-section analysis has been first applied for buckling analysis in Taig et al. (2016), where a detailed analysis of the effect, in terms of critical load, of including the cross-section deformability in both pre-buckling and buckling analyses has been proposed.

The introduction of non-conventional modes allowed to further extend the GBT capabilities in modeling TWMs. An important contribution is available in Natário et al. (2012), where the localized web buckling analysis of beams subjected to concentrate loads has been analyzed. The essential contribution of transverse and shear pre-stresses, described by transverse extension and shear modes, respectively, has been pointed out. Similar results have been obtained in Basaglia and Camotim (2013) in analyzing the effect of transverse load application on buckling analysis. In this sense, authors developed a simplified procedure, where the external work of applied transverse load has been assumed as internal work of pre-buckling stresses (i.e., the exact procedure). It has been shown that the simplified formulation, which is much more computationally efficient than its exact counterpart, is able to provide very good results if the relevant buckling mode does not involve heavy local deformations in the transverse loaded cross-section. Non-conventional modes, in particular shear distributions, also play an important role in describing the behavior of regular polygonal tubes. Significant contributions have been proposed in Gonçalves and Camotim (2013a,b,c), where the cross-section and buckling analyses of members subjected to compression, bending or torsion have been completely detailed. Analytical expressions were provided for some cross-section modal properties, and compari-

son in terms of critical load with some closed-form solutions available in the Literature were proposed. Non-conventional modes, in particular out-of-plane shear-deformable fields, play a fundamental role in the analysis of composite orthotropic TWMs. The first model for the buckling analysis of FRP composite beams with open branched cross-section was proposed by Silva et al. (2006) and then extended in Silva, Silvestre and Camotim (2010) for the analysis of FRP composite open-section thin-walled columns. The effect of shear modes in critical loads and buckling modes has been analyzed in the contribution. In particular, shear modes are essential to capture the correct critical load in case of orthotropic behavior. In case of isotropic material, no significant difference can be seen in considering the shear deformability as regards the critical load, providing that conventional local modes are included in the analysis. However, shear modes always influence buckling modal shapes. A complete and extended analysis on the interaction between (transverse) extension, shear and (conventional) local deformation modes in the static bifurcation of thin-walled composite members is presented in Silvestre and Camotim (2013b).

The capability to include non-standard support conditions in GBT formulation has represented a fundamental improvement. The first model was proposed in Camotim et al. (2008) and includes full and partial (i.e., elastically deformable) local constraints. The need of expressing constraints as function of the assumed deformation modes through a modal description has been pointed out. The capability to include local restraints allowed the development of a GBT for linear and buckling analysis of thin-walled frames. The first proposal is available in Basaglia et al. (2008), where the sole (conventional) rigid-body modes have been included in the analysis. Thus, each TWM composing the frame behaves according with the classic Vlasov beam theory, limiting the formulation to the sole global buckling analysis. The connection between the various beams composing the frame is realized by means of a (nodal) *joint element*, placed at the (idealized) point where the connection is deemed to take place, where the modal degrees-of-freedom (i.e., the amplitude functions) are transformed into generalized nodal displacements. In this way and within a Finite Element (FE)-based procedure, the obtained total stiffness matrix includes the effects of ensuring degree of freedom compatibility in the joints connecting adjacent members. A total warping transmission is enforced at each frame joint by means of kinematic relations, thus assuming that web stiffening plates are included at joint locations to prevent the occurrence of distortions. A full GBT formulation for thin-walled frames, including cross-section distortions and therefore suitable for the local, distorsional and global buckling analysis has been proposed in Basaglia et al. (2009). The formulation extends the concept of joint element to arbitrary constraint conditions taking place at the frame joints, thus removing the hypothesis of perfectly-rigid joints (i.e. total warping transmission) introduced in the previous contribution. Formulations outlined so far are suitable for open cross-section TWMs and rely on the sole set of conventional modes provided in Silvestre and Camotim (2002a). Non-conventional fields are included in the buckling analysis of thin-walled frames in Basaglia et al. (2010), thus extending the model for the analysis of arbitrary loading conditions. A complete state-of-the-art report on the buckling analysis of steel thin-walled frames is available in Camotim et al. (2010). Formulations here described have been suited for the analysis of thin-walled structural systems. Cold-formed steel purlins restrained by sheetings are analyzed in Basaglia, Camotim, Gonçalves and Graça (2013), where the latter are simulated by means of elastic rotational and translational supports (springs) located at the purlin upper flange mid-width. A more

general approach suitable for thin-walled systems, such as rack systems, pitched-roof industrial frames, portal frames made with cold-formed hollow section (RHS) profiles and roof-supporting trusses has been proposed in Basaglia and Camotim (2015).

GBT has successfully applied for the analysis of composite steel-concrete beams. The first model is reported in Gonçalves and Camotim (2010), based on the static approach for the cross-section analysis described in Gonçalves et al. (2009). The shear deformability in the longitudinal direction of the interface connections between steel and concrete component was included by means of a subsequent set of deformation fields, obtained by imposing unitary relative displacement (i.e., slip) at each connection interface. This cause a non-zero cross-section warping, inducing non-zero in plane displacement because of the Vlasov unshearability hypothesis (V2). The set of deformation modes including the connection deformability therefore belongs to conventional modes. The proposed model has recently been adopted in Gonçalves et al. (2016); Henriques et al. (2016) for the formulation of a GBT-based beam finite element suitable for the buckling analysis of steel-concrete composite beams. A slightly different approach was introduced in Taig and Ranzi (2015), based on the dynamic approach for the cross-section analysis. The shear deformability of the interface, commonly referred to as partial interaction, has been taken into account in the longitudinal direction by means of linear elastic springs uniformly distributed along the beam length and placed at the interface connections, according to the Newmark model (Newmark et al., 1951). The approach has been recently extended, for the first time in GBT, to the transverse partial interaction behavior of composite beams in Taig and Ranzi (2016). It is worth to be noted that, while proper-defined conventional modes need to be further included when using the static approach to account for the partial interaction analysis, the latter is automatically included in the obtained set of deformation modes provided by the dynamic approach. Some other successful applications of the GBT framework have been recently proposed. A GBT-based model for the analysis of TWMs with variable (open) cross-section have been outlined in Nedelcu (2010). The model has been obtained under the approximation of warping displacements still perpendicular to the cross-section plane. The effect of shear stress has been neglected in the pre-buckling analysis. It has been shown that the proposed model provides good results for members with small tapering slopes. The model was then extended to the analysis of isotropic (closed cross-section) conical shells under compression in Nedelcu (2011). A GBT approach for the linear analysis of TWMs with locally stiffened sections has been proposed in Taig and Ranzi (2014). The contribution is based on the dynamic approach for the cross-section analysis. In particular, the sole set of conventional modes has been used in the analysis. Two approaches have been formulated to include the plate stiffeners, both providing good results. The first approach relies on elastic springs placed on the stiffened cross-section elements, thus providing two different sets of modes (i.e., for the unstiffened and stiffened sections, respectively) requiring a high level of care in their combination. The second approach introduces a set of internal constraints to be enforced in the member analysis. A first-order GBT has been developed in Peres et al. (2016) for curved TWMs with circular axis. An original method for analysis of TWMs with squared holes using GBT has been first presented in Nedelcu (2014). The approach is based on the analysis of a full (i.e., unperforated) TWMs from which the contribution, in terms of global stiffness matrix, of the missing (i.e., perforated) region has been subtracted. A different approach has been proposed in Cai and Moen (2015); Casafont et al. (2015); Cai and Moen (2016); Casafont et al. (2018). The latter contributions

treat the TWM as an assembly of prismatic sub-members having constant cross-section. A set of compatibility constraints on the GBT modal amplitudes have been introduced according to the procedure outlined in Camotim et al. (2008) to connect the mentioned sub-members at their interfaces.

The development of material and geometrical nonlinear GBT formulations has represented a fundamental advancement, extending the approach to the plastic bifurcation and post-buckling analyses of TWMs. The first geometrically nonlinear GBT formulation was presented in Silvestre and Camotim (2003b) for the analysis of cold-formed steel members with open cross-section. The proposal constitute a fundamental reference in the field since it outlines a GBT-based methodology for the geometrically nonlinear analysis which has never been substantially modified in further contributions. It is based on the use of the linear GBT kinematic commonly adopted for first- (i.e., linear) and second-order (i.e., buckling) analyses (e.g., Silvestre and Camotim, 2002a,b) together with an incomplete expression of the Green-Lagrange strain tensor. In particular, the sole membrane nonlinear strain components related to the cross-section displacement in its own plane are considered in the analysis, similarly to as done in Silvestre and Camotim (2002b). A fundamental contribution is represented by the introduction of a set of so called *shear* modes, as mentioned so far, to be added to the *fundamental* ones to account of effects associated to large displacements, such as the approaching of cross-section natural nodes (i.e., shortening effect) induced by the in-plane deflection of plates. In this sense, the paper represents the first contribution in which non-conventional modes, definitively formalized in Gonçalves et al. (2010), have been presented and used in the analysis. A FE procedure has been also proposed to solve the GBT (nonlinear) equations, where Hermitian cubic polynomial shape functions have been used to interpolate the modal amplitudes. The proposed FE procedure has had a great diffusion in the GBT framework and constitutes the approach commonly adopted for the solution of GBT equations in both linear, buckling and nonlinear analyses. The geometrically nonlinear GBT has been adopted for the post-buckling analysis of stiffened lipped channel columns in Silvestre and Camotim (2006b), pointing out the significant role played by stiffeners in distortional post-critical behavior. The model has been extended to account for arbitrary support conditions in Basaglia et al. (2011), and thus adopted for the post-buckling analysis of thin-walled steel frames in Basaglia, Camotim and Silvestre (2013). It is worth to be noted that, since the model benefits of a linear GBT kinematics, arbitrary restraints conditions developed for linear and buckling analyses (e.g., Camotim et al., 2008; Basaglia et al., 2009; Camotim et al., 2010) can be included in the nonlinear model in a very straightforward manner. The proposed nonlinear approach has been then used for the post-buckling analysis of laminated CFRP stiffened panels in Silva, Camotim and Silvestre (2010) and GFRP pultruded beams in Silva et al. (2011). Once again, the use of linear GBT kinematics allows the orthotropic model previously proposed (e.g., Silvestre and Camotim, 2002a; Silva et al., 2006) to be included in the nonlinear analysis in a natural way. Very recently, a corotational based geometrically nonlinear GBT formulation has been presented in de Miranda et al. (2017). The approach follows the main idea first proposed in Silvestre and Camotim (2003b), adopting a linear GBT kinematics and including the sole nonlinear membrane strains, however the full set of deformation fields, including the non-conventional ones involving shear deformation within the plate thickness (de Miranda et al., 2013), have been considered in the analysis. The first material nonlinear GBT formulation has been presented in Gonçalves and Camotim (2004) for

the analysis of aluminum and stainless steel columns subjected to uniform compression. Both J_2 -flow and J_2 -deformation theories of plasticity, suitable for a small strain (i.e. geometrically linear) analysis, have been considered in order to include the so-called *plate buckling paradox* (e.g., Hutchinson, 1974). The sole conventional modes have been included in the analysis. The contribution is remarkable since it allows to deal with closed cross-section, thanks to the inclusion of the torsion (Bredt-like) shear mode, which will be later classified as conventional according to Gonçalves et al. (2010). The approach has been extended to include general load conditions in Gonçalves and Camotim (2007). A GBT-based FE formulation for the elasto-plastic analysis of TWMs has been proposed in Gonçalves and Camotim (2011), based on the sole set of conventional modes, and then extended including non-conventional fields for the first time in Abambres et al. (2013). The proposed GBT-based formulation has been used very recently in Silvestre et al. (2017) to study the influence of the mode nature (local, distortional, global) on the load carrying capacity of TWMs beyond the yield load. It was shown that, under the hypothesis of small strain regime, a significant post-yielding strength is available in case of local/distorsional failure modes, while the opposite occurs when failure modes are global in nature. The material nonlinear GBT-based FE formulation has been extended to the inclusion of geometrically nonlinear effects in Gonçalves and Camotim (2012). Consistently with the original proposal for geometrically nonlinear analysis (Silvestre and Camotim, 2003b), an incomplete Green-Lagrange strain tensor expression has been adopted, accounting for the sole nonlinear membrane strain terms, while material non-linearities are included according to as proposed in Gonçalves and Camotim (2011), thus limiting the analysis to conventional modes. The model is suitable for small-to-moderate displacement range, since nonlinear curvature have been neglected. A full material and geometric nonlinear GBT approach, suitable for large displacement regime, has been proposed in Abambres, Camotim and Silvestre (2014), where both nonlinear curvatures and non-conventional fields have been included in the analysis. Based on the latter contribution, a nonlinear GBT-based FE formulation have been developed in Abambres, Camotim, Silvestre and Rasmussen (2014) and then adopted for modeling steel-concrete composite beams in Henriques et al. (2014), limited to material non-linearities, and Henriques et al. (2015) for full material and geometrical nonlinear analysis. The interaction between steel and concrete components is included in the analysis according to as presented in Gonçalves and Camotim (2010).

The GBT approach have been suited for dynamic analyses of TWMs. The first model is available in Silvestre and Camotim (2006c). The formulation is based on demanding the time-dependency to the unknown amplitude functions and describing the latter with the classic free vibration mode superposition (e.g., Inman, 2013) widely adopted in structural dynamic. In this way, a member modal analysis is performed, thus identifying a set of member vibration modes (to not be confused with the cross-section GBT deformation modes). A set of uncoupled ordinary differential equations is then obtained in the unknown time functions describing the time variation of vibration (member) modes previously identified. The modal nature of the GBT approach, given by the introduction of cross-section deformation fields, allows to understand the contribution of each cross-section (GBT) mode on the configuration of each (member) vibration mode. In this sense, one can intend the dynamic analysis performed within the GBT framework as a *double modal analysis*. The approach for the GBT dynamic analysis initially proposed in Silvestre and Camotim (2006c) has kept substantially unchanged in further contributions, anal-

ogously to what had happened for the geometrically nonlinear GBT formulation. The original proposal deals with the dynamic analysis of axially compressed open section cold-formed steel members and includes the sole set of conventional GBT modes, similarly to as proposed, e.g., in Silvestre and Camotim (2002a); Basaglia et al. (2009). Its extension to composite orthotropic materials is proposed in Silvestre and Camotim (2006a) and calls for both conventional and shear-deformable GBT modes, thus adopting the GBT kinematics and cross-section analysis proposed in Silva et al. (2006). Bebiano et al. (2008b) extended the formulation to include non-uniform bending by adopting a very similar procedure to as done in Bebiano et al. (2007). A general GBT-based approach for the dynamic analysis of TWMs subjected to arbitrary dynamic loads was proposed in Bebiano, Camotim and Silvestre (2013) for steel members and in Silvestre and Camotim (2013a) for composite open cross-section beams, while the contribution in Gonçalves et al. (2014) for the analysis of complex multi-cell cross-sections has been suited in the dynamic analysis in Gonçalves et al. (2015). Very recently, the GBT-based dynamic analysis has been adopted for investigating the dynamic response of high-speed railway bridge decks in Bebiano et al. (2017).

The intense research on the GBT allowed the method to become a reliable approach for the analysis of TWMs, very competitive indeed with respect to more refined shell-based Finite Element analyses (FEAs) as regards the linear and buckling analyses. The computer code GB-TUL has been developed by Camotim and co-workers for the GBT-based analysis of arbitrary TWMs with various load and support conditions (e.g., Bebiano et al., 2008a; Bebiano, Camotim and Gonçalves, 2013). Thanks to the modal nature of the approach, GBT is particularly suitable in understanding the behavior of TWMs, in particular as regard interactions between local/distorsional/global buckling modes. Analysis in this sense has been proposed in Dinis et al. (2010) regarding angle, T-section and cruciform TWMs. Mode interaction in equal-leg angle columns has been investigated in Dinis et al. (2012); Mesacasa et al. (2014). An interesting contribution is represented by Dinis and Camotim (2011), where the buckling mode interactions of cold-formed steel lipped channel columns have been investigated. Columns analyzed had cross-sections dimensions and length ensuring equal local, distorsional and global critical loads, thus maximizing the mode interaction phenomenon. The local/distorsional interaction in lipped channels beams has been very recently analyzed in Martins, Camotim, Gonçalves and Dinis (2016). The modal nature of GBT has been very recently suited through the GBTUL code for developing a “trial-and error” procedure aimed to the geometry optimization of TWMs with various support conditions, in order to enforce particular buckling behaviors, both pure (i.e., local or distorsional or global) and with interaction. Such TWMs were further investigate through a full material- and geometrical- nonlinear FEA, to predispose DSM-based design procedures. Several recent contributions can be found in this sense for lipped channel columns (e.g., Martins et al., 2015; Cava et al., 2016; Martins, Camotim and Dinis, 2017c), web/flange stiffened channel columns (e.g., Martins, Dinis and Camotim, 2016; Landesmann et al., 2016; Martins, Camotim and Dinis, 2017a) and beams (e.g., Martins, Landesmann, Camotim and Dinis, 2017; Martins, Camotim and Dinis, 2017b). An alternative and reliable approach is represented by the so-called constrained Finite Strip Method (cFSM), developed by Schafer and co-workers (e.g., Ádány and Schafer, 2006b, 2008) and implemented in the open source software CUFSM (e.g., Schafer and Ádány, 2006; Li and Schafer, 2010). The approach make use of internal constraints to direct the TWM behavior, thus identifying local, distorsional and global buckling

modes very similarly to what GBT naturally provides. Some interesting comparisons between GBT and cFSM are available in the Literature. The first comparison is reported in Ádány and Schafer (2006a), while an extended comparison between the two approaches, in terms of critical loads and buckling modes on open (unbranched) TWMs, have been proposed in Ádány et al. (2009). The latter contribution lead to a revisited GBT (Silvestre et al., 2011), where the kinematic assumptions and procedures adopted by GBT to identify and characterize the cross-section deformation modes have been revisited in order to make the GBT framework more suitable for a true comparison with the displacement fields constraints employed in cFSM. A full comparison between FEA, cFSM and GBT is available in Casafont et al. (2009) in terms of pure distortional elastic buckling loads and limited to open TWMs. It is worth to be mentioned that the GBT distortional (conventional) modes have been used in the latter contribution as internal constraints, in order to limit the FEA to pure distortional behavior. A very similar procedure has been proposed in Casafont et al. (2011) and thus extended in Nedelcu (2012); Nedelcu and Cucu (2014) to account for global, distortional and local buckling loads. A similar procedure has been proposed in Ádány (2017); Ádány et al. (2017) for developing a constrained shell-FEA, making use of the displacement fields constraints employed in cFSM. Very recently, a new approach, namely the method of Generalized Eigenvectors (GE), has been proposed for the analysis of beams (e.g., Genoese et al., 2014a,b). The method is valid for both compact and thin-walled beams and is based on a semi-analytic finite element formulation for the analysis of the cross-section. A generalized eigenproblem is obtained, in particular eigenvectors associated with zero eigenvalues denotes cross-section displacements according to the classic de Saint-Venant solution, while eigenvectors with positive real-part eigenvalues denotes generalized warping modes describing cross-section distortions. An interesting comparison between GE and GBT approaches is available in Garcea et al. (2016), where both cross-section deformation modes and critical loads and modes stemming from a static bifurcation (buckling) analysis are analyzed and compared for different cross-section shapes.

2.3 Linear GBT formulation

A brief overview on the GBT approach for linear elastic analysis of TWMs is presented in this Section. A generic TWM is considered, with arbitrary open, closed or partially-closed cross-section, made of flat plates connected along edges. The displacement field of the mid-surface \mathcal{S} of the plates (i.e., at $y = 0$) can be expressed as (Fig. 2.1):

$$\mathbf{u}(s, z) = u(s, z)\mathbf{e}_s(s) + v(s, z)\mathbf{e}_y(s) + w(s, z)\mathbf{e}_z(s) \quad (2.1)$$

where s is the curvilinear abscissa along the mid-line of the cross-section profile \mathcal{C} , z is the abscissa along the beam axis, $\mathbf{e}_s(s)$ ($\mathbf{e}_y(s)$) is a unit versor tangent (normal) to \mathcal{C} , $\mathbf{e}_z(s)$ is a unit versor parallel to the TWM axis, respectively, and $u(s, z)$, $v(s, z)$, $w(s, z)$ are the relevant scalar displacement components in the same triad. In the framework of GBT, these latter are expressed as linear combination of *assumed* (known) deformation fields $U_k(s)$, $V_k(s)$ and $W_k(s)$, commonly referred to as *deformation modes* and defined on \mathcal{C} , and corresponding (unknown)

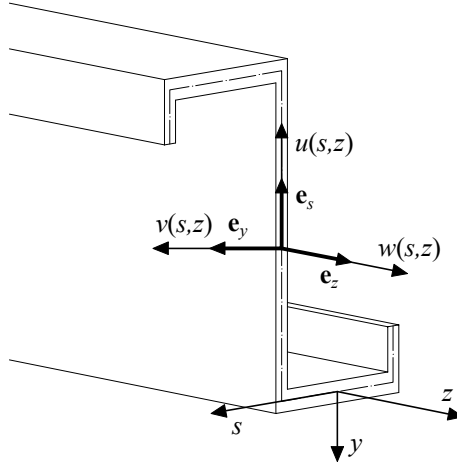


Figure 2.1: GBT displacement field.

amplitude functions $\varphi_k(z)$, defined along the beam abscissa, as (e.g., Ranzi and Luongo, 2011):

$$u(s, z) = \sum_{k=1}^K U_k(s) \varphi_k(z) \quad (2.2a)$$

$$v(s, z) = \sum_{k=1}^K V_k(s) \varphi_k(z) \quad (2.2b)$$

$$w(s, z) = \sum_{k=1}^K W_k(s) \varphi'_k(z) \quad (2.2c)$$

where the prime symbol denotes differentiation with respect to the corresponding function variable. The displacement field $\mathbf{d}(s, y, z) = d_s(s, y, z)\mathbf{e}_s(s) + d_y(s, y, z)\mathbf{e}_y(s) + d_z(s, y, z)\mathbf{e}_z(s)$ at a point $P(s, y, z)$ located within the plate thickness (i.e., external to \mathcal{S}) is evaluated according to the Kirchhoff model as (e.g., Ranzi and Luongo, 2011):

$$d_s(s, y, z) = \sum_{k=1}^K [U_k(s) - yV'_k(s)] \varphi_k(z) \quad (2.3a)$$

$$d_y(s, y, z) = \sum_{k=1}^K V_k(s) \varphi_k(z) \quad (2.3b)$$

$$d_z(s, y, z) = \sum_{k=1}^K [W_k(s) - yV_k(s)] \varphi'_k(z) \quad (2.3c)$$

With the adopted formulation, the (linear) strain field $\boldsymbol{\varepsilon}(s, y, z) = \{\varepsilon_s^m, \varepsilon_z^m, \gamma_{sz}^m, \varepsilon_s^f, \varepsilon_z^f, \gamma_{sz}^f\}^T$ can be written as:

$$\varepsilon_s^m = \sum_{k=1}^K U_k'(s) \varphi_k(z) \quad (2.4a)$$

$$\varepsilon_z^m = \sum_{k=1}^K W_k(s) \varphi_k''(z) \quad (2.4b)$$

$$\gamma_{sz}^m = \sum_{k=1}^K [U_k(s) + W_k'(s)] \varphi_k'(z) \quad (2.4c)$$

$$\varepsilon_s^f = \sum_{k=1}^K -y V_k''(s) \varphi_k(z) \quad (2.4d)$$

$$\varepsilon_z^f = \sum_{k=1}^K -y V_k(s) \varphi_k''(z) \quad (2.4e)$$

$$\gamma_{sz}^f = \sum_{k=1}^K -2y V_k'(s) \varphi_k'(z) \quad (2.4f)$$

where membrane strain components, relevant to $y = 0$ and denoted with superscript m , have been distinguished from flexural components, relevant to $y \neq 0$ and denoted with superscript f . A linear elastic law is commonly adopted, thus expressing membrane and flexural stresses as $\boldsymbol{\sigma} = \mathbf{E}\boldsymbol{\varepsilon}$, where the elastic matrix \mathbf{E} is defined as:

$$\mathbf{E} = \begin{bmatrix} \frac{E}{1-\nu^2} & \frac{\nu E}{1-\nu^2} & 0 & 0 & 0 & 0 \\ \frac{\nu E}{1-\nu^2} & \frac{E}{1-\nu^2} & 0 & 0 & 0 & 0 \\ 0 & 0 & G & 0 & 0 & 0 \\ 0 & 0 & 0 & \frac{E}{1-\nu^2} & \frac{\nu E}{1-\nu^2} & 0 \\ 0 & 0 & 0 & \frac{\nu E}{1-\nu^2} & \frac{E}{1-\nu^2} & 0 \\ 0 & 0 & 0 & 0 & 0 & G \end{bmatrix} \quad (2.5)$$

where E , G and ν are the longitudinal, tangential and Poisson moduli, respectively. Corresponding (linear) stress field $\boldsymbol{\sigma}(s, y, z) = \{\sigma_s^m, \sigma_z^m, \tau_{sz}^m, \sigma_s^f, \sigma_z^f, \tau_{sz}^f\}^T$ can be written as:

$$\sigma_s^m = \sum_{k=1}^K \frac{E}{1-\nu^2} [U_k'(s) \varphi_k(z) + \nu W_k(s) \varphi_k''(z)] \quad (2.6a)$$

$$\sigma_z^m = \sum_{k=1}^K \frac{E}{1-\nu^2} [\nu U_k'(s) \varphi_k(z) + W_k(s) \varphi_k''(z)] \quad (2.6b)$$

$$\tau_{sz}^m = \sum_{k=1}^K G [U_k(s) + W_k'(s)] \varphi_k'(z) \quad (2.6c)$$

$$\sigma_s^f = \sum_{k=1}^K -\frac{yE}{1-\nu^2} [V_k''(s) \varphi_k(z) + \nu V_k(s) \varphi_k''(z)] \quad (2.6d)$$

$$\sigma_z^f = \sum_{k=1}^K -\frac{yE}{1-\nu^2} [\nu V_k''(s) \varphi_k(z) + V_k(s) \varphi_k''(z)] \quad (2.6e)$$

$$\tau_{sz}^f = \sum_{k=1}^K -2yG V_k'(s) \varphi_k'(z) \quad (2.6f)$$

The weak formulation of the elasticity problem can be derived through the Principle of Virtual Works. This can be expressed, assuming external forces to be constant (or averaged) over the plate thickness, as (e.g., Piccardo et al., 2014a):

$$\int_{\mathcal{V}} \boldsymbol{\varepsilon}^T \mathbf{E} \delta \boldsymbol{\varepsilon} dV - \int_S \mathbf{f}^T \delta \mathbf{u} dS - \int_C \sum_B \mathbf{F}_B^T \delta \mathbf{u}_B ds = 0 \quad (2.7)$$

where \mathcal{V} is the volume of the TWM, $\mathbf{f}(s, z) = f_s(s, z)\mathbf{e}_s(s) + f_y(s, z)\mathbf{e}_y(s) + f_z(s, z)\mathbf{e}_z(s)$ are forces per unit area acting on the middle surface \mathcal{S} , $\mathbf{F}_B(s) = F_{Bs}(s)\mathbf{e}_s(s) + F_{By}(s)\mathbf{e}_y(s) + F_{Bz}(s)\mathbf{e}_z(s)$ are forces per unit length applied on the boundaries $B : z = 0, \mathcal{L}$ (i.e., on the mid-line \mathcal{C} of the end cross-sections at $z = 0, \mathcal{L}$, respectively, \mathcal{L} being the TWM length), and the δ -operator denotes virtual quantities. By making use of Eqs. (2.2), (2.4) and (2.5), the following field equations can be obtained from Eq. (2.7) by performing the standard steps of variational calculus (e.g., Berdichevsky, 2009):

$$\mathbf{C}\varphi^{IV} - (\mathbf{D} - \mathbf{F} - \mathbf{F}^T)\varphi'' + \mathbf{B}\varphi - \mathbf{p} = \mathbf{0} \quad (2.8)$$

with corresponding boundary conditions terms to be applied at $z = 0, \mathcal{L}$:

$$\delta\varphi'^T (\mathbf{C}\varphi'' + \mathbf{F}^T\varphi - \mathbf{P}^W) = \mathbf{0} \quad (2.9a)$$

$$\delta\varphi^T [\mathbf{C}\varphi''' - (\mathbf{D} - \mathbf{F}^T)\varphi' - \mathbf{P}^M] = \mathbf{0} \quad (2.9b)$$

where the vector $\varphi = \{\varphi_1(z), \dots, \varphi_k(z), \dots, \varphi_K(z)\}^T$ collects the K unknown amplitude functions. Eq. (2.8) are commonly referred to as *GBT equations*. They consist on a set of K coupled ordinary differential equations in the amplitude functions $\varphi_k(z)$. Eq. (2.9) generate the mechanical boundary conditions (i.e., the *natural conditions*) to be applied to the end cross-sections once the geometric constraints (i.e., the *essential conditions*) have been prescribed. In Eqs. (2.8) and (2.9), the following positions hold for structural matrices:

$$B_{hk} = B_{hk}^e + B_{hk}^f = \frac{Et}{1 - \nu^2} \int_{\mathcal{C}} U'_h(s)U'_k(s)ds + \frac{Et^3}{12(1 - \nu^2)} \int_{\mathcal{C}} V''_h(s)V''_k(s)ds \quad (2.10a)$$

$$C_{hk} = C_{hk}^a + C_{hk}^f = \frac{Et}{1 - \nu^2} \int_{\mathcal{C}} W_h(s)W_k(s)ds + \frac{Et^3}{12(1 - \nu^2)} \int_{\mathcal{C}} V_h(s)V_k(s)ds \quad (2.10b)$$

$$\begin{aligned} D_{hk} &= D_{hk}^s + D_{hk}^t = \\ &= Gt \int_{\mathcal{C}} [U_h(s) + W'_h(s)][U_k(s) + W'_k(s)] ds + \frac{Gt^3}{3} \int_{\mathcal{C}} V'_h(s)V'_k(s)ds \end{aligned} \quad (2.10c)$$

$$F_{hk} = F_{hk}^s + F_{hk}^f = \frac{\nu Et}{1 - \nu^2} \int_{\mathcal{C}} U'_h(s)W_k(s)ds + \frac{\nu Et^3}{12(1 - \nu^2)} \int_{\mathcal{C}} V''_h(s)V_k(s)ds \quad (2.10d)$$

where superscripts f, t, e, a and s refer to the flexural, torsional, (transverse) extensional, axial (longitudinal) and shear nature of the underlying energy terms, respectively. The relevant loading vectors included in both Eqs. (2.8) and (2.9) are defined as:

$$p_k = \int_{\mathcal{C}} [f_s(s, z)U_k(s) + f_y(s, z)V_k(s) - f_{z,z}(s, z)W_k(s)] ds \quad (2.11a)$$

$$P_k^W = \int_{\mathcal{C}} \left[\sum_B F_{Bz}(s)W_k(s) \right] ds \quad (2.11b)$$

$$P_k^M = \int_{\mathcal{C}} \left\{ \sum_B [F_{Bs}(s)U_k(s) + F_{By}(s)V_k(s)] + f_z(s, z)W_k(s) \right\} ds \quad (2.11c)$$

where the comma denotes differentiation with respect to the following variable.

GBT equations are commonly solved numerically by means of a Finite Element (FE) procedure (e.g., Bathe, 2014). The beam is discretized along its longitudinal axis by means of N_E finite elements and the unknown amplitude functions are approximated, in the spirit of the displacement-based FE formulations, by means of Hermite cubic polynomial shape functions. This approximation can be described by:

$$\varphi_k(z) \cong \sum_{i=1}^2 \left[H_{2i-1}(z) \varphi_k^{(i)} + H_{2i}(z) \varphi_k'^{(i)} \right] \quad (2.12)$$

where $\varphi_k^{(i)}, \varphi_k'^{(i)}$ are the (unknown) nodal values of the amplitude functions, while $H_i(z)$ are polynomials shape functions that can be expressed in non-dimensional form as:

$$H_1(z) = 1 - 3 \left(\frac{z}{l_E} \right)^2 + 2 \left(\frac{z}{l_E} \right)^3; \quad H_2(z) = l_E \left[\frac{z}{l_E} - 2 \left(\frac{z}{l_E} \right)^2 + \left(\frac{z}{l_E} \right)^3 \right] \quad (2.13a,b)$$

$$H_3(z) = 3 \left(\frac{z}{l_E} \right)^2 - 2 \left(\frac{z}{l_E} \right)^3; \quad H_4(z) = l_E \left[- \left(\frac{z}{l_E} \right)^2 + \left(\frac{z}{l_E} \right)^3 \right] \quad (2.13c,d)$$

with l_E being the length of the E -th FE. By making use of Eq. (2.12) and performing the standard steps of the FE procedure, the following stiffness relationship can be obtained for each GBT-based FE:

$$\mathbf{K}_E \mathbf{d}_E = \mathbf{q}_E \quad (2.14)$$

where \mathbf{d}_E is a $4K \times 1$ vector collecting the unknown nodal values of the amplitude functions, while \mathbf{K}_E and \mathbf{q}_E are $4K \times 4K$ stiffness matrix and $4K \times 1$ load vector, respectively, defined as follows:

$$\mathbf{K}_E = \int_{l_E} [\mathbf{H}^T (\mathbf{B} \mathbf{H} + \mathbf{F}^T \mathbf{H}'') + \mathbf{H}'^T \mathbf{D} \mathbf{H}' + \mathbf{H}''^T (\mathbf{C} \mathbf{H}'' + \mathbf{F} \mathbf{H})] dz \quad (2.15a)$$

$$\mathbf{q}_E = \int_{l_E} [\mathbf{H}^T \mathbf{q}_1 + \mathbf{H}'^T \mathbf{q}_2] dz \quad (2.15b)$$

being:

$$q_{1k} = \int_{\mathcal{C}} [f_s(s, z) U_k(s) + f_y(s, z) V_k(s)] ds; \quad q_{2k} = \int_{\mathcal{C}} f_z(s, z) W_k(s) ds \quad (2.16a,b)$$

and:

$$\mathbf{H}(z) = [H_1(z) \mathbf{I} \quad H_2(z) \mathbf{I} \quad H_3(z) \mathbf{I} \quad H_4(z) \mathbf{I}] \quad (2.17)$$

with \mathbf{I} being a $K \times K$ identity matrix.

From a mathematical viewpoint, GBT can be classified as a semi-variational approach, where a linear Galerkin method is used to reduce the original elastic three-dimensional problem described by partial differential equations to an equivalent one-dimensional problem dealing with ordinary differential equations. Semi-variational approaches stem from the so called

Kantorovich-Vlasov method (e.g., Prokopov et al., 1982), which originates from the work done by Kantorovich on the use of Galerkin method for reducing complex problems to ordinary differential equations (Kantorovich, 1933, 1942; Kantorovich and Krylov, 1958). Nevertheless a similar procedure was earlier proposed by Vlasov for the analysis of shells (Vlasov, 1932). In the context of the Kantorovich-Vlasov method, GBT involves the use of a linear Galerkin methods (Kantorovich and Krylov, 1958; Fletcher, 1984), in which the displacement field is expressed by means of *linear trial functions* $U_k(s), V_k(s)$ and $W_k(s)$ affected by *linear coordinates* $\varphi_k(z)$. GBT presents lots of similarities with the procedure commonly adopted in elastic buckling and bifurcation analysis (e.g., Budiansky, 1974; Luongo and Pignataro, 1988 for applications in the context of thin-walled beams), however a fundamental difference exists between the two approaches. In fact, while the set of trial functions of the latter is made of *critical* (i.e., *buckling*) *modes*, the former relies on generic functions $U_k(s), V_k(s)$ and $W_k(s)$ describing congruent deformed configurations of the beam cross-section. Therefore, the use of the nomenclature *modes* for functions $U_k(s), V_k(s)$ and $W_k(s)$ seems to be ambiguous, since it might lead to consider the GBT trial functions as the critical modes depicted by the TWM. For this reasons and in spite of the wide diffusion in the Literature of the nomenclature “*deformation modes*”, functions $U_k(s), V_k(s)$ and $W_k(s)$ will be referred in this work to as “*trial functions*”, or alternatively “*functions*” or “*fields*”.

The GBT approach requires two steps to be carried out, in particular: (a) *cross-section analysis*, where a suitable set of trial functions $U_k(s), V_k(s)$ and $W_k(s)$ is identified; (b) *member analysis*, where matrices and vectors in Eqs. (2.10) and (2.11) are first evaluated, then GBT equations and corresponding boundary conditions, Eqs. (2.8) and (2.9), are solved, either analytically or numerically, in terms of unknowns coordinates $\varphi_k(z)$. The choice of the set of trial functions is a fundamental step for the numerical efficiency of a Galerkin approach. As a matter of facts, despite the convergence of the method is guaranteed providing that the set of trial functions is (i) complete in energy, and (ii) made of linearly independent functions, it is well known (e.g., Fletcher, 1984) that the use of local-type functions strongly reduces the accuracy of the method. Therefore, the use of fields $U_k(s), V_k(s)$ and $W_k(s)$ involving nontrivial displacement in a limited portion of the cross-section requires, in order to obtain accurate results, the use of a large number of functions. On the contrary, fields that are global in nature and hierarchically ordered allow to well model the TWM behavior by using a very limited number of trial functions, making the GBT very efficient. The cross-section analysis is therefore the leading step in the GBT approach, since it is strictly related to the accuracy and efficiency of the methodology.

Chapter 3

Novel straightforward dynamic approach for the GBT cross-section analysis

The classic cross-section analysis (e.g., Davies and Leach, 1994; Silvestre and Camotim, 2002a) is based on the two fundamental Vlasov hypotheses: (V1) all the members composing the cross-section are in-plane inextensible, and (V2) they are unshearable. Due to V2 hypothesis, tangential in-plane displacements and warping are mutually linked so that, once one is known, the other can be consequently evaluated. The set of in-plane and warping deformation fields that identically satisfy Vlasov hypotheses refers to as *conventional* trial functions. In some case however, these latter may not be sufficient to accurately describe the TWM behavior, and other deformation fields, referred to as *non-conventional* trial functions, were introduced (e.g., Silvestre and Camotim, 2003b; Gonçalves et al., 2010; Piccardo et al., 2014a). Non-conventional trial functions include *extension* and *shear* fields; they are obtained by releasing the V1 and V2 assumptions and, together with conventional ones, they constitute a complete set of linear trial functions, able to span the whole space of the admissible configurations of the problem. The importance of non-conventional fields in the GBT-based analysis has been repeatedly pointed out in the Literature. They play a fundamental role in the buckling analysis of TWMs subjected to concentrated and transverse loads (e.g., Natário et al., 2012; Basaglia and Camotim, 2013), regular polygonal tubes (e.g., Gonçalves and Camotim, 2013a,c) and composite orthotropic TWMs (e.g., Silva et al., 2006; Silva, Camotim and Silvestre, 2010), while they are essential to include geometrically non-linear effects in GBT-based non-linear analyses (e.g., Silvestre and Camotim, 2003b; Silva et al., 2011).

The classic static approach that allows to evaluate both conventional and non-conventional functions (e.g., Silvestre and Camotim, 2002a, 2003b; Gonçalves et al., 2010) arises from a discretization of the cross-section in a finite number of plate segments by introducing “natural” nodes (corresponding to wall mid-line intersections or free edges) and “intermediate” nodes (arbitrarily located between the natural nodes of each wall). Each trial function is defined as the static solution (by classic methods of structural mechanics) of a linear elastic planar frame, representing the cross-section, subjected to unitary generalized displacement at each node. In this way, obtained displacement fields are generally *local-type* in nature since they involve non-trivial displacements only in a few adjacent segments. It is then introduced an orthogonalization procedure (e.g., Silvestre and Camotim, 2002a; Gonçalves et al., 2010) which serves the purpose of hierarchizing trial functions in a well-defined way, with the aim to obtain *global type* deformation fields and a partial decoupling of the GBT equations. Very recently, a step forward has been proposed within the static approach to the cross-section analysis in Bebiano et al. (2015), in order to obtain a “rational” and “automate” procedure, according to the definition of the authors. Although this procedure is undeniably more direct and less involved than those previously cited, it maintains complexity and problems intrinsic to the static approach. In particular, the procedure still requires, as a first step, the determination of an exhaustive set of node-based elementary deformation fields as solutions of static problems, arising from the

individual imposition of four unit generalized displacements at each (natural and intermediate) node. Then, the obtained elementary trial functions must be combined through a number of eigenvalue problems (greater than 10; see Figure 13 in Bebiano et al., 2015), in order to provide the final set of GBT (global) trial functions. Moreover, the whole procedure is not based on purely kinematic concepts (as it would be definitely possible at least for isotropic material) but it is, in some sense, mixed and recursive: the physical characterization of GBT functions is obtained by the mentioned eigenvalue problems that are defined through stiffness matrices arising from the member analysis and then depending on the trial functions themselves. Nevertheless, this action is necessary to give physical meaning to static elementary deformation fields initially determined, in addition to make less coupled the GBT equations (without reaching a complete decoupling anyway). A completely innovative dynamic approach for the cross-section analysis was first proposed in Ranzi and Luongo (2011), limited to conventional trial functions, and later extended to non-conventional ones in Piccardo et al. (2014a). In this new context, referred to as GBT-D, the set of trial functions is directly achieved from the eigenvectors of a positive semi-definite eigenvalue problem. The free dynamics of the unconstrained planar frame, represented by the mid-lines of plate segments forming the cross-section, is chosen as the eigenvalue problem. In this way, deformation fields arise naturally from the solution of a small number of eigenvalue problems (only 3) without any preliminary static evaluation and without the need for further orthogonalization involving stiffness matrices. The complete procedure consists of three steps (Piccardo et al., 2014a): (1) a first constrained planar eigenvalue problem (PEP) is performed for a linear elastic planar frame having the shape of the TWM mid-line, whose members are assumed to be inextensible; obtained fields are then supplied by warping components ensuring (a) zero membrane shear-strains in open branches, and (b) constant shear-stress flow along closed loops (*conventional* trial functions); (2) a second constrained PEP is solved for an extensional planar frame of the same shape, where obtained fields are the orthogonal supplement to the inextensional ones (*extension* trial functions); (3) a warping eigenvalue problem (WEP) is performed for a pure shear beam, supplying purely warping fields for the TWM (*shear* trial functions). Thanks to the intrinsic characteristics of the dynamic approach, the obtained conventional and shear fields are directly global in nature and hierarchically ordered. Moreover, the approach results very simple from a mathematical viewpoint and easy to be implemented in a computer code. Despite the many advantages provided, the original GBT-D approach sometimes leads to localized extension fields (i.e., having displacements localized in few natural nodes of the profile). This aspect does not imply any problem in the solution, but it seems in contrast with the GBT spirit as reduced method, that should try to find a well approximated solution of structural behavior using the smallest possible number of trial functions. To avoid this problem, an unconstrained dynamic approach for the cross-section analysis was introduced in Taig et al. (2015). In the contribution, a set of mixed in-plane flexure-extension fields is obtained at first, then conventional and extension functions are separated through properly defined eigenvalue problems that are very similar to those present in the static procedure. The proposed methodology allows to overcome the localized nature of extension fields shown by the original GBT-D approach. However, resulting conventional and extension trial functions seem to be slightly imprecise, especially as regards higher ones that sometimes lose their symmetry. Due to this fact, the whole set of trial functions have to be considered in the analysis in order to correctly describe the structural behavior, as happened for the GBT-D procedure and in contrast to

the original spirit of GBT earlier mentioned. Moreover, as in the static procedure, this method is partially mixed since member stiffness matrices depending on trial function themselves are necessary to perform the whole procedure. In this chapter, a new procedure is developed within the GBT-D approach originally proposed in Piccardo et al. (2014a), in order to overcome the possible localized character of extension trial functions. To this end, a new constrained PEP is formulated, where members are assumed to be unshearable and unflexible (i.e., they can only show purely in-plane elongations) in order to obtain a subset of planar, non-conventional, purely extension fields which arise naturally of global type for both mono-connected (i.e. open) and multiply-connected (i.e. closed or partially closed) TWM cross-sections. Regarding these latter, the need of hybrid trial functions (i.e., mixed in-plane flexure-extension fields) is pointed out. They include flexural deformation involving frame elasticity associated to the effect of non-simultaneous elongations on elements belonging to closed branches. A further constrained PEP is presented, where hybrid functions are asked to be energetically orthogonal to remaining in-plane (conventional and pure extension) deformation fields. The chapter is organized as follows. An exhaustive overview on the available approaches for the cross-section analysis within the GBT-D approach (Piccardo et al., 2014a; Taig et al., 2015) is first presented in Section 3.1. The continuous formulations for both PEP and WEP are briefly presented, then the corresponding discrete FE-based versions, commonly preferred in the Literature, are illustrated in detail. The new procedure for (pure and mixed) extension trial functions is then introduced in Section 3.2, pointing out a couple of alternative and equivalent procedures for the determination of the constraint matrix required in the new PEP. An illustrative example of a generic partially closed cross-section taken from Bebiano et al. (2015) is presented throughout Sections 3.1 and 3.2, in order to highlight the differences, in terms of obtained trial functions, between the three approaches, while three additional examples are presented in Section 3.2, illustrating the versatility of the new procedure. The set of trial functions obtained from the dynamic approach are summarized in Section 3.3. Finally, a brief discussion on the influence in adopting different interpolating polynomial functions for the discrete FE-based cross-section analysis is addressed in Section 3.4.

3.1 Overview on the GBT-D approach

A segment of TWM with length dz is considered to be free in space (i.e., unconstrained), weightless, with mass proportional to the local thickness (see Fig. 3.1a, where a channel section is considered as example). The segment is susceptible of two types of motion: (a) in-plane oscillations, in which all points move transversely to the beam axis z (i.e., the segment behaves as an unconstrained planar extensible frame, see Fig. 3.1b), and (b) out-of-plane (warping) oscillations, in which all points move parallel to the beam axis (i.e., the segment behaves as an unconstrained pure shear beam, see Fig. 3.1c). Since dz is infinitesimal, it can be assumed that both in-plane and out-of-plane motions are not dependent on z ; therefore, the previous two problems are governed by two independent sets of uncoupled differential equations, referred to as Planar Eigenvalue Problem (PEP) and Warping Eigenvalue Problem (WEP), respectively, which are now outlined in separate sections.

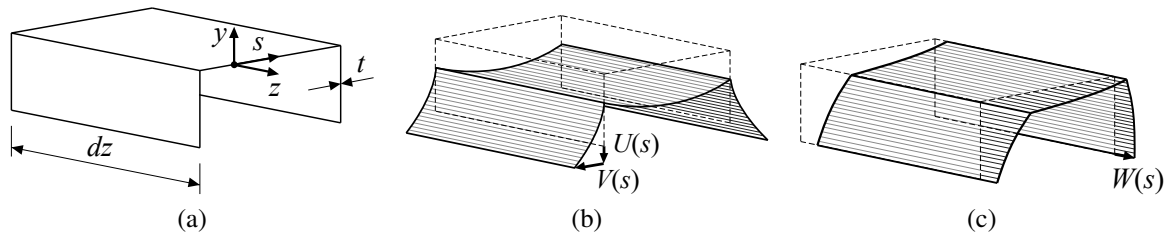


Figure 3.1: Free oscillations of a segment of TWM: (a) undeformed configuration, (b) in-plane oscillations, (c) out-of-plane (warping) oscillations.

3.1.1 Planar Eigenvalue Problem (PEP)

The PEP is governed by the well-known equations for axial and transverse vibrations of a beam, which are expressed as (Piccardo et al., 2014a):

$$U''(s) + \lambda \frac{m}{EA} U(s) = 0 \quad (3.1a)$$

$$V^{IV}(s) + \lambda \frac{m}{EJ} V(s) = 0 \quad (3.1b)$$

where m , A , J , E are the mass per unit length, area, second moment of area and elastic modulus, respectively, of each beam element used in discretizing the cross-section as a planar frame, while λ depicts the unknown eigenvalue, defined as the square of the frame natural circular frequency (i.e., $\lambda = \omega^2$). Eq. (3.1) are the fields equations applicable to each beam element, providing that parameters m , A , J , E remain constant along each segment. By following the standard steps of structural dynamics (e.g., Inman, 2013), a transcendent characteristic equation of the type $f(\lambda) = 0$ can be obtained, which admits an infinite number of eigenvalues λ_k and associated eigenfunctions $U_k(s)$, $V_k(s)$, $k = 1, 2, \dots$.

Although the continuous problem is in principle simple and suitable for matrix formulation (e.g., Ranzi and Luongo, 2014), its discrete version is preferred in the Literature. The planar frame representative of the TWM cross-section is subdivided into M finite elements by interposing possible additional nodes between the natural ones (i.e., the corners of the profile). By using the classic six degree-of-freedom (DOF) FE illustrated in Fig. 3.2a, being n the total number of nodes (both natural and intermediate) adopted for the frame discretization, the problem is reduced to $N = 3n$ DOF. Following standard steps of the FE procedure (e.g., Ranzi and Gilbert, 2015) and assuming Hermite cubic and Lagrangian linear polynomial interpolating functions for the transverse and axial displacements, respectively, the local stiffness and mass matrices \mathbf{K}_p^e and \mathbf{M}_p^e (with $e = 1, 2, \dots, M$ and subscript p identifying the *planar* problem) are evaluated for each element (see Appendix A), and then suitably assembled. The following algebraic eigenvalue problem is thus obtained:

$$(\mathbf{K}_p - \lambda_p \mathbf{M}_p) \mathbf{q}_p = \mathbf{0} \quad (3.2)$$

where \mathbf{K}_p and \mathbf{M}_p are the $N \times N$ global stiffness and mass matrices and \mathbf{q}_p is a N -vector collecting nodal displacements. Since the matrices \mathbf{K}_p and \mathbf{M}_p are real symmetric, their eigenvectors \mathbf{q}_{pk} ($k = 1, \dots, N$) constitutes a complete set that spans the whole space of the admissible configurations of the system. It is here highlighted the fact that eigenvectors are normalized in

the present work, unless otherwise specified, in such a way the maximum nodal displacement they describe is unitary in magnitude. Corresponding trial functions describe mixed flexure-extension deformation fields. Any non-singular change of basis leads to a set of deformation fields that still represent a complete basis for the considered space. Thus, consistently to as commonly done in the GBT framework (e.g., Gonçalves et al., 2010) and to facilitate the physical interpretation of the problem, it is convenient to divide the whole space into supplementary subspaces leading to a mechanical characterization of deformation fields. The first subspace concerns the *conventional* fields, in which the planar frame undergoes flexure without extension, satisfying the Vlasov's V1 hypothesis. The second subspace includes the *non-conventional* (transverse) *extension* fields, in which elements composing the cross-section are free to depict in-plane elongations, thus violating the inextensibility (V1) condition. Two distinct procedures have been proposed in the context of the GBT-D approach, in order to identify the aforementioned subspaces. The first one is based on introducing suitable sets of internal constraints in the PEP depicted in Eq. (3.2). The procedure can be thus referred to as *constrained approach* and has been first introduced in Ranzi and Luongo (2011), limited to conventional fields, and then extended in Piccardo et al. (2014a) to account for extension trial functions. The second procedure was first proposed in Taig et al. (2015) and, on the contrary, it does not involve any internal constraints, since conventional and extension fields are separated by performing subsequent changes of basis very similar to those present in the static procedure. For this reasons, it is referred to as *unconstrained approach*. For the seek of clarity, the two methodologies will be illustrated separately in the following.

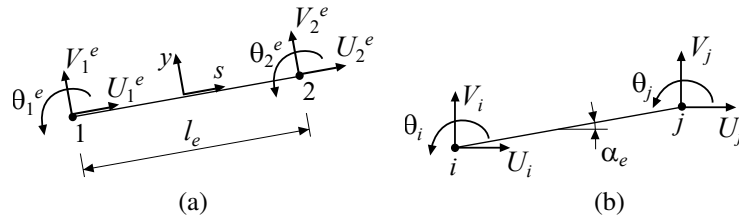


Figure 3.2: In-plane 6 DOF FE for the cross-section analysis: nodal displacements in (a) local, and (b) global coordinates.

Constrained approach for conventional and extension trial functions

The first procedure for conventional fields in the context of the constrained (GBT-D) approach has been proposed in Ranzi and Luongo (2011). It is based on the introduction of suitable internal constraints in Eq. (3.2), equal in number to the M elements used in the FE discretization of the planar frame. Referring to the generic element e in the plane of the cross-section (Fig. 3.2a) and interpreting it as a generalized elastic spring as provided by Luongo and Paolone (1997) (see Appendix B), its global axial deformation is defined in local coordinates as:

$$\varepsilon_e = U_2^e - U_1^e \quad (3.3)$$

The inextensibility constraint $\varepsilon_e = 0$ can be rewritten in global coordinates as:

$$(U_j - U_i) \cos \alpha_e + (V_j - V_i) \sin \alpha_e = 0 \quad (3.4)$$

obtaining M linearly independent equations representative of a purely-extensional internal constraint; they can be collected in a linear system of the type (subscript i being referred to *inextensible* trial functions):

$$\mathbf{A}_i \mathbf{q}_p = \mathbf{0} \quad (3.5)$$

where \mathbf{A}_i is a $M \times N$ matrix. Eq. (3.5) can be solved with respect to $N_i = N - M$ master variables \mathbf{q}_{iM} , as provided in Appendix C. Based on this technique, a *constrained* PEP is obtained:

$$(\mathbf{K}_i - \lambda_i \mathbf{M}_i) \mathbf{q}_{iM} = \mathbf{0} \quad (3.6)$$

where:

$$\mathbf{K}_i = \mathbf{R}_i^T \mathbf{K}_p \mathbf{R}_i; \quad \mathbf{M}_i = \mathbf{R}_i^T \mathbf{M}_p \mathbf{R}_i \quad (3.7a,b)$$

are $N_i \times N_i$ reduced-order stiffness and mass matrices, respectively, and \mathbf{R}_i is a $N \times N_i$ constraint matrix (see Appendix C). Eq. (3.6) provides N_i eigenvectors $\mathbf{q}_{ik} = \mathbf{R}_i \mathbf{q}_{iMk}$ that can be collected in the $N \times N_i$ matrix $\mathbf{Q}_i = [\mathbf{q}_{i1}, \mathbf{q}_{i2}, \dots, \mathbf{q}_{iN_i}]$: they span a N_i -dimensional subspace of the original N -dimensional one. From them the conventional (inextensional) planar trial functions $U_k^i(s), V_k^i(s)$ ($k = 1, 2, \dots, N_i$) are determined, based on the adopted interpolating functions. Since the frame is unconstrained (i.e., \mathbf{K}_p is positive semi-definite) and the constraint matrix \mathbf{R}_i is a full-rank matrix, the problem admits the triple eigenvalue $\lambda_i = 0$, to which three eigenvectors, describing rigid motions of the cross-section, are associated. These can be freely and conveniently chosen as two translations along the principal inertia axes of the cross-section, and a rotation around its shear center.

Conventional planar trial functions can be conveniently supplemented by warping distributions $W_k^i(s)$ whose associate membrane shear strain γ_{sz}^m is required to be either (a) nil along open branches of \mathcal{C} (i.e., satisfying the Vlasov unshearability condition), or (b) constant on each closed branch of \mathcal{C} (i.e., satisfying the Bredt's condition). Recalling Eq. (2.4c) and considering that $U_k^i(s)$ are piecewise constant functions (i.e., $U_k^i(s) = U_k^e, e = 1, 2, \dots, M$) due to the Vlasov inextensibility condition V1 enforced in Eq. (3.5), it follows that warping distributions are piecewise linear function and can be expressed as function of their (unknown) nodal values as:

$$W_k^i(s) = \frac{W_{2k}^e - W_{1k}^e}{l_e} s + W_{1k}^e \quad e = 1, 2, \dots, M \quad (3.8)$$

where W_{1k}^e and W_{2k}^e depict the values of warping distribution associated to the k -th trial function at the first node (i.e., $s = 0$) and end node (i.e., $s = l_e$), respectively, of element e possessing length l_e . The Vlasov unshearability (V2) condition can thus be expressed as:

$$U_k^e + \frac{W_{2k}^e - W_{1k}^e}{l_e} = 0 \quad (3.9)$$

to be applied on elements belonging to open branches of \mathcal{C} , while the following relationship holds on closed branches:

$$G t_e \left(U_k^e + \frac{W_{2k}^e - W_{1k}^e}{l_e} \right) = \sum_{l=1}^L (\pm) Q_k^l \quad (3.10)$$

where t_e is the thickness of the e -th element and Q_k^l is the (unknown) tangential stress flow associated with the k -th trial function and acting of the l -th closed loop (being L the total

number of closed loops composing the cross-section). An arbitrary positive rotation is assigned to each loop and a positive (negative) sign is used in the summation for Q_k^l in the right-hand side of Eq. (3.10) when the direction identified by the local coordinate s and the one consequent to the rotation previously introduced coincide (differ). Eqs. (3.9) and (3.10) represent a linear system of M equations and $n + L$ unknowns. Since the number of cross-section elements can be expressed as $M = n - 1 + L$, one of these unknowns remains arbitrary. It describes the uniform (longitudinal) extension of the member. To make the warping orthogonal to the extension, it is convenient to choose the remaining arbitrary unknown in such a way that the average k -th warping function is zero, i.e.:

$$\int_C W_k^i(s) ds = \sum_{e=1}^M \frac{l_e}{2} (W_{1k}^e + W_{2k}^e) = 0 \quad (3.11)$$

An illustrative example of a generic partially closed cross-section taken from Bebiano et al. (2015) and shown in Fig. 3.3a is proposed to illustrate the GBT-D procedure. In perfect

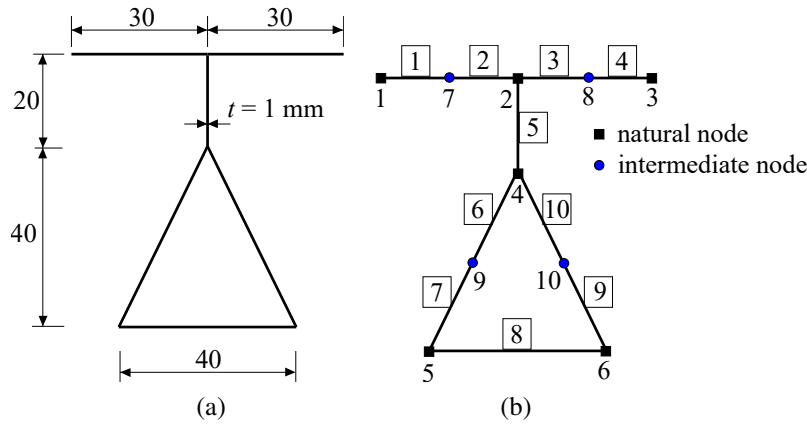


Figure 3.3: Illustrative example of dynamic cross-section analysis: (a) geometry, (b) cross-section discretization.

analogy with Bebiano et al. (2015), the cross-section is discretized with $n = 10$ nodes, then $N = 30$ and $M = 10$ elements (Fig. 3.3b). Conventional trial functions $U_k^i(s)$, $V_k^i(s)$, $W_k^i(s)$ ($k = 1, 2, \dots, N_i$) for the illustrative example are shown in Fig. 3.4; they are in number $N_i = N - M = 20$. The first three functions describe rigid-body motions corresponding to null eigenvalues. Other fields involve in-plane flexure without elongation of the cross-section elements, in accordance with Vlasov's V1 hypothesis. Corresponding warping distributions enforce the unshearability V2 hypothesis on open branches, and the Bredt's conditions on closed cells.

Extension fields are assumed, accordingly to Piccardo et al. (2014a), as the orthogonal supplement to the conventional subset \mathbf{Q}_i previously identified. Any vector \mathbf{q}_e orthogonal to the latter subspace must satisfy N_i orthogonality conditions which can be expressed in matrix form as $\mathbf{Q}_i^T \mathbf{G} \mathbf{q}_p = \mathbf{0}$, being \mathbf{G} any definite positive matrix. In the following, the identity matrix (i.e., $\mathbf{G} = \mathbf{I}$) is adopted. The set of N_i orthogonality conditions are used as internal constraints in the dynamic problem of Eq. (3.2). They can be solved in terms of $N_e = N - N_i = M$ master

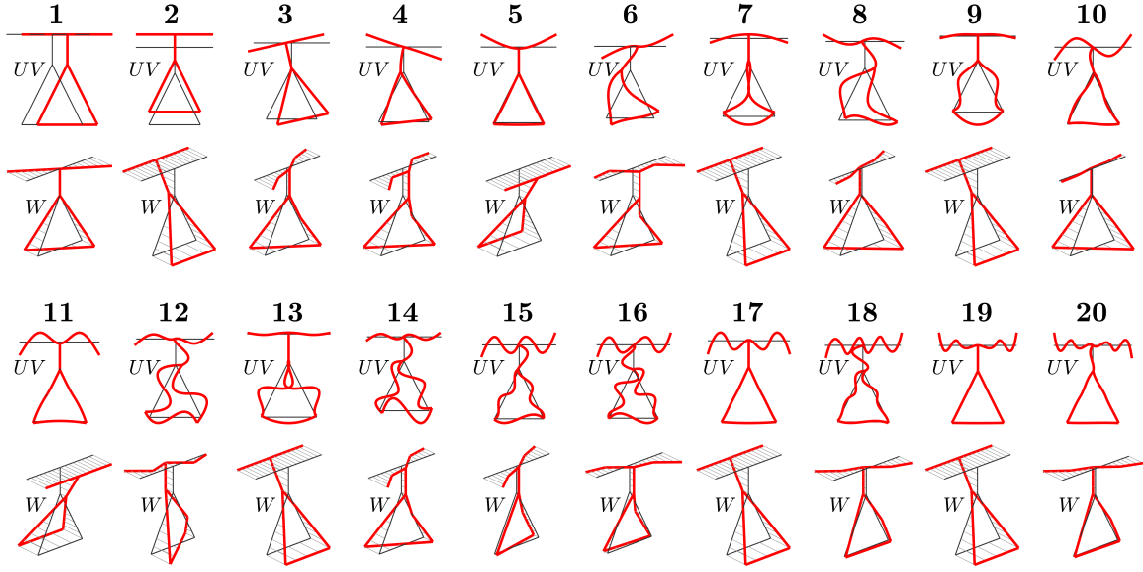


Figure 3.4: Illustrative example of dynamic cross-section analysis: conventional planar and warping trial functions obtained with the GBT-D approach (Piccardo et al., 2014a).

variable \mathbf{q}_{eM} , as provided in Appendix C, thus obtaining the following constrained PEP:

$$(\mathbf{K}_e - \lambda_e \mathbf{M}_e) \mathbf{q}_{eM} = 0 \quad (3.12)$$

where:

$$\mathbf{K}_e = \mathbf{R}_e^T \mathbf{K}_p \mathbf{R}_e; \quad \mathbf{M}_e = \mathbf{R}_e^T \mathbf{M}_p \mathbf{R}_e \quad (3.13a,b)$$

are $M \times M$ reduced-order stiffness and mass matrices, respectively, and \mathbf{R}_e is a $N \times M$ constraint matrix (see Appendix C). Eq. (3.12) provides M eigenvectors $\mathbf{q}_{ek} = \mathbf{R}_e \mathbf{q}_{eMk}$ orthogonal to the inextensional eigenvectors \mathbf{q}_{ik} , thus completing the basis sought. Transverse extension planar trial functions $U_k^e(s)$, $V_k^e(s)$ ($k = 1, 2, \dots, M$) are determined, based on the adopted interpolating functions. They are associated to nil warping components (i.e., $W_k^e(s) = 0$). Extension planar trial functions for the illustrative example are shown in Fig. 3.5, where both the full in-plane cross-section displacement UV and the sole transverse displacement U have been reported, the latter using the y -axis convention (i.e., they are plotted as a diagram with positive values in the local y -axis direction). Obtained axial displacements $U_k^e(s)$ are global in type since they involve non-trivial displacements in sufficiently wide portions of the cross-section (i.e., more than one node adopted in the discretization). On the contrary, transverse displacements $V_k^e(s)$ are localized nearby one single node in almost all obtained extension trial functions. This might be due to internal constraints enforcing orthogonality with conventional fields, which seems to prevent rigid translations of elements not depicting axial displacements. The phenomenon may influence the computational efficiency of the GBT approach, since a large number of local-type trial functions may be required to obtain accurate results. Moreover, such localized bending behavior is not related to any physical evidence.

Unconstrained approach for conventional and extension trial functions

An alternative procedure was developed in Taig et al. (2015) for the identification of conventional and extension planar trial functions. The procedure is referred to *unconstrained* approach

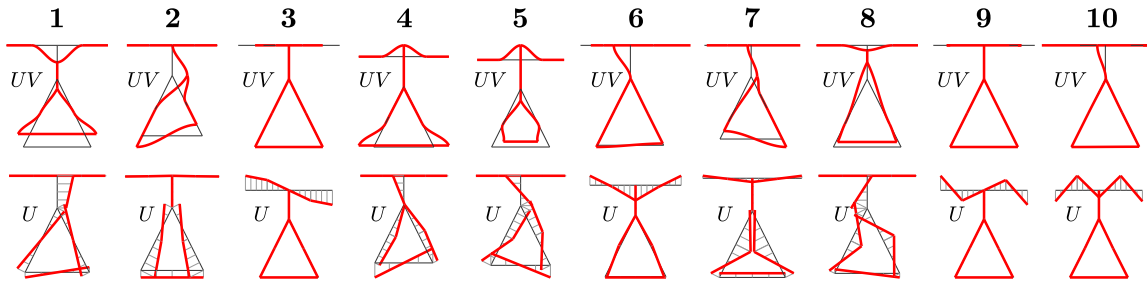


Figure 3.5: Illustrative example of dynamic cross-section analysis: non-conventional extension (planar) trial functions obtained with the GBT-D approach (Piccardo et al., 2014a).

since it does not employ any internal constraint, differently to as done in Ranzi and Luongo (2011); Piccardo et al. (2014a). A first set of planar trial function is evaluated, in terms of nodal values, through the dynamic analysis of the unconstrained frame representing the cross-section, Eq. (3.2), thus obtaining mixed flexure-extensional deformation fields. They are collected in the $N \times N$ matrix $\mathbf{Q}_p = [\mathbf{q}_{p1}, \mathbf{q}_{p2}, \dots, \mathbf{q}_{pN}]$, where the first three eigenvectors depict rigid-body motions: they are associated to the triple multiplicity nil eigenvalue stemming from Eq. (3.2) and due to the fact that matrix \mathbf{K}_p is positive semi-definite (i.e., the frame is unconstrained). Subsets of conventional and extension fields are then obtained by performing a change of basis to the original set after removing the three rigid-body deformation fields, i.e. $\mathbf{Q}_p^* = [\mathbf{q}_{p4}, \mathbf{q}_{p5}, \dots, \mathbf{q}_{pN}]$, by solving the following eigenproblem:

$$(\mathbf{B}^e - \mu \mathbf{B}^f) \mathbf{u} = 0 \quad (3.14)$$

where μ and \mathbf{u} depict an eigenpair, while matrices \mathbf{B}^e and \mathbf{B}^f are defined in Eq. (2.10a) and account for the axial and flexural deformation, respectively, of plate elements composing the cross-section. Eq. (3.14) admits $N_c (= N_i - 3)$ zero eigenvalues that are related to planar inextensible fields (i.e., the subset of conventional functions without the three describing rigid-body motions), while the remaining M non-zero eigenvalues identify planar deformation fields involving transverse extension (i.e., the subset of extension functions). By collecting the eigenvectors \mathbf{u}_j corresponding to zero eigenvalues ($j = 1, 2, \dots, N_c$) in the transformation matrix $\mathbf{T}_c^* = [\mathbf{u}_1, \mathbf{u}_2, \dots, \mathbf{u}_{N_c}]$ and the remaining ones \mathbf{u}_k corresponding to non-zero eigenvalues ($k = N_c + 1, \dots, N - 3$) in the transformation matrix $\mathbf{T}_e^* = [\mathbf{u}_{N_c+1}, \dots, \mathbf{u}_k, \dots, \mathbf{u}_{N-3}]$, conventional and extension subsets can be separated through the following linear transformations:

$$\begin{bmatrix} \mathbf{Q}_c^{*T} \\ \mathbf{Q}_e^{*T} \end{bmatrix} = \begin{bmatrix} \mathbf{T}_c^{*T} \\ \mathbf{T}_e^{*T} \end{bmatrix} \mathbf{Q}_p^{*T} \quad (3.15)$$

where \mathbf{Q}_c^* and \mathbf{Q}_e^* are $(N \times N_c)$ and $(N \times M)$ matrices, respectively, whose columns identify eigenvectors describing planar inextensible and extensible configurations, respectively. Although corresponding trial functions could already be used in the member analysis, a further post-processing is performed to ensure that all identified fields reflect the response of the entire cross-section, rather than just displacements of localized parts of it. This is achieved by performing two further change of basis defined by the following eigenproblems:

$$(\mathbf{T}_c^{*T} \mathbf{B}^f \mathbf{T}_c^* - \mu_i \mathbf{I}) \mathbf{u}_c = 0 \quad (3.16a)$$

$$(\mathbf{T}_e^{*T} \mathbf{B}^e \mathbf{T}_e^* - \mu_e \mathbf{I}) \mathbf{u}_e = 0 \quad (3.16b)$$

from which the following transformation matrices are obtained:

$$\mathbf{T}_c = [\mathbf{u}_{c1}, \mathbf{u}_{c2}, \dots, \mathbf{u}_{N_c}]; \quad \mathbf{T}_e = [\mathbf{u}_{e1}, \mathbf{u}_{e2}, \dots, \mathbf{u}_M] \quad (3.17a,b)$$

The final subsets of conventional and extension trial functions can be finally achieved, in terms of nodal values, through the following linear transformations:

$$\mathbf{Q}_c^T = \mathbf{T}_c \mathbf{Q}_c^{*T}; \quad \mathbf{Q}_e^T = \mathbf{T}_e \mathbf{Q}_e^{*T} \quad (3.18a,b)$$

The subset of conventional planar trial functions must be finally completed by adding the three rigid-body motions removed at the beginning of the procedure, i.e. $\mathbf{Q}_i = [\mathbf{q}_{p1}, \mathbf{q}_{p2}, \mathbf{q}_{p3}, \mathbf{Q}_c]$, and by supplying warping distributions $W_k^i(s)$ able to satisfy the Vlasov's unshearability (V2) condition on open branches and the Bredt's conditions on closed cells (Eqs. (3.9) to (3.11)).

The complete subsets of conventional trial functions $U_k^i(s)$, $V_k^i(s)$, $W_k^i(s)$ ($k = 1, 2, \dots, N_i$) and transverse extension trial functions $U_k^e(s)$, $V_k^e(s)$ ($k = 1, 2, \dots, N_e$) for the illustrative example obtained with the unconstrained approach are shown in Figs. 3.6a and 3.6b, respectively. Obtained extension fields seems to overcome the localized character affecting the ones illustrated in Fig. 3.5. Pure elongations of cross-section elements can be observed on open branches, while mixed extensional-flexure deformations can be observed on closed branches (see fields 3 and 4). The latter phenomenon is meaningful since the problem governing in-plane extension of elements belonging to closed branches is hyperstatic and, thus, profile elements may exhibit flexural deformation involving frame elasticity. In contrast, both conventional and extension fields seems to be imprecise, since they lose their symmetry properties, especially in higher functions. This phenomenon lead to the fact the whole set of deformation modes have to be considered in order to correctly describe the structural behavior, in contrast with the spirit of the GBT approach as a reduction method.

3.1.2 Warping Eigenvalue Problem

The WEP governs the free oscillations of a pure shear beam in the $s - z$ plane. This is an internally constrained Timoshenko beam, in which cross-section rotations are prevented, so that elements are only permitted to slide orthogonally to the axis. Therefore, the shear γ is the only strain, and the shear force T the only active stress. The vibration of the beam in the out-of-plane (warping) direction is governed by the following differential equation (Piccardo et al., 2014a):

$$W''(s) + \lambda \frac{m}{GA} U(s) = 0 \quad (3.19)$$

which is formally identical to Eq. (3.1a). Providing that parameters m , A , G , the latter being the tangential modulus, remain constant along each segment composing the cross-section, Eq. (3.19) is the field equation of the problem, applicable to each beam element. Similarly to as done in the PEP, a transcendent characteristic equation of the type $f(\lambda) = 0$ can be obtained, whose roots λ_k , which are infinite in number, represent the warping eigenvalues, with associated eigenfunctions $W_k(s)$, $k = 1, 2, \dots$.

The discrete version of the WEP is obtained by using the same discretization adopted for the previous PEP. By using the 2 DOF FE shown in Fig. 3.7, the system is reduced, in the WEP

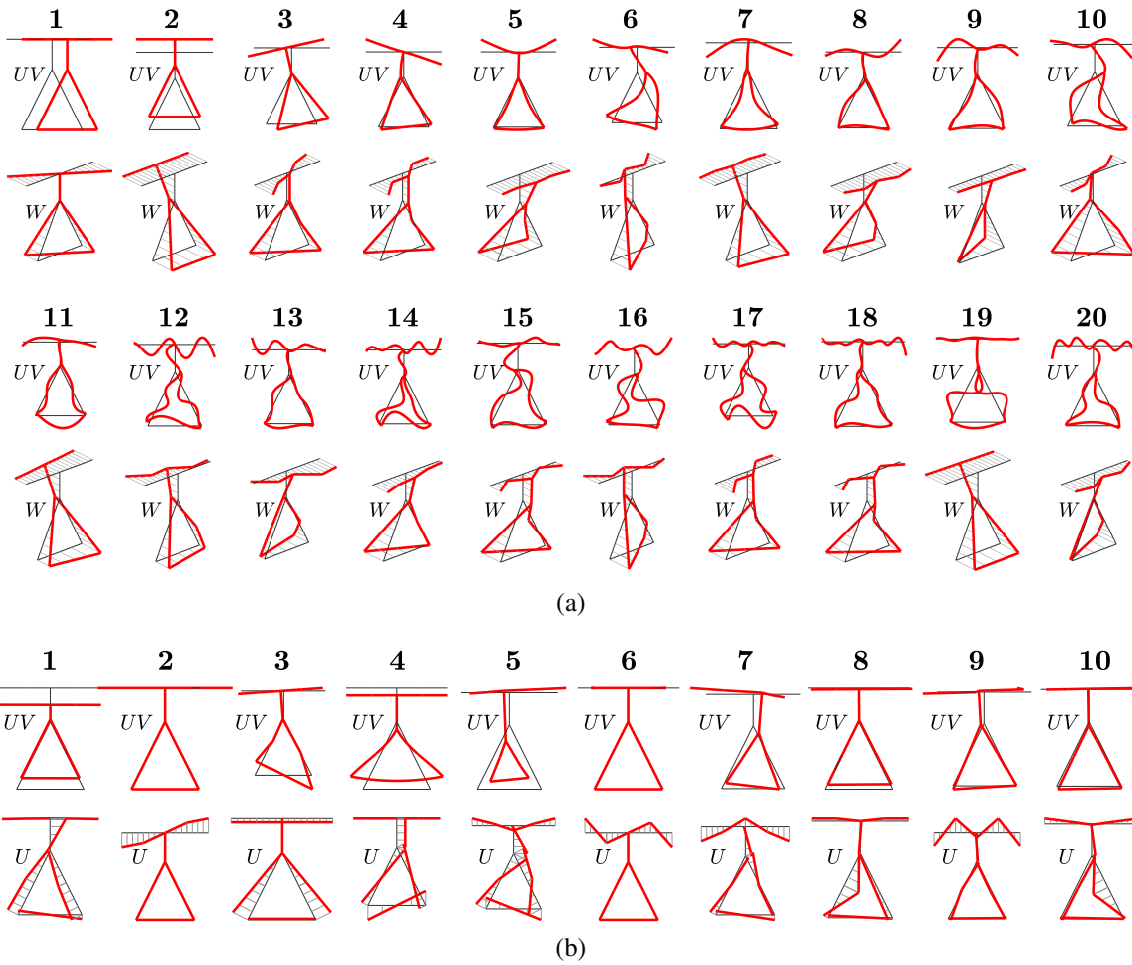


Figure 3.6: Illustrative example of dynamic cross-section analysis:(a) conventional planar and warping trial functions, (b) non-conventional extension (planar) trial functions, obtained with the unconstrained approach (Taig et al., 2015).

context, to n DOF. By assuming linear Lagrangian polynomials as interpolating functions, the local stiffness and mass matrices \mathbf{K}_w^e and \mathbf{M}_w^e (with $e = 1, 2, \dots, M$ and subscript w identifying the *warping* problem) are evaluated for each element (see Appendix A), and then assembled. The following WEP is obtained:

$$(\mathbf{K}_w - \lambda_w \mathbf{M}_w) \mathbf{q}_w = \mathbf{0} \quad (3.20)$$

where \mathbf{K}_w and \mathbf{M}_w are the $n \times n$ global (real symmetric) stiffness and mass matrices, respectively, and \mathbf{q}_w is a n -vector collecting nodal displacements. Eq. (3.20) provides n eigenvectors \mathbf{q}_{wk} which can be collected in the $n \times n$ matrix $\mathbf{Q}_w = [\mathbf{q}_{w1}, \mathbf{q}_{w2}, \dots, \mathbf{q}_{wn}]$. Since the frame is unconstrained (i.e., \mathbf{K}_w is positive semi-definite), the problem admits the nil eigenvalue $\lambda_w = 0$, whose corresponding eigenvector describes the rigid out-of-plane displacement of the TWM profile (i.e., a *global longitudinal shortening* effect). Corresponding warping (out-of-plane) trial functions, determined based on the adopted interpolating functions, describe pure warping displacement fields and violate the Vlasov unshearability hypothesis V2. Accordingly to

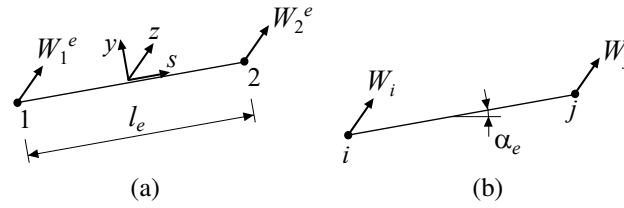


Figure 3.7: Out-of-plane 2 DOF FE for the cross-section analysis: nodal displacements in (a) local, and (b) global coordinates.

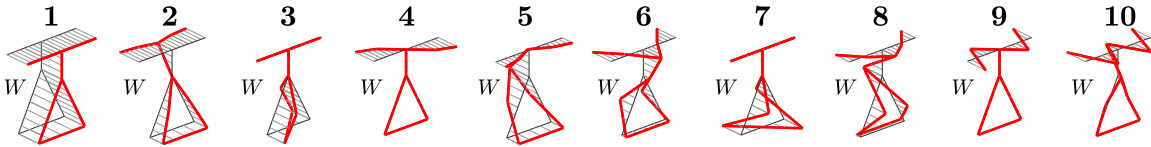


Figure 3.8: Illustrative example of dynamic cross-section analysis: non-conventional shear (warping) trial functions

Gonçalves et al. (2010), they constitute the set of *non-conventional shear* trial functions $W_k^s(s)$ ($k = 1, 2, \dots, n$) and are associated with nil in-plane displacements (i.e., $U_k^s(s) = V_k^s(s) = 0$). Shear functions for the illustrative example are shown in Fig. 3.8: they are in number of $n = 10$. It is worth to be noted that the first function, which corresponds to null eigenvalue and describing the global longitudinal shortening effect, satisfies both V1 and V2 Vlasov's hypothesis. For these reasons, it is usually classified as a conventional warping field, associated to the trivial in-plane trial functions $U_k(s) = V_k(s) = 0$ (Gonçalves et al., 2010). All the other $(n - 1)$ warping fields obtained by the WEP are, instead, non-conventional shear trial functions in the proper meaning of the term and describe a pure-shear behavior.

3.2 Novel straightforward dynamic approach for the evaluation of extension trial functions

The original GBT-D procedure (Piccardo et al., 2014a) defines extension planar trial functions as the orthogonal supplement to the conventional subset Q_i calculated in Eq. (3.6). Although this definition is perfectly suited to determine a planar subset of functions able to complete the conventional ones, it sometimes leads to localized displacement fields, as previously discussed. The unconstrained procedure (Taig et al., 2015) allows to overcome this aspect, however resulting conventional and extension fields seems to be slightly imprecise, especially as regards higher functions that sometimes lose their symmetry. This may be due to the fact that eigenvalue problems used to separate conventional and extension trial functions introduce and/or magnify numerical errors that are intrinsic to a discrete (FE-based) procedure such as the cross-section analysis. For this reasons, a new improved approach for the calculation of extension (non-conventional) trial functions within GBT-D is here proposed. Extension trial functions are here defined as those planar deformation fields where plates forming the cross-section depict *pure elongation* in the s direction (i.e., they cannot depict bending within the

cross-section plane and they possess nil warping). Such a behavior can be modeled by requiring the beam elements composing the frame used in the PEP to be *globally undeformable against shear and flexure*, as it will be better clarified in the following. As a result, obtained trial function are *purely-extensional* deformation fields.

Referring to the generic element e in the plane of the cross-section (Fig. 3.2), by interpreting it as a generalized elastic spring (Luongo and Paolone (1997); see Appendix B), its global shear γ_e and bending κ_e deformations can be expressed in local coordinates:

$$\gamma_e = V_2^e - V_1^e - \theta_1^e l_e \quad (3.21a)$$

$$\kappa_e = \theta_2^e - \theta_1^e \quad (3.21b)$$

The M planar unshearability conditions, $\gamma_e = 0$, can be rewritten in global coordinates as:

$$-(U_j - U_i) \sin \alpha_e + (V_j - V_i) \cos \alpha_e - \theta_i l_e = 0 \quad (3.22)$$

whereas the M conditions describing indeformability under flexure, $\kappa_e = 0$, simply become:

$$\theta_j - \theta_i = 0 \quad (3.23)$$

Eqs. (3.22) and (3.23), representative of shear and flexural internal constraints, can be collected in a new linear system (subscript e being referred to *extensible* deformation modes):

$$\mathbf{A}_e \mathbf{q}_p = \mathbf{0} \quad (3.24)$$

where \mathbf{A}_e is a $2M \times N$ matrix. Whereas the M equations described in Eq. (3.22) deriving from unshearability conditions are always linearly independent, only $M - L$ among conditions of indeformability under flexure, depicted in Eq. (3.23), are linearly independent, L being the number of cross-section closed branches. As a consequence, in case of $L > 0$ (i.e., multiply-connected cross-section, that is closed or partially-closed section), \mathbf{A}_e is not a full-rank matrix and must be further reduced. In particular, Eq. (3.24) can be solved with respect to $N_e = N - 2M + L$ master variables \mathbf{q}_{eM} . Details on implementation of a constrained algebraic eigenvalue problem are provided in Appendix C. Based on this technique, a new constrained PEP is obtained:

$$(\mathbf{K}_e - \lambda_e \mathbf{M}_e) \mathbf{q}_{eM} = \mathbf{0} \quad (3.25)$$

where:

$$\mathbf{K}_e = \mathbf{R}_e^T \mathbf{K}_p \mathbf{R}_e; \quad \mathbf{M}_e = \mathbf{R}_e^T \mathbf{M}_p \mathbf{R}_e \quad (3.26a,b)$$

are $N_e \times N_e$ reduced-order stiffness and mass matrices, respectively, and \mathbf{R}_e is a $N \times N_e$ constraint matrix (see Appendix C). The problem still admits the triple eigenvalue $\lambda_e = 0$, to which the usual three rigid-body planar motions are associated. The latter can be disregarded indeed since they are already included in the subset of conventional planar functions. Therefore, Eq. (3.25) actually provides only $N_e - 3$ new linearly independent eigenvectors corresponding to non-zero distinct eigenvalues. They can be collected in the $N \times (N_e - 3)$ matrix $\mathbf{Q}_e = [\mathbf{q}_{e4}, \mathbf{q}_{e5}, \dots, \mathbf{q}_{eN_e}]$. This set of planar orthogonal (linearly independent) eigenvectors \mathbf{Q}_e spans a $(N_e - 3)$ -dimensional subspace of the original N -dimensional one. Corresponding non-conventional, planar, extension trial functions $U_k^e(s)$, $V_k^e(s)$ ($k = 1, 2, \dots, N_e - 3$) are

determined based on the adopted interpolating polynomial functions, to be associated to null warping components, $W_k^e(s) = 0^1$.

Extension trial functions obtained with the new proposed procedure are shown for the illustrative example in Fig. 3.9; they are in number $N_e - 3 = 8$. Pure elongations of cross-section elements, together with rigid-body motions (that do not make global elastic shear and flexural work) are present. These latter arise from the dynamic nature of the equilibrium imposed by Eq. (3.25), that includes inertial terms. Because of the symmetry of the cross-section, a rigid rotation is involved to restore the dynamic equilibrium when the diagonal branches of the closed triangular cell admit skew-symmetric U displacements, whereas rigid motion does not occur for symmetric extensions. Moreover, the single elements of the closed triangular cell can not be deformed individually. Since a closed cell is an internally hyperstatic system, an axial deformation of a unique element would cause flexure of all the other elements: this behavior may not occur because of the constraints prescribing indeformability under flexure, Eq. (3.23). Extension trial functions obtained from this new procedure are naturally global in type, without the need for any further operation.

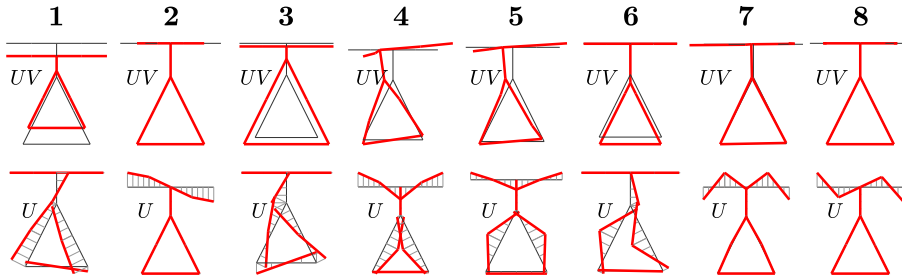


Figure 3.9: Illustrative example of dynamic cross-section analysis: non-conventional extension (planar) trial functions obtained with the proposed GBT-D approach.

Conventional and non-conventional (i.e. extension) planar trial functions form a basis of $N_i + N_e - 3 = 2N - 3(M + 1) + L$ eigenvectors. It is easy to prove that this basis is not sufficient to span a N -dimensional space in case of multiply-connected cross-section. As a matter of fact, since the number M of cross-section elements can be expressed as $M = n - 1 + L$, conventional and non-conventional planar fields are in number of $(N - 2L)$ on the whole. Therefore, they are able to span a N -dimensional space if and only if $L = 0$, i.e. the TWM cross-section is made of open branches. In case of closed or partially-closed cross-section there should exist further $2L$ trial functions able to complete the previous two subsets. In these cases, it is clear that the problem governing in-plane extension of elements is hyperstatic and, thus, profile elements may exhibit flexural deformation involving frame elasticity. Then, purely-extensible functions are no longer sufficient to describe all the extensional deformation fields that the cross-section may experience. Additional mixed extensional-flexural functions may occur, referred to as *hybrid* fields. They are necessarily non-conventional since they involve extension, in violation of the

¹The assumption $W_k^e(s) = 0$ violates in principle the V2 hypothesis; therefore, extension trial functions are not associate to pure in-plane axial membrane elongations ε_s^m , but they induce also non-nil membrane shear strains γ_{sz}^m . This fact could be avoided by introducing the V2 hypothesis of membrane unsharability, thus providing a warping supplement $W_k^e(s) \neq 0$ to be associated to in-plane trial functions, similarly to as done for conventional fields. This case, however, has not been analyzed in the present Thesis.

Vlasov's V1 hypothesis.

Hybrid trial functions are defined as those deformation fields able to make null mutual (elastic) work with others planar (conventional and purely-extension) functions. Referring to the generic element e (Fig. 3.2) interpreted as a generalized elastic spring by its global axial, shear and flexural deformations ε_e , γ_e , κ_e , defined by Eqs. (3.4), (3.22) and (3.23), the elastic potential energy \mathcal{U} of the planar frame representative of the TWM cross-section can be expressed as:

$$\mathcal{U} = \frac{1}{2} \sum_{e=1}^M (C_e^a \varepsilon_e^2 + C_e^s \gamma_e^2 + C_e^f \kappa_e^2 - \gamma_e \kappa_e C_e^s l_e) \quad (3.27)$$

where C_e^a , C_e^s , C_e^f are the axial, shear and flexure stiffness of the element e , respectively. Details about these expressions are provided in Luongo and Paolone (1997) and in Appendix B. Based on the GBT displacement field, Eq. (2.2), the energy \mathcal{U} , Eq. (3.27), can be rewritten in the following form:

$$\mathcal{U} = \frac{1}{2} \sum_{h=1}^K \sum_{k=1}^K \mathcal{U}_{hk} \quad (3.28)$$

\mathcal{U}_{hk} being the mutual elastic work, defined as:

$$\mathcal{U}_{hk} = \sum_{e=1}^M \left[C_e^a \varepsilon_{eh} \varepsilon_{ek} + C_e^s \gamma_{eh} \gamma_{ek} + C_e^f \kappa_{eh} \kappa_{ek} - C_e^s \frac{l_e}{2} (\gamma_{eh} \kappa_{ek} + \kappa_{eh} \gamma_{ek}) \right] \quad (3.29)$$

where ε_{ej} , γ_{ej} , κ_{ej} are the global deformations of the generic element e expressed by the j -th GBT-D trial function. Eq. (3.29) can be suitably simplified by accounting the fact that conventional planar fields have null axial deformation by definition (i.e., $\varepsilon_{ej} = 0$). By denoting with the subscript h the generic h -th hybrid field and with subscript j the generic j -th conventional planar field, the constraint condition of null mutual hybrid-conventional work is:

$$\mathcal{U}_{hj} = \sum_{e=1}^M \left[C_e^s \gamma_{eh} \gamma_{ej} + C_e^f \kappa_{eh} \kappa_{ej} - C_e^s \frac{l_e}{2} (\gamma_{eh} \kappa_{ej} + \kappa_{eh} \gamma_{ej}) \right] = 0 \quad (3.30)$$

with $j = 4, \dots, N_i$, since the rigid-body motions involve null deformations. In a similar fashion, the following constraint condition of null mutual hybrid-extensional work can be obtained by denoting with the subscript k the generic k -th planar extension trial function and remembering that these latter can only exhibit elongation by definition (i.e., $\gamma_{ek} = \kappa_{ek} = 0$):

$$\mathcal{U}_{hk} = \sum_{e=1}^M C_e^a \varepsilon_{eh} \varepsilon_{ek} = 0 \quad (3.31)$$

with $k = 1, \dots, N_e - 3$. Eqs. (3.30) and (3.31) constitute a linear system of $(N_i + N_e - 6)$ linearly independent equations that can be expressed in matrix form through the global coordinates as (subscript h being referred to hybrid trial functions):

$$\mathbf{A}_h \mathbf{q}_p = \mathbf{0} \quad (3.32)$$

where \mathbf{A}_h is a $(N_i + N_e - 6) \times N$ matrix.

In alternative, a completely equivalent and even more direct procedure for the determination of the matrix \mathbf{A}_h consists in imposing the same orthogonality conditions in terms of displacements. By collecting nodal values of both conventional (except for rigid-body motions) and non-conventional trial functions in the $N \times (N_i + N_e - 6)$ matrix $\mathbf{Q}_h = [\mathbf{q}_{i4}, \mathbf{q}_{i5}, \dots, \mathbf{q}_{iN_i}, \mathbf{q}_{e4}, \mathbf{q}_{e5}, \dots, \mathbf{q}_{e(N_e-3)}]$, the orthogonality condition in terms of displacements between the h -th hybrid function and the k -th conventional or extensional field becomes:

$$\mathbf{f}_k^T \mathbf{q}_h = 0 \quad k = 1, 2, \dots, N_i + N_e - 6 \quad (3.33)$$

where \mathbf{f}_k is the N -vector of the nodal forces induced by the general conventional or extensional k -th displacement field, given by $\mathbf{f}_k = \mathbf{K}_p \mathbf{q}_k$. Eq. (3.33) provide a linear system of $N_i + N_e - 6$ linearly independent equations, that can be rewritten in the form (3.32) by assuming $\mathbf{A}_h = \mathbf{Q}_h^T \mathbf{K}_p$.

The system (3.32) can be solved with respect to $N_h = N - (N_i + N_e - 6) = 2L + 3$ master variables \mathbf{q}_{hM} ; the implementation of the constrained algebraic eigenvalue problem is exactly equivalent to the previous problems (see Appendix C). Through this classic technique, the following constrained PEP is obtained:

$$(\mathbf{K}_h - \lambda_h \mathbf{M}_h) \mathbf{q}_{hM} = 0 \quad (3.34)$$

where:

$$\mathbf{K}_h = \mathbf{R}_h^T \mathbf{K}_p \mathbf{R}_h; \quad \mathbf{M}_h = \mathbf{R}_h^T \mathbf{M}_p \mathbf{R}_h \quad (3.35a,b)$$

are $N_h \times N_h$ reduced-order stiffness and mass matrices, respectively, and \mathbf{R}_h is a $N \times N_h$ constraint matrix (see Appendix C). Since the frame is always unconstrained and \mathbf{R}_h is a full-rank matrix, the problem still admits the triple nil eigenvalue $\lambda_h = 0$, whose associated eigenvectors describe rigid-body planar displacements of the cross-section. Since they are already included in the conventional subset of trial functions, only $N_h - 3$ eigensolutions are acceptable, leading to $2L$ eigenvectors spanning a $2L$ -dimensional subspace of the original N -dimensional one. Hybrid (non-conventional) trial function $U_k^h(s)$, $V_k^h(s)$ ($k = 1, 2, \dots, 2L$) are determined based on the adopted interpolating polynomial functions and associated to null warping components, $W_k^h(s) = 0$. It is worth to be noted that, differently to what happens to conventional, extension and shear trial functions whose number is directly related to the number of nodes adopted in discretizing the cross-section, the number of hybrid fields is independent from the adopted discretization, being related only to the cross-section geometry, in particular to the number of closed branches possessed.

Hybrid non-conventional functions for the illustrative example are shown in Fig. 3.10, reporting both the in-plane and the tangential displacement (the latter as a diagram). They are, as expected, in number $N_h - 3 = 2L = 2$, and involve mixed flexure-extensional deformations of the closed branches and consistent rigid-body motions of the remaining open branches. As in the previous PEPs, rigid-body motions are present to ensure the dynamic equilibrium to inertial terms. These motions, however, don't affect the energetic orthogonality constraints since they make null elastic work. Also the hybrid trial functions are of global-type naturally, without the need of any further manipulation. A comparison with the results obtained by the classic static approach for the cross-section analysis points out some differences. In particular, the first hybrid field in Fig. 3.10 looks much better compared to the corresponding static one (see mode

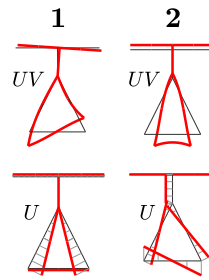


Figure 3.10: Illustrative example of dynamic cross-section analysis: non-conventional hybrid (planar) trial functions obtained with the proposed GBT-D approach.

25, Figure 12 in Bebiano et al., 2015), which also involves flexure in the vertical open branch, thus not respecting the vertical symmetry axis of the section.

In order to illustrate the capabilities and the versatility of the novel method, three additional illustrative applications are presented. The first two are classic TWM examples: (i) an open cross-section, having lipped channel profile with an intermediate node in the web in addition to natural nodes (Fig. 3.11a); and (ii) a closed cross-section, having rectangular profile and schematized with the natural nodes only (Fig. 3.11b). In the following figures, in-plane conventional fields are shown together with their warping supplement, while both the full in-plane cross-section displacement UV and the sole transverse displacement U , the latter using the y -axis convention, have been reported for extension trial functions. The first three conventional trial functions (corresponding to nil eigenvalues) describes the planar rigid-body motions; the first shear trial function is related to the out-of-plane rigid-body motion (i.e., global longitudinal shortening).

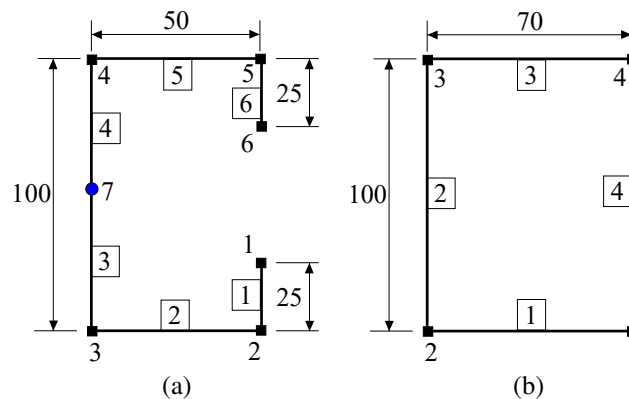


Figure 3.11: Additional examples of dynamic cross-section analysis: (a) lipped channel and (b) boxed cross-sections

Conventional trial functions of the lipped-channel section are shown in Fig. 3.12; non-conventional extension and shear fields are reported in Figs. 3.13a and 3.13b, respectively. Since $n = 7$, $M = 6$ and $L = 0$ (i.e., open cross-section), therefore $N_i = 15$, $N_e = 6$. As expected for an isostatic system, extension fields experience only purely elongations of the plate elements and rigid translations and rotations; no hybrid functions have been obtained and purely extension fields are sufficient to complete, together with conventional ones, the basis de-

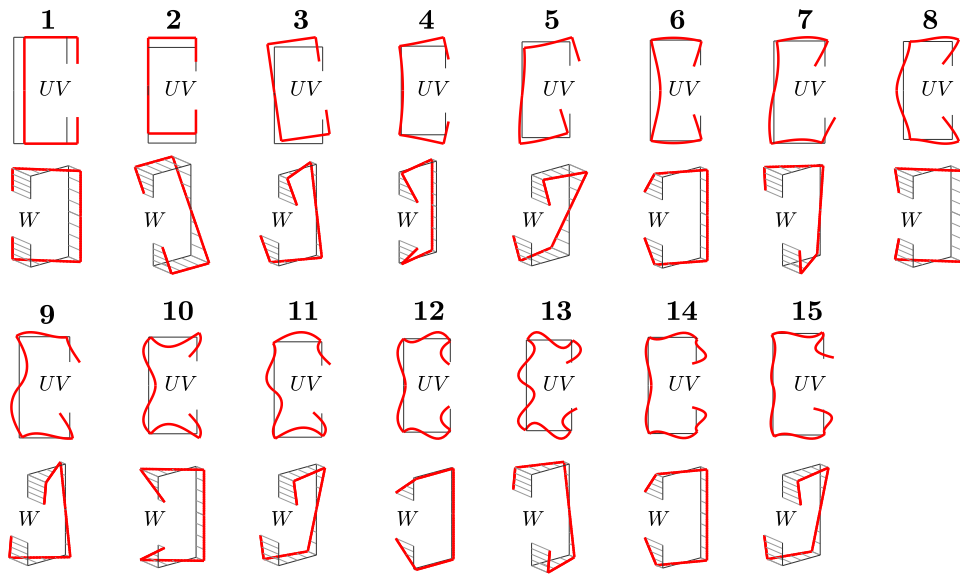
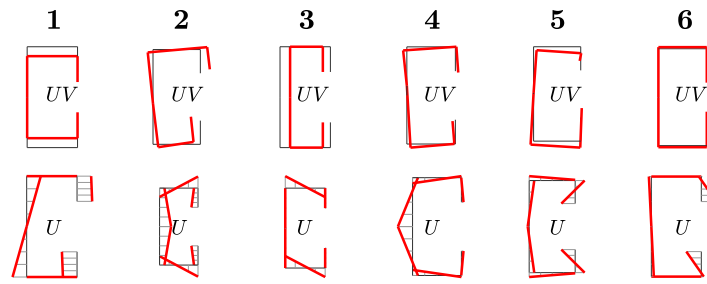


Figure 3.12: Lipped-channel profile: conventional planar and warping trial functions obtained with the proposed GBT-D approach.

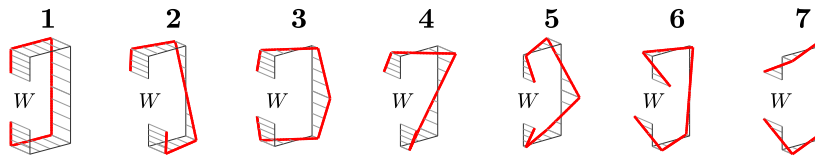
scribing all the possible planar deformations of the TWM cross-section. Concerning extension trial functions, as previously discussed, rigid-body rotations are required to restore the global dynamic equilibrium when the tangential displacements are in phase opposition as regards the symmetry axis of the cross-section. Obtained functions appear very clean, in a natural way from the solution of two constrained PEP and one WEP only.

Concerning the rectangular boxed section, $n = 4$, $M = 4$ and $L = 1$ (i.e., closed cross-section with a unique cell), therefore $N_i = 8$, $N_e = 2$, $N_h = 2$. Conventional trial functions are shown in Fig. 3.14; extension, hybrid and shear fields are reported in Figs. 3.15a to 3.15c, respectively. The hyperstatic nature of this closed boxed section leads to hybrid functions involving both extension and flexure, that appear when pure, in phase opposition elongations of two opposite elements occur. On the contrary, due to the double symmetry of the cross-section, extension trial functions does not involve rigid rotations. All obtained deformation fields are very precise and clean and derive from the simple solution of three constrained PEP and one WEP without further orthogonalization procedures.

The last application concerns the two-cell bridge-deck section depicted in Fig. 3.16. The proposed cross-section combines closed cells with open branches, and represents a summary example on the capabilities of the new method. Conventional trial functions are shown in Fig. 3.17; extension and hybrid functions are detailed in Figs. 3.18a and 3.18b; shear fields are depicted in Fig. 3.19. Since $n = 8$ (i.e., only the natural nodes are taken into account, as in Bebiano et al., 2015), $M = 9$ and $L = 2$ (i.e., closed cross-section with two cells), therefore $N_i = 15$, $N_e = 5$, $N_h = 4$. As in the previous examples, the dynamic approach lead in its simplicity to very precise and clean trial functions. In hybrid trial functions, the symmetry of tangential displacements is fully respected leading to perfect flexure-extension mixed deformations, as it does not seem to be fully respected in an analogous example presented in Bebiano et al. (2015). In fact, subsequent operations of manipulation, such as those required for the static approach, necessarily lead to higher numerical approximations with respect to the



(a)



(b)

Figure 3.13: Lipped channel profile: (a) extension and (b) shear (warping) trial functions obtained with the proposed GBT-D approach.

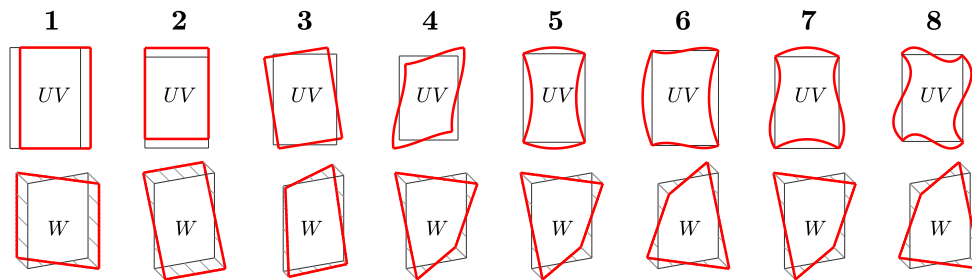
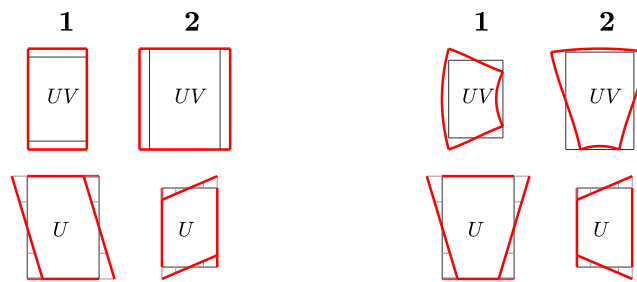
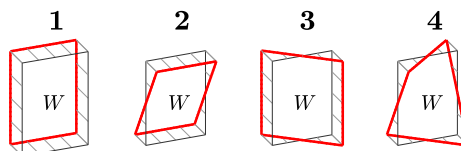


Figure 3.14: Boxed rectangular profile: conventional planar and warping trial functions obtained with the proposed GBT-D approach.



(a)

(b)



(c)

Figure 3.15: Boxed rectangular profile: (a) extension, (b) hybrid and (c) shear (warping) trial functions obtained with the proposed GBT-D approach.

single eigenvalue problem required by the dynamic approach, besides being most costly from an operational point of view.

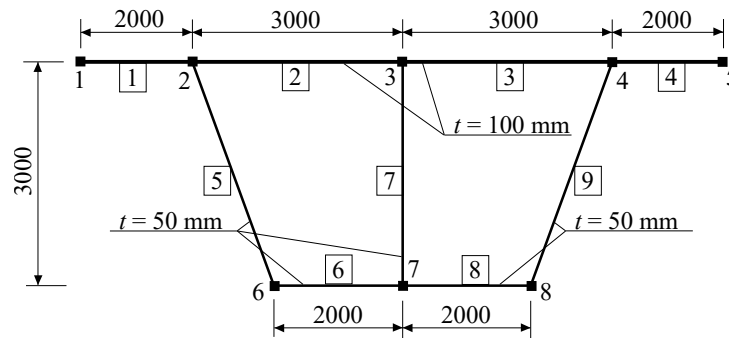


Figure 3.16: Bridge deck cross-section: (a) geometry and (b) discretization.

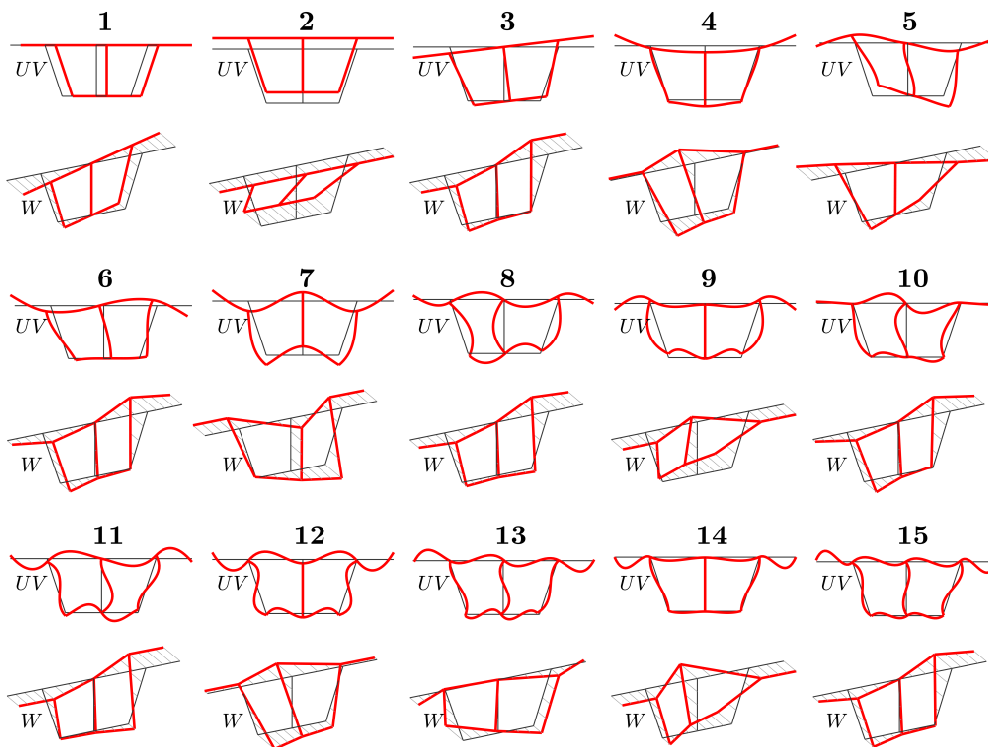


Figure 3.17: Bridge-deck cross section: conventional planar and warping trial functions obtained with the proposed GBT-D approach.

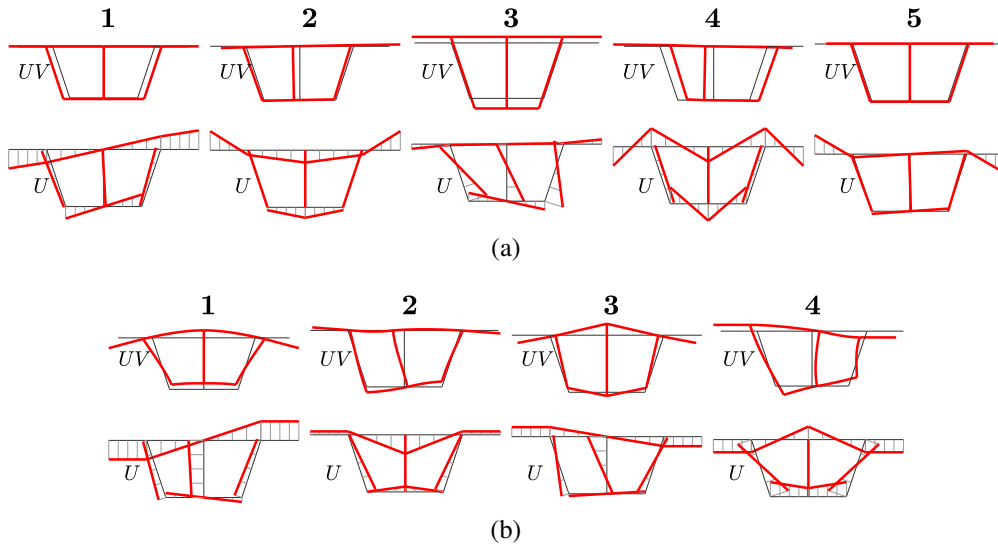


Figure 3.18: Bridge-deck cross section: (a) extension and (b) hybrid trial functions obtained with the proposed GBT-D approach.

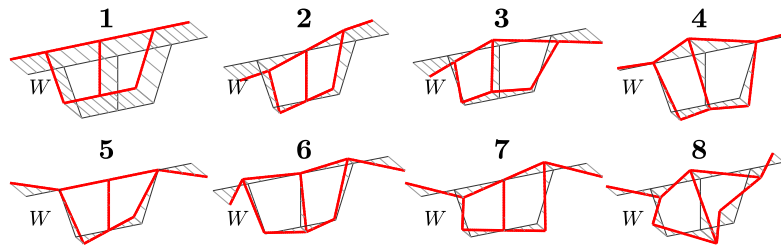


Figure 3.19: Bridge-deck cross section: shear (warping) trial functions obtained with the proposed GBT-D approach.

3.3 Conventional and non-conventional trial functions within the GBT-D approach

The improved GBT-D approach can be summarized in the following four steps leading to linear trial functions to be used within the GBT framework with straightforward mechanical characteristics directly deriving from their dynamic nature:

1. derivation of a subset of $N_i = (3n - M)$ *conventional* trial functions, $U_k^i(s), V_k^i(s), W_k^i(s)$, $k = 1, 2, \dots, N_i$, whose in-plane and out-of-plane components are obtained by a first constrained planar PEP and by the imposition of Vlasov's V2 hypothesis and Bredt's conditions (once planar values are known), respectively, with $M = n - 1 + L$;
2. obtaining a subset of $(N_e - 3) = (3n - 2M + L - 3)$ *extension* trial functions, $U_k^e(s), V_k^e(s)$, $k = 1, 2, \dots, (N_e - 3)$, through a second constrained planar PEP, L being the number of possible cross-section closed branches;
3. in case of multiply-connected (i.e., closed or partially closed) cross-section, determination

of an additional subset of $2L$ hybrid (flexure-extensional) trial functions, $U_k^h(s), V_k^h(s)$, $k = 1, 2, \dots, 2L$, by a supplementary third constrained planar PEP, whose expression can be equivalently obtained in terms of mutual works or displacement fields;

4. derivation of a subset of n shear (or purely warping) trial functions, $W_k^s(s)$, $k = 1, 2, \dots, n$, through a global out-of-plane WEP. The first warping field (i.e., the longitudinal shortening one) is often considered to belong rightfully to the subset of conventional trial functions.

The union of the first three subsets forms a basis that is able to completely span the original $3n$ -dimensional space composed by all planar deformation fields that a TWM cross-section can experience. This basis combined with the subset of the shear fields allows to obtain $4n$ trial functions, that represents the totality of the possible configurations for a discretized cross-section. The last three subsets (extension, hybrid and shear fields) constitutes the set of the non-conventional trial functions (Gonçalves et al., 2010). Often, under the heading of “conventional”, it includes the first shear (rigid) trial functions implying global longitudinal shortening, bringing the number of conventional fields to $(N_i + 1)$. All these results are obtained with only three eigenvalue problems for open sections and four eigenvalue problems for multiply-connected sections, without the need of additional orthogonalization operations.

3.4 On the influence of the polynomial order in the FE-based GBT cross-section analysis

In this Section, the influence of the order of polynomial adopted as interpolating functions in a FE-based GBT cross-section analysis is discussed. The illustrative example shown in Fig. 3.20 is proposed for the seek of clarity. It consists on a steel lipped channel beam having the cross-section shown in Fig. 3.11a. The beam is 2 m long and is assumed to be simply-supported and free to warp at the end supports, while it is restrained from warping at mid-span (Fig. 3.20). Elastic modulus of 200 GPa and Poisson’s ration of 0.3 are specified for the beam. A uniform pressure of 10 kPa is applied to the upper flange, as shown in Fig. 3.20. The simplest choice,

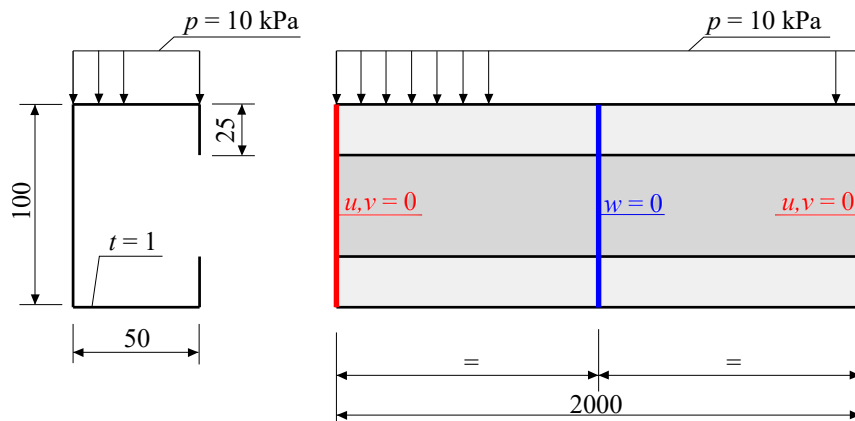


Figure 3.20: Lipped channel member: load arrangement and restraints conditions.

in terms of FEs to be employed in the discrete cross-section analysis, consists in using the 6 DOF FE shown in Fig. 3.2 and the 2 DOF FE in Fig. 3.7 for PEP and WEP, respectively. The choice is denoted in the following as FE_1 and calls for linear Lagrangian, cubic Hermite and linear Lagrangian polynomial shape functions for $U_k(s)$, $V_k(s)$ and $W_k(s)$, respectively. Results obtained for the illustrative example are shown in Fig. 3.21 in terms of displacements and stresses. They have been obtained by using the same cross-section discretization reported in Fig. 3.11a, while the member have been subdivided into 20 GBT-based FEs. All variables have been plotted at the member coordinate in which they reach their maximum values, which occur at mid-span (i.e., $z = \mathcal{L}/2$) for the in-plane displacement uv and transverse and normal membrane and flexural stresses (i.e., σ_s^m , σ_s^f , σ_z^m , σ_z^f), and at the end sections (i.e., $z = 0, \mathcal{L}$) for warping displacement w and shear stress components (i.e., τ_{sz}^m , τ_{sz}^f). For clarity, the plotted variables have been suitably scaled, and scale coefficient is reported for each plot. Results obtained with the GBT approach have been compared with the ones obtained with a shell element model developed in ABAQUS/Standard (Simulia, 2010) for validation purposes. The whole beam is discretized through quadrangular shell elements S4R5 available in the software library and suitable for first-order (linear) analysis, having 5 mm width, altogether 20,000 finite elements.

Comparison between results provided by the GBT approach and the ABAQUS solution shows a very good agreement as regards displacements (i.e., u , v and w) and membrane longitudinal stress σ_z^m , with differences between the two models lesser than the 2% considering the results obtained via ABAQUS for reference in the following. Concerning flexural stresses (i.e., σ_s^f , σ_z^f and τ_{sz}^f), a less accurate agreement can be noticed, especially as regard the loaded plate, where differences between GBT and ABAQUS up to the 20%. This can be attributed to the poor discretization adopted for the cross-section analysis, where no intermediate nodes have been introduced on the loaded element. Different results are obtained when considering the membrane transverse stress σ_s^m and membrane shear stress τ_{sz}^m , where significant discontinuities can be observed between adjacent elements. This fact is a direct consequence of the polynomial order adopted in the cross-section analysis to approximate non-conventional trial functions, whilst conventional functions have limited influence on the considered stresses since they obey the Vlasov hypothesis. More in detail, membrane transverse stress σ_s^m , Eq. (2.6a), depends on $U_k'(s)$, $W_k(s)$, which are described by piece-wise constant and linear polynomial interpolating functions, respectively, while membrane tangential stress τ_{sz}^m , Eq. (2.6c), is described by $U_k(s)$, $W_k'(s)$, interpolated by linear and piece-wise constant functions, respectively. Step-wise variations for $U_k'(s)$ and $W_k'(s)$ are responsible for the discontinuous patterns depicted by the aforementioned stresses.

The simplest way to address the problem consists in enhancing the polynomial order of interpolating functions, by adopting quadratic Lagrange polynomials for non-conventional trial functions $U_k(s)$ and $W_k(s)$, thus obtaining continuous distributions of their first derivative. Corresponding FE to be adopted in the PEP is the 7 DOF element illustrated in Fig. 3.22a, while the WEP calls for the 3 DOF element depicted in Fig. 3.22b. They are referred in the following as FE_2 , while stiffness and mass matrices to be used in the discrete PEP and WEP are reported in Appendix A. Results for the illustrative example obtained by adopting FE_2 are reported in Fig. 3.23. Membrane transverse stress σ_s^m and membrane shear stress τ_{sz}^m match very well with the reference solutions obtained with ABAQUS, with differences within the 5%, and their

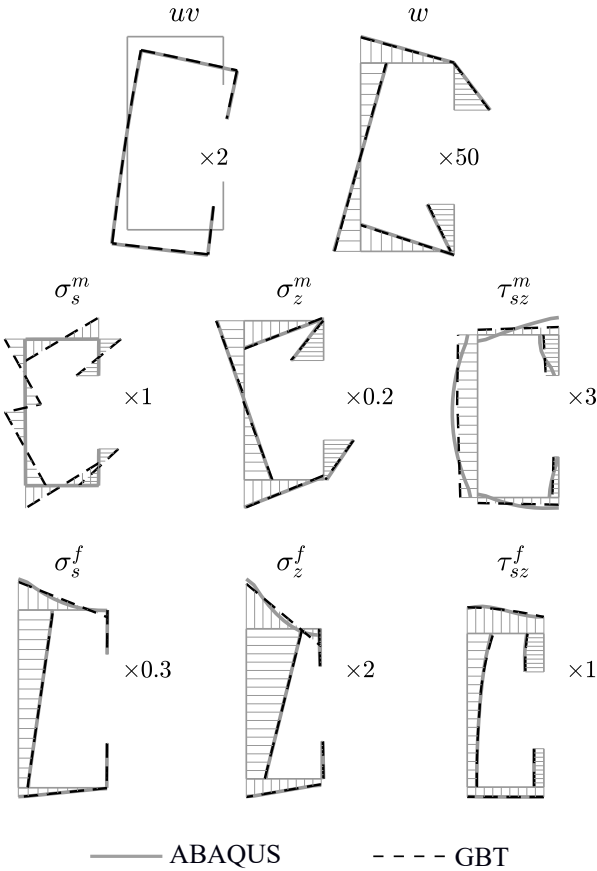


Figure 3.21: Lipped channel member: displacements and stress fields obtained with FE₁.

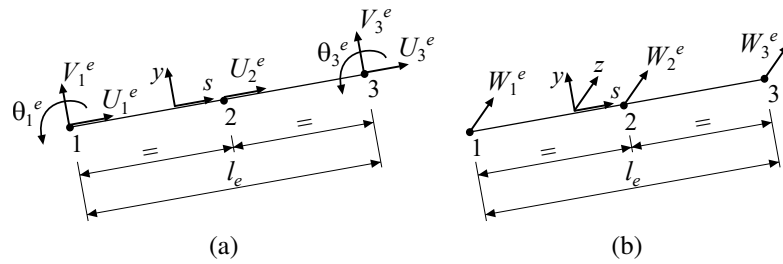


Figure 3.22: FE₂: (a) In-plane seven DOF FE and (b) out-of-plane three DOF FE elements for the cross-section analysis (local coordinates).

patterns are continuous. It has to be noted that the use of FE₂ does not provide any improvement as regard flexural stresses provided by GBT, which still manifest some small differences with respect to the reference solutions. This is due to the polynomial order of interpolating functions for $V_k(s)$ adopted in FE₂, on which flexural stresses are relied to (Eqs. (2.6d) to (2.6f)), which has not been changed. More refined solutions can be obtained by increasing the cross-section discretization or, alternatively, by using more refined FEs as the ones described in Fig. 3.24. They

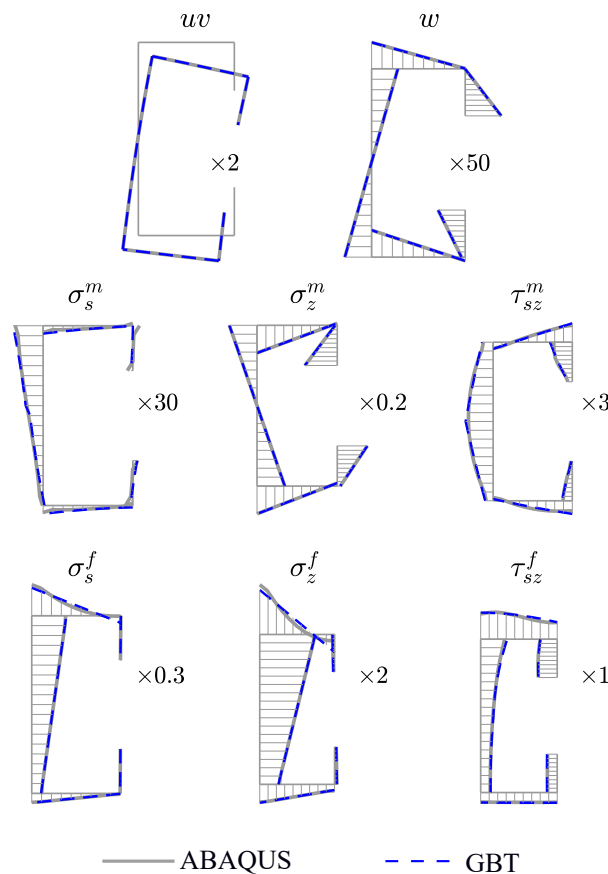


Figure 3.23: Lipped channel member: displacements and stress fields obtained with FE₂.

are referred to in the following as FE₃ and consists on an 11 DOF FE to be used in the PEP and calling for 4th order Lagrangian and 5th order Hermite polynomial interpolating functions

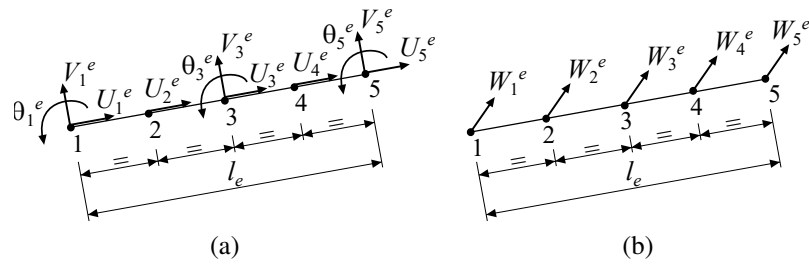


Figure 3.24: FE_3 : (a) In-plane eleven DOF FE and (b) out-of-plane five DOF FE elements for the cross-section analysis (local coordinates).

for $U_k(s)$ and $V_k(s)$, respectively, while a 5 DOF FE is adopted in the WEP calling for 4th order Lagrangian polynomial interpolating functions for $W_k(s)$. Corresponding stiffness and mass matrices to be used in the discrete PEP and WEP are reported in Appendix A. Results for the illustrative example obtained by adopting FE_3 are reported in Fig. 3.25, showing an excellent correspondence between GBT and ABAQUS solutions for all stresses, with maximum differences lesser than 2% .

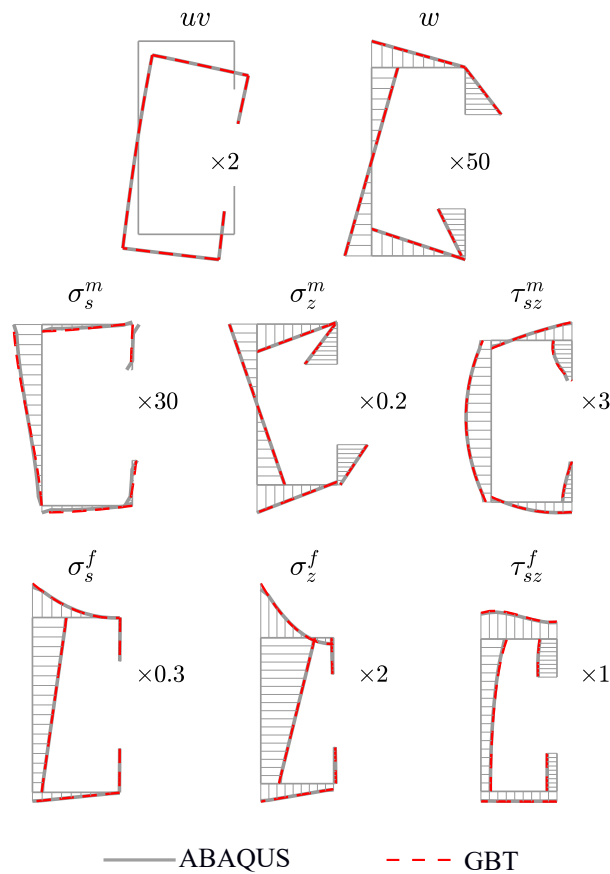


Figure 3.25: Lipped channel member: displacements and stress fields obtained with FE_3 .

Chapter 4

Partial interaction analysis of multi-component TWMs within the GBT framework

Multi-component Thin-Walled Members (TWMs) represent an efficient form of construction increasingly used for both bridge and building applications. Their main advantage relies in their capability to combine the contribution of different components, eventually made of different materials, by means of mechanical devices, commonly shear-deformable connectors, installed at their interface. This leads to high flexibility in assembling the member as well as in a greater structural performance of the multi-component member than the one exhibited by the combined contribution of the structural elements considered in isolation. The behavior of a multi-component member is strongly influenced by the deformability of the interface connections, leading the various elements to depict relative displacements taking place at the interface locations. This kinematic behavior is usually referred as *partial interaction*, and the first model dealing with such a response for two-layered composite members was due to Newmark et al. (1951). The model was based on the coupling of two Euler-Bernoulli beams by means of a shear connection uniformly distributed along the interface and able to deform in the longitudinal direction. Since then, the model has been widely extended in the field of composite constructions, accounting for transverse partial interaction (e.g., Nguyen et al., 2001; Ranzi et al., 2006), material and geometric non-linearities (e.g., Ranzi and Bradford, 2009; Ranzi et al., 2010; Zona and Ranzi, 2011), the use of Timoshenko beam model for one or both components (e.g., Xu and Wang, 2013) and shear lag effects (e.g., Dezi et al., 2001, 2003; Gara et al., 2010).

The first GBT model in the field of composite structures was proposed in Gonçalves and Camotim (2010) for composite steel-concrete members. It was based on the classic static procedure for the cross-section analysis (e.g., Silvestre and Camotim, 2002a; Gonçalves et al., 2010). The proposed model takes into account the partial interaction behavior in the longitudinal direction of the member by introducing appropriate trial functions, in addition to the ones obtained for the whole cross-section assumed as single component, to account for the longitudinal slip. The proposed formulation have been adopted for developing a GBT-based beam nonlinear FE suitable for modeling steel-concrete composite beams in Henriques et al. (2014), limited to material non-linearities, and Henriques et al. (2015) for full material and geometrical nonlinear analysis. Recently, the same model has been extended for the buckling analysis of steel-concrete composite beams in Gonçalves et al. (2016); Henriques et al. (2016). A complete different approach was proposed in Taig and Ranzi (2015) for the partial interaction analysis of composite TWMs accounting for longitudinal partial interaction and recently extended in Taig and Ranzi (2016) to account, for the first time within the GBT approach, for both transverse and longitudinal partial interaction. Proposed models are based on the unconstrained (dynamic) approach for the cross-section analysis (Taig et al., 2015) previously outlined in Section 3.1.1.

In this Chapter, a GBT approach for the longitudinal and transverse partial interaction analysis of multi-component TWMs is developed. The main contribution consists on a dynamic procedure for the GBT cross-section analysis used to determine the set of conventional and

non-conventional (i.e., extension and shear) trial functions. The proposed approach relies on the formulation of two distinct eigenvalue problems describing the free oscillation of a unitary segment of TWM, namely: (i) Planar Eigenvalue Problem (PEP), governing the in-plane motion of the segment, and (ii) Warping Eigenvalue Problem (WEP), governing the out-of-plane (warping) motion of the segment. The partial interaction is included in the analysis by means of shear deformable linear elastic springs placed at the interface between adjacent components and assumed to be uniformly distributed along the member length. While the complete set of shear trial functions can be directly identified from the eigenvectors of the WEP, deformation fields described by the PEP depict a mixed flexure-extension behavior and need to be “separated” into conventional and extension trial functions. To this end, two procedures are developed in the context of the dynamic approach for the cross-section analysis. The first one stems from the unconstrained approach proposed in Taig et al. (2015) and extended in Taig and Ranzi (2016) for the partial interaction analysis of composite steel-concrete beams. The approach relies on three eigenvalue problems involving the in-plane extension and bending stiffness matrices. The unconstrained approach presents the great advantage of providing a complete set of GBT trial functions with a very limited number of analysis. Therefore, it is undeniably more direct and less involved than the static approach, which requires a large number of eigenvalue problems to be performed in addition to as many static analysis as GBT trial functions (e.g., Bebiano et al., 2015). Nevertheless, analogously to as occurs for single-component cross-sections, obtained planar conventional and extension fields seems to be slightly imprecise, with higher functions that sometimes lose their symmetry. Although obtained fields are perfectly suitable for the analysis, a large number of trial functions has to be considered to properly describe the structural behavior, in contrast with the original spirit of GBT as reduction method. The second dynamic procedure for the cross-section analysis of multi-component TWMs is based on the novel GBT-D procedure outlined in Section 3.2, which has been shown to provide very precise and clean trial functions by adopting a simple straightforward and not recursive procedure. The full set of in-plane (conventional and non-conventional) trial functions is obtained through a very limited number of PEPs (from two to three). In particular, a first PEP is solved, where members composing the cross-section are forced to be inextensible, according to the Vlasov hypothesis V1, thus leading to the set of planar conventional functions. A second PEP is then formulated, where members are assumed to be unshearable and unflexurable (i.e., they can only show purely in-plane elongations) in order to obtain a subset of planar, non-conventional, purely extension fields. Finally, a third PEP is presented in case of multi-connected (i.e. closed or partially closed) TWM cross-sections, supplying the set of hybrid trial functions (i.e., mixed in-plane flexure-extension fields). The Chapter is organized as follows: a brief overview on the GBT framework for the partial interaction analysis of multi-component TWMs is presented in Section 4.1. The new dynamic procedures for the cross-section analysis are then presented in Section 4.2, where an illustrative example of multi-component TWM taken from the Literature (Georgieva et al., 2012) is presented in order to highlight the differences, in terms of obtained trial functions, between the two proposals. Finally, the proposed GBT approach is validated using the numerical results determined with a refined finite element model developed in ABAQUS/Standard (Simulia, 2010) as reference. To this end, the linear elastic analysis of two real multi-component TWMs taken from the Literature (Hanaor, 2000; Georgieva et al., 2012) are presented.

4.1 Basis of the GBT approach for the partial interaction analysis of multi-component TWMs

A prismatic multi-component TWM is considered as assembly of N_m components having arbitrary open, closed or partially-closed cross-section. Each component is assumed as a set of flat plates connected along edges and free to bend in their own plane. The triad $\{\mathbf{e}_s, \mathbf{e}_y, \mathbf{e}_z\}$ is identified for any arbitrary point $P(s, z)$ lying on the mid-surface \mathcal{S}_α of the α -th component ($\alpha = 1, \dots, N_m$) composing the TWM (i.e., at $y = 0$) (Fig. 4.1), being \mathbf{e}_z the versor parallel to the beam axis z , \mathbf{e}_s the versor tangent to the curvilinear abscissa s lying along the mid-line of the transverse profile \mathcal{C}_α and $\mathbf{e}_y = \mathbf{e}_z \times \mathbf{e}_s$ defined accordingly to the right-hand rule. The displacement field can thus be expressed as:

$$\mathbf{u}(s, z) = u(s, z)\mathbf{e}_s + v(s, z)\mathbf{e}_y + w(s, z)\mathbf{e}_z \quad (4.1)$$

where $u(s, z)$, $v(s, z)$ and $w(s, z)$ are the relevant displacement components in the direction identified by the corresponding versors (Fig. 4.1). Within the GBT formulation and according to the Kantorovich semi-variational approach, a linear Galerkin approach is used to express the displacement field in Eq. (4.1) by means of *linear trial functions* $U_k(s), V_k(s)$ and $W_k(s)$ affected by *linear coordinates* $\varphi_k(z)$, as described in Eq. (2.2). The Kirchhoff plate model is adopted to evaluate the displacement field $\mathbf{d}(s, y, z) = d_s(s, y, z)\mathbf{e}_s + d_y(s, y, z)\mathbf{e}_y + d_z(s, y, z)\mathbf{e}_z$ in an arbitrary point located within the plate thickness (e.g., Piccardo et al., 2014a). The infinitesimal strains $\boldsymbol{\varepsilon}(s, y, z)$ are calculated by distinguishing membrane strains components, related to the mid-surfaces \mathcal{S}_α , from the flexural components (Eq. (2.4)). Corresponding membrane and flexural stress collected in vector fields $\boldsymbol{\sigma}(s, y, z)$ are then calculated adopting a linear elastic constitutive law (Eq. (2.6)).

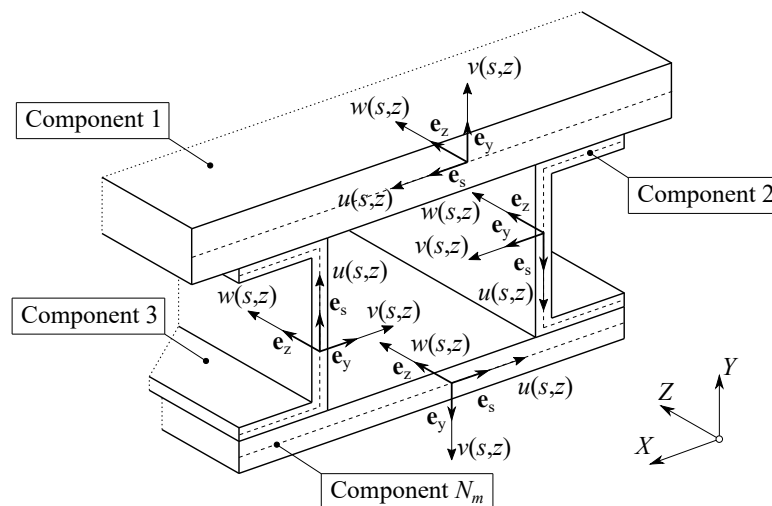


Figure 4.1: Multi-component TWM: displacement field.

The interaction between adjacent members composing the cross-section is introduced by placing N_{sc} connectors along rectilinear lines Λ_n ($n = 1, \dots, N_{sc}$) at the interface location (Taig and Ranzi, 2016, Fig. 4.2a). They are assumed to prevent separation between connected

elements, while relative displacement (i.e., slips) in longitudinal (i.e., along z) and transverse directions (i.e., along s) are permitted. For the n -th connector, linking the i -th and the j -th components of the cross-section, longitudinal slip $\delta_L^n(z)$ and transverse slips $\delta_T^n(z)$ (Fig. 4.2b) can be expressed as function of GBT trial functions as follows (Taig and Ranzi, 2016):

$$\delta_T^n(z) = \sum_{k=1}^K \bar{V}_k^n \varphi_k(z) \quad (4.2a)$$

$$\delta_L^n(z) = \sum_{k=1}^K \bar{W}_k^n \varphi_{k,z}(z) \quad (4.2b)$$

where \bar{V}_k^n is the transverse slip induced by the k -th planar trial functions, while \bar{W}_k^n is the longitudinal slips induced by the k -th warping field, respectively. They can be expressed as (Taig and Ranzi, 2016):

$$\bar{V}_k^n = [U_k(s_n^j) - y_n^j V_{k,s}(s_n^j)] - [U_k(s_n^i) - y_n^i V_{k,s}(s_n^i)] \quad (4.3a)$$

$$\bar{W}_k^n = [W_k(s_n^j) - y_n^j V_k(s_n^j)] - [W_k(s_n^i) - y_n^i V_k(s_n^i)] \quad (4.3b)$$

being s_n^j (s_n^i) the location of the n -th connector on the cross-section mid-line \mathcal{C}_j (\mathcal{C}_i) of the j -th (i -th) component, y_n^j (y_n^i) the perpendicular distance of the extreme fiber of the j -th (i -th) component from the mid-surface \mathcal{S}_j (\mathcal{S}_i) (Fig. 4.2c). The partial interaction behavior is considered by placing linear elastic springs uniformly distributed along Λ_n . A linear elastic uncoupled constitutive law is adopted to express the composite action, in particular:

$$f_T^n(z) = k_T^n \sum_{k=1}^K \bar{V}_k^n \varphi_k(z) \quad (4.4a)$$

$$f_L^n(z) = k_L^n \sum_{k=1}^K \bar{W}_k^n \varphi_{k,z}(z) \quad (4.4b)$$

being f_L^n and f_T^n the longitudinal and transverse forces shear per unit length, respectively, induced in the spring, while k_L^n and k_T^n are the longitudinal and transverse shear connection rigidities, respectively.

The weak formulation of the elasticity problem can be derived through the Principle of Virtual Works. This can be expressed, including the work done by the (longitudinal and transverse) shear forces along interfaces between components and assuming external forces to be constant (or averaged) over the plate thickness, as (Piccardo et al., 2014b; Taig and Ranzi, 2016):

$$\sum_{\alpha=1}^{N_m} \left\{ \int_{\mathcal{V}_\alpha} \boldsymbol{\varepsilon}^T \mathbf{E}_\alpha \delta \boldsymbol{\varepsilon} d\mathcal{V} - \int_{\mathcal{S}_\alpha} \mathbf{f}^T \delta \mathbf{u} dS - \int_{\mathcal{C}_\alpha} \sum_B \mathbf{F}_B^T \delta \mathbf{u}_B ds \right\} + \sum_{n=1}^{N_{sc}} \int_{\Lambda_n} \mathbf{f}_n \delta \boldsymbol{\delta}_n^T dz = 0 \quad (4.5)$$

where \mathcal{V}_α and \mathbf{E}_α are the volume and the elastic tensor, respectively, of the α -th component of the multi-component TWM, $\mathbf{f}(s, z)$ and $\mathbf{F}_B(s)$ are forces per unit area acting on the middle surfaces \mathcal{S}_α and forces per unit length applied on the mid-lines \mathcal{C}_α of the end cross-sections,

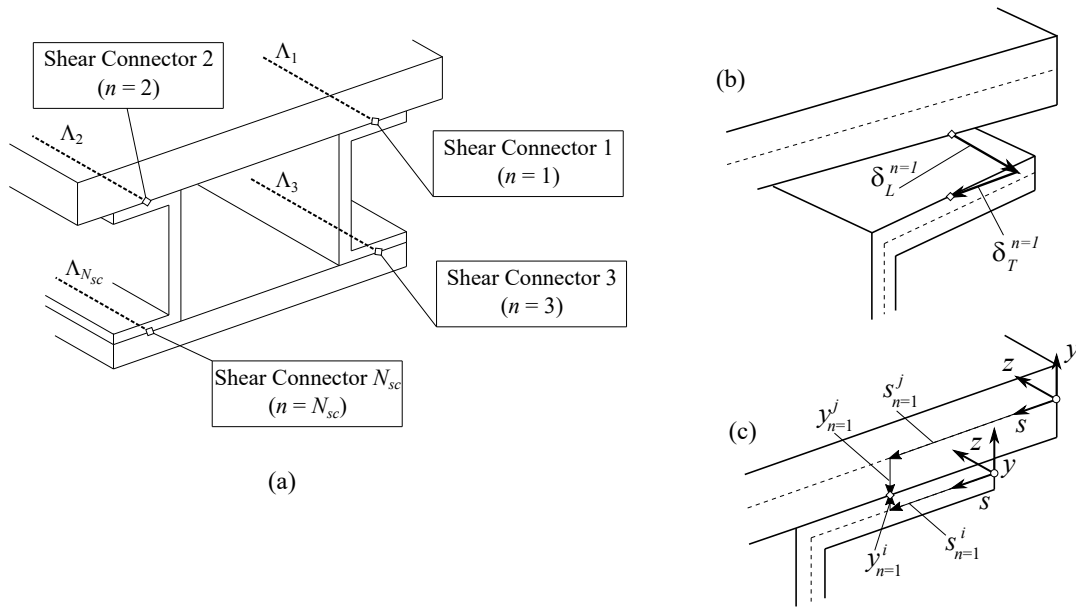


Figure 4.2: Multi-component TWM: interface connection details. (a) Cross-section with shear connectors. (b) Longitudinal and transverse slips. (c) Location of shear connectors.

respectively (see Section 2.3), the δ -operator denotes virtual quantities, while δ_n and \mathbf{f}_n are 2×1 vectors collecting slips and shear forces associated to the n -th connector. By making use of Eqs. (2.4), (2.5), (4.2) and (4.4) and performing the standard steps of variational calculus (e.g., Berdichevsky, 2009), the following system of K coupled ordinary differential equations, commonly referred to as *GBT equations*, can be obtained from Eq. (4.5):

$$\mathbf{C}\varphi^{IV} - (\mathbf{D} - \mathbf{F} - \mathbf{F}^T)\varphi'' + \mathbf{B}\varphi - \mathbf{p} = \mathbf{0} \quad (4.6)$$

with corresponding boundary conditions terms to be applied at $z = 0, L$:

$$\delta\varphi^T (\mathbf{C}\varphi'' + \mathbf{F}^T\varphi - \mathbf{P}^W) = \mathbf{0} \quad (4.7a)$$

$$\delta\varphi^T [\mathbf{C}\varphi''' - (\mathbf{D} - \mathbf{F}^T)\varphi' - \mathbf{P}^M] = \mathbf{0} \quad (4.7b)$$

where the vector $\varphi = \{\varphi_1(z), \dots, \varphi_k(z), \dots, \varphi_K(z)\}^T$ collects the K unknown amplitude functions. In Eqs. (4.6) and (4.7), the following positions hold for loading vectors:

$$p_k = \sum_{\alpha=1}^{N_m} \int_{\mathcal{C}_\alpha} [f_s(s, z)U_k(s) + f_y(s, z)V_k(s) - f_{z,z}(s, z)W_k(s)] ds \quad (4.8a)$$

$$P_k^W = \sum_{\alpha=1}^{N_m} \int_{\mathcal{C}_\alpha} \sum_B [F_{Bz}(s)W_k(s)] ds \quad (4.8b)$$

$$P_k^M = \sum_{\alpha=1}^{N_m} \int_{\mathcal{C}_\alpha} \left\{ \sum_B [F_{Bs}(s)U_k(s) + F_{By}(s)V_k(s)] + f_z(s, z)W_k(s) \right\} ds \quad (4.8c)$$

and structural matrices:

$$B_{hk} = B_{hk}^e + B_{hk}^f; \quad B_{hk}^e = \sum_{\alpha=1}^{N_m} \frac{E_\alpha t_\alpha}{1 - \nu_\alpha^2} \int_{\mathcal{C}_\alpha} U_h'(s) U_k'(s) ds + \sum_{n=1}^{N_{sc}} k_T^n \bar{V}_h^n \bar{V}_k^n \quad (4.9a,b)$$

$$B_{hk}^f = \sum_{\alpha=1}^{N_m} \frac{E_\alpha t_\alpha^3}{12(1 - \nu_\alpha^2)} \int_{\mathcal{C}_\alpha} V_h''(s) V_k''(s) ds \quad (4.9c)$$

$$C_{hk} = C_{hk}^a + C_{hk}^f; \quad C_{hk}^a = \sum_{\alpha=1}^{N_m} \frac{E_\alpha t_\alpha}{1 - \nu_\alpha^2} \int_{\mathcal{C}_\alpha} W_h(s) W_k(s) ds \quad (4.9d,e)$$

$$C_{hk}^f = \sum_{\alpha=1}^{N_m} \frac{E_\alpha t_\alpha^3}{12(1 - \nu_\alpha^2)} \int_{\mathcal{C}_\alpha} V_h(s) V_k(s) ds \quad (4.9f)$$

$$D_{hk} = D_{hk}^s + D_{hk}^t; \quad D_{hk}^t = \sum_{\alpha=1}^{N_m} \frac{G_\alpha t_\alpha^3}{3} \int_{\mathcal{C}_\alpha} V_h'(s) V_k'(s) ds \quad (4.9g,h)$$

$$D_{hk}^s = \sum_{\alpha=1}^{N_m} G_\alpha t_\alpha \int_{\mathcal{C}_\alpha} [U_h(s) + W_h'(s)] [U_k(s) + W_k'(s)] ds + \sum_{n=1}^{N_{sc}} k_L^n \bar{W}_h^n \bar{W}_k^n \quad (4.9i)$$

$$F_{hk} = F_{hk}^s + F_{hk}^f; \quad F_{hk}^s = \sum_{\alpha=1}^{N_m} \frac{\nu_\alpha E_\alpha t_\alpha}{1 - \nu_\alpha^2} \int_{\mathcal{C}_\alpha} U_h'(s) W_k(s) ds \quad (4.9j,k)$$

$$F_{hk}^f = \sum_{\alpha=1}^{N_m} \frac{\nu_\alpha E_\alpha t_\alpha^3}{12(1 - \nu_\alpha^2)} \int_{\mathcal{C}_\alpha} V_h''(s) V_k(s) ds \quad (4.9l)$$

where superscripts f , t , e , a and s refer to the flexural, torsional, (transverse) extensional, axial (longitudinal) and shear nature of the underlying energy terms, respectively, the comma denotes differentiation with respect to the following variable, while E_α , G_α , ν_α and t_α are the longitudinal, tangential, Poisson moduli and thickness, respectively, of the α -th component ($\alpha = 1, \dots, N_m$). GBT equations are commonly solved numerically by means of a FE procedure (e.g., Bathe, 2014), as outlined in Section 2.3 and leading to the following representation:

$$\mathbf{K}_E \mathbf{d}_E = \mathbf{q}_E \quad (4.10)$$

where \mathbf{d}_E is a $4K \times 1$ vector collecting the unknown nodal values of linear coordinates $\varphi_k(z)$, while \mathbf{K}_E and \mathbf{q}_E are $4K \times 4K$ stiffness matrix and $4K \times 1$ load vectors, respectively (see Section 2.3).

4.2 GBT-D cross-section analysis for multi-component TWMs

This Section presents the procedure to evaluate the basis of GBT trial functions suitable to describe the behavior of multi-component members. According to the dynamic approach for the GBT cross-section analysis (GBT-D), trial functions are obtained from the dynamic analysis of an infinitesimal segment of multi-component TWM assumed to be free in space (i.e., unconstrained), weightless, with mass proportional to the local thickness. Two independent eigenvalue problems are obtained, referred to as Planar Eigenvalue Problem (PEP), governing the in-plane oscillations of the beam segment, and Warping Eigenvalue Problem (WEP), governing its out-of-plane (i.e., warping) oscillations. Their discrete version, commonly preferred in the Literature, calls for the discretization of the planar frame representative of the TWM cross-section into M finite elements by interposing possible additional nodes between the natural ones (i.e., the corners of the profile). The 7 DOF FE and the 3 DOF FE illustrated in Figs. 3.22a and 3.22b, respectively, are adopted for the PEP and WEP, respectively, in order to avoid locking problems outlined in Section 3.4. Within this arrangement and being n the total number of nodes (both natural and intermediate) adopted for the frame discretization, the PEP is reduced to $N = 3n + M$ DOF, while the WEP possesses $N_s = n + M$ DOF. Following standard steps of the FE procedure (e.g., Ranzi and Gilbert, 2015) and assuming Hermite cubic for the transverse displacement $V(s)$ and Lagrangian parabolic polynomial interpolating functions for the axial displacements $U(s)$ and warping displacement $W(s)$, the (local) planar stiffness and mass matrices \mathbf{K}_p^e and \mathbf{M}_p^e ($e = 1, 2, \dots, M$ and subscript p identifying the *planar* problem) and warping stiffness and mass matrices \mathbf{K}_w^e and \mathbf{M}_w^e ($e = 1, 2, \dots, M$ and subscript w identifying the *warping* problem) are evaluated for each element (see Appendix A). To account for the partial interaction in both (in-plane) transverse and (out-of-plane) longitudinal directions, linear elastic springs with negligible masses are specified at the location of the shear connections to account for their flexibility present between adjacent components. This is carried out in the PEP by using a 6 DOF spring element (Fig. 3.2), whose stiffness matrix \mathbf{K}_p^n ($n = 1, 2, \dots, N_{sc}$) can be expressed, assuming the order $[U_1^e V_1^e \theta_1^e U_2^e V_2^e \theta_2^e]^T$ as regards the element DOF, as follows:

$$\mathbf{K}_p^n = k_T^n \cdot \begin{bmatrix} 0 & 0 & 0 & 0 & 0 & 0 \\ & 1 & 0 & 0 & -1 & 0 \\ & & 0 & 0 & 0 & 0 \\ & & & 0 & 0 & 0 \\ \text{sym} & & & & 1 & 0 \\ & & & & & 0 \end{bmatrix} \quad (4.11)$$

A 2 DOF spring element (Fig. 3.7) is used in the WEP, whose stiffness matrix \mathbf{K}_w^n ($n = 1, 2, \dots, N_{sc}$) is:

$$\mathbf{K}_w^n = k_L^n \cdot \begin{bmatrix} 1 & -1 \\ -1 & 1 \end{bmatrix} \quad (4.12)$$

After assembling the contribution of each (beam and connector) element, the following WEP is obtained:

$$(\mathbf{K}_w - \lambda_w \mathbf{M}_w) \mathbf{q}_w = \mathbf{0} \quad (4.13)$$

where \mathbf{K}_w and \mathbf{M}_w are the $N_s \times N_s$ global (real symmetric) stiffness and mass matrices, respectively. Since the frame is unconstrained (i.e., \mathbf{K}_w is positive semi-definite), the problem admits

the nil eigenvalue $\lambda_w = 0$, whose corresponding eigenvector describes the rigid out-of-plane displacement of the TWM profile (i.e., a *global longitudinal shortening* effect). Corresponding warping (out-of-plane) trial functions, determined based on the adopted interpolating functions, describe pure warping displacement fields and violate the Vlasov unshearability hypothesis V2. Accordingly to Gonçalves et al. (2010), they constitute the set of *non-conventional shear* trial functions $W_k^s(s)$ ($k = 1, 2, \dots, N_s$) and are associated with nil in-plane displacements (i.e., $U_k^s(s) = V_k^s(s) = 0$). Obtained non-conventional shear functions include the partial interaction behavior in the longitudinal direction.

To clarify the procedure, all steps involved in the proposed GBT will be followed by an illustrative example of the built-up cross-section taken from Georgieva et al. (2012) shown in Fig. 4.3a. It is composed by four components (i.e., $N_m = 4$), in particular two “ Σ ” profiles and two lipped channel profiles, whose dimensions are shown in Figs. 4.3b and 4.3c, respectively. Four shear connectors are placed at the interface locations (i.e., $N_{sc} = 4$) to include interactions between adjacent members (Fig. 4.3a). Resulting multi-component cross-section is then multi-connected and possesses one closed loops (i.e., $L = 1$, being L the number of closed branches). For ease of notations, shear connectors rigidities have been considered by means of the dimensionless parameters α_L and α_T , according to as commonly provided in the Literature for two-layered composite beams (e.g., Girhammar and Gopu, 1993). In particular, the case of medium shear connection ($\alpha_L \mathcal{L} = 5$, $\alpha_T \mathcal{L} = 5$, \mathcal{L} being the member length) has been considered to highlight the partial interaction between components. The normalized longitudinal and transverse slips, Eq. (4.3), will be presented for each trial function; they are defined as the ratio between the slip itself and the maximum displacement of the corresponding function, as follows:

$$\tilde{V}_k^n = \frac{|\bar{V}_k^n|}{\max(|U_k^n|, |V_k^n|)}; \quad \tilde{W}_k^n = \frac{|\bar{W}_k^n|}{\max(|W_k^n|)} \quad (4.14a,b)$$

The first 18 shear functions for the illustrative example are shown in Fig. 4.4. The first function,

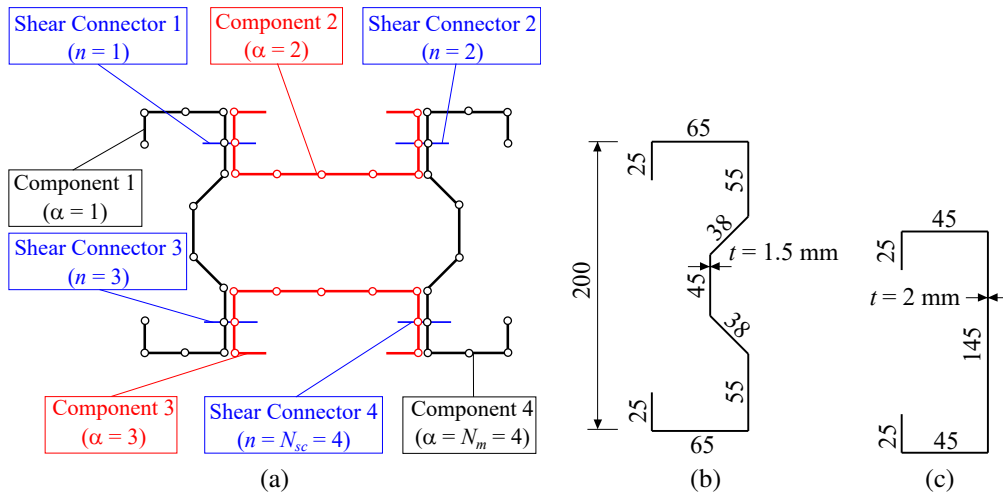


Figure 4.3: Illustrative example of dynamic cross-section analysis of a multi-component cross-section (Georgieva et al., 2012). (a) Built-up box girder cross-section and adopted cross-section discretization, (b) “ Σ ” profile dimensions, (c) lipped Channel profile dimensions.

which corresponds to null eigenvalue and describing the global longitudinal shortening effect,

satisfies both V1 and V2 Vlasov's hypothesis. For these reasons, it is usually classified as a conventional warping field, associated to the trivial in-plane trial functions $U_k(s) = V_k(s) = 0$ (Gonçalves et al., 2010). All the other warping fields obtained by the WEP are, instead, non-conventional shear trial functions in the proper meaning of the term and describe a pure-shear behavior. They describe warping fields where component motions are paired up in twos, with each component alternatively in phase or in opposition with the adjacent ones. Corresponding jumps in the warping functions localized at shear connection locations describe the partial shear interaction behavior in the longitudinal direction. Obtained shear trial functions are naturally global in shape and their warping distributions are in agreement with the cross-section symmetries. Moreover, deformation fields are, as expected, automatically hierarchically ordered.

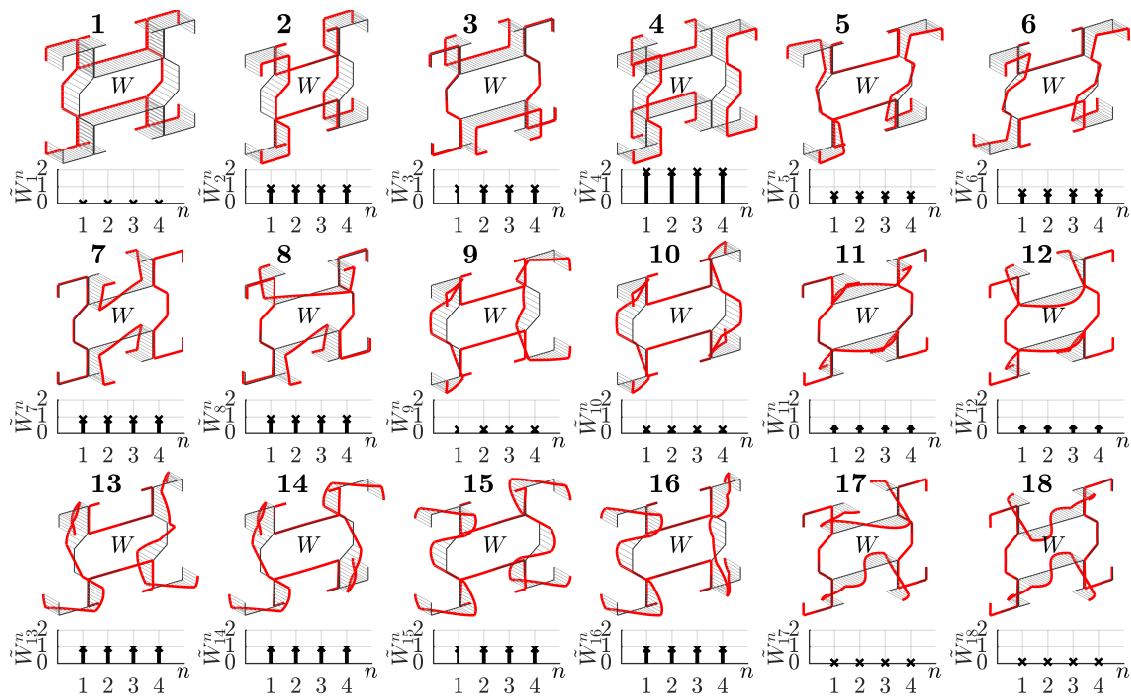


Figure 4.4: Illustrative example of dynamic cross-section analysis of a multi-component cross-section (Georgieva et al., 2012): non-conventional shear (warping) trial functions.

Concerning the planar analysis, the following PEP is obtained after assembling the contribution of each (beam and connector) element:

$$(\mathbf{K}_p - \lambda_p \mathbf{M}_p) \mathbf{q}_p = \mathbf{0} \quad (4.15)$$

where \mathbf{K}_p and \mathbf{M}_p are the $N \times N$ global stiffness and mass matrices obtained by assembling the contribution of each (beam and connector) cross-section element, and \mathbf{q}_p is a N -vector collecting nodal displacements. However, separation or penetration between adjacent components at their interface has to be prevented by enforcing an internal axial restraint to the 6 DOF link elements representing the shear connection (Fig. 3.2), therefore ensuring that the element remains inextensible along its length. In local coordinates, this can be written for the n -th link element

by requiring its global elongation to be zero:

$$\varepsilon_n = U_2^n - U_1^n = 0 \quad (4.16)$$

A further internal constraint prescribing indeformability under flexure is applied to each link element, to satisfy the in-plane rotations' compatibility. This can be written in local coordinates as:

$$\kappa_n = \theta_2^n - \theta_1^n = 0 \quad (4.17)$$

The N_{sc} inextensibility constraints, $\varepsilon_n = 0$, can be rewritten in global coordinates as:

$$(U_j - U_i) \cos \alpha_n + (V_j - V_i) \sin \alpha_n = 0 \quad (4.18)$$

whereas the N_{sc} conditions describing indeformability under flexure, $\kappa_n = 0$, simply become:

$$\theta_j - \theta_i = 0 \quad (4.19)$$

Eqs. (4.18) and (4.19) can be collected in a linear system:

$$\mathbf{A}_{sc} \mathbf{q}_p = \mathbf{0} \quad (4.20)$$

By applying the procedure illustrated in Appendix C and widely employed in the previous Chapter, Eq. (4.20) can be solved in terms of $N_p = N - 2N_{sc}$ master variables \mathbf{q}_{scM} , thus leading to the following (constrained) PEP:

$$(\mathbf{K}_{sc} - \lambda_{sc} \mathbf{M}_{sc}) \mathbf{q}_{scM} = \mathbf{0} \quad (4.21)$$

where:

$$\mathbf{K}_{sc} = \mathbf{R}_{sc}^T \mathbf{K}_p \mathbf{R}_{sc}; \quad \mathbf{M}_{sc} = \mathbf{R}_{sc}^T \mathbf{M}_p \mathbf{R}_{sc} \quad (4.22a,b)$$

are $N_p \times N_p$ reduced-order stiffness and mass matrices, respectively, and \mathbf{R}_{sc} is a $N \times N_p$ constraint matrix (see Appendix C). Eigenvectors $\mathbf{q}_{scMk} = \mathbf{R}_{sc} \mathbf{q}_{scMk}$ ($k = 1, \dots, N_p$) constitutes a complete set that spans the whole space of the admissible in-plane configuration of the system. Corresponding trial functions describe mixed flexure-extensional deformation fields and include the partial interaction behavior in the transverse direction. Consistently to as commonly done in the GBT framework (e.g., Gonçalves et al., 2010) and to facilitate the physical interpretation of the problem, the whole configuration space is subdivided into conventional and extension subspaces. Two procedures are presented to this end. The first one stems for the unconstrained approach proposed in Taig et al. (2015) and recently extended in Taig and Ranzi (2015, 2016) for the partial interaction analysis of composite steel-concrete beams. The second proposal is based on the novel GBT-D procedure outlined in Section 3.2. For clarity, the two procedures will be outlined separately in the following.

4.2.1 Conventional and extensional trial functions for multi-component members: an unconstrained approach

A first set of planar trial function is evaluated, in terms of nodal values, by solving the PEP outlined in Eq. (4.21), thus obtaining mixed flexure-extensional deformation fields. Their

nodal values are collected in the $N \times N_p$ matrix $\mathbf{Q}_{sc} = [\mathbf{q}_{sc1}, \mathbf{q}_{sc2}, \dots, \mathbf{q}_{scN_p}]$. Similarly to as illustrated in Section 3.1.1, subsets of conventional and extension fields are obtained by performing a change of basis to the original set after removing the three rigid-body deformation fields, i.e. $\mathbf{Q}_{sc}^* = [\mathbf{q}_{sc4}, \mathbf{q}_{sc5}, \dots, \mathbf{q}_{scN_p}]$, by solving the following eigenproblem:

$$(\mathbf{B}^e - \mu \mathbf{B}^f) \mathbf{u} = \mathbf{0} \quad (4.23)$$

where μ and \mathbf{u} depict an eigenpair, while matrices \mathbf{B}^e and \mathbf{B}^f are defined in Eq. (4.9) and account for the axial and flexural deformation, respectively, of plate elements composing the cross-section. The influence of the connection deformability in the transverse direction is accounted in the analysis. Due to the use of the 7 DOF planar FE (Fig. 3.22a), Eq. (4.23) admits $N_c = N_p - 2M - 3$ zero eigenvalues that are related to planar inextensible fields (i.e., the subset of conventional functions without the three describing rigid-body motions), while the remaining $N_e = 2M$ non-zero eigenvalues identify planar deformation fields involving transverse extension (i.e., the subset of extension functions). By collecting the eigenvectors \mathbf{u}_j corresponding to zero eigenvalues ($j = 1, 2, \dots, N_c$) in the transformation matrix $\mathbf{T}_c^* = [\mathbf{u}_1, \mathbf{u}_2, \dots, \mathbf{u}_{N_c}]$ and the remaining ones \mathbf{u}_k corresponding to non-zero eigenvalues ($k = N_c + 1, \dots, N_p - 3$) in the transformation matrix $\mathbf{T}_e^* = [\mathbf{u}_{N_c+1}, \dots, \mathbf{u}_k, \dots, \mathbf{u}_{N_p-3}]$, conventional and extension subsets can be separated through the following linear transformations:

$$\begin{bmatrix} \mathbf{Q}_c^{*\text{T}} \\ \mathbf{Q}_e^{*\text{T}} \end{bmatrix} = \begin{bmatrix} \mathbf{T}_c^{*\text{T}} \\ \mathbf{T}_e^{*\text{T}} \end{bmatrix} \mathbf{Q}_p^{*\text{T}} \quad (4.24)$$

where \mathbf{Q}_c^* and \mathbf{Q}_e^* are $N \times N_c$ and $N \times N_e$ matrices, respectively, whose columns identify eigenvectors describing planar inextensible and extensible, respectively, configurations. Although corresponding trial functions could already be used in the member analysis, a further post-processing is performed to ensure that all identified fields reflect the response of the entire cross-section, rather than just displacements of localized parts of it. This is achieved by performing two further change of basis defined in Eqs. (3.16) to (3.18). The subset of conventional planar trial functions must be finally completed by adding the three rigid-body motions removed at the beginning of the procedure.

Conventional planar trial functions can be conveniently supplemented by warping distributions $W_k^i(s)$ satisfying the Vlasov's unshearability (V2) condition on open branches of \mathcal{C} and the Bredt's condition on closed cells, as outlined in Section 3.1.1. A key step in the definition of the warping profiles of the conventional modes is the inclusion of the longitudinal slip at the locations of the shear connections. For those belonging to open branches, the unshearability condition (V2) can be enforced by requiring link elements to depict nil longitudinal slip, i.e. $\bar{W}_k^n = 0$. Since, due to the Vlasov's hypothesis and regardless from interpolating functions adopted in the PEP, trial functions $U_k^i(s)$ and $W_k^i(s)$ are piece-wise constant and piece-wise linear functions, respectively, longitudinal slips \bar{W}_k^n can be conveniently rewritten as:

$$\bar{W}_k^n = W_{2k}^n - W_{1k}^n + h_n U_k^n \quad (4.25)$$

where W_{1k}^n and W_{2k}^n depict the values of warping distribution associated to the k -th trial function at the first node (i.e., $s = 0$) and end node (i.e., $s = h_n$), respectively, of the n -th connector

possessing length h_n , while U_k^n is the value of function $U_k(s)$ on the n -th connector. The zero shear strain (V1) condition for can thus be rewritten as:

$$W_{2k} - W_{1k} + h_n U_k^n = 0 \quad (4.26)$$

Regarding connectors belonging to closed branches, the Bredt's condition can be enforced by relating the longitudinal distributed shear force $f_{kL}^n = k_L^n \bar{W}_k^n$ acting on the n -th connection induced by the k -th trial function to the unknown tangential stress flow Q_k^l acting of the l -th closed loop, as follows:

$$k_L^n (W_{2k} - W_{1k} + h_n U_k^n) = \sum_{l=1}^L (\pm) Q_k^l \quad (4.27)$$

where a positive (negative) sign is used in the summation for Q_k^l in the right-hand side of Eq. (4.27) when the direction identified by the local coordinate s and the one consequent to an arbitrary positive rotation assigned to the l -th loop coincide (differ). The remaining arbitrary unknown describing the uniform (longitudinal) extension of the member can be determined by requiring that the average k -th warping function is zero, thus making the warping orthogonal to the extension, i.e.:

$$\sum_{\alpha=1}^{N_m} \int_{C_\alpha} W_k^i(s) ds = \sum_{e=1}^M \frac{l_e}{2} (W_{1k}^e + W_{2k}^e) + \sum_{n=1}^{N_{sc}} \frac{h_n}{2} (W_{1k}^n + W_{2k}^n) = 0 \quad (4.28)$$

The first 15 conventional trial function for the illustrative example are shown in Fig. 4.5. First three functions are associated to nil eigenvalues of Eq. (4.21) and describe in-plane rigid-body motions. They do not depict transverse slips at shear connectors locations. Following conventional fields depict pure in-plane flexural behavior with no axial elongations of plates composing the cross-section, according to Vlasov's hypothesis V1. Slips in the transverse direction may occur at shear connection locations, describing the partial interaction behavior in the transverse direction. Analogously, conventional warping complements may include longitudinal slips at shear connection locations. Conventional warping fields describe, in conjunction with corresponding in-plane distribution, displacement configurations that possess nil membrane shear strain (or constant shear stress flow) along the beam axis, according to the Vlasov's hypothesis V2 (Bredt's condition). In this sense, longitudinal slips occurring at shear connection location participate in restoring the beam unsharability. The first 15 non-conventional extension trial function for the illustrative example are shown in Fig. 4.6, where both the full in-plane cross-section displacement UV and the sole transverse displacement U have been reported, the latter using the y -axis convention. They contribute in describing the partial shear interaction thanks to slips depicted at shear connection locations.

Analogously to what occurs for single-component cross-section, the unconstrained approach leads to slightly imprecise fields, where symmetry properties possessed by the cross-section seems to be lost, especially in higher functions. In case of multi-component TWMs, this phenomenon appears particularly evident as regards extension fields. Referring to as depicted in Fig. 4.6, it is evident that all obtained displacement fields violate the cross-section double-symmetry. The same can be concluded as regards transverse slips, resulting non symmetric

in both conventional and extension planar trial functions. This phenomenon might be due to the fact that the subsequent operations of manipulation required to separate conventional fields from extension ones lead to higher numerical approximations with respect to a single eigenvalue problem procedure such as the one adopted in the GBT-D procedure introduced in Section 3.2. Obtained set of functions can still be adopted in the analysis, however, as already pointed out in previous Sections, they would reduce the numerical efficiency of the GBT approach, since the entire set of trial functions must be employed in the analysis to obtain accurate results.

4.2.2 Enhanced GBT-D approach to evaluate conventional and extension trial functions for multi-component members

The proposed approach for the cross-section analysis is based on the GBT-D approach introduced in Section 3.2. Planar conventional and non-conventional (i.e., extension and, in case of multi-connected cross-section, hybrid) trial functions are evaluated by means of three constrained PEP where suitable sets of internal constrained equations expressed in the form $\mathbf{A}\mathbf{q}_p = \mathbf{0}$ are introduced in the unconstrained PEP described in Eq. (4.15). Based on the procedure outlined in Appendix C and widely used in previous Sections, the following constrained problem can be obtained by solving the system of internal constraints in terms of a reduced number of master variables \mathbf{q}_{pM} :

$$(\mathbf{K}_p^* - \lambda_p^* \mathbf{M}_p^*) \mathbf{q}_{pM} = \mathbf{0} \quad (4.29)$$

where:

$$\mathbf{K}_p^* = \mathbf{R}^T \mathbf{K}_p \mathbf{R}; \quad \mathbf{M}_p^* = \mathbf{R}^T \mathbf{M}_p \mathbf{R}_c \quad (4.30a,b)$$

are reduced-order stiffness and mass matrices, respectively, and \mathbf{R} is a constraint matrix (see Appendix C).

Conventional trial functions are defined as the in-plane and warping displacement fields obeying the Vlasov's hypothesis of (V1) in-plane inextensibility, and (V2) out-of-plane un-shearability, the latter substituted by the Bredt's condition of constant shear stress flow on closed branches. According to as proposed in Ranzi and Luongo (2011), their in-plane component can be obtained by introducing suitable internal constraints requiring each element axial deformation to vanish. Referring to the 7 DOF beam FE (Fig. 3.22a), this condition can be expressed in local coordinates as:

$$U_3^e - U_2^e = 0; \quad U_2^e - U_1^e = 0 \quad e = 1, \dots, M \quad (4.31a,b)$$

The inextensibility conditions can be enforced on each link element (Fig. 3.2a) as:

$$U_2^n - U_1^n = 0 \quad n = 1, \dots, N_{sc} \quad (4.32)$$

Further internal constraints prescribing indeformability under flexure are applied to each link element, to satisfy the in-plane rotations' compatibility (e.g., Taig and Ranzi, 2016). They can be written in local coordinates as:

$$\theta_2^n - \theta_1^n = 0 \quad n = 1, \dots, N_{sc} \quad (4.33)$$

Eqs. (4.31) to (4.33) constitute the full set of internal constraints for obtaining conventional planar trial functions. They can be written in compact form as $\mathbf{A}_i \mathbf{q}_p = \mathbf{0}$, where \mathbf{A}_i is a $2(M + N_{sc}) \times N$ full-rank matrix (subscript i being referred to *inextensible* trial functions). It can be solved with respect to $N_i = N_p - 2M$ master variables \mathbf{q}_{iM} . Corresponding constrained PEP (Eq. (3.6)) provides N_i independent eigenvectors $\mathbf{q}_{ik} = \mathbf{R}_i \mathbf{q}_{iMk}$ ($k = 1, \dots, N_i$), being \mathbf{R}_i a $N \times N_i$ constraint matrix (see Appendix C). They can be collected in the $N \times N_i$ matrix $\mathbf{Q}_i = [\mathbf{q}_{i1}, \mathbf{q}_{i2}, \dots, \mathbf{q}_{iN_i}]$. From them the conventional (inextensional) planar trial functions $U_k^i(s)$, $V_k^i(s)$ ($k = 1, 2, \dots, N_i$) are determined, based on the adopted interpolating functions. Corresponding (piece-wise linear) conventional warping distributions $W_k^i(s)$, $k = 1, \dots, N_i$, can be obtained based on the procedure outlined in previous Sections. The first 15 conventional functions for the illustrative example are depicted in Fig. 4.7. As for single component cross-sections, first three fields describe rigid in-plane rigid-body motions and they are associated to nil eigenvalues of Eq. (4.29). They do not depict transverse slips at shear connector locations. Following conventional functions depict pure in-plane flexural behavior with no axial elongations of plates composing the cross-section. Slips in the transverse direction may occur at shear connection locations, thus including the partial shear interaction in the transverse direction. Transverse slips are not visible in trial functions proposed in Fig. 4.7 since they occur on higher functions. The first one involving significant transverse slips is the 29th trial function, depicting $\tilde{V}_{29}^n \cong 0.11$ at all shear connections (i.e., $n = 1, \dots, 4$). Obtained conventional fields are very clean and naturally global in shape. Moreover, according to the cross-section symmetry, they are always symmetric (or anti-symmetric) with respect to the vertical and horizontal barycentric directions. Longitudinal slips may occur at shear connection location, participating in restoring the beam unshearability condition. As expected, conventional warping distributions are linear.

Extension trial functions are defined as those deformation fields where the plate elements composing the TWM cross-section are supposed to be in-plane globally unshearable and undeformable under flexure. The latter conditions can be expressed in local coordinates, for the seven DOF FE adopted in the discrete planar analysis (Fig. 3.22a), as:

$$V_3^e - V_1^e - \theta_1^e l_e = 0 \quad e = 1, \dots, M \quad (4.34a)$$

$$\theta_3^e - \theta_1^e = 0 \quad e = 1, \dots, M \quad (4.34b)$$

while the same conditions can be enforced on each 6 DOF link element (Fig. 3.2a), as: }

$$V_2^n - V_1^n - \theta_1^n h_n = 0 \quad n = 1, \dots, N_{sc} \quad (4.35a)$$

$$\theta_2^n - \theta_1^n = 0 \quad n = 1, \dots, N_{sc} \quad (4.35b)$$

Additional internal constraints must be applied on each link element prescribing its axial deformation to vanish (i.e., in-plane inextensibility, Eq. (4.32)), to prevent interpenetration between adjacent components. The $2M + 3N_{sc}$ internal constraints identified by Eqs. (4.32), (4.34) and (4.35) constitute the full set of internal constraints to be enforced in the PEP for obtaining extension planar trial functions. They can be written in compact form as $\mathbf{A}_e \mathbf{q}_p = \mathbf{0}$, where \mathbf{A}_e is a $(2M + 3N_{sc}) \times N$ matrix (subscript e being referred to *extension* trial functions). Analogously to what happens for single-component cross-sections, only $(M + N_{sc} - L)$ among unflexural conditions, Eqs. (4.34b) and (4.35b), are linearly independent, L being the number of cross-section closed branches. As a consequence, in case of $L > 0$ (i.e., multiply-connected cross-section),

\mathbf{A}_e is not a full-rank matrix and it must be further reduced. In particular, the set of internal constraints can be solved with respect to $N_e = N_p - 2M - N_{sc} + L$ master variables \mathbf{q}_{eM} . Corresponding constrained PEP (Eq. (3.25)) provides N_e independent eigenvectors $\mathbf{q}_{ek} = \mathbf{R}_e \mathbf{q}_{eMk}$ ($k = 1, \dots, N_e$), being \mathbf{R}_e a $N \times N_e$ constraint matrix (see Appendix C). They include the three rigid-body motions corresponding to the triple multiplicity nil eigenvalue of the constrained PEP, which have to be disregarded. Relevant eigenvectors can be collected in the $N \times (N_e - 3)$ matrix $\mathbf{Q}_e = [\mathbf{q}_{e4}, \mathbf{q}_{e5}, \dots, \mathbf{q}_{eN_e}]$. From them, extension planar trial functions $U_k^e(s), V_k^e(s)$ ($k = 1, 2, \dots, N_e - 3$) are determined, based on the adopted interpolating functions, and associated to null warping components, $W_k^e(s) = 0$. Extension trial functions obtained with the new proposed procedure are shown for the illustrative example in Fig. 4.8. Analogously to single-component cross-sections, obtained fields depict pure elongations of cross-section elements, together with rigid-body motions. Because of internal constraints, each single element belonging on closed cell can not be deformed individually, since it would cause bending of all other elements belonging to the same loop. It is noteworthy the fact that, within extension trial functions, link elements modeling shear deformable connectors are prevented to deform within the cross-section plane. As a matter of facts, they are asked to be (i) axially undeformable, (ii) in-plane unsharable, and (iii) in-plane unflexurable. While the assumption (i) serves the purpose to prevent separation between adjacent components, conditions (ii) and (iii) are a direct consequence of the kinematic assumptions used in defining extension fields within the GBT-D approach. As a consequence and differently to what happened in the unconstrained approach, shear connectors act as a perfectly in-plane rigid connection. Therefore, obtained (pure) extension fields do not include the transverse partial interaction. Obtained fields appear to be very clean and naturally global in shape, and they respect the cross-section double symmetry.

In case of multi-connected cross-section (i.e., $L > 0$), subsets of conventional and extension planar fields are not sufficient to span the entire N_p -dimensional space of admissible planar configurations the multi-component cross-section may describe. As a matter of fact, since the number M of cross-section elements can be expressed as $M = n - 1 - N_{sc} + L$, conventional and non-conventional planar fields are in number of $(N_p - 2L)$ on the whole. Then, in case of closed or partially-closed cross-section there should exist further $2L$ trial functions able to complete the previous two subsets. They are referred to as *hybrid* fields and, analogously to single-component cross-sections, they describe mixed extensional-flexural deformations induced by non-simultaneous elongations of elements belonging to closed loops. Hybrid trial functions are defined as those deformation fields able to make null mutual (elastic) work with others planar (conventional and purely-extension) functions. This condition can be easily enforced in terms of displacements, as provided in Section 3.2, by enforcing:

$$[\mathbf{Q}_i \quad \mathbf{Q}_e]^T \mathbf{K}_p \mathbf{q}_p = \mathbf{0} \quad (4.36)$$

The set of $N_i + N_e - 3$ internal constraints described in Eq. (4.36) must be supplied by the $2N_{sc}$ nil elongation and nil flexural deformation conditions on link elements (Eqs. (4.32) and (4.33), respectively) to restore the in-plane displacement compatibility, i.e. avoiding interpenetration between adjacent components. The full set of constraints to be enforced to obtain hybrid functions can be written in compact form as $\mathbf{A}_h \mathbf{q}_p = \mathbf{0}$, where \mathbf{A}_h is a $(N_p - 2L + 2N_{sc}) \times N$ matrix (subscript h being referred to *hybrid* trial functions). It has to be noted that rigid-body motions do not spend elastic work, since they do not depict any non-rigid deformation. Therefore, \mathbf{A}_h is not a full-rank matrix, and the set of internal constraints can be solved with respect

to $N_h = 2L + 3$ master variables \mathbf{q}_{hM} . Corresponding constrained PEP, Eq. (3.34), provides N_h independent eigenvectors $\mathbf{q}_{hk} = \mathbf{R}_h \mathbf{q}_{hMk}$ ($k = 1, \dots, N_h$), being \mathbf{R}_h a $N \times N_h$ constraint matrix (see Appendix C). They include the three rigid-body motions corresponding to the triple multiplicity nil eigenvalue of the constrained PEP, which have to be disregarded. Relevant eigenvectors can be collected in the $N \times 2L$ matrix $\mathbf{Q}_h = [\mathbf{q}_{h4}, \mathbf{q}_{h5}, \dots, \mathbf{q}_{hN_h}]$. From them, hybrid planar trial functions $U_k^h(s), V_k^h(s)$ ($k = 1, 2, \dots, 2L$) are determined, based on the adopted interpolating functions, and associated to null warping components, $W_k^h(s) = 0$. Hybrid non-conventional functions for the illustrative example are shown in Fig. 4.9, reporting both the in-plane and the tangential displacement (the latter as a diagram). They are, as expected, in number $N_h - 3 = 2L = 2$, and involve mixed flexure-extensional deformations of the closed branches and consistent rigid-body motions of the remaining open branches. As in the previous PEPs, rigid-body motions are present to ensure the dynamic equilibrium to inertial terms. Also the hybrid trial functions are global-type in a natural way, without the need of any further manipulation. Hybrid modes may depict slips in the transverse direction, thus contributing in modeling the transverse partial shear interaction. As regard the illustrative example, however, slips at shear connections are negligible.

4.3 Applications

Two applications are considered in the following to outline the ease of use of the GBT formulation proposed and to validate its accuracy. The first application considers the built-up multi-component box girder presented in Georgieva et al. (2012) and already used as illustrative example in previous Sections (Fig. 4.3). The beam is 3.0 m long and it is subjected to an eccentric pressure distributed along the member (Fig. 4.10). The beam is assumed to be simply supported, with boundary conditions allowing free warping at end supports and restraining warping at mid-span (Fig. 4.10b). The material properties for the steel components are described by an elastic modulus of 200 GPa and a Poisson's ratio of 0.3. Different levels of shear connection rigidities are considered in the following to highlight their influence on the partial interaction behavior of the multi-component member. The former are expressed in term of dimensionless parameters $\alpha_L \mathcal{L}$ and $\alpha_T \mathcal{L}$ (\mathcal{L} being the member length) as regards the interaction in the longitudinal and transverse directions, respectively, as commonly provided in the Literature for two-layered composite beams (e.g., Girhammar and Gopu, 1993). In particular, results are provided in the following for weak shear connection (i.e., $\alpha_L \mathcal{L} = 1, \alpha_T \mathcal{L} = 1$), medium shear connection (i.e., $\alpha_L \mathcal{L} = 5, \alpha_T \mathcal{L} = 5$) and strong shear connection (i.e., $\alpha_L \mathcal{L} = 20, \alpha_T \mathcal{L} = 20$). Results calculated with the proposed GBT approach have been compared with those determined with a shell element model developed in the software ABAQUS/Standard (Simulia, 2010), where the general purpose shell element S4 has been adopted for plate segments. All materials have been modeled as linear-elastic isotropic. The shear connection is implemented through the ABAQUS planar connection type, which is able to allow relative displacement on the selected plane and avoid relative displacement along the direction normal to that plane. In order to describe the continuous interface connection model formulated in the GBT approach, closely-spaced wires spread along the rectilinear lines of the shear connection have been specified. The planar connection type has been assigned to each wire with the constitutive relationship

described by:

$$\begin{bmatrix} f_T \\ f_L \end{bmatrix} = \begin{bmatrix} K_T & 0 \\ 0 & K_L \end{bmatrix} \begin{bmatrix} \Delta u_T \\ \Delta u_L \end{bmatrix} \quad (4.37)$$

where f_T (f_L) are the induced forces in transverse (longitudinal) direction of the member, Δu_T (Δu_L) are the relative displacement of the two connected components at wire's location in the transverse (longitudinal) direction and K_T (K_L) are the associated spring stiffness in the two directions. These latter rigidities are obtained by multiplying the distributed spring stiffness k_T^n (k_L^n) adopted in the GBT model by the wire (longitudinal) spacing. Concerning the adopted member discretization, the GBT model has been subdivided into 30 GBT-based FEs, while quadrilateral elements with almost 5 mm width have been used in ABAQUS, altogether 168,000 finite elements. Comparisons between the GBT and ABAQUS results are presented in Figs. 4.11 to 4.13. The former have been obtained by using the trial functions calculated by adopting the enhanced GBT-D approach described in Section 4.2.2. All variables have been plotted at the member coordinate in which they reach their maximum values, which occur at mid-span (i.e., $z = \mathcal{L}/2$) for the in-plane displacement uv and transverse and normal membrane and flexural stresses (i.e., σ_s^m , σ_s^f , σ_z^m , σ_z^f), and at the end sections (i.e., $z = 0, \mathcal{L}$) for warping displacement w and shear stress components (i.e., τ_{sz}^m , τ_{sz}^f). For clarity, proposed results have been scaled based on their maximum (absolute) value observed along the member length and the adopted scale coefficient is plotted on each graph. Moreover, the response of each component is outlined by using different colors. Excellent match is obtained in these comparisons for all the three levels of shear connection stiffness adopted for the longitudinal and transverse shear connector stiffness. Differences between GBT and ABAQUS solutions are lesser than 4%, having considered the results obtained via ABAQUS for reference. The influence of the partial shear interaction on the overall behavior of the multi-component TWM is noteworthy. As expected, member with lower shear connection rigidities undergoes larger deflections than the member with stiffer interface properties. In case of weak shear connection, the interaction between components is negligible, and the structural response is given by the sum of the contribution of the individual components considered in isolation. As a matter of fact, the structural response for the considered load condition is almost entirely resisted by the loaded “ Σ ” profile, as well depicted by the shape of the warping distribution w and membrane longitudinal stress σ_z^m (Fig. 4.11). For medium shear connection, components forming the cross-section start to interact, as highlighted by warping profile and relevant stress distribution (i.e., σ_z^m). In this case, significant stress levels are induced throughout the cross-section, in particular on the lipped channel adjacent to the loaded profile. Same considerations can be made for the case of strong shear connection rigidities.

The second application consists on the linear elastic analysis of a multi-component member taken from Hanaor (2000), whose geometry is described in Fig. 4.14. It consists of a partially-closed built-up TWM formed by a concrete slab and three thin-walled cold-formed steel elements (i.e., two “Z” profiles and one thin plate element), subjected to an eccentric uniformly distributed pressure of 5 kPa applied to the right-hand third of the beam (Fig. 4.14a). The beam is 5.0 m long, the concrete slab is 50 mm thick, while all steel elements possess thickness of 2 mm. Material properties include an elastic modulus of 200 GPa and 35 GPa for steel and concrete, respectively, and a Poisson' ratio of 0.2 and 0.3 for concrete and steel, respectively. The beam is simply supported, in particular it is assumed in-plane fully restrained and warping free

at $z = 0, \mathcal{L}$, while a global warping restraint is imposed at mid-span. Similarly to the previous application, different levels in terms of shear connectors rigidities have been considered in the following, in order to outline the influence of the partial shear behavior in the multi-component member. In particular, cases of weak ($\alpha_L L = 1, \alpha_T L = 1$), intermediate ($\alpha_L L = 5, \alpha_T L = 5$) and strong ($\alpha_L L = 20, \alpha_T L = 20$) shear connection have been taken into account. The FE GBT model has been obtained by discretizing the member into 30 GBT-based FEs. Concerning the shell-based FE model, steel elements have been subdivided by means of quadrilateral elements having almost 5 mm width, while the ones composing the concrete slab possess 200 mm width. The ABAQUS model possesses about 240,000 shell FEs. The cross-section analysis is performed with the proposed enhanced GBT-D approach (Section 4.2.2), and subsets of the obtained conventional and non-conventional trial functions are shown for illustrative purposes in Figs. 4.15 to 4.18. They have been obtained for the case of weak shear connectors rigidities (i.e., $\alpha_L L = 1, \alpha_T L = 1$). All trial functions are very precise and clean and derive from the simple solution of three constrained PEP and one WEP without further orthogonalizations. Partial shear interaction in the transverse direction is included in conventional in-plane and non-conventional hybrid fields, as depicted by transverse slips occurring at shear connection locations, while in-plane extension include a perfect (i.e., rigid) interaction between components. Longitudinal partial shear interaction is included in both conventional and non-conventional shear warping fields.

Calculated results with the proposed approach are reported in Figs. 4.19a to 4.19c, respectively, in terms of in-plane displacement uv and out-of-plane displacement w , while results in terms of membrane normal longitudinal stress σ_z^m and shear distribution τ_{sz}^m have been plotted in Figs. 4.20a to 4.20c. Plots are referred to the member coordinate in which they reach their maximum values and they have been suitably scaled for clarity, with the scale coefficient reported in each plot. Numerical results obtained with ABAQUS have been plotted to show the accuracy of the proposed model. The agreement of the two solutions is excellent for all shear connection levels, with differences between the GBT and ABAQUS solution within 5%. The influence of shear connection levels can easily be evidenced by the global deformation of the member, which diminishes with increasing the shear connection rigidity (Fig. 4.19). It is also evident that, in case of weak shear connection, components forming the cross-section behaves independently. Considering that the horizontal slab and bottom thin plate possess low flexural (and shear) rigidity in the plane of the cross-section, the structural response is mainly resisted by the relatively stiffer rigidities of the two Z sections. This behavior is well depicted by observing that high stress levels are induced in the Z profiles, e.g. for the membrane stresses σ_z^m and membrane shear stresses τ_{sz}^m , and that the remaining two cross-sectional components (i.e. concrete slab and bottom thin plate) exhibit negligible stresses (Fig. 4.20a). On the contrary, the shape of warping and stress fields for the case of strong shear connection, Figs. 4.19c and 4.20c, indicate that all components forming the cross-section are participating in resisting external loads. The case of intermediate shear connections is collocated between the previous two (Figs. 4.19b and 4.20b).

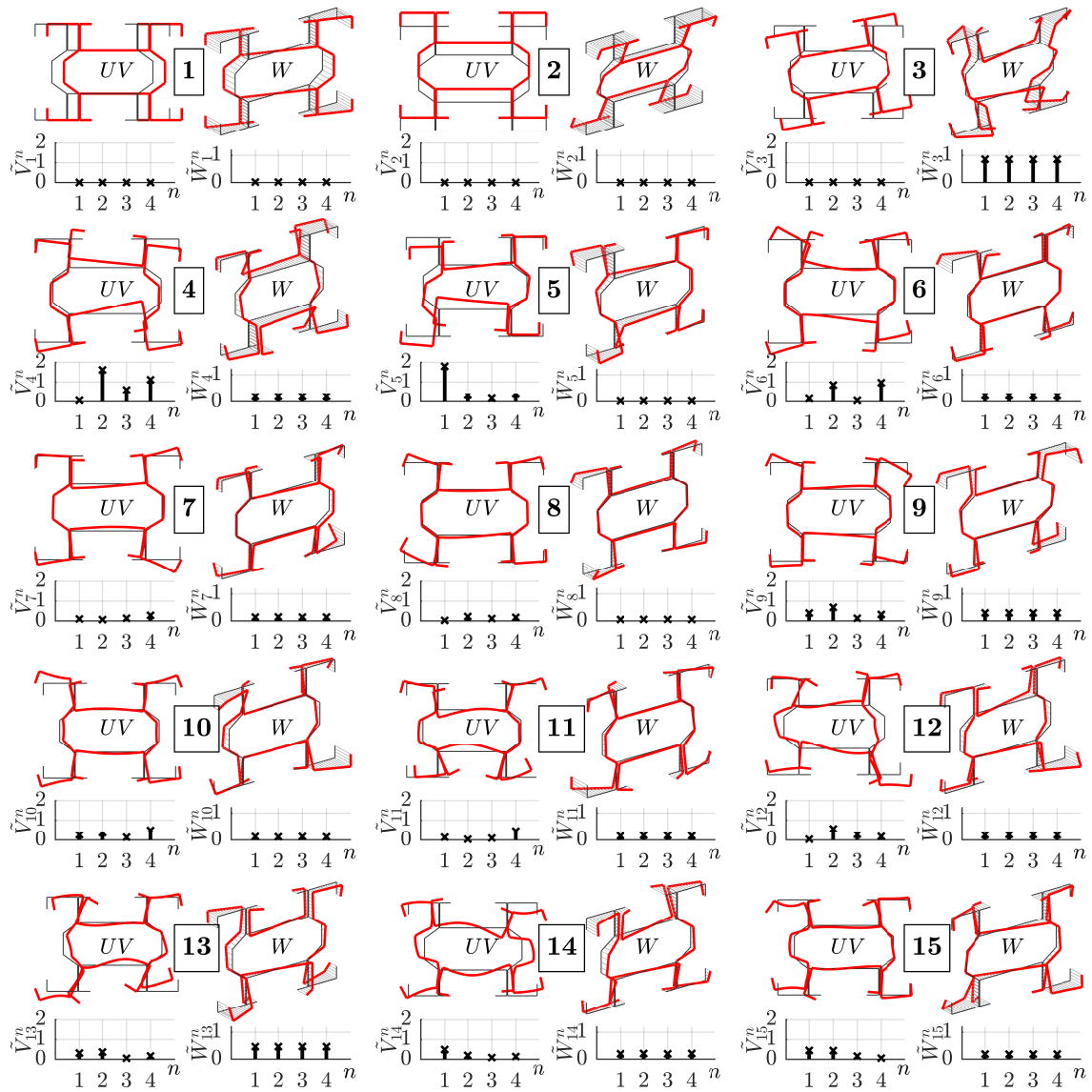


Figure 4.5: Illustrative example of dynamic cross-section analysis of a multi-component cross-section (Georgieva et al., 2012): conventional in-plane and out-of-plane (warping) trial functions obtained with the unconstrained approach.

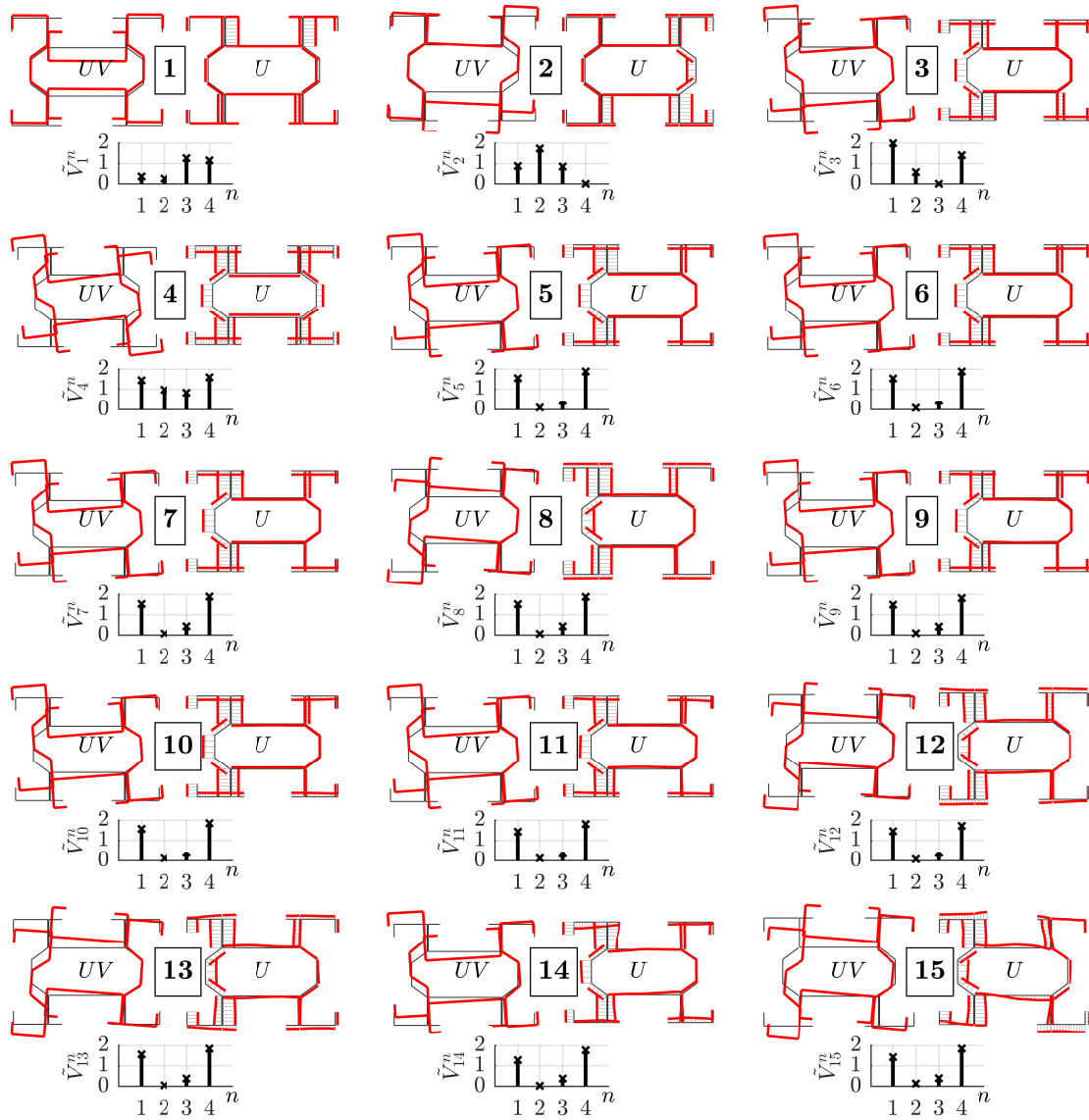


Figure 4.6: Illustrative example of dynamic cross-section analysis of a multi-component cross-section (Georgieva et al., 2012): non-conventional extension trial functions obtained with the unconstrained approach.

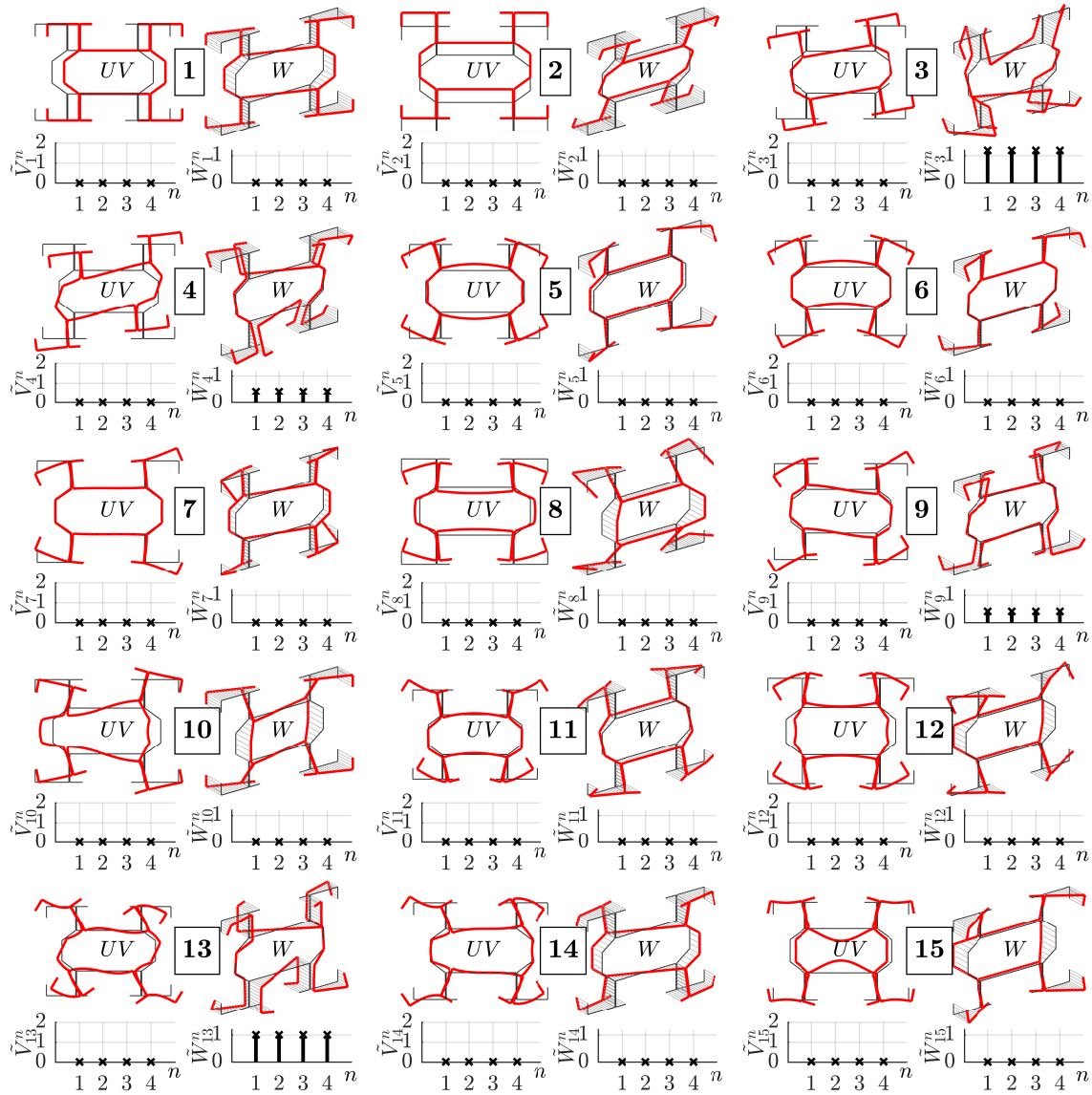


Figure 4.7: Illustrative example of dynamic cross-section analysis of a multi-component cross-section (Georgieva et al., 2012): conventional in-plane and out-of-plane (warping) trial functions obtained with the enhanced GBT-D approach.

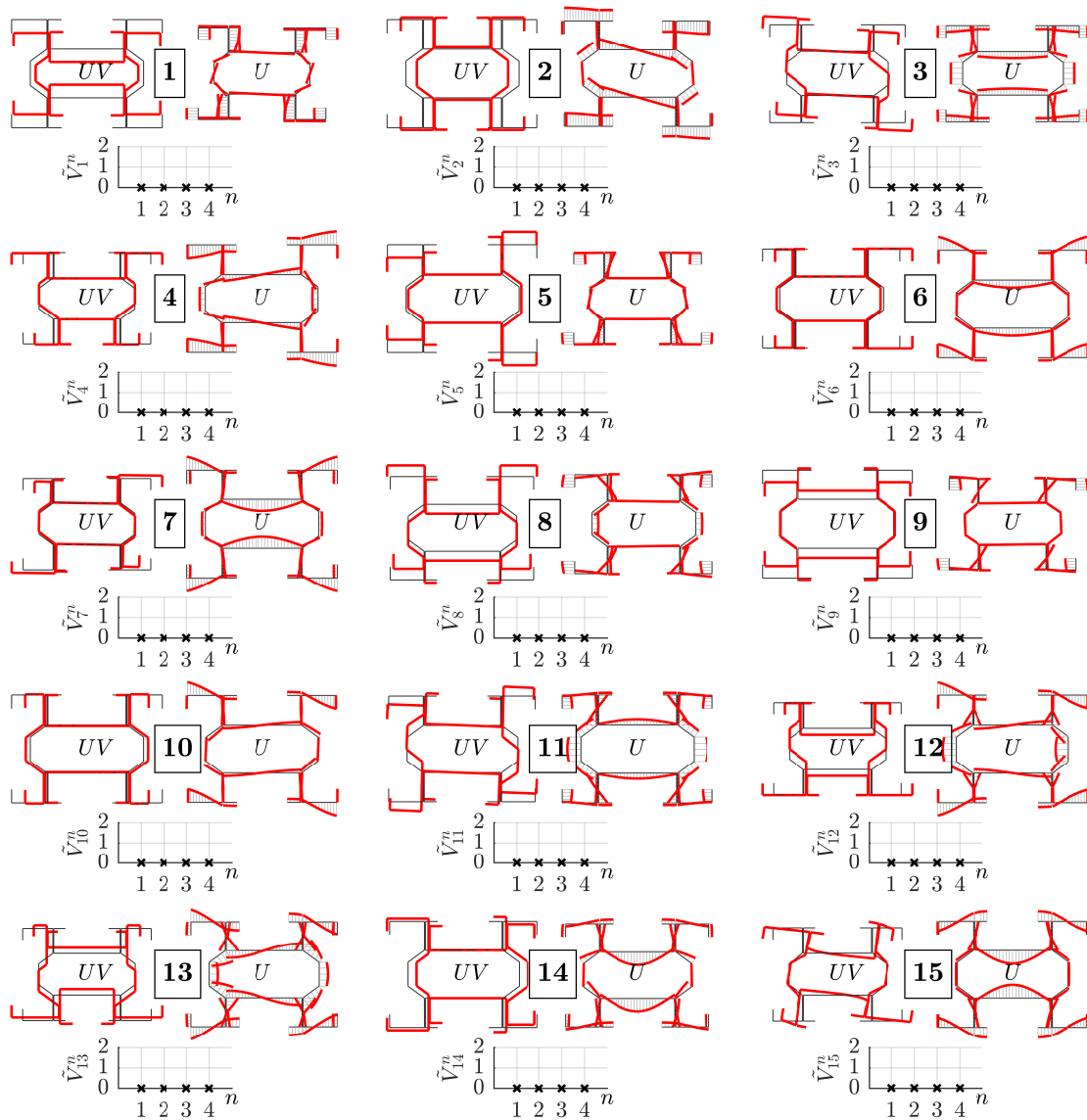


Figure 4.8: Illustrative example of dynamic cross-section analysis of a multi-component cross-section (Georgieva et al., 2012): non-conventional extension trial functions obtained with the enhanced GBT-D approach.

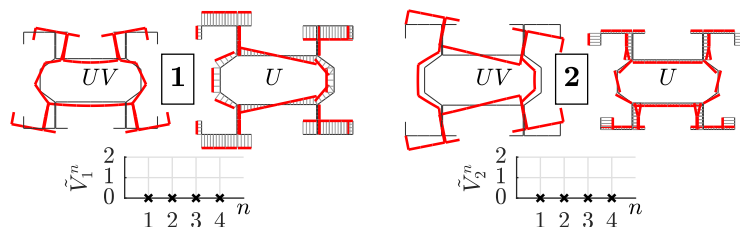


Figure 4.9: Illustrative example of dynamic cross-section analysis of a multi-component cross-section (Georgieva et al., 2012): non-conventional hybrid trial functions obtained with the enhanced GBT-D approach.

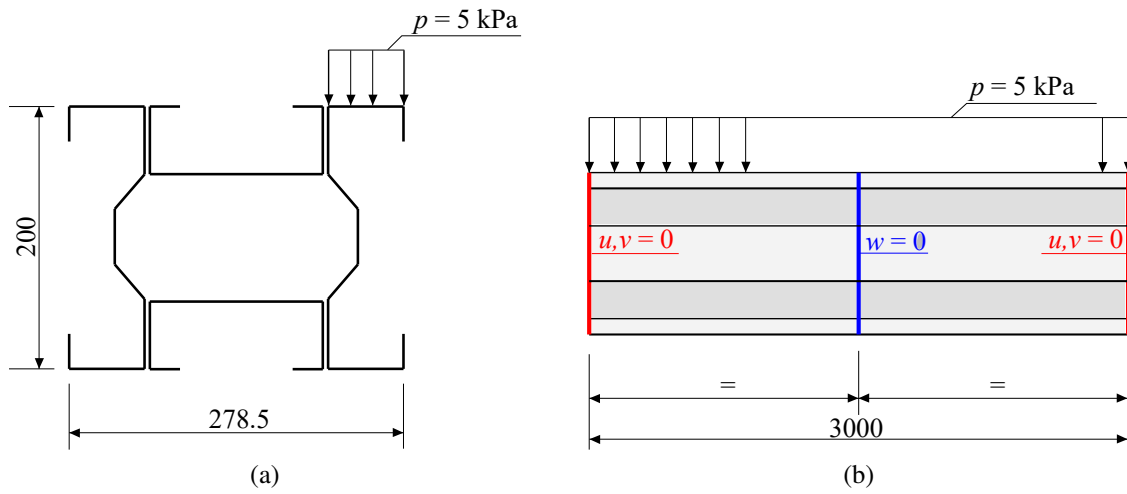


Figure 4.10: Box girder built-up multi-component member (Georgieva et al., 2012): member geometry and load arrangement.

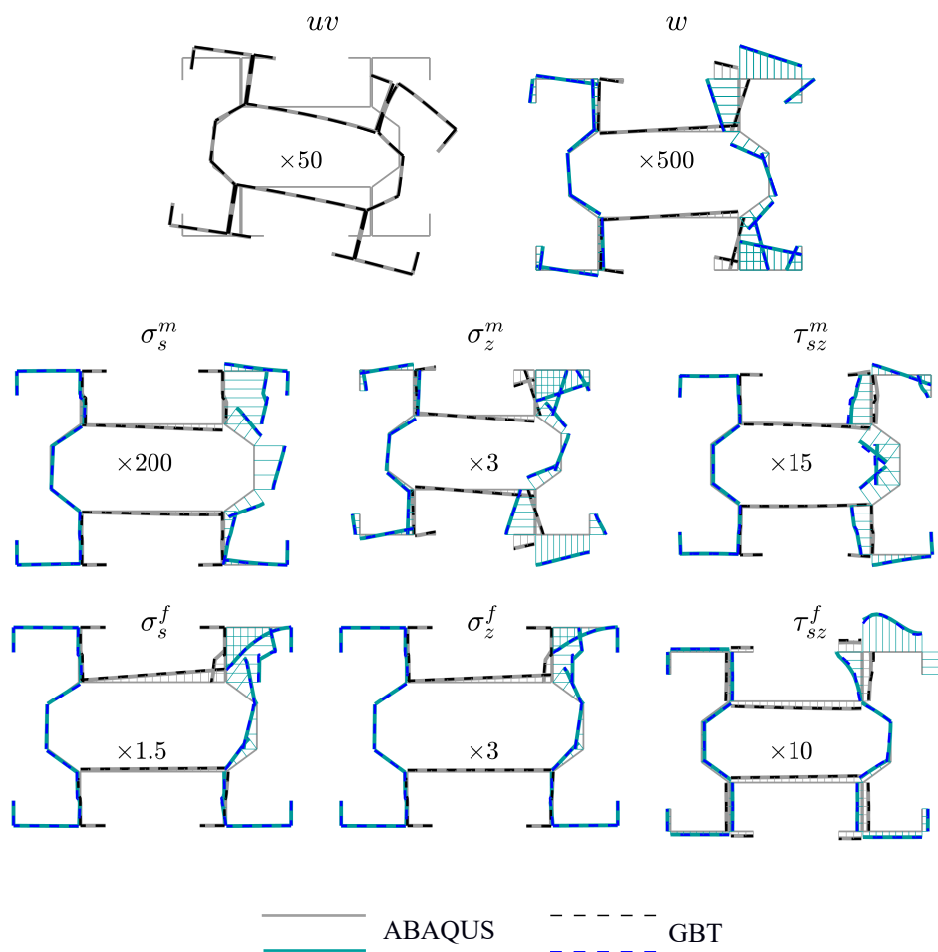


Figure 4.11: Box girder built-up multi-component member (Georgieva et al., 2012): displacements and stress fields with weak shear connection ($\alpha_L \mathcal{L} = 1$, $\alpha_T \mathcal{L} = 1$).

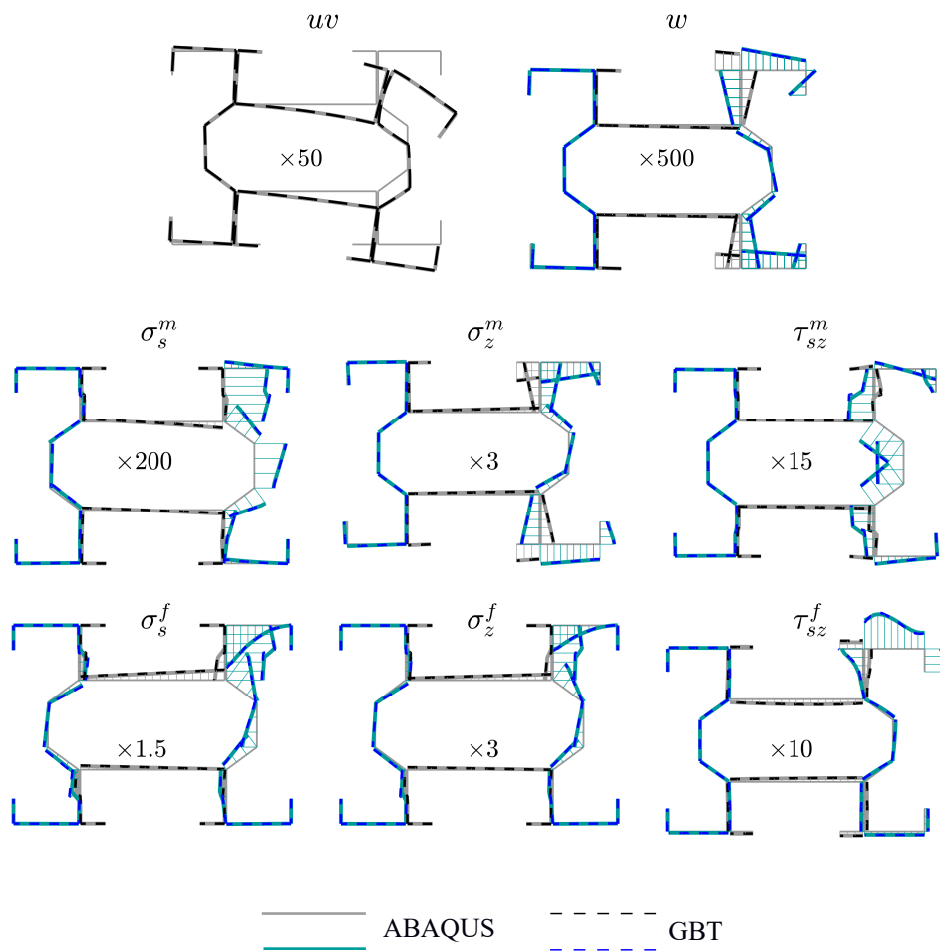


Figure 4.12: Box girder built-up multi-component member (Georgieva et al., 2012): displacements and stress fields with medium shear connection ($\alpha_L \mathcal{L} = 5$, $\alpha_T \mathcal{L} = 5$).

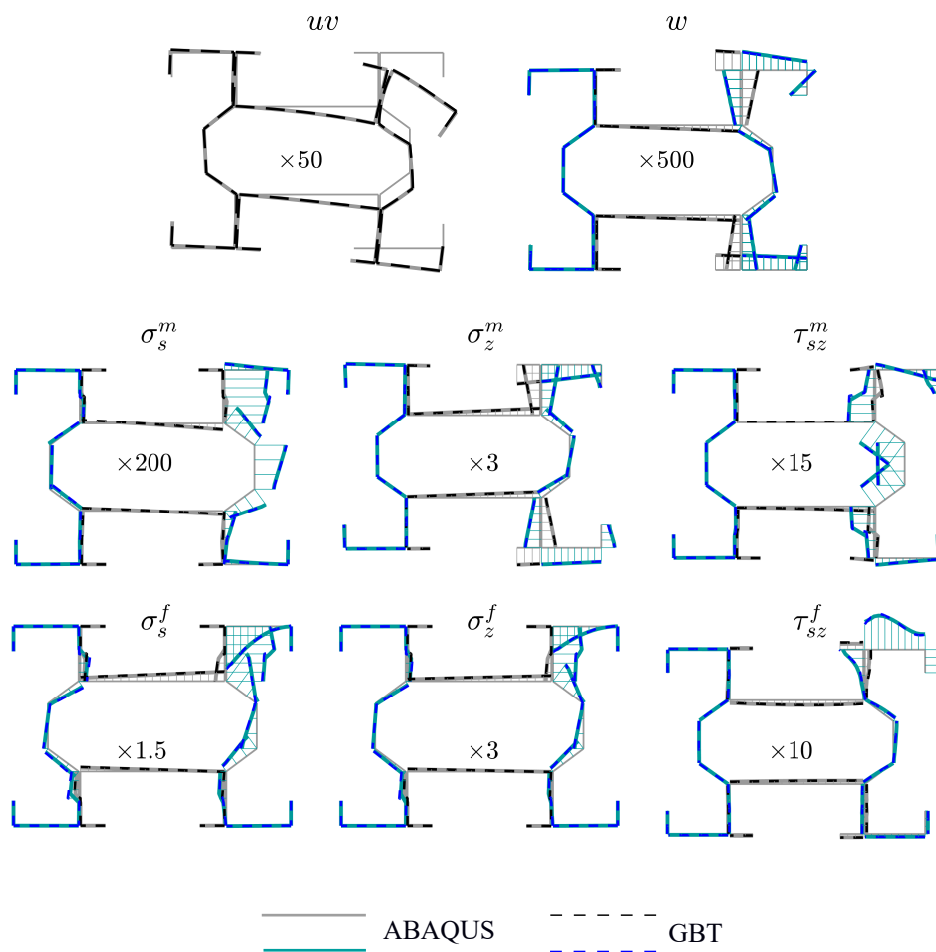


Figure 4.13: Box girder built-up multi-component member (Georgieva et al., 2012): displacements and stress fields with weak shear connection ($\alpha_L \mathcal{L} = 20$, $\alpha_T \mathcal{L} = 20$).

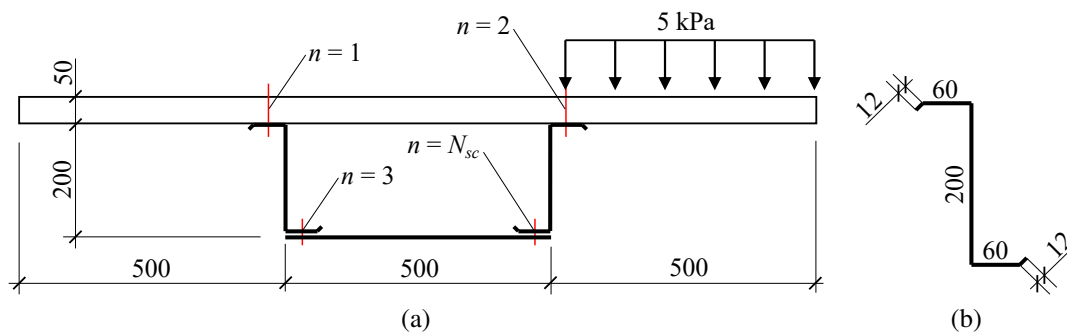


Figure 4.14: Partially-closed multi-component member (Hanaor, 2000): (a) built-up cross-section and load arrangement; (b) geometry of the cold-formed “Z” profile.

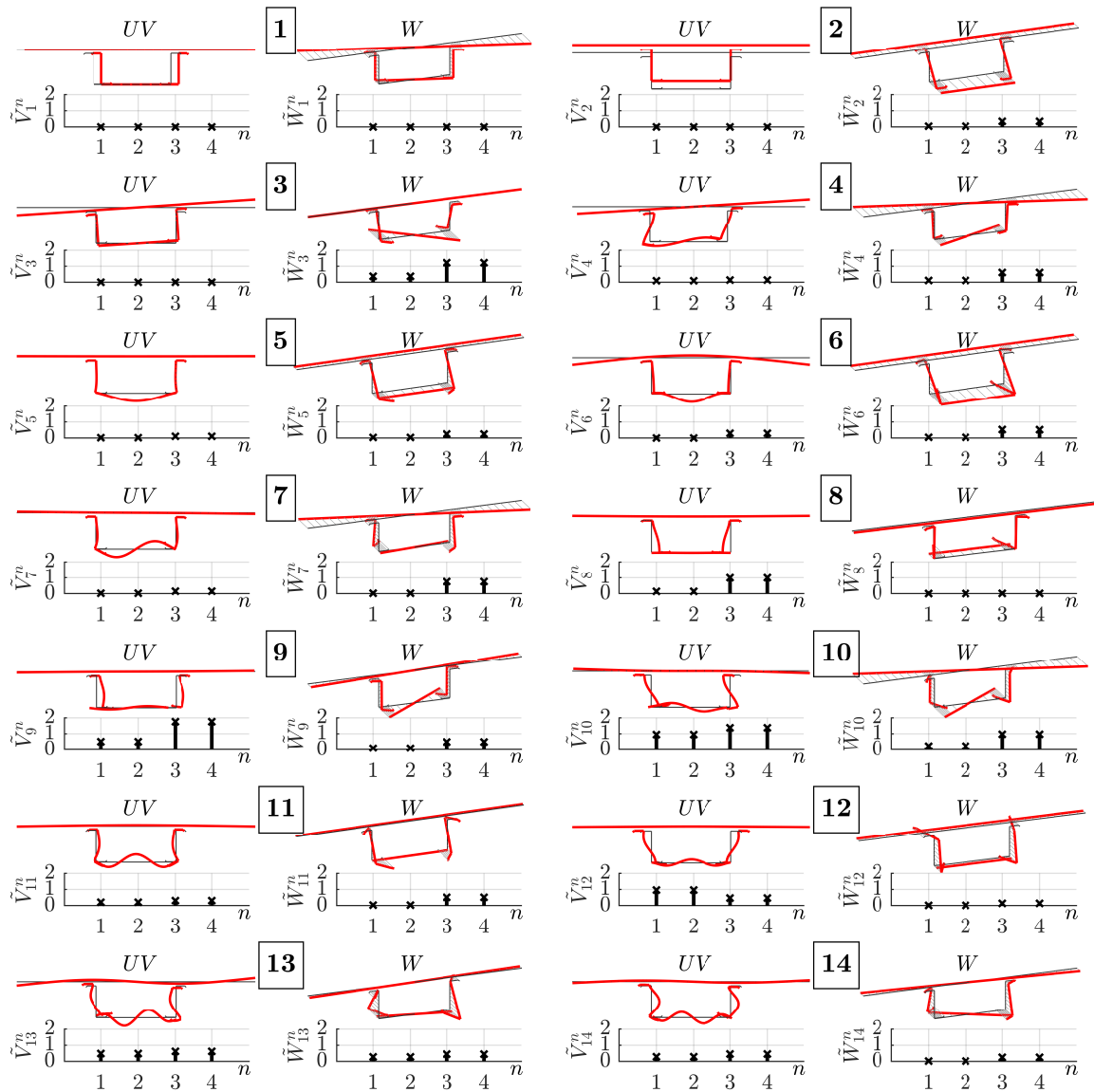


Figure 4.15: Partially-closed multi-component member (Hanaor, 2000): conventional in-plane and out-of-plane (warping) trial functions obtained with the enhanced GBT-D approach.

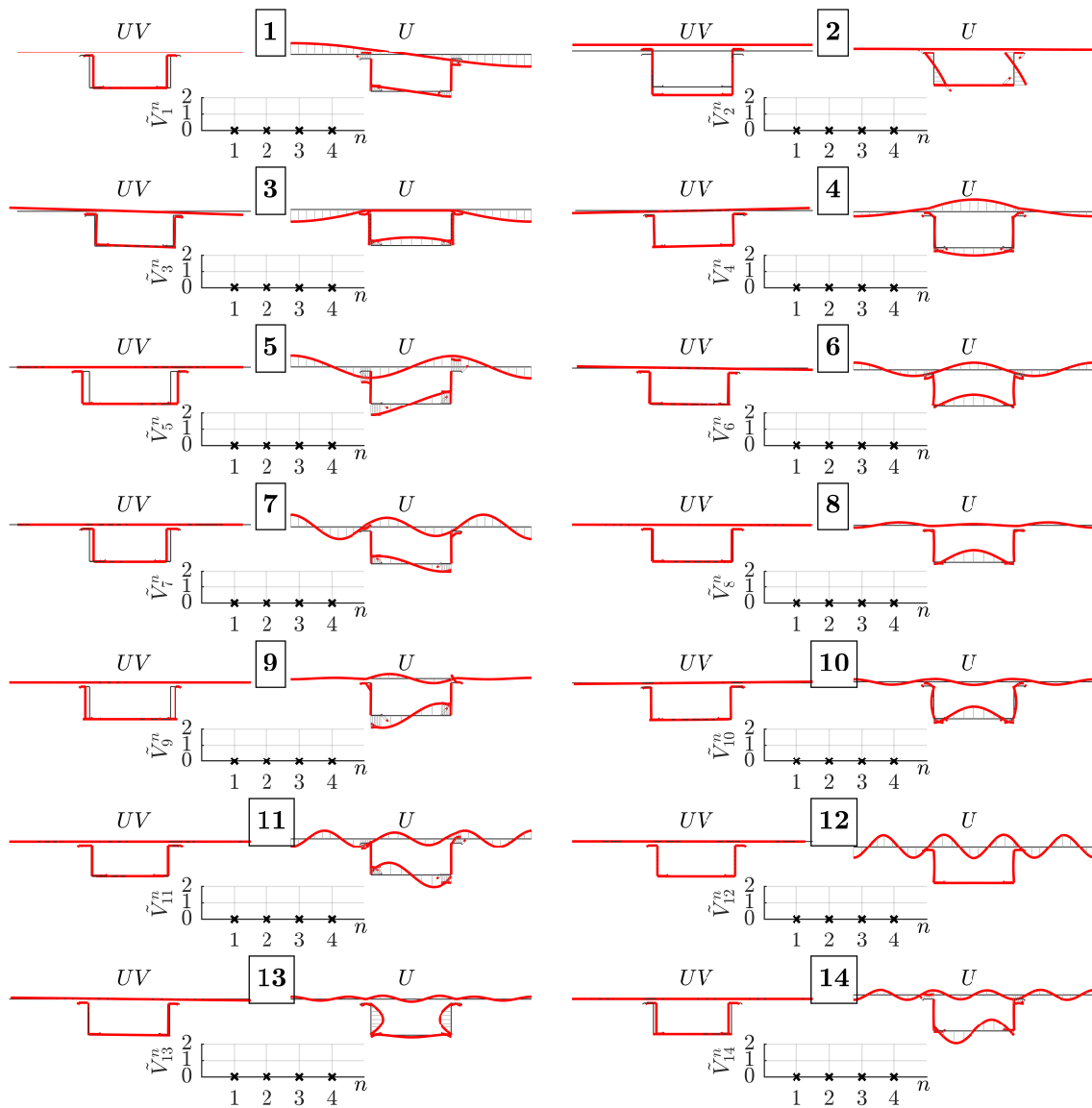


Figure 4.16: Partially-closed multi-component member (Hanaor, 2000): non-conventional extension trial functions obtained with the enhanced GBT-D approach.

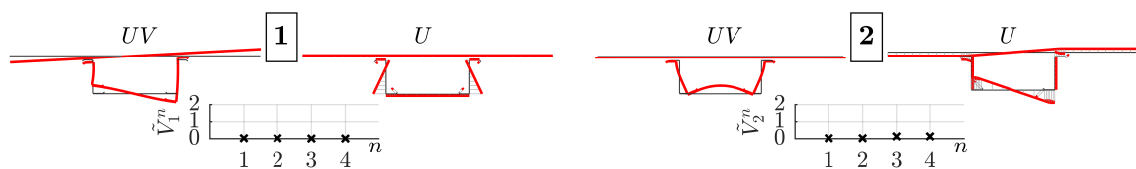


Figure 4.17: Partially-closed multi-component member (Hanaor, 2000): non-conventional hybrid trial functions obtained with the enhanced GBT-D approach.

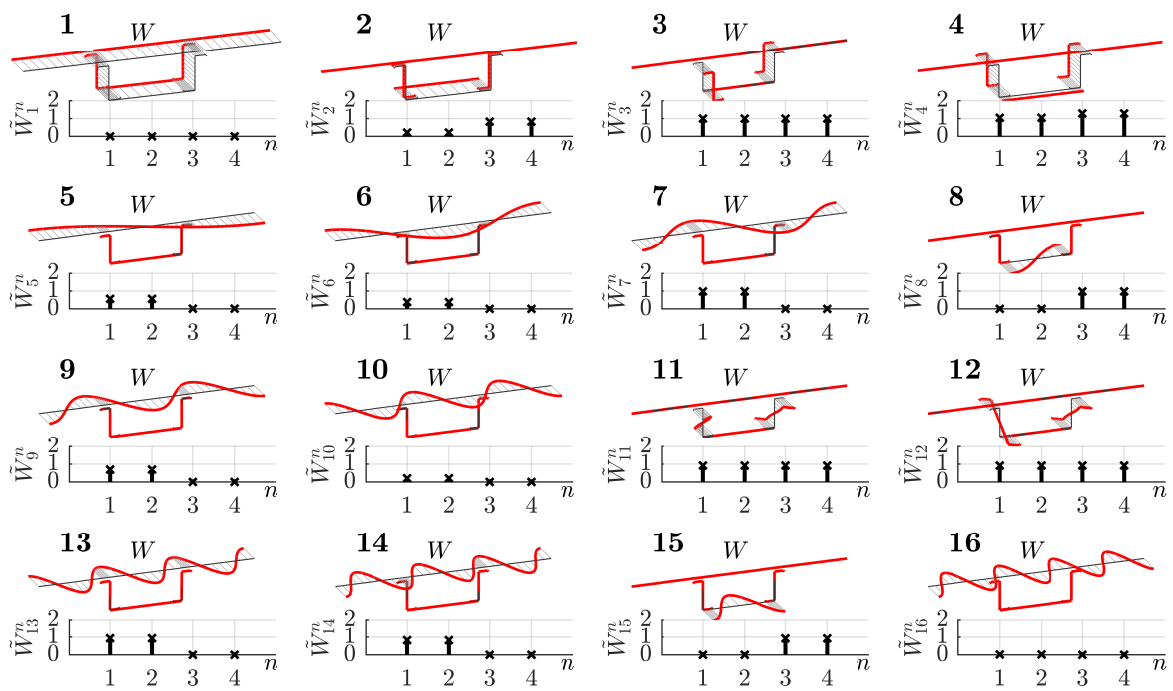


Figure 4.18: Partially-closed multi-component member (Hanaor, 2000): non-conventional shear (warping) trial functions.

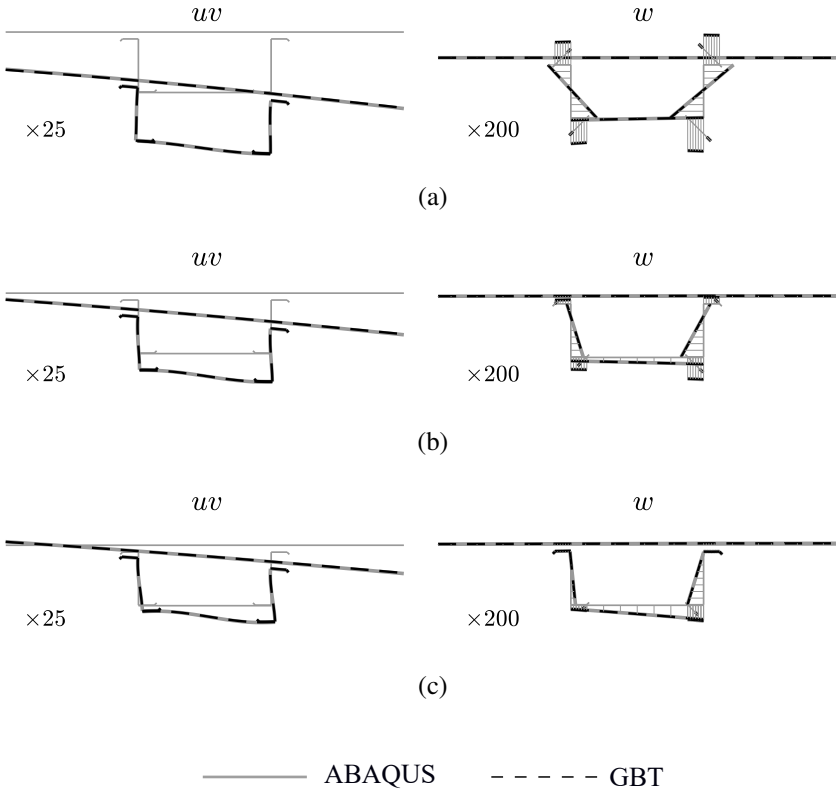


Figure 4.19: Partially-closed multi-component member (Hanaor, 2000): displacement fields uv and w in case of: (a) weak shear connection ($\alpha_L L = 1, \alpha_T L = 1$), (b) intermediate shear connection ($\alpha_L L = 5, \alpha_T L = 5$) and (c) strong shear connection ($\alpha_L L = 20, \alpha_T L = 20$).

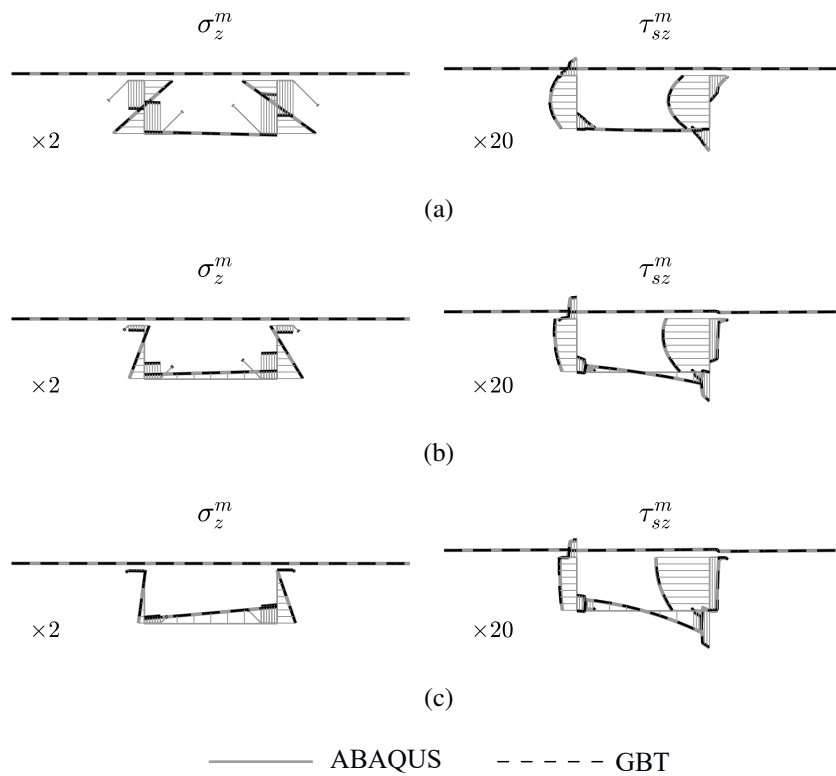


Figure 4.20: Partially-closed multi-component member (Hanaor, 2000): significant stress fields σ_z^m and τ_{sz}^m : (a) weak shear connection ($\alpha_L L = 1, \alpha_T L = 1$), (b) intermediate shear connection ($\alpha_L L = 5, \alpha_T L = 5$) and (c) strong shear connection ($\alpha_L L = 20, \alpha_T L = 20$).

Chapter 5

Displacement-based GBT for composite TWMs with large web penetrations

Composite steel-concrete members represent a very efficient structural solution for simply-supported elements undergoing bending, thanks to their capability in combining concrete slabs with steel thin-walled profiles. In particular, their resisting capacity is optimized by confining compression stresses in the concrete components, thus limiting steel members to withstand pure tensile stresses. For these reasons, they are increasingly used throughout the world, especially for bridges and large span building floors. Regarding these latter, it is common practice to perform large penetrations in webs of steel members (Fig. 5.1a,b), in order to accommodate building services such as plumbing, electrical and heating systems. Penetrations may be reinforced with localized longitudinal stiffeners (Fig. 5.1c,d), in order to limit the beam overall deflection. The behavior of composite members is strongly influenced by the shear deformability of mechanical devices placed at the interfaces between concrete and steel members, which leads to a relative displacement developing between components, that is, slip. This behavior is commonly referred to as partial shear interaction. When dealing with thin-walled profiles, the deformability of steel cross-section in both in-plane and out-of-plane directions must be taken into account to obtain accurate results. Finally, the presence of penetrations and stiffeners may significantly influence the beam overall deformability, in addition to cause stress concentration phenomena in their neighborhoods.

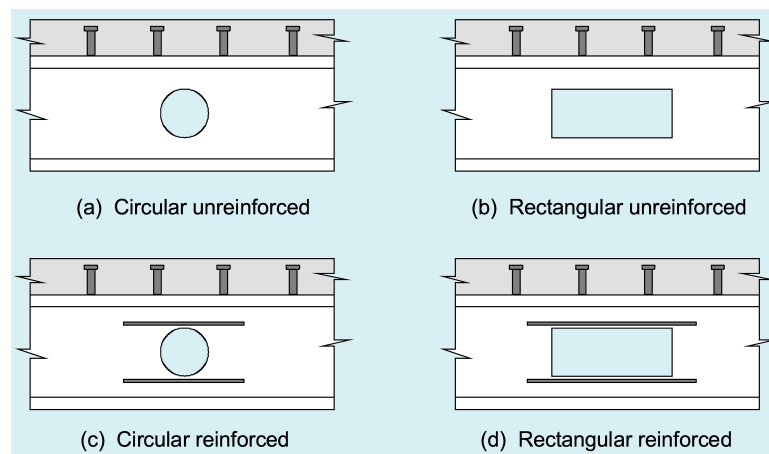


Figure 5.1: Types of large web penetrations (from Mills, 2001)

Composite TWMs with large web penetrations can be accurately modeled by using refined shell-based FE procedures. However, resulting models are usually burdensome and very time consuming and may not be suitable for design purposes. For these reasons, reduced approaches for the analysis of TWMs have been developed in recent years, including the Finite Strip Methods (FSM; e.g., Cheung, 1976; Ádány and Schafer, 2006b) and Generalized Beam The-

ory (GBT; e.g., Schardt, 1989; Silvestre and Camotim, 2002a). Concerning single-component TWMs, a FSM-based approach for linear and non-linear analysis of members with arbitrary shaped perforations is available in Eccher et al. (2009); Pham (2017), while a GBT-based approach is available limited to squared holes in Cai and Moen (2015, 2016); Casafont et al. (2015, 2018). To the knowledge of the author, reduced approaches for composite TWMs with large web penetrations are not yet available in the Literature. Within the GBT, a TWM with perforations, taperings and localized stiffeners (Fig. 5.2a) can be modeled as a structural system composed by sub-members possessing uniform cross-section along their length (Fig. 5.2b). Trial functions are first evaluated for each cross-section, then independent sets of GBT equations are written in terms of the unknown linear coordinates for each sub-member. The global model is finally obtained by coupling the aforementioned sets by means of compatibility conditions, enforcing displacement and strain fields to be continuous on interfaces between sub-members. Due to the nature of the GBT approach, displacements and strains must be expressed in terms of trial functions. Since the latter are related to the cross-section properties and are in general different for each sub-member, required compatibility constraints may be large in number and quite involved, leading to burdensome and computationally inefficient GBT models.

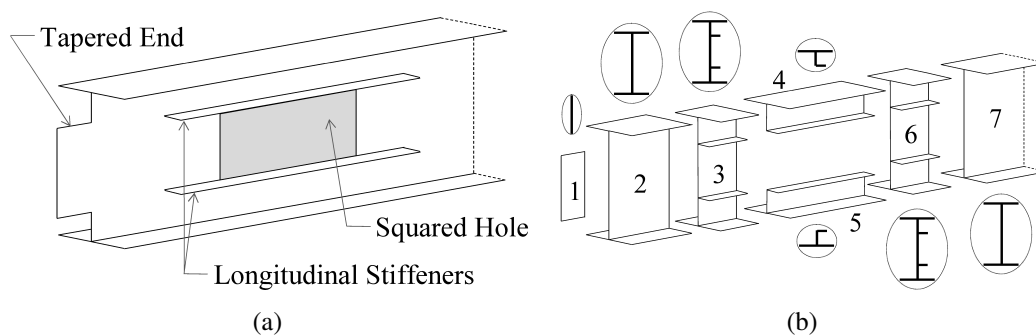


Figure 5.2: (a) TWM with tapered end and stiffened squared web perforation. (b) Decomposition into sub-members.

The first attempt to overcome a very similar problem was presented in Basaglia et al. (2008); Camotim et al. (2010) concerning the analysis of thin-walled frames. In order to facilitate the assembly between various sub-members composing the structural system, joint elements were added at end nodes of each beam, where unknown linear coordinates were expressed in terms of (unknown) cross-section nodal displacements and rotations through a variable transformation. Although this strategy does not allow to completely avoid the use of constraint equation in modeling connections between sub-members, required restraints were reduced in number and significantly simplified. This technique constitutes the basis of the so-called *displacement-based GBT approach*. It is based on the use of linear trial functions to perform a variable transformation and express the (unknown) linear coordinates in terms of (unknown) displacements and rotations at nodes adopted for the cross-section discretization. In this way, each GBT-based beam FE is transformed into an assembly of M flat quadrilateral GBT-based shell elements (M being the number of elements used for discretizing the cross-section), whose kinematic description corresponds to an enhancement of the standard GBT one with cross-section in-plane nodal rotations. The displacement-based GBT approach has been formalized very recently in Gonçalves and Camotim (2017a,b) and it has been successfully adopted in developing a corotational based

approach for geometrically nonlinear analysis in de Miranda et al. (2017). Since obtained GBT-based shell FE can benefit of assembly procedures commonly adopted in standard FE models, the displacement-based GBT approach constitutes a systematic and straightforward fashion for modeling structural systems. The approach combines the capability of the original GBT in reducing the problem dimensionality with the flexibility of standard shell-based FE procedures in dealing with complex geometries. Referring in particular to perforated, tapered and locally stiffened members, the displacement-based GBT allows to completely avoid the aforementioned constraint equation, thus obtaining very simple and numerically efficient models.

In this Chapter, the original displacement-based GBT approach is extended to the analysis of composite steel-concrete TWMs depicting large web penetration. The proposed approach is developed starting to the GBT formulation for the partial interaction analysis of multi-component TWM proposed in Chapter 4. The set of trial functions, which include the shear deformability of connectors placed at the interface between steel and concrete components, is first evaluated with the enhanced GBT-D approach proposed in Section 4.2.2 and then suited to perform a variable transformation and express unknown coordinates in terms of unknown nodal displacements and rotations. Since connectors were asked to be inextensible and undeformable against flexure to prevent detachment and/or interpenetration between components, they introduce a set of internal constraints in the cross-section analysis. As a consequence, planar trial functions are lesser in number than planar nodal DOF possessed by the composite (multi-component) cross-section. The variable transformation is therefore performed by relating (unknown) linear coordinates to a reduced number of planar nodal DOF, referred to as “master” DOF (to be distinguished from “slave” ones) and equal in number to the planar trial functions. The set of internal constraints mentioned above is suited to identify the required set of master variables and expressing slave DOF as function of master ones. The present Chapter is structured as follows: the displacement-based GBT formulation for single-component TWM is first outlined in detail in Section 5.1. An application on a I-shaped steel beam with mid-span stiffened perforation and tapered ends provided with bolted connection is presented for illustrative purposes. The new displacement-based GBT approach for composite TWM is then developed in Section 5.2. An application on a large-span composite beam with multiple web-perforations taken from Mills (2001) is then proposed to outline the capabilities and ease-to-use of the approach. Obtained results are compared with the ones obtained by means of a refined shell-based FE model developed with ABAQUS/Standard (Simulia, 2010) for validation purposes.

5.1 Displacement-based GBT: formulation

Linear trial functions obtained with the discrete FE-based dynamic approach for the cross-section analysis illustrated in Chapter 3 are identified starting from their (discrete) nodal values by means of the adopted interpolating functions. As shown in Section 3.4, the simplest choice, in terms of polynomial orders for interpolating functions, to avoid discontinuous stress paths induced by different order contributions of non-conventional trial functions in the expression of strain fields, consists on a 7 DOF FE (Fig. 3.22a) and a 3 DOF FE (Fig. 3.22b) to be adopted in the PEP and WEP, respectively. Corresponding obtained nodal values are illustrated in Figs. 5.3a and 5.3b, respectively, where superscript i refers to the i -th node adopted in the cross-

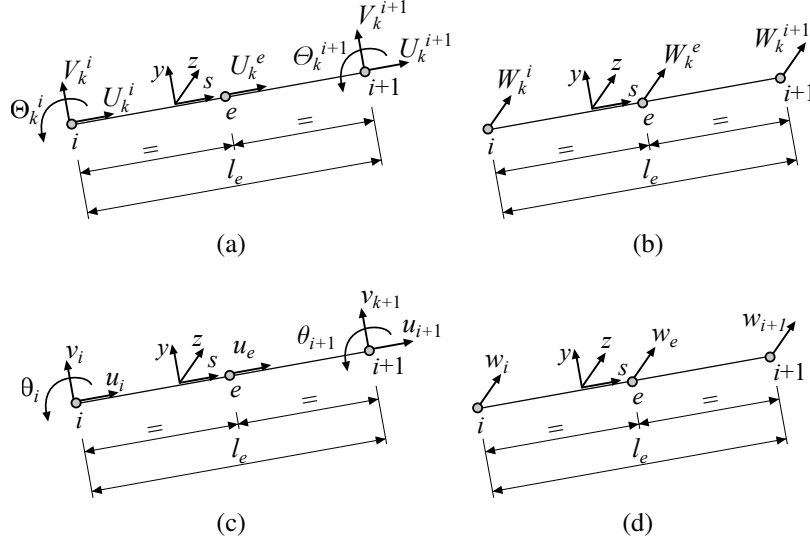


Figure 5.3: (a) Nodal values of in-plane trial functions; (b) nodal values of out-of-plane (warping) trial functions; (c) in-plane nodal DOF; (d) out-of-plane (warping) nodal DOF.

section discretization (i.e., $i = 1, \dots, n$, n being the total number of nodes, both natural and intermediate), superscript e refers to the e -th beam finite element (i.e., $e = 1, \dots, M$, M being the number of elements), while subscript k identifies the k -th trial function (i.e., $k = 1, \dots, K$, $K = 4n + 2M$ being the total number of DOF, including planar and warping ones, possessed by the discrete cross-section). By making use of the linear GBT kinematics (Eq. (2.2)), nodal DOF corresponding to nodal values of the obtained trial functions (i.e., displacements and in-plane rotation evaluated in correspondence of known values of trial functions) can be expressed as follows (Figs. 5.3c and 5.3d):

$$u_i(z) = \sum_{k=1}^K U_k^i \varphi_k(z) \quad i = 1, \dots, n + M \quad (5.1a)$$

$$v_i(z) = \sum_{k=1}^K V_k^i \varphi_k(z) \quad i = 1, \dots, n \quad (5.1b)$$

$$\theta_i(z) = \sum_{k=1}^K \Theta_k^i \varphi_k(z) \quad i = 1, \dots, n \quad (5.1c)$$

$$w_i(z) = \sum_{k=1}^K W_k^i \varphi_k'(z) \quad i = 1, \dots, n + M \quad (5.1d)$$

Starting from Eq. (5.1) and collecting the $K_p (= 3n + M)$ in-plane DOF $u_i(z)$, $v_i(z)$, $\theta_i(z)$ and $u_e(z)$ in the vector $\mathbf{u}(z)$, the $K_w (= n + M)$ warping DOF $w_i(z)$ and $w_e(z)$ in the vector $\mathbf{w}(z)$, then assembling the K linear coordinates $\varphi_k(z)$ in the vector $\boldsymbol{\varphi}(z)$, the following two linear

systems can be written:

$$\mathbf{U} \boldsymbol{\varphi}(z) = \mathbf{u}(z) \quad (5.2)$$

$$\begin{bmatrix} \mathbf{U} \\ \mathbf{W} \end{bmatrix} \boldsymbol{\varphi}'(z) = \begin{bmatrix} \mathbf{u}'(z) \\ \mathbf{w}(z) \end{bmatrix} \quad (5.3)$$

The following positions hold for matrices involved in Eqs. (5.2) and (5.3):

$$\mathbf{U} = \begin{bmatrix} \mathbf{Q}_p & \mathbf{0}_{K_p}^{K_w} \end{bmatrix} \quad (5.4a)$$

$$\mathbf{W} = [\mathbf{Q}_\Omega \quad \mathbf{Q}_w] ; \quad \mathbf{Q}_\Omega = \begin{bmatrix} \boldsymbol{\Omega} & \mathbf{0}_{K_w}^{K_p - N_c} \end{bmatrix} \quad (5.4b,c)$$

where \mathbf{Q}_p and \mathbf{Q}_w are $K_p \times K_p$ and $K_w \times K_w$ matrix, respectively, collecting nodal values of planar and shear trial functions, respectively (Figs. 5.3a and 5.3b, respectively), arranged by column (i.e., their generic k -th column collects nodal values of the k -th trial function), $\boldsymbol{\Omega}$ is a $K_w \times N_c$ matrix (N_c being the number of conventional functions) collecting nodal values of conventional warping distributions $W_k^i(s)$ (Fig. 5.3b) arranged by columns, while $\mathbf{0}_a^b$ is a $a \times b$ nil matrix. The presence of 0-submatrices is due to shear trial functions having nil in-plane displacements (Eq. (5.4a)) and to extension and hybrid (non-conventional) in-plane functions depicting nil warping displacement (Eq. (5.4c)). Systems (5.2) and (5.3) can in principle be suited to express linear coordinates $\boldsymbol{\varphi}(z)$ (and corresponding first derivative $\boldsymbol{\varphi}'(z)$) as function of nodal DOF $\mathbf{u}(z)$, $\mathbf{u}'(z)$, $\mathbf{w}(z)$, thus defining a variable transformation. However, while a unique solution can be obtained for $\boldsymbol{\varphi}'(z)$ by solving Eq. (5.3), system (5.2) is indeterminate, since it possess $K_p (< K)$ equations in front of K unknowns. It is easy to prove that redundant unknowns are represented by linear coordinates $\varphi_k(z)$ related to non-conventional shear functions. As a matter of fact, the latter depict trivial in-plane distributions, therefore corresponding linear coordinates $\varphi_k(z)$ are irrelevant and can assume arbitrary distributions. The simplest way to address the problem is to adopt a slightly modified GBT linear kinematics, where an independent set of linear coordinates $\psi_k(z)$ is introduced for non-conventional shear trial functions, as follows:

$$u(s, z) = \sum_{k=1}^{K_p} U_k(s) \varphi_k(z) \quad (5.5a)$$

$$v(s, z) = \sum_{k=1}^{K_p} V_k(s) \varphi_k(z) \quad (5.5b)$$

$$w(s, z) = \sum_{k=1}^{K_p} \Omega_k(s) \varphi_k'(z) + \sum_{k=1}^{K_w} W_k(s) \psi_k(z) \quad (5.5c)$$

where $W_k(s)$ represent the k -th non-conventional *shear* functions, while $\Omega_k(s)$ depict the warping distribution associated to the k -th *planar* trial function: they are nil in case of non-conventional (i.e., extension and hybrid) fields, while they coincide with conventional warping complement $W_k^i(s)$ in case of conventional planar functions. Within the new arrangement, (linear) strain field

$\boldsymbol{\varepsilon}(s, y, z) = \{\varepsilon_s^m, \varepsilon_z^m, \gamma_{sz}^m, \varepsilon_s^f, \varepsilon_z^f, \gamma_{sz}^f\}^T$ and stress field $\boldsymbol{\sigma}(s, y, z) = \{\sigma_s^m, \sigma_z^m, \tau_{sz}^m, \sigma_s^f, \sigma_z^f, \tau_{sz}^f\}^T$ can be written as:

$$\varepsilon_s^m = \sum_{k=1}^{K_p} U'_k(s) \varphi_k(z) \quad (5.6a)$$

$$\varepsilon_z^m = \sum_{k=1}^{K_p} \Omega_k(s) \varphi_k''(z) + \sum_{k=1}^{K_w} W_k(s) \psi_k'(z) \quad (5.6b)$$

$$\gamma_{sz}^m = \sum_{k=1}^{K_p} [U_k(s) + \Omega'_k(s)] \varphi_k'(z) + \sum_{k=1}^{K_w} W'_k(s) \psi_k(z) \quad (5.6c)$$

$$\varepsilon_s^f = \sum_{k=1}^{K_p} -y V_k''(s) \varphi_k(z) \quad (5.6d)$$

$$\varepsilon_z^f = \sum_{k=1}^{K_p} -y V_k(s) \varphi_k''(z) \quad (5.6e)$$

$$\gamma_{sz}^f = \sum_{k=1}^{K_p} -2y V'_k(s) \varphi_k'(z) \quad (5.6f)$$

and

$$\sigma_s^m = \sum_{k=1}^{K_p} \frac{E}{1-\nu^2} [U'_k(s) \varphi_k(z) + \nu \Omega_k(s) \varphi_k''(z)] + \sum_{k=1}^{K_w} \frac{\nu E}{1-\nu^2} W_k(s) \psi_k'(z) \quad (5.7a)$$

$$\sigma_z^m = \sum_{k=1}^{K_p} \frac{E}{1-\nu^2} [\nu U'_k(s) \varphi_k(z) + \Omega_k(s) \varphi_k''(z)] + \sum_{k=1}^{K_w} \frac{E}{1-\nu^2} W_k(s) \psi_k'(z) \quad (5.7b)$$

$$\tau_{sz}^m = \sum_{k=1}^{K_p} G [U_k(s) + \Omega'_k(s)] \varphi_k'(z) + \sum_{k=1}^{K_w} G W'_k(s) \psi_k(z) \quad (5.7c)$$

$$\sigma_s^f = \sum_{k=1}^{K_p} -\frac{yE}{1-\nu^2} [V_k''(s) \varphi_k(z) + \nu V_k(s) \varphi_k''(z)] \quad (5.7d)$$

$$\sigma_z^f = \sum_{k=1}^{K_p} -\frac{yE}{1-\nu^2} [\nu V_k''(s) \varphi_k(z) + V_k(s) \varphi_k''(z)] \quad (5.7e)$$

$$\tau_{sz}^f = \sum_{k=1}^{K_p} -2yG V'_k(s) \varphi_k'(z) \quad (5.7f)$$

By making use of Eq. (5.5), Eqs. (5.2) and (5.3) can be rewritten as:

$$\mathbf{Q}_p \boldsymbol{\varphi}(z) = \mathbf{u}(z) \quad (5.8)$$

$$\begin{bmatrix} \mathbf{Q}_p & \mathbf{0}_{K_p}^{K_w} \\ \mathbf{Q}_\Omega & \mathbf{Q}_w \end{bmatrix} \begin{bmatrix} \boldsymbol{\varphi}'(z) \\ \boldsymbol{\psi}(z) \end{bmatrix} = \begin{bmatrix} \mathbf{u}'(z) \\ \mathbf{w}(z) \end{bmatrix} \quad (5.9)$$

where $\boldsymbol{\varphi}(z)$ and $\boldsymbol{\psi}(z)$ are $K_p \times 1$ and $K_w \times 1$ vectors, respectively, collecting the (unknown) linear coordinates $\varphi_k(z)$ and $\psi_k(z)$, respectively. Eqs. (5.8) and (5.9) can now be solved independently in terms of linear coordinates. Since matrices \mathbf{Q}_p and \mathbf{Q}_w are non-singular (i.e., planar and shear warping trial functions constitutes complete basis), the following can be obtained (e.g., Bernstein, 2005):

$$\boldsymbol{\varphi}(z) = \mathbf{T}_p \mathbf{u}(z) \quad (5.10a)$$

$$\boldsymbol{\varphi}'(z) = \mathbf{T}_p \mathbf{u}'(z) \quad (5.10b)$$

$$\boldsymbol{\psi}(z) = \mathbf{T}_w \mathbf{w}(z) + \mathbf{T}_{wp} \mathbf{u}'(z) \quad (5.10c)$$

where:

$$\mathbf{T}_p = \mathbf{Q}_p^{-1}; \quad \mathbf{T}_w = \mathbf{Q}_w^{-1}; \quad \mathbf{T}_{wp} = -\mathbf{T}_w \mathbf{Q}_\Omega \mathbf{T}_p \quad (5.11a-c)$$

Eq. (5.10) represents a variable transformation which allows to express unknown linear coordinates as function of nodal DOF (i.e., nodal displacements, rotations and curvatures at nodes used in the cross-section discretization (Figs. 5.3c and 5.3d).

The weak formulation of the elasticity problem can be derived through the Principle of Virtual Works, as illustrated in Section 2.3. By making use of Eqs. (5.5) to (5.7), Eq. (2.7) can be rewritten in compact form as follows:

$$\int_{\mathcal{L}} \{ \delta \boldsymbol{\varphi}^T (\mathbf{B} \boldsymbol{\varphi} + \mathbf{F}^T \boldsymbol{\phi}' - \mathbf{q}_1) + \delta \boldsymbol{\phi}'^T (\mathbf{F} \boldsymbol{\varphi} + \mathbf{C} \boldsymbol{\phi}') + \delta \boldsymbol{\phi}^T (\mathbf{D} \boldsymbol{\phi} - \mathbf{q}_2) \} dz + \sum_B (\delta \boldsymbol{\varphi}^T \mathbf{P}_1 + \delta \boldsymbol{\phi}^T \mathbf{P}_2) = 0 \quad (5.12)$$

where the δ -operator denotes virtual quantities, structural matrices \mathbf{B} , \mathbf{C} , \mathbf{D} , \mathbf{F} and load vectors \mathbf{q}_1 , \mathbf{q}_2 , \mathbf{P}_1 , \mathbf{P}_2 are detailed in Appendix D, and:

$$\boldsymbol{\phi}(z) = \begin{bmatrix} \boldsymbol{\varphi}'(z) \\ \boldsymbol{\psi}(z) \end{bmatrix} \quad (5.13)$$

By making use of the variable transformation defined in Eq. (5.10), Eq. (5.12) can be rewritten as follows:

$$\int_{\mathcal{L}} \left\{ \delta \mathbf{u}^T \mathbf{T}_p^T (\mathbf{B} \mathbf{T}_p \mathbf{u} + \mathbf{F}^T \mathbf{T} \mathbf{d}' - \mathbf{q}_1) + \delta \mathbf{d}'^T \mathbf{T}^T (\mathbf{F} \mathbf{T}_p \mathbf{u} + \mathbf{C} \mathbf{T} \mathbf{d}') + \delta \mathbf{d}^T \mathbf{T}^T (\mathbf{D} \mathbf{T} \mathbf{d} - \mathbf{q}_2) \right\} dz - \sum_B (\delta \mathbf{u}^T \mathbf{T}_p^T \mathbf{P}_1 + \delta \mathbf{d}^T \mathbf{T}^T \mathbf{P}_2) = 0 \quad (5.14)$$

where:

$$\mathbf{d}(z) = \begin{bmatrix} \mathbf{u}'(z) \\ \mathbf{w}(z) \end{bmatrix}; \quad \mathbf{T} = \begin{bmatrix} \mathbf{T}_p & \mathbf{0}_{K_p}^{K_w} \\ \mathbf{T}_{wp} & \mathbf{T}_w \end{bmatrix} \quad (5.15a,b)$$

The set of K displacement-based GBT equations and relevant boundary conditions can be derived from Eq. (5.14) by performing standard steps of calculus of variations (e.g., Berdichevsky, 2009). They are reported in Appendix D. Their solution is achieved numerically, as commonly done in the Literature, by means of a Finite Element (FE) procedure (e.g., Bathe, 2014). The member is discretized into N_E finite elements and following descriptions are adopted for approximating the unknowns:

$$\mathbf{u}(z) \cong \mathbf{H}(z) \mathbf{u}_E; \quad \mathbf{w}(z) \cong \mathbf{L}(z) \mathbf{w}_E \quad (5.16a,b)$$

where \mathbf{u}_E (\mathbf{w}_E) are $4K_p \times 1$ ($3K_w \times 1$) vectors collecting values of unknown functions at nodes of the member FE, $\mathbf{H}(z)$ is a $K_p \times 4K_p$ matrix collecting Hermite cubic polynomial interpolating functions and defined in Eq. (2.17), while:

$$\mathbf{L}(z) = [L_1(z)\mathbf{I} \quad L_2(z)\mathbf{I} \quad L_3(z)\mathbf{I}] \quad (5.17)$$

is a $K_w \times 3K_w$ matrix (\mathbf{I} being a $K_w \times K_w$ identity matrix) collecting Lagrange parabolic polynomial interpolating functions defined as:

$$L_1(z) = 1 - 3\frac{z}{l_E} + 2\left(\frac{z}{l_E}\right)^2; \quad L_2(z) = 4\frac{z}{l_E} - 4\left(\frac{z}{l_E}\right)^2 \quad (5.18a,b)$$

$$L_3(z) = -\frac{z}{l_E} + 2\left(\frac{z}{l_E}\right)^2 \quad (5.18c)$$

with l_E being the length of the E -th FE. It is pointed out that the choice of parabolic polynomials for warping DOF $\mathbf{w}(z)$ allows to avoid the so called *shear locking* (e.g., Ranzi and Gilbert, 2015), occurring when terms participating in the shear strain term γ_{sz} contribute with different order. The same choice is commonly performed in the definition of the Timoshenko beam FE, where in fact the axial (i.e., along z) displacement needs to be interpolated by means of parabolic shape functions. This allows to avoid locking phenomena induced by the linear shape functions commonly used in defining the standard Euler-Bernoulli beam FE (e.g., Ranzi and Gilbert, 2015). After performing the standard steps of the FE procedure, the following stiffness relationship can be obtained for each GBT-based FE:

$$\mathbf{K}_E \mathbf{x}_E = \mathbf{q}_E \quad (5.19)$$

where \mathbf{x}_E is a $(4K_p + 3K_w) \times 1$ vector collecting values of unknown functions at nodes of the member FE, while \mathbf{K}_E and \mathbf{q}_E are $(4K_p + 3K_w) \times (4K_p + 3K_w)$ stiffness matrix and $(4K_p + 3K_w) \times 1$ load vector, respectively, defined as follows:

$$\mathbf{K}_E = \int_{l_E} \mathbf{N}^T \begin{bmatrix} \mathbf{T}_p^T \mathbf{B} \mathbf{T}_p & \mathbf{0}_{K_p}^K & \mathbf{T}_p^T \mathbf{F}^T \mathbf{T} \\ \mathbf{0}_K^{K_p} & \mathbf{T}^T \mathbf{D} \mathbf{T} & \mathbf{0}_K^K \\ \mathbf{T}^T \mathbf{F} \mathbf{T}_p & \mathbf{0}_K^K & \mathbf{T}^T \mathbf{C} \mathbf{T} \end{bmatrix} \mathbf{N} dz; \quad \mathbf{N} = \begin{bmatrix} \mathbf{H} & \mathbf{0}_{K_p}^{3K_w} \\ \mathbf{H}' & \mathbf{0}_{K_p}^{3K_w} \\ \mathbf{0}_{K_w}^{4K_p} & \mathbf{L} \\ \mathbf{H}'' & \mathbf{0}_{K_p}^{3K_w} \\ \mathbf{0}_{K_w}^{4K_p} & \mathbf{L}' \end{bmatrix} \quad (5.20a,b)$$

$$\mathbf{q}_E = \int_{l_E} \begin{bmatrix} \mathbf{H}^T & \mathbf{H}'^T & \mathbf{0}_{K_w}^{K_p} \\ \mathbf{0}_{3K_w}^{K_p} & \mathbf{0}_{3K_w}^{K_p} & \mathbf{L}^T \end{bmatrix} \begin{bmatrix} \mathbf{T}_p^T \mathbf{q}_1 \\ \mathbf{T}^T \mathbf{q}_2 \end{bmatrix} dz \quad (5.20c)$$

The displacement-based GBT approach allows to transform each GBT-based beam FE into an assembly of M GBT-based shell FE, M being the number of elements used to discretize the cross-sections. Nodal DOF possessed by each shell FE are outlined in Table 5.1. According to Gonçalves and Camotim (2017b), obtained shell elements are equivalent to the classic Bogner-Fox-Schmit plate element with added (Lagrangian) quadratic membrane displacements, except for the longitudinal interpolation of the in-plane axial displacement u , in which case Hermite cubic functions are employed.

The main advantage of the proposed approach consists on the possibility to assemble obtained shell elements by following procedures commonly adopted in standard shell-based FE models. This allows to significantly reduce and, in many cases such as TWMs with squared perforations, taperings and longitudinal stiffeners, to avoid the use of constraint equations in modeling the structural systems. GBT-based models can thus be obtained with a systematic and

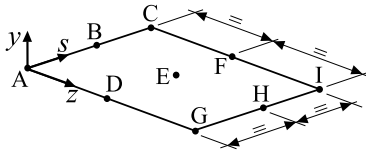
	Nodal DOF for the GBT-based shell element		
	Displacements	Rotations	Curvatures
	u_A, v_A, w_A	$\xi_A(=v_{A,z}), \eta_A(=u_{A,z}),$ $\zeta_A(=v_{A,s})$	$\kappa_A(=v_{A,sz})$
	u_B, w_B	$\eta_B(=u_{B,z})$	
	u_C, v_C, w_C	$\xi_C(=v_{C,z}), \eta_C(=u_{C,z}),$ $\zeta_C(=v_{C,s})$	$\kappa_C(=v_{C,sz})$
	w_D		
	w_E		
	w_F		
	u_G, v_G, w_G	$\xi_G(=v_{G,z}), \eta_G(=u_{G,z}),$ $\zeta_G(=v_{G,s})$	$\kappa_G(=v_{G,sz})$
	u_H, w_H	$\eta_H(=u_{H,z})$	
	u_I, v_I, w_I	$\xi_I(=v_{I,z}), \eta_I(=u_{I,z}),$ $\zeta_I(=v_{I,s})$	$\kappa_I(=v_{I,sz})$

Table 5.1: GBT-based shell FE: coordinate system and nodal DOF.

straightforward fashion. Similar advantages can be obtained also when dealing with localized support conditions. As a matter of fact, they can be directly enforced by removing restrained DOF from the discrete system, Eq. (5.19), thus avoiding the use of constraint equations expressing them as function of the unknown coordinates, as otherwise required by the standard GBT approach.

An illustrative example is proposed to illustrate the ease-to-use of the displacement-based GBT approach. It concerns the linear elastic analysis of the steel I-shaped beam illustrated in Fig. 5.4. The beam is 1.50 m long and specifies elastic modulus of 200 GPa and Poisson's ratio of 0.3. It depicts tapered ends and a stiffened mid-span squared web perforation. In particular, web perforation possesses dimension 400 mm \times 220 mm, while local longitudinal stiffeners are realized means of plates depicting 60 mm width; they are placed on only one side of the web and they are longitudinally extended both forward and backward with respect to web penetration for a length equal to 200 mm. All steel members are 5 mm thick and the gross cross-section dimensions are depicted in Fig. 5.4b. The beam is supposed to be locally restrained by mean of bolted connections on tapered end regions. Restrained DOF are reported in Fig. 5.4a, while bolts geometry is illustrated in Fig. 5.4c. The beam is subjected to a vertical pressure equal to 0.1 MPa applied on the top flange (Fig. 5.4a). The displacement-based GBT approach is used to model the TWM. In particular, the beam is subdivided into eight sub-members possessing uniform cross-section along their length, as depicted in Fig. 5.5. For each sub-member, the cross-section analysis is first performed, then stiffness relation depicted in Eq. (5.19) is written. The global GBT-based model is then obtained by assembling the contribution of each sub-members by following the common procedures adopted for shell-based FE models. To this scope, no constraint equations have been used. Local constraint conditions represented by bolted connections are finally included by removing constrained nodal DOF from the analysis.

Results obtained with the displacement-based GBT formulation are compared with the so-

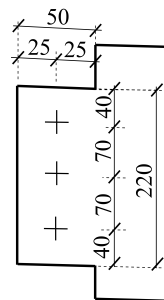
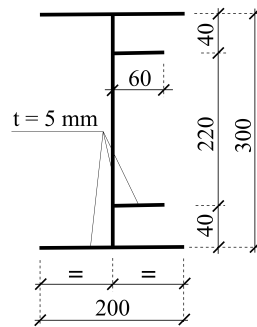
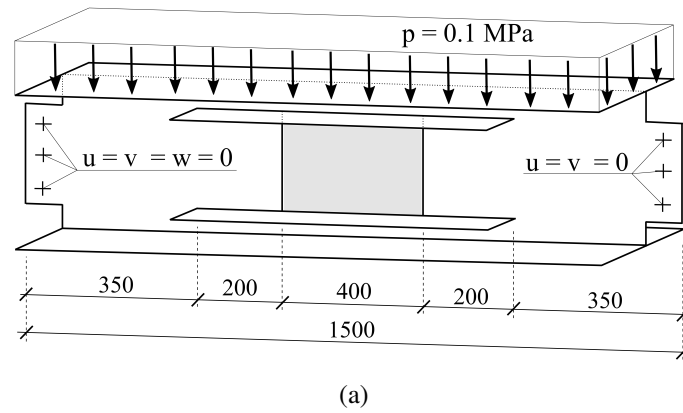


Figure 5.4: I-shaped TWM with tapered ends and central stiffened squared hole. (a) Member dimensions, load arrangement and boundary conditions. (b) Gross cross-section dimensions. (c) Bolted connection geometry.

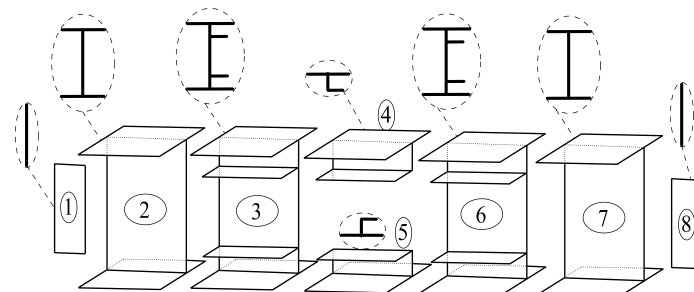


Figure 5.5: I-shaped TWM with tapered ends and central stiffened squared hole: sub-members decomposition.

lution calculated through a three-dimensional finite element analysis (FEA) performed with the commercial software ABAQUS/Standard (Simulia, 2010). Reduced-integration S4R shell finite elements available in the software library have been used for this purpose. Quadrangular shell FE adopted in the ABAQUS member discretization possess width equal about to 10 mm; they are altogether 8900 shell finite elements. Corresponding discretization adopted in the GBT-based model is made with spacing equal to 20 mm as regard the cross-section, which corresponds in discretizing the gross cross-section (Fig. 5.4b) into 37 segments, and about 50 mm concerning the one along the member length. Representative comparison in terms of displacements fields are reported in Fig. 5.6. In particular, Fig. 5.6a reports the in-plane displacement at mid-span, while warping fields at the interface between sub-members 1-2 and 6-7 are represented in Figs. 5.6b and 5.6c, respectively. For clarity, plotted variables have been properly scaled, with the adopted scale coefficient reported on each plot. The agreement between the calculated GBT solution and the FEA results is excellent. Comparisons in terms of stress fields are reported in Fig. 5.7. Stress distributions are in general well predicted by the displacement-based GBT model, particularly near local restraints, penetration, stiffeners and any other geometrical and mechanical discontinuity.

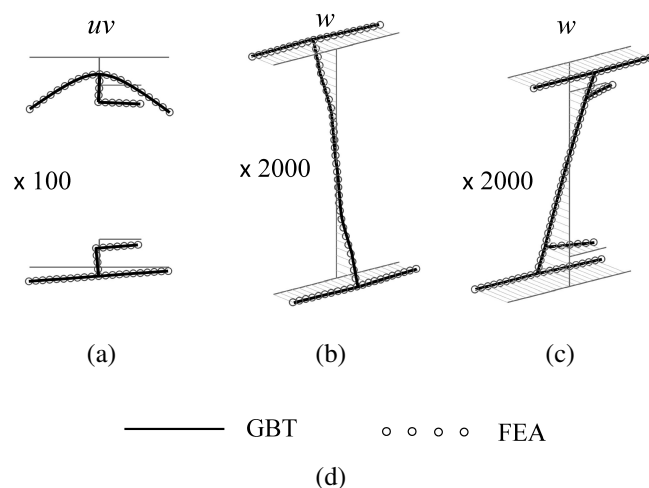


Figure 5.6: I-shaped TWM with tapered ends and central stiffened squared hole: (a) in-plane displacement at mid-span. (b) warping at interface between sub-members 1-2. (c) warping at interface between sub-members 6-7.

5.2 Displacement-based GBT for composite TWMs

Composite TWMs can be analyzed within the GBT framework by following the procedure proposed in Chapter 4. The interaction between steel and concrete members composing the cross-section is introduced by placing N_{sc} connectors along rectilinear lines at the interface location. They allow relative displacement (i.e., slips) in both longitudinal (i.e., along z) and transverse directions (i.e., along s), while separation between components is prevented. The composite action is included by means of linear elastic spring placed in correspondence of

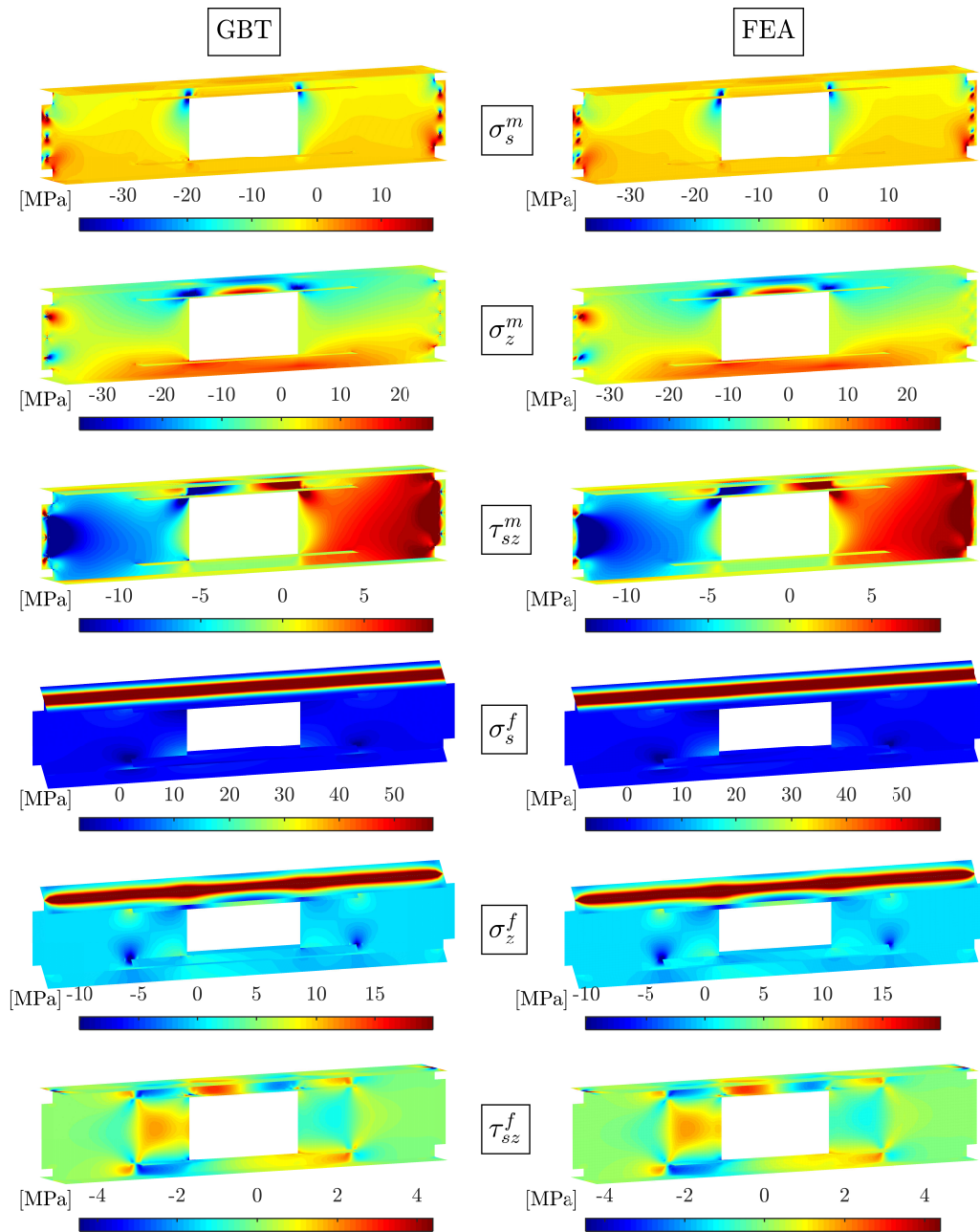


Figure 5.7: I-shaped TWM with tapered ends and central stiffened squared hole: stress distributions.

shear connectors. Within this arrangement, obtained trial functions automatically include the longitudinal and transverse partial interaction behavior. To prevent separation and interpenetration between adjacent components, internal constraints specified in Eqs. (4.32) and (4.33) are included in the PEP. They are in number $2N_{sc}$ and they prescribe shear connectors to be (i) axially inextensible, and (ii) undeformable under flexure. As a consequence, obtained planar trial functions $\varphi_k(z)$ are in number $N_p = K_p - 2N_{sc}$ (i.e., $\varphi(z)$ is a $N_p \times 1$ vector).

As a result of the inclusion of internal constraints into the PEP, planar nodal DOF belonging to the n -th shear connector ($n = 1, \dots, N_{sc}$) and linking the i -th and j -th components obey the

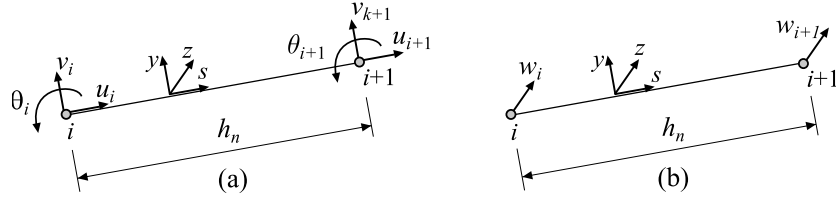


Figure 5.8: Shear connector element. (a) in-plane nodal DOF; (b) out-of-plane (warping) nodal DOF.

following constraint conditions (Fig. 5.8):

$$u_j - u_i = 0 \quad (5.21a)$$

$$\theta_j - \theta_i = 0 \quad (5.21b)$$

Eq. (5.21) can be re-written in compact form as follows:

$$\mathbf{A}_{sc} \mathbf{u}(z) = 0 \quad (5.22)$$

being \mathbf{A}_{sc} a $2N_{sc} \times K_p$ coefficient matrix. As a consequence, variable transformation defined in Eqs. (5.8) and (5.9) must be solved with respect to a reduced number of planar nodal DOF. This can be achieved by suiting Eq. (5.22) in order to identify $2N_{sc}$ “slave” planar nodal DOF $\mathbf{u}_S(z)$ to be expressed in terms of the N_p “master” planar nodal DOF $\mathbf{u}_M(z)$. After the latter have been isolated, Eqs. (5.8) and (5.9) are rewritten as:

$$\mathbf{Q}_{pM} \boldsymbol{\varphi}(z) = \mathbf{u}_M(z) \quad (5.23)$$

$$\begin{bmatrix} \mathbf{Q}_{pM} & \mathbf{0}_{N_p}^{K_w} \\ \mathbf{Q}_{\Omega} & \mathbf{Q}_w \end{bmatrix} \begin{bmatrix} \boldsymbol{\varphi}'(z) \\ \boldsymbol{\psi}(z) \end{bmatrix} = \begin{bmatrix} \mathbf{u}'_M(z) \\ \mathbf{w}(z) \end{bmatrix} \quad (5.24)$$

where \mathbf{Q}_{pM} is a $N_p \times N_p$ matrix collecting the nodal values of planar trial functions corresponding to master planar nodal DOF. Analogously to as described in previous Section, a variable transformation can be defined by means of Eqs. (5.23) and (5.24), in particular:

$$\boldsymbol{\varphi}(z) = \mathbf{T}_{pM} \mathbf{u}_M(z) \quad (5.25a)$$

$$\boldsymbol{\varphi}'(z) = \mathbf{T}_{pM} \mathbf{u}'_M(z) \quad (5.25b)$$

$$\boldsymbol{\psi}(z) = \mathbf{T}_w \mathbf{w}(z) + \mathbf{T}_{wpM} \mathbf{u}'_M(z) \quad (5.25c)$$

where:

$$\mathbf{T}_{pM} = \mathbf{Q}_{pM}^{-1}; \quad \mathbf{T}_w = \mathbf{Q}_w^{-1}; \quad \mathbf{T}_{wpM} = -\mathbf{T}_w \mathbf{Q}_{\Omega} \mathbf{T}_{pM} \quad (5.26a-c)$$

By making use of Eq. (5.25), the weak form of the elasticity problem can be rewritten as follows:

$$\int_{\mathcal{L}} \left\{ \delta \mathbf{u}_M^T \mathbf{T}_{pM}^T (\mathbf{B} \mathbf{T}_{pM} \mathbf{u} + \mathbf{F}^T \mathbf{T}_M \mathbf{d}'_M - \mathbf{q}_1) + \delta \mathbf{d}'_M^T \mathbf{T}_M^T (\mathbf{F} \mathbf{T}_{pM} \mathbf{u}_M + \mathbf{C} \mathbf{T}_M \mathbf{d}'_M) + \right. \\ \left. + \delta \mathbf{d}_M^T \mathbf{T}_M^T (\mathbf{D} \mathbf{T}_M \mathbf{d}_M - \mathbf{q}_2) \right\} dz - \sum_B (\delta \mathbf{u}_M^T \mathbf{T}_{pM}^T \mathbf{P}_1 + \delta \mathbf{d}_M^T \mathbf{T}_M^T \mathbf{P}_2) = 0 \quad (5.27)$$

where:

$$\mathbf{d}_M(z) = \begin{bmatrix} \mathbf{u}'_M(z) \\ \mathbf{w}(z) \end{bmatrix}; \quad \mathbf{T}_M = \begin{bmatrix} \mathbf{T}_{pM} & \mathbf{0}_{N_p}^{K_w} \\ \mathbf{T}_{wpM} & \mathbf{T}_w \end{bmatrix} \quad (5.28a,b)$$

In Eq. (5.27), relevant structural matrices \mathbf{B} , \mathbf{C} , \mathbf{D} and \mathbf{F} include the work done by the (longitudinal and transverse) shear forces along interfaces between components and are detailed in Appendix D. Starting from Eq. (5.27), the set of $K^* = N_p + K_w$ displacement-based GBT equations is solved numerically, as commonly done in the Literature, by means of a Finite Element (FE) procedure (e.g., Bathe, 2014). The member is discretized into N_E finite elements and following descriptions are adopted for approximating the unknowns:

$$\mathbf{u}_M(z) \cong \mathbf{H}(z) \mathbf{u}_{EM}; \quad \mathbf{w}(z) \cong \mathbf{L}(z) \mathbf{w}_E \quad (5.29)$$

where \mathbf{u}_{EM} and \mathbf{w}_E are $4N_p \times 1$ and $3K_w \times 1$ vectors, respectively, collecting values of unknown functions at nodes of the member FE, while $\mathbf{H}(z)$ and $\mathbf{L}(z)$ are $N_p \times 4N_p$ and $K_w \times 3K_w$ matrices, respectively, collecting Hermite cubic and Lagrange parabolic polynomial interpolating functions, respectively. After performing the standard steps of the FE procedure, the following stiffness relationship can be obtained for each GBT-based FE:

$$\mathbf{K}_E \mathbf{x}_{EM} = \mathbf{q}_E \quad (5.30)$$

where \mathbf{x}_{EM} is a $(4N_p + 3K_w) \times 1$ vector collecting values of unknown functions at nodes of the member FE, while \mathbf{K}_E and \mathbf{q}_E are $(4N_p + 3K_w) \times (4N_p + 3K_w)$ stiffness matrix and $(4N_p + 3K_w) \times 1$ load vector, respectively, defined in Eq. (5.20). Slave planar nodal DOF $\mathbf{u}_S(z)$, which have been removed at the beginning of the procedure, can be finally calculated starting from master ones. In fact, after partitioning Eq. (5.22) as:

$$[\mathbf{A}_{scM} \quad \mathbf{A}_{scS}] \begin{bmatrix} \mathbf{u}_M \\ \mathbf{u}_S \end{bmatrix} = \mathbf{0} \quad (5.31)$$

and assuming \mathbf{A}_{scS} to be a non-singular matrix, the following holds:

$$\mathbf{u}_S(s) = -\mathbf{A}_{scS}^{-1} \mathbf{A}_{scM} \mathbf{u}_M(s) \quad (5.32)$$

The capabilities and ease-to-use of the proposed displacement-based GBT approach for composite TWM with large web perforations are outlined by means of an illustrative example. It consists on the linear elastic analysis of a composite member taken from Mills (2001). It is composed by a concrete slab with thickness 120 mm and an I-shaped steel member type 410UB53.7 (Fig. 5.9a), whose dimensions are shown in Fig. 5.9b. The interaction between steel and concrete members is included by means of one shear connector in the cross-section, as shown in Fig. 5.9b. The beam is 10.5 m long and it is assumed to be simply supported, with boundary conditions restraining the warping of the composite section at the member mid-span and the in-plane displacements at the end supports (Fig. 5.9c). The external load consists of a 30 kPa uniform pressure load applied to the right-hand half of the concrete slab as illustrated in Fig. 5.9a. The beam possesses four web penetrations with dimensions 225 mm \times 440 mm, equally spaced along the member length. Regarding these latter, two configurations have been considered, namely: (i) Set 01, where web penetrations are unstiffened, as shown in Fig. 5.10a,

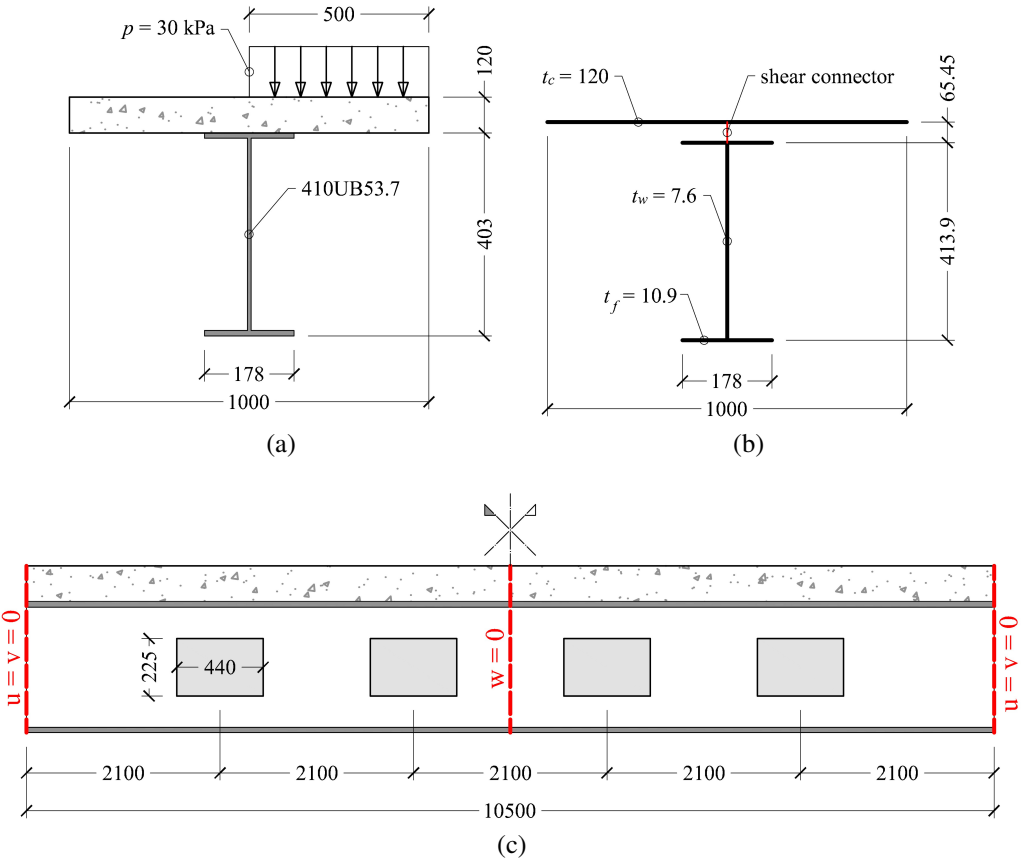


Figure 5.9: Composite TWB with web penetrations (from Mills, 2001). (a) Cross-section geometry and load arrangement; (b) cross-section idealization and shear connectors definition; (c) member geometry and constraints.

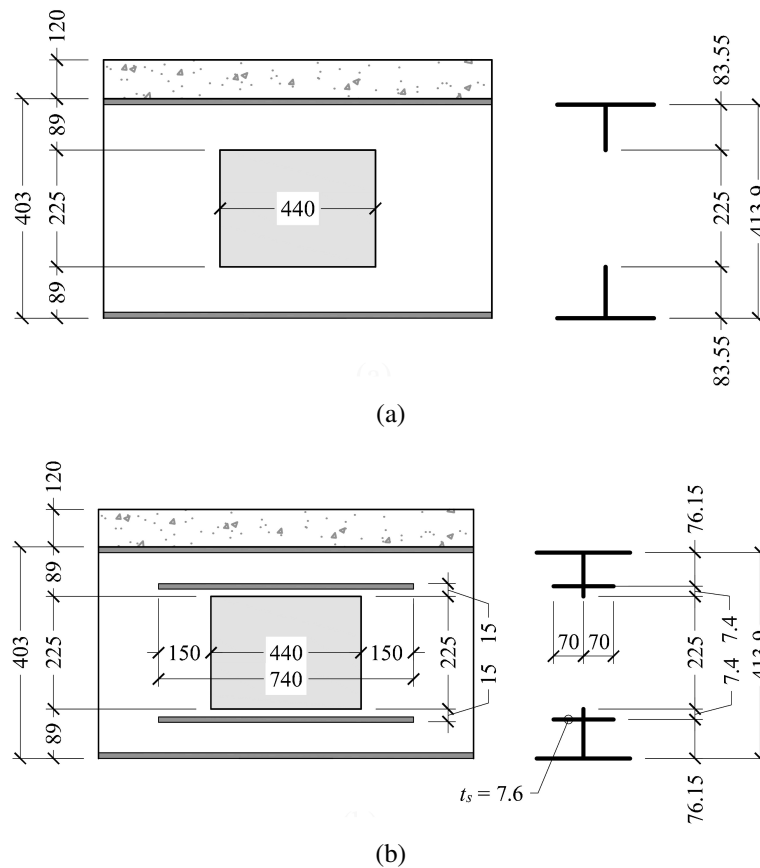


Figure 5.10: Geometry of web penetrations. (a) Set 01: unstiffened penetrations. (b) Set 02: stiffened penetrations.

and (ii) Set 02, where web penetrations are reinforced by means of longitudinal stiffeners placed on both sides of the web, as illustrated in Fig. 5.10b. The material properties adopted in the simulation specify an elastic modulus of 35 GPa and 200 GPa for the concrete and steel, respectively, and corresponding Poisson's ratios of 0.2 and 0.3, respectively. Different levels of shear connection rigidities are considered in the following to highlight their influence on the partial interaction behavior of the composite member. Similarly to as done in Chapter 4, the former are expressed in term of dimensionless parameters $\alpha_L \mathcal{L}$ and $\alpha_T \mathcal{L}$ (\mathcal{L} being the member length) as regards the interaction in the longitudinal and transverse directions, respectively, as commonly provided in the Literature for two-layered composite beams (e.g., Girhammar and Gopu, 1993). In particular, results are provided in the following for weak shear connection (i.e., $\alpha_L \mathcal{L} = 1$, $\alpha_T \mathcal{L} = 1$), medium shear connection (i.e., $\alpha_L \mathcal{L} = 5$, $\alpha_T \mathcal{L} = 5$) and strong shear connection (i.e., $\alpha_L \mathcal{L} = 20$, $\alpha_T \mathcal{L} = 20$). Results calculated with the proposed GBT approach have been compared with those determined with a shell element model developed in the software ABAQUS/Standard (Simulia, 2010), where the general purpose shell element S4 has been adopted for plate segments. All materials have been modeled as linear-elastic isotropic. The shear connection is implemented through the ABAQUS planar connection type, which is able to allow relative displacement on the selected plane and avoid relative displacement along the direction normal to that plane. In order to describe the continuous interface connection

model formulated in the GBT approach, closely-spaced wires spread along the rectilinear lines of the shear connection have been specified. The planar connection type has been assigned to each wire with the uncoupled constitutive relationship described in Eq. (4.37), where involved rigidities are obtained by multiplying the distributed spring stiffness k_T^n (k_L^n) adopted in the GBT model by the wire (longitudinal) spacing.

The global displacement-based GBT FE model is obtained by assembling the contribution of each sub-member composing the composite TWM. Differently to as required in standard GBT approaches, no constraint equations have been adopted in the proposed procedure. The solution is first obtained in terms of warping and planar master nodal variables, then planar slave DOF are calculated by post-processing the planar master ones. The case of TWM with unstiffened web penetrations (i.e., Set 01) is first analyzed. Comparisons between the GBT and ABAQUS results are presented in Figs. 5.11 and 5.12 in terms of membrane and flexural stresses, respectively. They have been obtained for the case of medium shear connection (i.e., $\alpha_L \mathcal{L} = 5$, $\alpha_T \mathcal{L} = 5$) and they are representative of all shear connection levels. Flexural stresses shown in Fig. 5.12 refer to surfaces characterized by $y = +t/2$, being t the plate thickness of walls composing the cross-section. The accuracy of results obtained with the proposed displacement-based GBT approach is remarkable. It is worth to be pointed out that membrane and flexural stresses depict different behavior in the neighborhood of web penetration. In particular, the membrane stresses significantly increase close to the edges and the corners of the holes, while the membrane stresses in the steel flanges and the concrete slab do not seem to be affected by the holes. On the contrary, flexural stresses depict strong variations on steel flanges and concrete slabs; they are, as expected, moderately influenced by holes on steel web since this latter is not subject to bending. This particular phenomenon seems to be confirmed by the longitudinal trend of membrane and flexural stresses illustrated in Figs. 5.13 and 5.14, respectively. In those diagrams, stresses in two representative points of the composite cross-section have been plotted in terms of their variation along the beam length. To show the accuracy of the obtained GBT results, stress distributions on the cross-section have been illustrated in correspondence of two member coordinates, referred to as sections A-A and B-B, whose positions along the beam length are highlighted on corresponding longitudinal plots. Reported results have been obtained for the case of medium shear connection (i.e., $\alpha_L \mathcal{L} = 5$, $\alpha_T \mathcal{L} = 5$), however their trend is representative of all shear connection levels. Results obtained with the proposed displacement-based GBT approach are in very good agreement with the ones obtained with ABAQUS. Large web penetrations induce significant stress concentrations in their neighborhoods. In particular, membrane stresses are mostly influenced on the web of steel member, that is very close to web penetrations (see, e.g., black curves in Fig. 5.13), while the influence of holes is negligible on the steel flange (see, e.g., blue curves in Fig. 5.13). On the contrary, flexural stresses significantly raises on the steel flange as consequence of web penetration (see, e.g., blue curves in Fig. 5.13), while their variation on the steel web (i.e., very close to web penetration) is less significant (see, e.g., black curves in Fig. 5.14).

Results for the case with stiffened web penetrations (i.e., Set 02) are reported in Fig. 5.15, where stress distributions in the neighborhood of the first web penetration have been shown for illustrative purposes. Similarly to the case of the unstiffened penetrations, the membrane stresses in the concrete slab and the steel flanges seem unaffected by the holes. On the contrary, they depict strong concentrations in correspondence of holes and stiffeners. Flexural stresses

are instead strongly influenced by penetrations almost everywhere on the cross-section. Similar considerations can be deduced from Figs. 5.16 and 5.17, where trends along the beam axis of stresses have been reported in two representative points of the composite cross-section. Obtained results concern the case of medium shear connection (i.e., $\alpha_L \mathcal{L} = 5$, $\alpha_T \mathcal{L} = 5$) and are representative of all shear connection levels. The agreement between ABAQUS and the proposed GBT approach is excellent.

The influence of shear connection levels is outlined in Figs. 5.18 and 5.19, as regards the case of unstiffened web penetrations (i.e., Set 01), and Figs. 5.20 and 5.21, as regards the case of stiffened web penetrations (i.e., Set 02). In particular, the trend along z of the vertical deflection v is shown in Figs. 5.18 and 5.20 as regards Set 01 and Set 02, respectively, while distributions along the member axis of the longitudinal slip depicted at the interface connection are reported in Figs. 5.19 and 5.21 concerning Set 01 and Set 02, respectively. The in-plane displacements w and longitudinal membrane stress σ_z^m are plotted in Figs. 5.18 and 5.20 for Set 01 and Set 02, respectively, in correspondence of two member coordinates, referred to as sections A-A and B-B and corresponding to the mid coordinate of the second web penetration and the beam mid-span, respectively. Warping distribution w and membrane tangential stress τ_{sz}^m are illustrated in Figs. 5.19 and 5.21 for Set 01 and Set 02, respectively, in correspondence of the left support (i.e., section A-A) and the mid-coordinate of the first web penetration (i.e., section B-B). It is specified that warping displacement w , longitudinal membrane stress σ_z^m and membrane tangential stress τ_{sz}^m are plotted in Figs. 5.18 to 5.21 as a diagram, with values directed along the y -axis (i.e., by using the y -axis convention). As expected, the composite TWM with lower shear connection rigidities undergoes larger deflections than the member with stiffer interface properties, as well depicted in Figs. 5.18 and 5.20. In case of weak shear connection, the interaction between components is negligible and strong slips take place at the interface connection. Steel and concrete components behave therefore independently. Considering that the concrete slab possesses low flexural (and shear) rigidity in the plane of bending, the structural response is mainly resisted by the relatively stiffer I-shaped steel profile. This behavior is well depicted by observing the shape of membrane stresses σ_z^m (Figs. 5.18 and 5.20), warping and membrane shear stresses τ_{sz}^m (Figs. 5.19 and 5.21). In particular, it is evident that the cross-section neutral axis almost coincides with the major bending axis of the steel I-shaped component. For medium shear connection, components forming the cross-section start to interact, as highlighted by warping profile and relevant stress distributions (i.e., σ_z^m and τ_{sz}^m), evidencing that the neutral axis has moved closer to the concrete slab. Similar considerations can be made for the case of strong shear connection rigidities.

Finally, the influence of large web penetrations is shown in Figs. 5.22 and 5.23, where trends along the member axis of vertical deflection and longitudinal membrane strains, respectively, are reported in one significant point within the cross-section for the cases of unperforated beam, unstiffened (i.e., Set 01) and stiffened (i.e., Set 02) penetrations considering different levels of shear connection rigidities. As expected, TWM with unstiffened web penetrations depict larger deflections than the unperforated ones (Fig. 5.22). This phenomenon seems to become more significant with increasing the shear rigidity of connections placed at the interface. On the contrary, TWM with stiffened web penetrations (i.e., Set 02) depict the same deflection of unperforated TWM for all shear connection rigidities (Fig. 5.22). Therefore, the use of longitudinal stiffeners for reinforcing large web penetrations seems to be a very efficient way to limit

the lost in terms of flexural and shear rigidities in the plane of the cross-section caused by web holes. Similar considerations can be made by analyzing the trend of longitudinal membrane strain depicted in Fig. 5.23. As a consequence of web penetrations, longitudinal membrane strain manifest a significant increase with respect to the case of unperforated member in correspondence of holes in case the latter are unstiffened (i.e., Set 01). Contrariwise, longitudinal strains remains equal or even lesser than the ones depicted by the unperforated TWM when web perforations are stiffened (i.e., Set 02). As shown in Fig. 5.23, this behavior is independent from the shear rigidity level depicted by connectors. It points out the fact that longitudinal stiffeners are efficient in limiting the strain concentration phenomenon in the neighborhood of web holes.

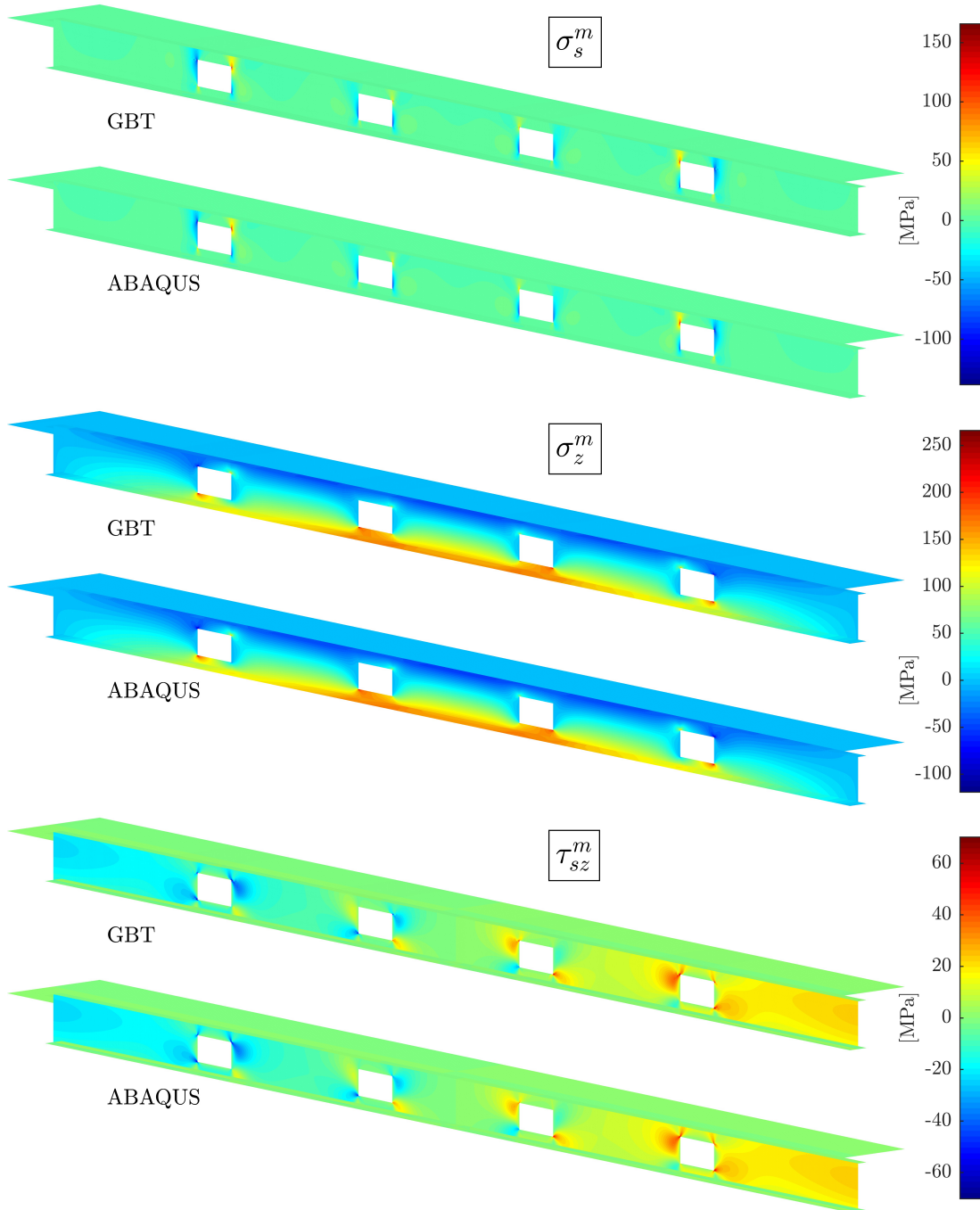


Figure 5.11: Composite TWB with unstiffened penetrations (Set 01). Global distributions of membrane stress fields for the case of medium shear connection ($\alpha_L \mathcal{L} = 5$, $\alpha_T \mathcal{L} = 5$).

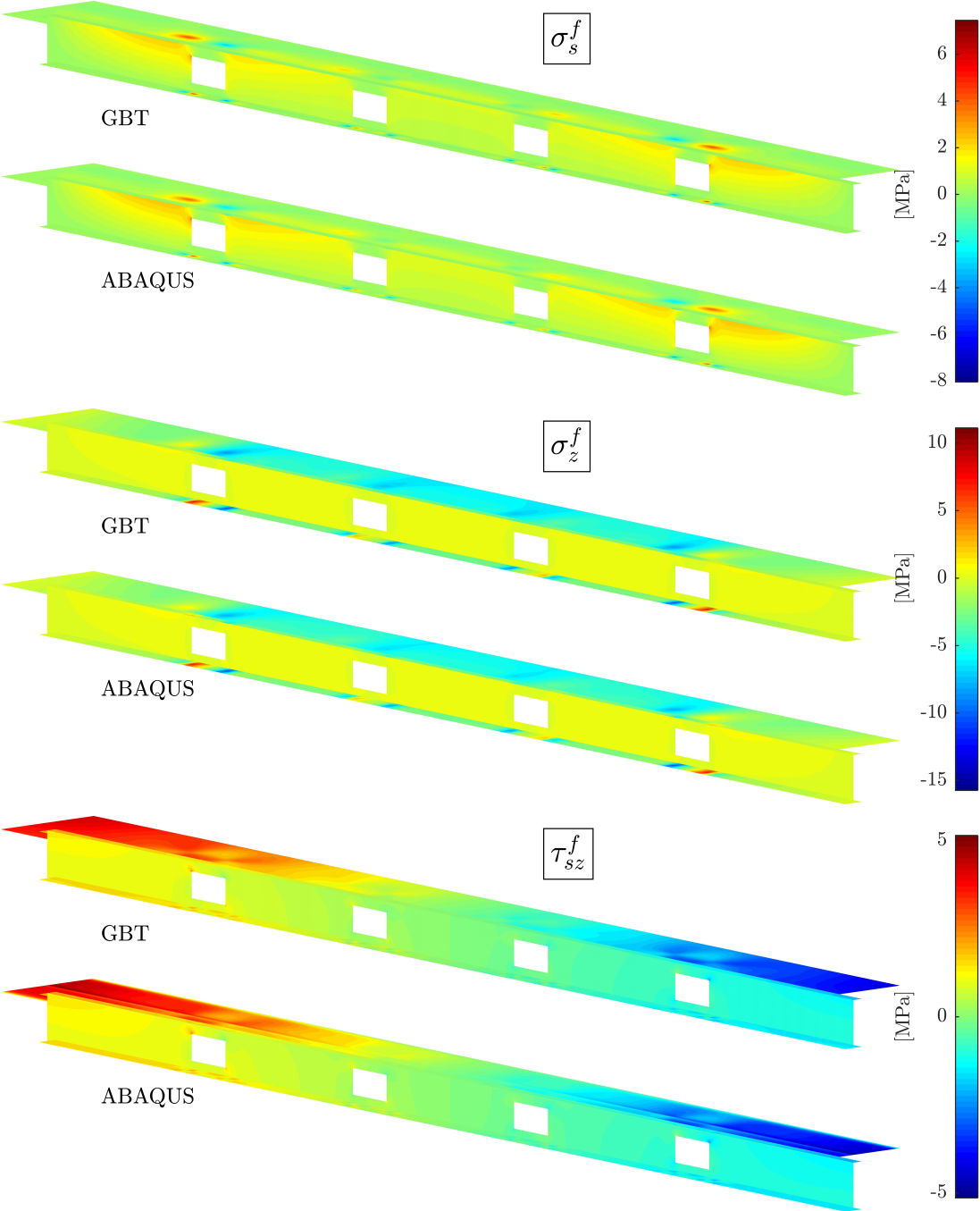


Figure 5.12: Composite TWB with unstiffened penetrations (Set 01). Global distributions of flexural stress fields for the case of medium shear connection ($\alpha_L \mathcal{L} = 5$, $\alpha_T \mathcal{L} = 5$).

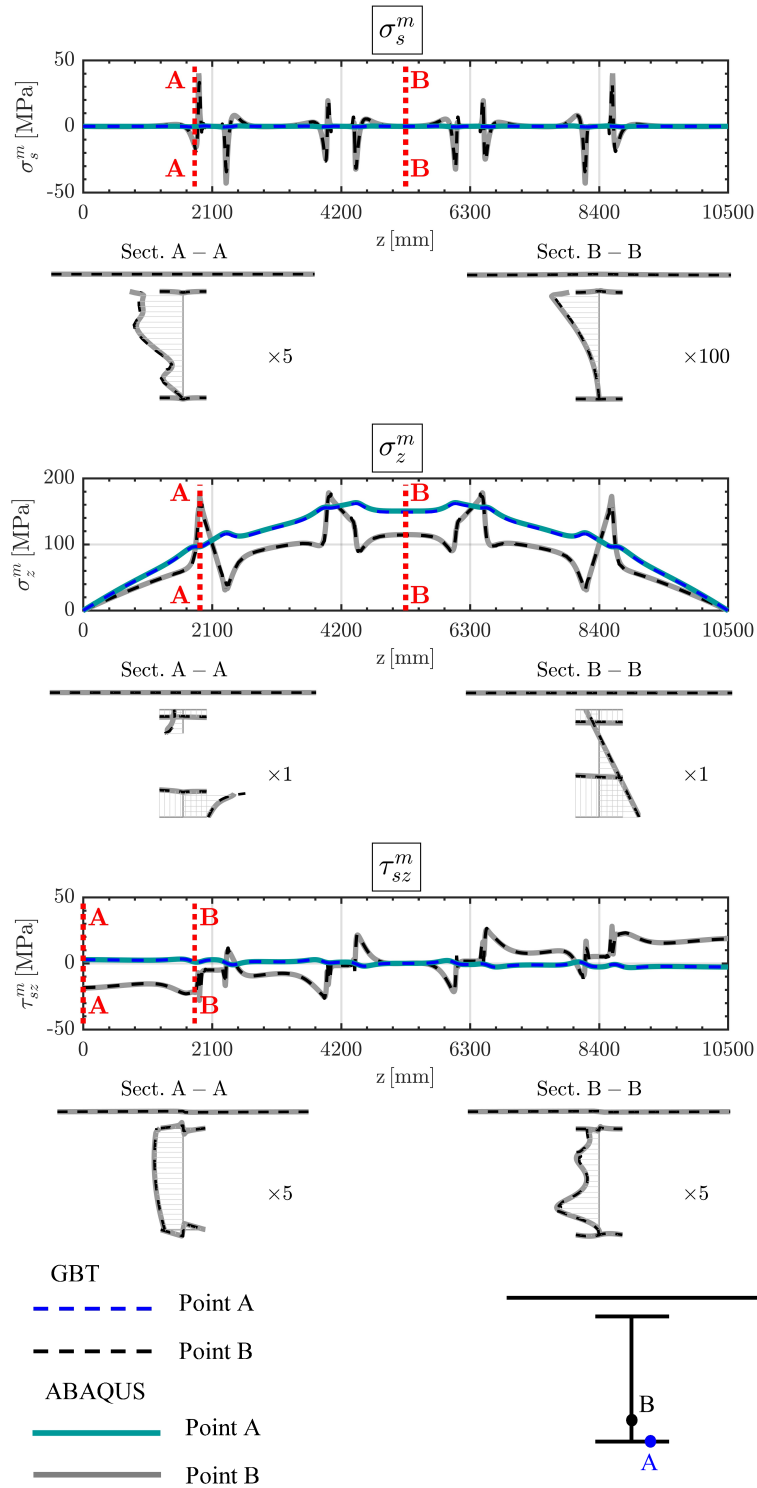


Figure 5.13: Composite TWB with unstiffened penetrations (Set O1). Representative trends along z and cross-section distributions of membrane stress fields for the case of medium shear connection ($\alpha_L \mathcal{L} = 5$, $\alpha_T \mathcal{L} = 5$).

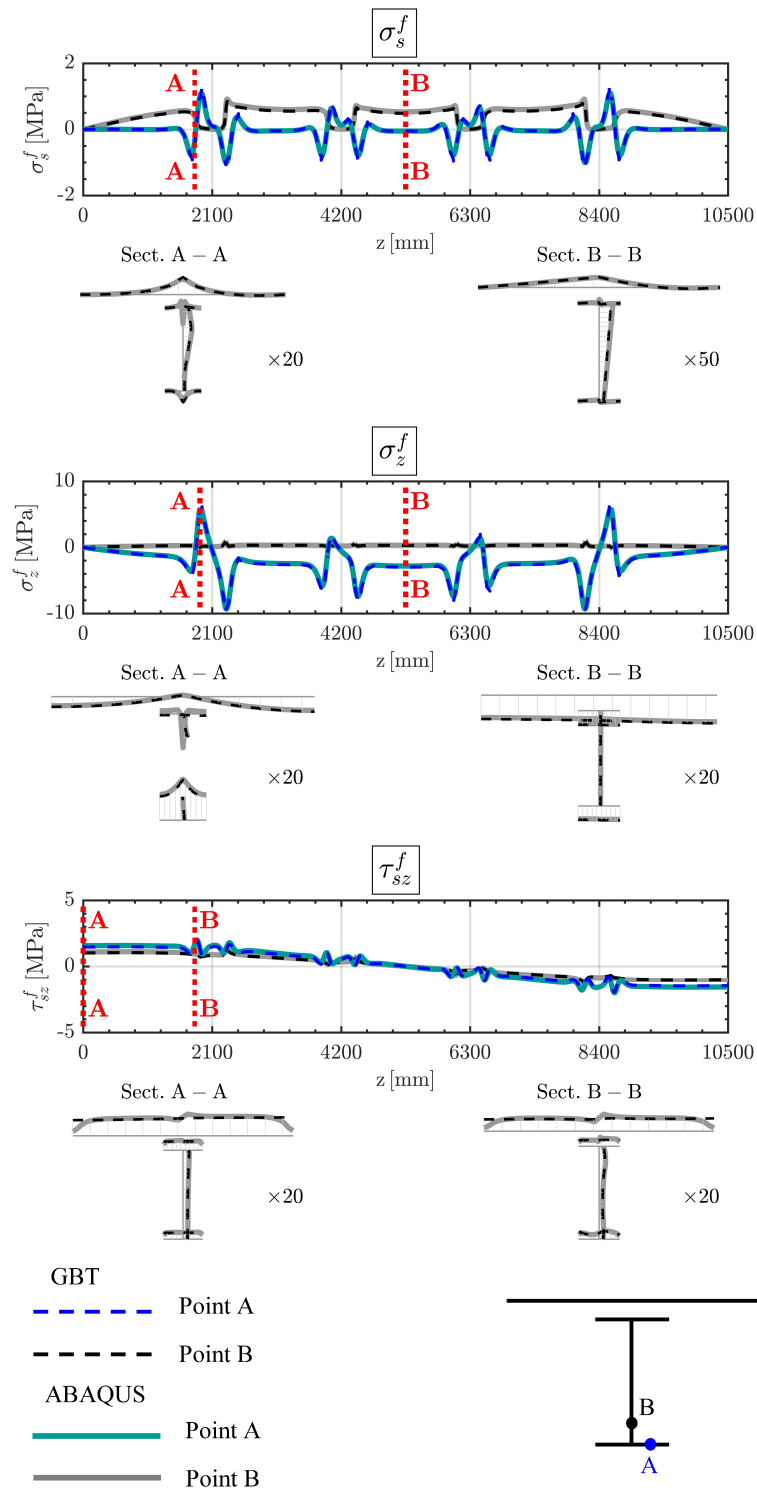


Figure 5.14: Composite TWB with unstiffened penetrations (Set 01). Representative trends along z and cross-section distributions of flexural stress fields for the case of medium shear connection ($\alpha_L \mathcal{L} = 5$, $\alpha_T \mathcal{L} = 5$).

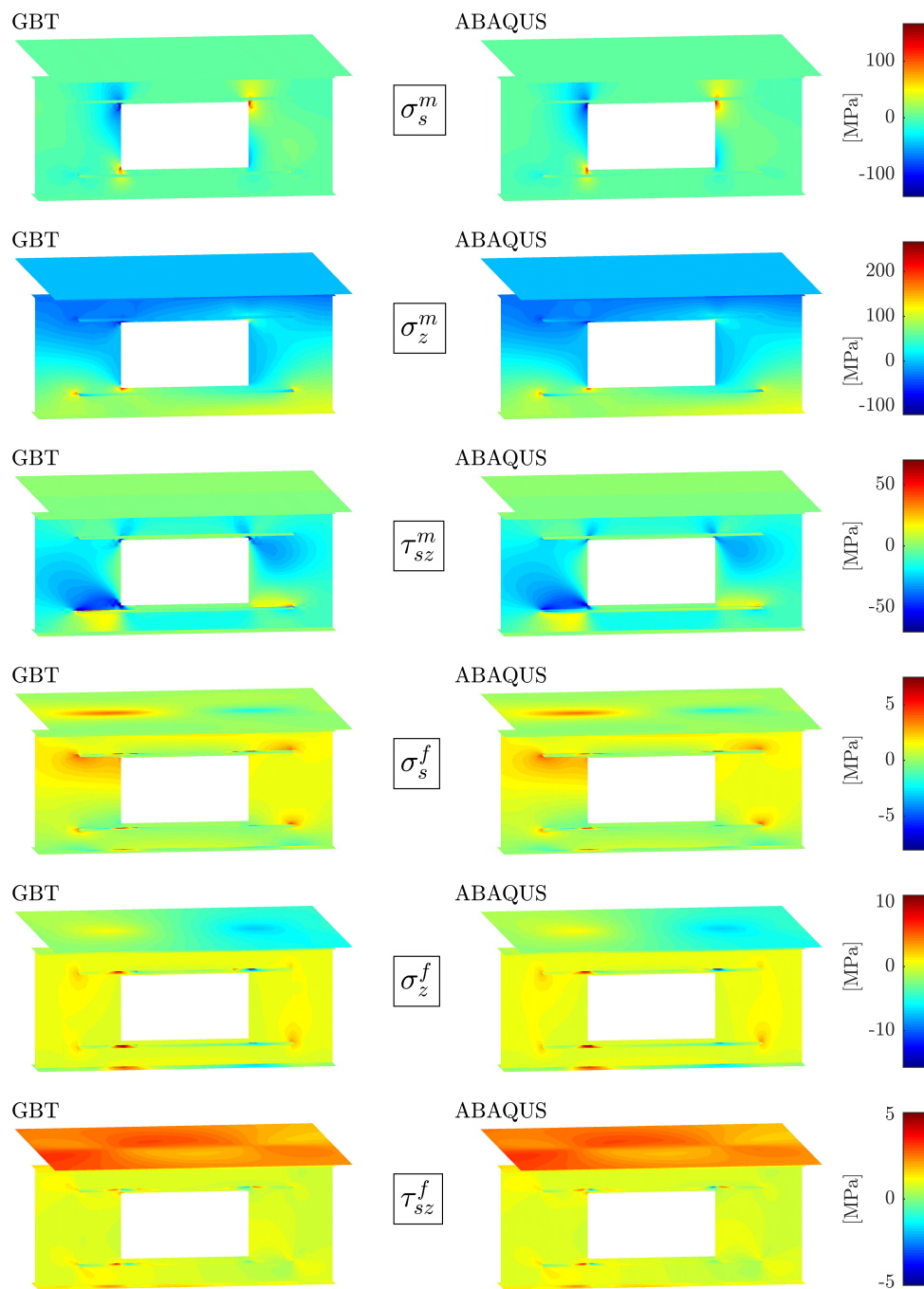


Figure 5.15: Composite TWB with stiffened penetrations (Set 02): stress fields in correspondence of the first penetration for the case of medium shear connection ($\alpha_L \mathcal{L} = 5$, $\alpha_T \mathcal{L} = 5$).

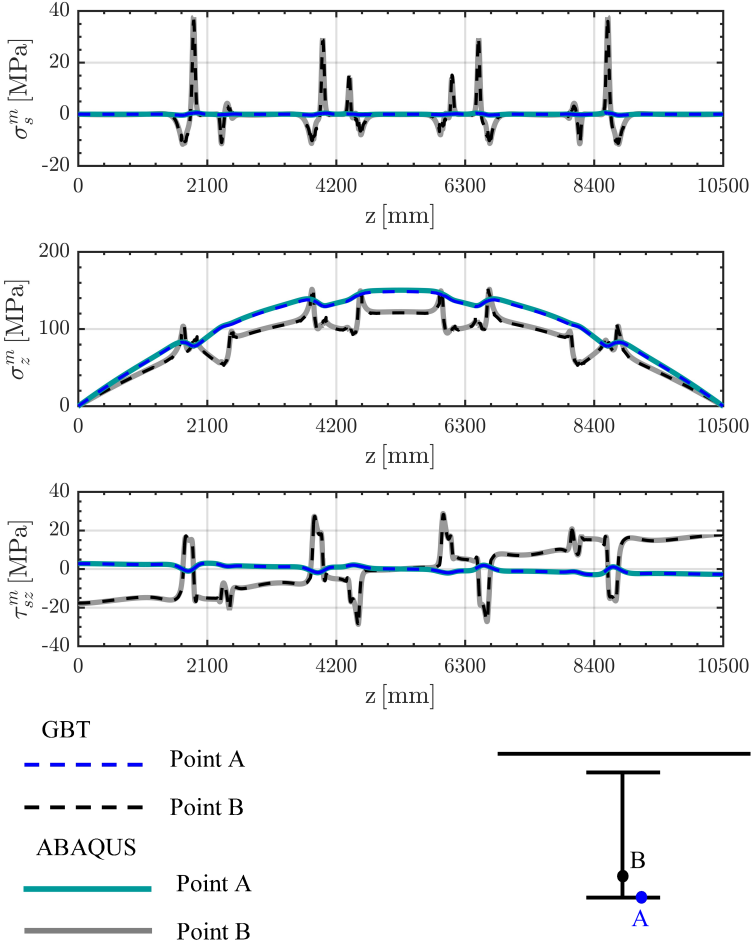


Figure 5.16: Composite TWB with stiffened penetrations (Set 02): trends along z of membrane stress fields in correspondence of the first penetration for the case of medium shear connection ($\alpha_L \mathcal{L} = 5$, $\alpha_T \mathcal{L} = 5$).

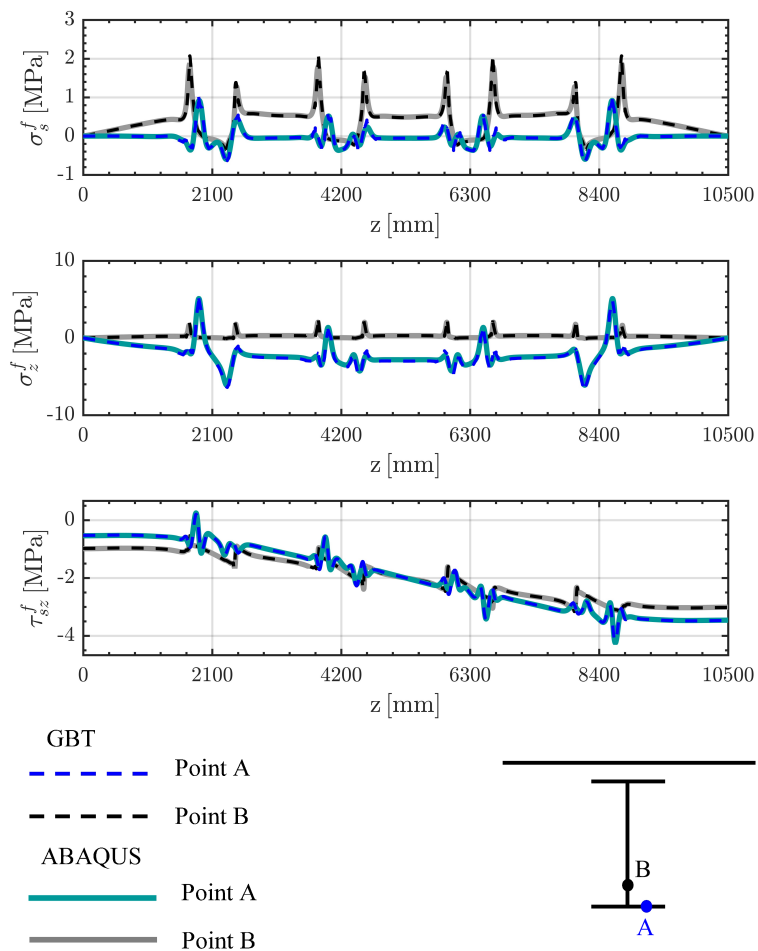


Figure 5.17: Composite TWB with stiffened penetrations (Set 02): trends along z of flexural stress fields in correspondence of the first penetration for the case of medium shear connection ($\alpha_L \mathcal{L} = 5$, $\alpha_T \mathcal{L} = 5$).

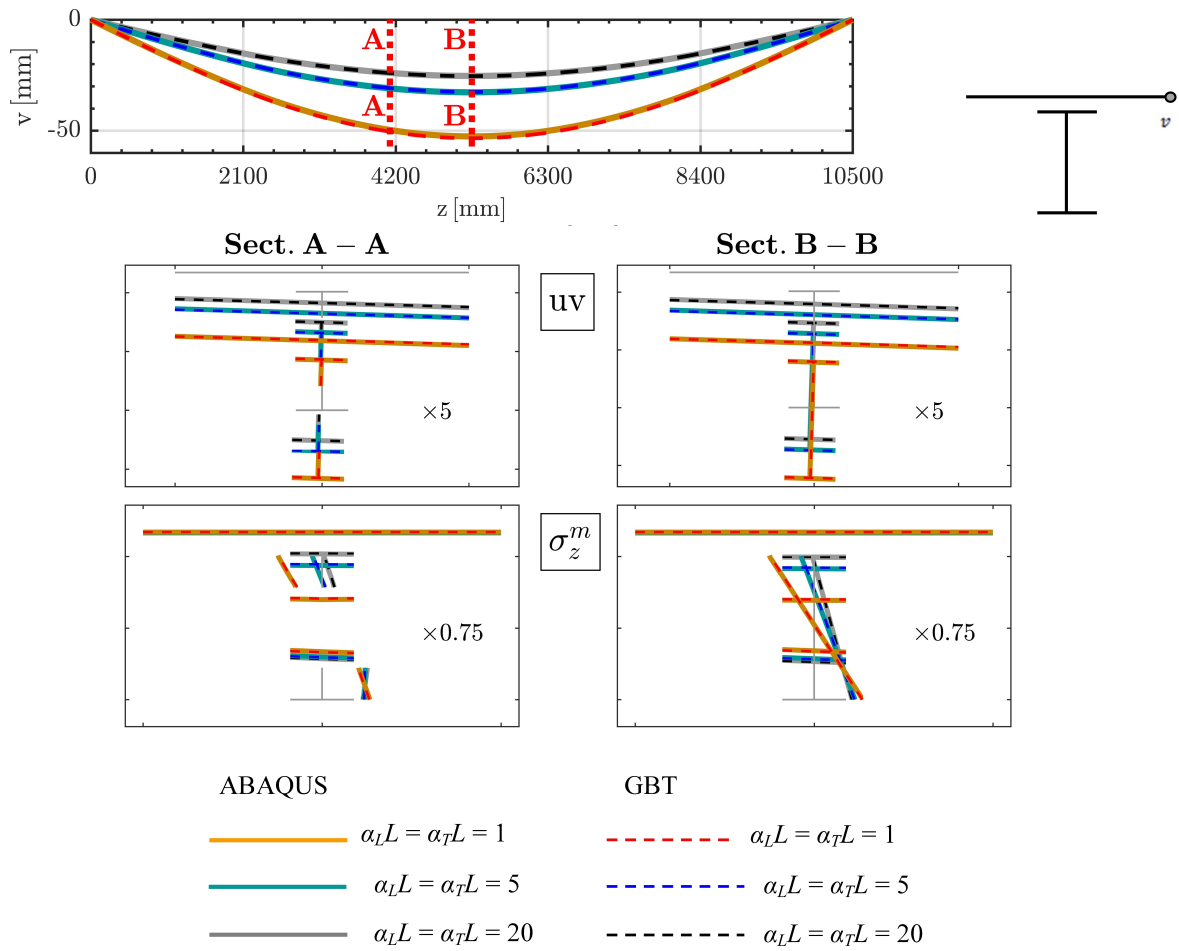


Figure 5.18: Composite TWB with unstiffened penetrations (Set 01). Trend along z of the overall deflection v for different levels of shear connection, in-plane displacement fields uv and membrane longitudinal stress distribution σ_z^m at specified locations along the beam axis. Note: σ_z^m displayed as a diagram, with values directed along the local y -axis.

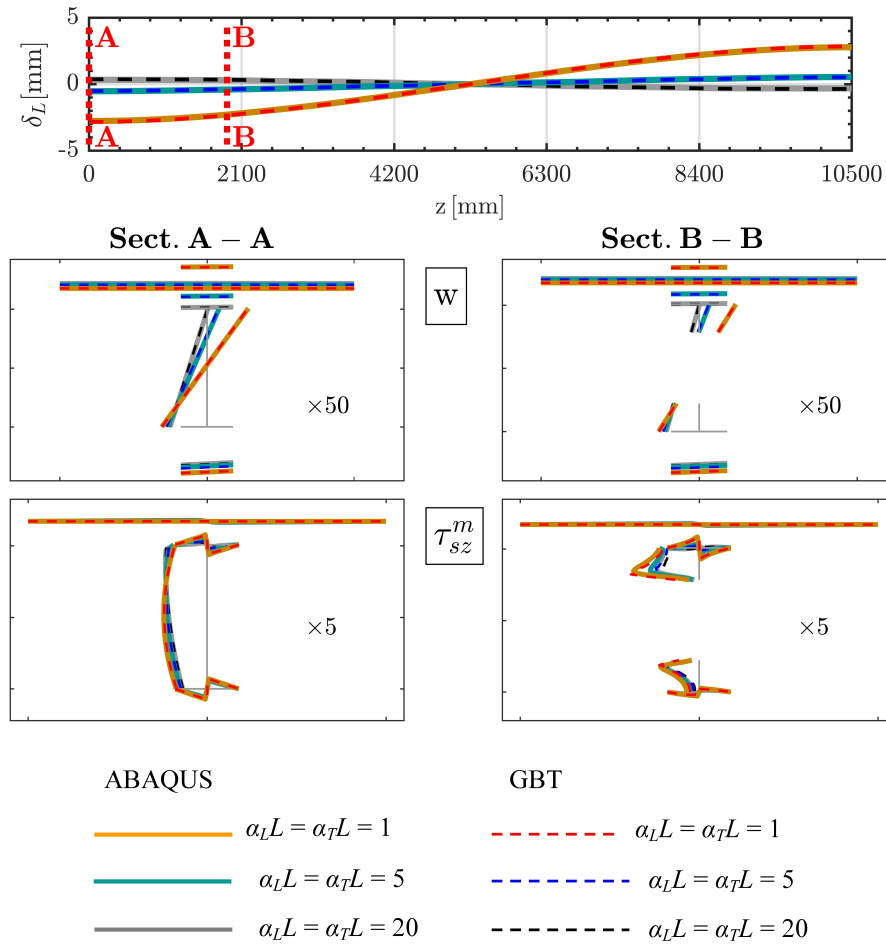


Figure 5.19: Composite TWB with unstiffened penetrations (Set 01). Trend along z of the longitudinal slip δ_L for different levels of shear connection, warping displacement fields w and membrane tangential stress distribution τ_{sz}^m at specified locations along the beam axis. Note: w and τ_{sz}^m displayed as a diagram, with values directed along the local y -axis.

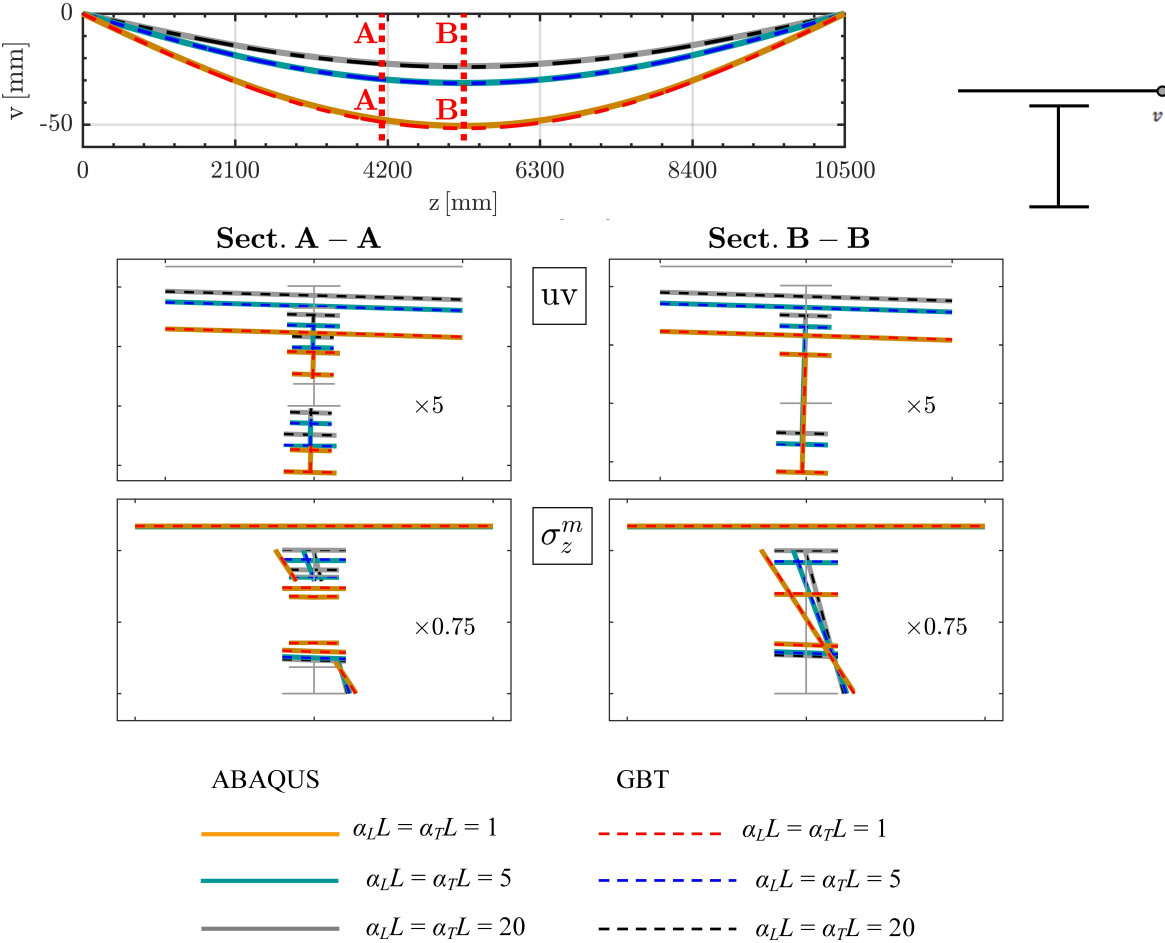


Figure 5.20: Composite TWB with stiffened penetrations (Set 02). Trend along z of the overall deflection v for different levels of shear connection, in-plane displacement fields uv and membrane longitudinal stress distribution σ_z^m at specified locations along the beam axis. Note: σ_z^m displayed as a diagram, with values directed along the local y -axis.

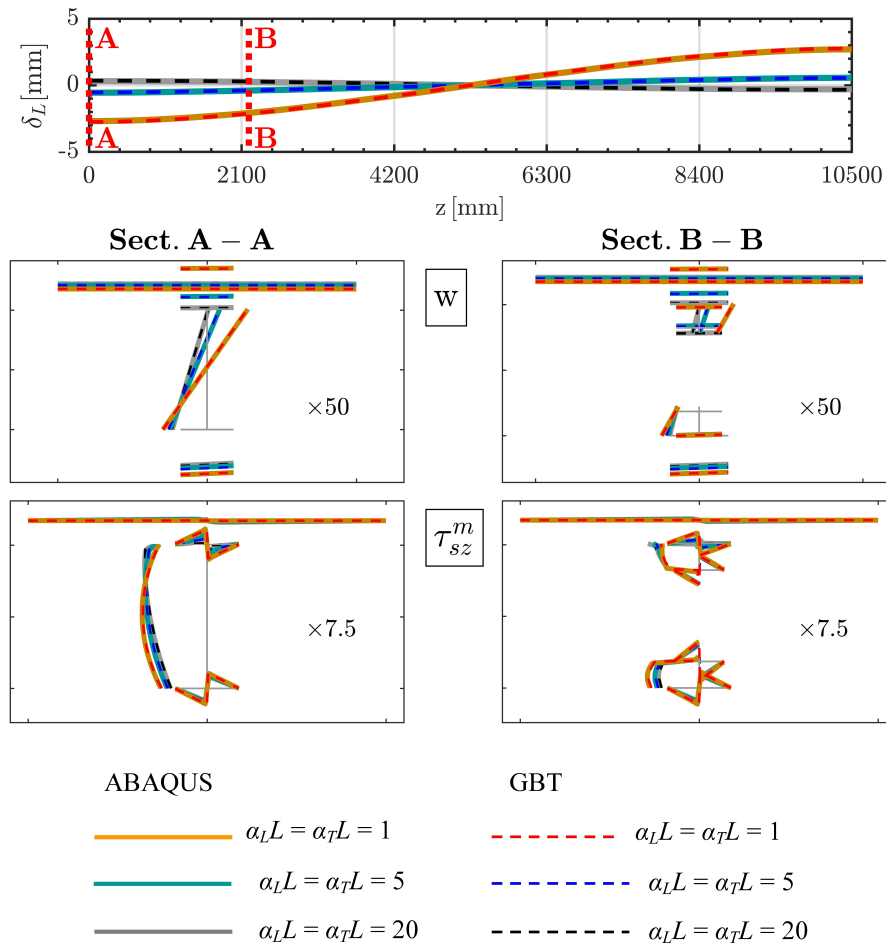


Figure 5.21: Composite TWB with stiffened penetrations (Set 02). Trend along z of the longitudinal slip δ_L for different levels of shear connection, warping displacement fields w and membrane tangential stress distribution τ_{sz}^m at specified locations along the beam axis. Note: w and τ_{sz}^m displayed as a diagram, with values directed along the local y -axis.

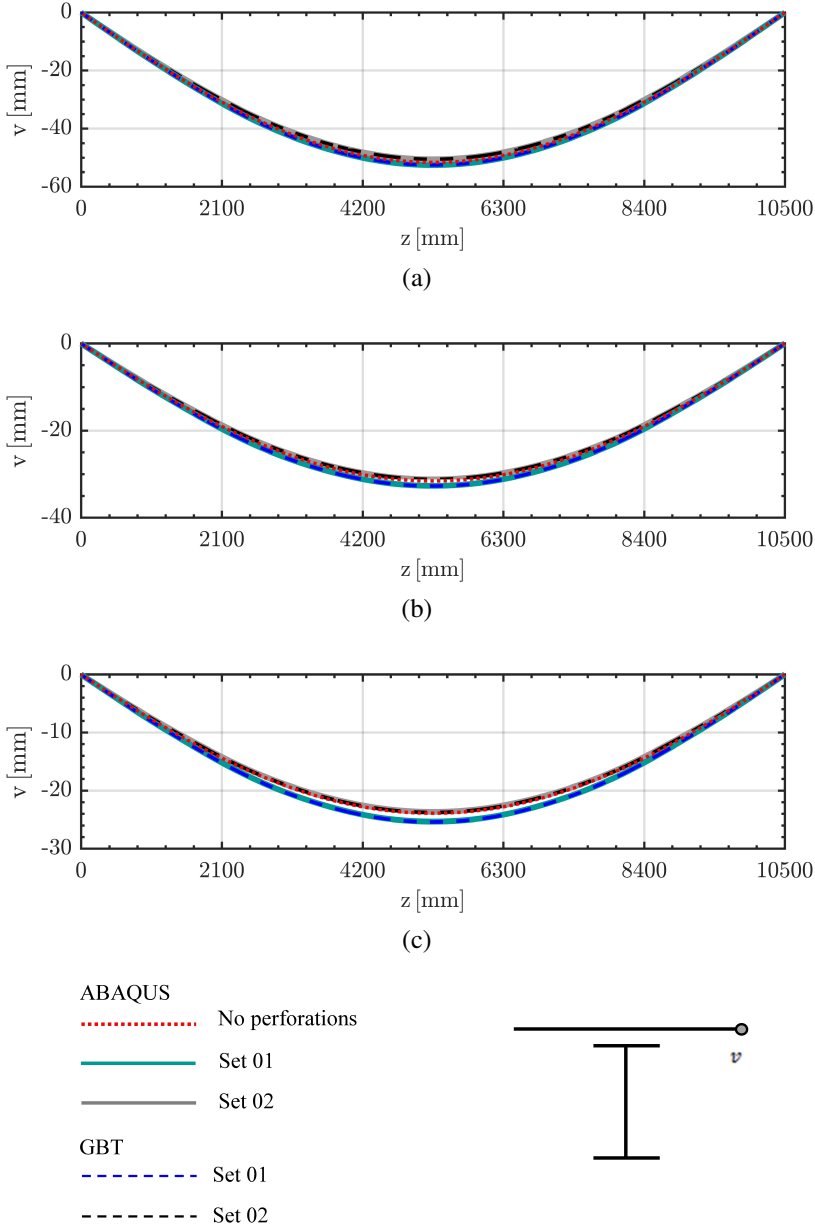


Figure 5.22: Comparison in terms of vertical deflection v between (i) unperforated TWB, (ii) TWB with unstiffened penetrations (Set 01) and (iii) TWB with stiffened penetrations (Set 02): (a) weak shear connection rigidity ($\alpha_L \mathcal{L} = 1, \alpha_T \mathcal{L} = 1$), (b) medium shear connection rigidity ($\alpha_L \mathcal{L} = 5, \alpha_T \mathcal{L} = 5$), (c) strong shear connection rigidity ($\alpha_L \mathcal{L} = 20, \alpha_T \mathcal{L} = 20$).

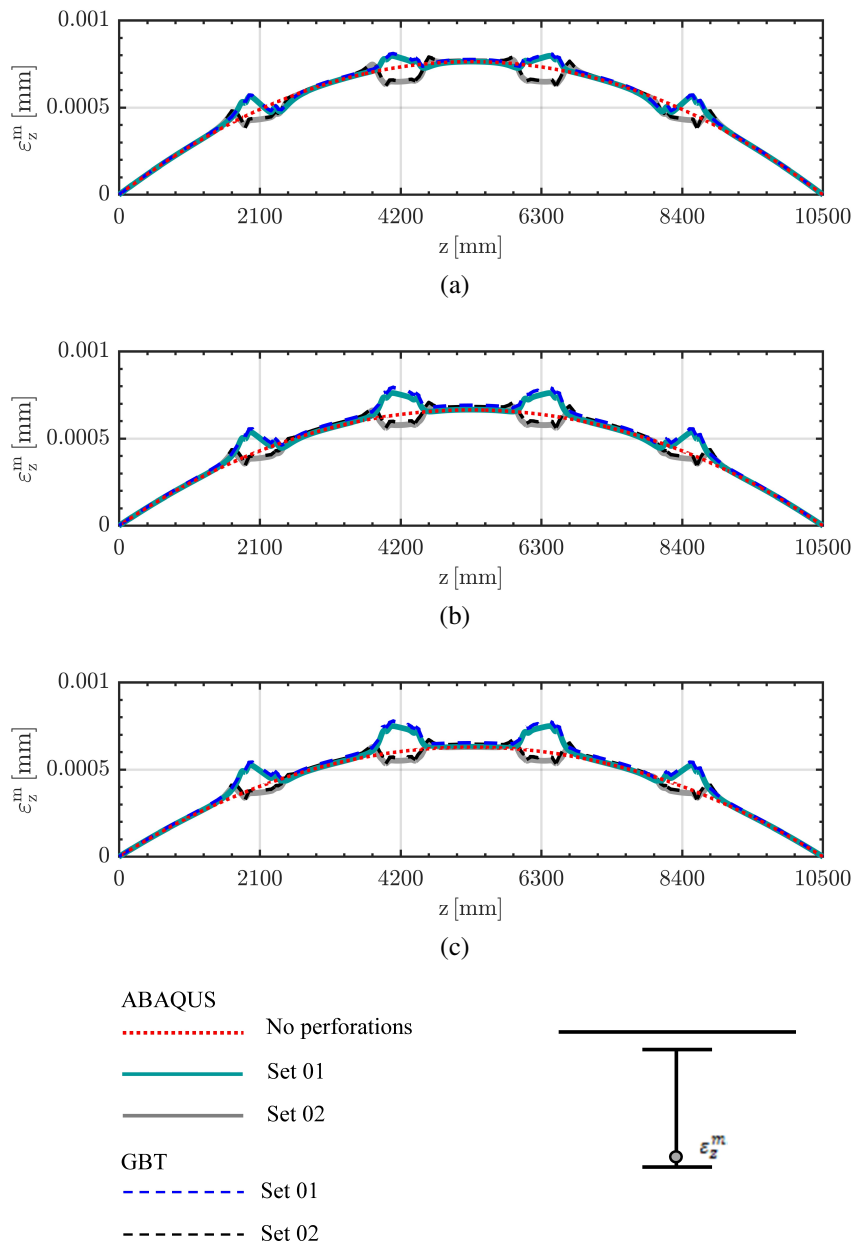


Figure 5.23: Comparison in terms of longitudinal membrane strain ε_z^m between (i) unperforated TWB, (ii) TWB with unstiffened penetrations (Set 01) and (iii) TWB with stiffened penetrations (Set 02): (a) weak shear connection rigidity ($\alpha_L \mathcal{L} = 1$, $\alpha_T \mathcal{L} = 1$), (b) medium shear connection rigidity ($\alpha_L \mathcal{L} = 5$, $\alpha_T \mathcal{L} = 5$), (c) strong shear connection rigidity ($\alpha_L \mathcal{L} = 20$, $\alpha_T \mathcal{L} = 20$).

Chapter 6

Nonlinear Generalized Beam Theory for arbitrary open and closed TWMs

The study of the geometrical nonlinear behavior of TWMs is of great interest for the analysis of elements potentially subject to large deformations (e.g. large deflections in cantilever beams) and of pre- and post-buckling equilibrium paths. In addition, the use of GBT models allows the study of local and global instabilities as a reliable and computationally efficient alternative to full numerical analysis through shell FE models or FSMs. The first geometrically nonlinear isotropic GBT formulation has been proposed in Silvestre and Camotim (2003b), limited to open-section TWMs. In the contribution, a nonlinear theory is formulated, leading to a system of equations valid for a large deformation range but retaining advantage of the GBT field decomposition feature. In more detail, the first step of the GBT procedure (i.e., the classic cross-section analysis - e.g., Silvestre and Camotim, 2002a; Gonçalves et al., 2010; Bebiano et al., 2015) is maintained unchanged compared with the linear case. Nonlinear GBT equations are obtained by adopting a not complete expression of the nonlinear Green-Lagrange strain-displacement relationships in the member strain energy, where in particular the sole membrane nonlinear strain components related to the cross-section displacement in its own plane are considered in the analysis, similarly to as done in Silvestre and Camotim (2002b). The proposed GBT-based methodology has been kept substantially unchanged in recent works addressed on both geometric and material non-linearities (see Section 2.2 for an extended review).

Geometric non-linearities produce, indeed, an alteration of beam deflection, both in transverse and longitudinal direction. Concerning the cross-section, distances between natural nodes, which are not modified in linear regime by the in-plane inflection of plates, change instead in the nonlinear regime (nodes usually approach each other, originating a transverse shortening effect). Regarding longitudinal deformations, beam deflection under transverse loading may involve an approach of end sections in the nonlinear field whereas their reciprocal distance is not modified in the linear regime. In the original nonlinear GBT (e.g., Silvestre and Camotim, 2003b), non-conventional trial functions play a key role in including those effects typical of a nonlinear regime. Fields obtained from a linear procedure (i.e., the usual cross-section analysis), although extended through the non-conventional set, may however not be entirely suitable to capture these effects typical of a nonlinear regime. It may take a large number of linear fields to approximate a typical nonlinear effect, losing the spirit of reduction method inherent in the GBT approach. This fact may also lead to a computationally inefficient formulation (see, e.g., Martins, Camotim, Gonçalves and Dinis, 2016). Moreover, the direct use of the GBT displacement field in the nonlinear expression of deformations can lead to locking problems due to different-order discrete description of involved displacements.

In this Chapter, a new GBT nonlinear formulation, namely NGBT, is proposed. The main contribution consists in the introduction of a set of *nonlinear* trial functions, resulting *slave* of linear ones and able to describe the nonlinear geometrical effects induced on the cross-section by linear trial functions themselves. The core of the NGBT formulation is represented by a

nonlinear cross-section analysis. It is based on the nonlinear Galerkin method (NGM) idea (e.g., Steindl and Troger, 2001), according to which the displacement field of the classic (linear) method, which calls for choosing linear trial functions (viz $U_k(s)$) affected by linear coordinates (viz $\varphi_k(z)$), is enriched by a nonlinear part, consisting of nonlinear trial functions (viz $U_{hk}(s)$, $U_{jhk}(s)$, ...) affected by quadratic, cubic, ..., combinations of the same linear coordinates, e.g.:

$$u(s, z) = \sum_{k=1}^K U_k(s)\varphi_k(z) + \sum_{h=1}^K \sum_{k=1}^K U_{hk}(s)\varphi_h(z)\varphi_k(z) + \dots \quad (6.1)$$

The nonlinear fields are able to describe changes of the sole transverse shapes, leaving to the weak formulation the task of describing longitudinal changes of shape. In this perspective, non-conventional (extensional and shear) linear fields do not offer a substantial advantage, since this kind of deformation is appropriately described by the passive fields.

It is worth noting that the dimensions of the resulting nonlinear and linear Galerkin equations are identical. The nonlinear Galerkin approach is usually adopted in bifurcation theory (Troger and Steindl, 1991) when the Center Manifold Method (CMM) is adopted. This approach is usually followed in elastic post-buckling theory (see, e.g., Budiansky, 1974; Luongo and Pignataro, 1988 for applications in the context of TWB). However, some differences between CMM and the procedure followed here exist, namely:

- in the CMM, the basis of linear trial functions $U_k(s)$ is made of critical modes (in the proper meaning of the word), whereas here $U_k(s)$ are taken as generic functions, with no special properties;
- in the CMM, the nonlinear trial functions $U_{hk}(s)$, $U_{jhk}(s)$, ... are determined by solving balance (equilibrium) equations, while here they are determined by kinematic conditions; in both cases, they are slave of the linear trial functions.

The present Chapter is structured as follows. The nonlinear cross-section analysis is first formulated in Section 6.1, where passive fields are determined. A formal analogy with a thermal problem is then suited in Section 6.2 to develop a direct and computationally efficient approach for the calculation of nonlinear trial functions within a FE-based (discrete) description. The nonlinear GBT equations are shortly described in Section 6.3, while the accuracy and efficiency of the proposed NGBT is pointed out in Section 6.4 by means of two examples, whose results are compared with traditional finite-element solutions obtained with ABAQUS/Standard (Simulia, 2010) for validation purposes.

6.1 Nonlinear cross-section analysis

A generic TWM is considered, with arbitrary open, closed or partially-closed cross-section, made of flat plates connected along edges (see Section 2.3). The displacement field of the mid-surface S of the plates (i.e., at $y = 0$) can be expressed as:

$$\mathbf{u}(s, z) = u(s, z)\mathbf{e}_s(s) + v(s, z)\mathbf{e}_y(s) + w(s, z)\mathbf{e}_z(s) \quad (6.2)$$

where s is the curvilinear abscissa along the mid-line of the cross-section profile \mathcal{C} , z is the abscissa along the beam axis, $\mathbf{e}_s(s)$, $\mathbf{e}_y(s)$, $\mathbf{e}_z(s)$ constitute a right-handed triad of unit vectors in the tangential (i.e., along s), normal (i.e., along y) and longitudinal (i.e., along z) directions, respectively, and $u(s, z)$, $v(s, z)$, $w(s, z)$ are the relevant scalar displacement components in the same triad. The following series representation is adopted to rewrite the relevant scalar displacement components:

$$u(s, z, \epsilon) = \epsilon \dot{u}(s, z) + \epsilon^2 \ddot{u}(s, z) + \dots \quad (6.3a)$$

$$v(s, z, \epsilon) = \epsilon \dot{v}(s, z) + \epsilon^2 \ddot{v}(s, z) + \dots \quad (6.3b)$$

$$w(s, z, \epsilon) = \epsilon \dot{w}(s, z) + \epsilon^2 \ddot{w}(s, z) + \dots \quad (6.3c)$$

where ϵ is an arbitrary small perturbation parameter and the dot symbols denotes differentiation with respect to ϵ . In the series (6.3), $(\dot{u}, \dot{v}, \dot{w})$ are *first-order* fields, $(\ddot{u}, \ddot{v}, \ddot{w})$ are *second-order* fields, etc. By taking into account terms up to ϵ^2 -order, first-order fields are defined as *active* or *master fields*, and second-order fields as *passive* or *slave fields*.

Active and passive fields are selected in order to fulfill the *Vlasov's conditions in the non-linear field*. Therefore, in case of open cross-section or open-branches of multi-connected ones, it is required that both the nonlinear transverse elongation ε_s^{NL} and the nonlinear shear strain γ_{zs}^{NL} are identically nil for each z along the beam axis. In case of closed or partially closed cross-section, the condition on shear strains is substituted with the *Bredt's condition in the non-linear field* (i.e., of constant shear stress flow on closed branches). By adopting the complete Green-Lagrange strain expression, the following is obtained:

$$\varepsilon_s^{NL} = u_{,s} + \frac{1}{2} (u_{,s}^2 + v_{,s}^2 + w_{,s}^2) = 0 \quad \forall z \quad (6.4a)$$

$$\gamma_{zs}^{NL} = w_{,s} + u_{,z} + u_{,s}u_{,z} + v_{,s}v_{,z} + w_{,s}w_{,z} = c_0 \quad \forall z \quad (6.4b)$$

where $c_0 = 0$ for open cross-sections and open branches on multi-connected cross-sections, while $c_0 = \sum_{l=1}^L \Gamma_l(z)/Gt(s)$ on closed loops, G and $t(s)$ being the tangential modulus and the thickness of cross-section plates, respectively, while $\Gamma_l(z)$ being the shear stress flow on the l -th closed loop possessed by the multi-component cross-section (being L the total number of closed loops). Shear stress flows are constant along s , according to the Bredt's condition, while they are in principle variable along z . By substituting Eq. (6.3) into Eq. (6.4) and separately equating to zero all terms with the same order of ϵ , the following perturbation equations are obtained:

$$\text{Order } \epsilon : \quad \dot{u}_{,s} = 0 \quad (6.5a)$$

$$\dot{w}_{,s} + \dot{u}_{,z} = c_0 \quad (6.5b)$$

$$\text{Order } \epsilon^2 : \quad \ddot{u}_{,s} + \frac{1}{2} (\dot{u}_{,s}^2 + \dot{v}_{,s}^2 + \dot{w}_{,s}^2) = 0 \quad (6.6a)$$

$$\ddot{w}_{,s} + \ddot{u}_{,z} - \dot{u}_{,s}\dot{u}_{,z} - \dot{v}_{,s}\dot{v}_{,z} - \dot{w}_{,s}\dot{w}_{,z} = 0 \quad (6.6b)$$

that can be sequentially solved up to the desired order to evaluate the u –(tangential) and w –(warping) components. It should be noted that Eqs. (6.5) and (6.6) allow an arbitrary choice of the v –(transverse) components. However, the latter should be selected in order to satisfy compatibility conditions at the cross-section nodes, as better explained hereinafter.

6.1.1 First-order (active) fields

First order conditions, Eq. (6.5), define the two fundamental Vlasov hypotheses (supplied by the Bredt's condition on closed loops) in a geometrically linear context. Therefore, first-order fields coincide with the classic *conventional* fields. Indeed, Eq. (6.5a) admits the separable variable solution:

$$\dot{u}(s, z) = \sum_{k=1}^K U_k(s) \varphi_k(z) \quad (6.7)$$

where $U_k(s) = \text{const}$ are piece-wise constant functions, and $\varphi_k(z)$ are arbitrary functions. In order to ensure compatibility conditions at the cross-section nodes (for any z along the beam axis), transverse and tangential displacements must have the same dependence on z , so that:

$$\dot{v}(s, z) = \sum_{k=1}^K V_k(s) \varphi_k(z) \quad (6.8)$$

where $V_k(s)$ are arbitrary functions, which must comply with $U_k(s)$ at nodes. In order to satisfy continuity of rotation at nodes, $V'_k(s)$ must be there continuous.

Once the $U_k(s)$ have been determined, Eq. (6.5b) is solved in chain. By substituting Eq. (6.7) in it, the following general expression can be obtained:

$$\dot{w}_{,s}(s, z) = - \sum_{k=1}^K \left[U_k(s) - \sum_{l=1}^L (\pm) \frac{Q_k^l}{t(s)G} \right] \varphi'_k(z) \quad (6.9)$$

with Q_k^l being the (unknown) tangential stress flow associated with the k -th trial function and acting of the l -th closed loop ($Q_k^l = 0$ on open branches). An arbitrary positive rotation is assigned to each loop and a positive (negative) sign is used in the summation for Q_k^l in the right-hand side of Eq. (6.9) when the direction identified by the local coordinate s and the one consequent to the rotation previously introduced coincide (differ). Eq. (6.9) admit the separable-variable solution:

$$\dot{w}(s, z) = \sum_{k=1}^K W_k(s) \varphi'_k(z) \quad (6.10)$$

in which:

$$W_k(s) = \int_{\mathcal{C}} \left[-U_k(s) + \sum_{l=1}^L (\pm) \frac{Q_k^l}{t(s)G} \right] ds + \bar{W}_k \quad (6.11)$$

are piece-wise linear functions which can be determined by following the procedure outlined in Section 3.1.1. The first-order field $U(s) = V(s) = 0$, $W(s) = \text{const}$, which identically satisfies the Vlasov's conditions, is worthy of attention. It models the longitudinal global shortening behavior, so that it could play an important role in geometric nonlinear analysis.

In conclusion, the solution of the first-order conditions, Eq. (6.5), leads to a complete set of first-order fields that are identical to the conventional fields of the classic linear GBT. They can be deduced using the proposed GBT-D approach as illustrated in Section 3.1.1.

6.1.2 Second-order (passive) fields

Second-order fields are conveniently derived in two successive steps: first, by enforcing nonlinear inextensibility, Eq. (6.6a), and then, nonlinear unshearability, Eq. (6.6b). The aforementioned conditions are treated in the following in separate Sections for clarity.

Inextensibility condition

The second-order inextensibility condition, Eq. (6.6a), is rewritten by taking into account the expression of the first-order fields. By remembering that $U_k(s)$ is piece-wise constant, i.e. $U'_k(s) = 0$, it reads:

$$\ddot{u}_{,s}(s, z) = -\frac{1}{2} \sum_{h=1}^K \sum_{k=1}^K [V'_h(s) V'_k(s) \varphi_h(z) \varphi_k(z) + W'_h(s) W'_k(s) \varphi'_h(z) \varphi'_k(z)] \quad (6.12)$$

The solution of Eq. (6.12) can be placed in the following form:

$$\ddot{u}(s, z) = \sum_{h=1}^K \sum_{k=1}^K \left[U_{hk}(s) \varphi_h(z) \varphi_k(z) + X_{hk}(s) \varphi'_h(z) \varphi'_k(z) \right] \quad (6.13)$$

which entails:

$$U'_{hk}(s) = -\frac{1}{2} V'_h(s) V'_k(s) \quad (6.14a)$$

$$X'_{hk}(s) = -\frac{1}{2} W'_h(s) W'_k(s) \quad (6.14b)$$

By integration, it follows:

$$U_{hk}(s) = -\frac{1}{2} \int_c V'_h(s) V'_k(s) ds + \bar{U}_{hk} \quad (6.15a)$$

$$X_{hk}(s) = -\frac{1}{2} \int_c W'_h(s) W'_k(s) ds + \bar{X}_{hk} \quad (6.15b)$$

The integration constants $\bar{U}_{hk}, \bar{X}_{hk}$ are selected in order to enforce continuity of displacement and rotation on the cross-section. Among all constants, those that still remain arbitrary are chosen by normalizing the second-order fields in order they have a zero-mean over \mathcal{C} . It should be noted that $U_{hk}(s), X_{hk}(s)$ are symmetric with respect to subscript indices; moreover, since $W_k(s)$ is a piece-wise linear function on the cross-section mid-line, then also $X_{hk}(s)$ are piece-wise linear functions.

As regards the transverse component $\ddot{v}(s, z)$, the same dependence on z is assumed:

$$\ddot{v}(s, z) = \sum_{h=1}^K \sum_{k=1}^K \left[V_{hk}(s) \varphi_h(z) \varphi_k(z) + Y_{hk}(s) \varphi'_h(z) \varphi'_k(z) \right] \quad (6.16)$$

in which functions $V_{hk}(s), Y_{hk}(s)$ should be selected in order to satisfy compatibility conditions at nodes.

Passive fields $U_{hk}(s)$, $V_{hk}(s)$ and $X_{hk}(s)$, $Y_{hk}(s)$ are *extensional fields*, having, however, a different meaning with respect to the non-conventional fields of the linear approach. Here, they describe innovative deformation fields which induce non-constant tangential displacement fields on each cross-section element, ensuring their inextensibility up to the second order. In other words, they describe *in-plane shortening* fields, able to compensate the second-order effects caused by the linear conventional fields.

Unshearability condition

The second-order unshearability condition, Eq. (6.6b), after substituting the expression of the first- and second-order fields so far determined in Eqs. (6.13) and (6.16), becomes:

$$\ddot{w}_{,s}(s, z) = - \sum_{h=1}^K \sum_{k=1}^K \left\{ \left[2U_{hk}(s) + V'_h(s) V_k(s) \right] \varphi_h(z) \varphi'_k(z) + \left[2X_{hk}(s) + W'_h(s) W_k(s) \right] \varphi'_h(z) \varphi''_k(z) \right\} \quad (6.17)$$

where it has been accounted that $U'_h(s) = 0$, and $U_{hk}(s)$, $X_{hk}(s)$ are symmetric with respect to subscripts. Solution of Eq. (6.17) can be placed in the following form:

$$\ddot{w}(s, z) = \sum_{h=1}^K \sum_{k=1}^K \left[W_{hk}(s) \varphi_h(z) \varphi'_k(z) + Z_{hk}(s) \varphi'_h(z) \varphi''_k(z) \right] \quad (6.18)$$

in which it must hold:

$$W'_{hk}(s) = -2U_{hk}(s) - V'_h(s) V_k(s) \quad (6.19a)$$

$$Z'_{hk}(s) = -2X_{hk}(s) - W'_h(s) W_k(s) \quad (6.19b)$$

with functions $U_{hk}(s)$, $X_{hk}(s)$ known from Eq. (6.15). Then, by integrating Eq. (6.19), it follows:

$$W_{hk}(s) = - \int_{\mathcal{C}} \left[2U_{hk}(s) + V'_h(s) V_k(s) \right] ds + \bar{W}_{hk} \quad (6.20a)$$

$$Z_{hk}(s) = - \int_{\mathcal{C}} \left[2X_{hk}(s) + W'_h(s) W_k(s) \right] ds + \bar{Z}_{hk} \quad (6.20b)$$

Arbitrary integration constants \bar{W}_{hk} , \bar{Z}_{hk} may be selected by enforcing continuity and normalizing out-of-plane displacements to have zero-mean over the cross-section \mathcal{C} . It should be noted that passive fields $W_{hk}(s)$, $Z_{hk}(s)$ are in general not symmetric with respect to subscript indices (i.e., $Z_{hk}(s) \neq Z_{kh}(s)$, $W_{hk}(s) \neq W_{kh}(s)$). Moreover, it can be easily proved that $Z_{hk}(s)$ is piece-wise linear on the cross-section mid-line. As a matter of fact, by differentiation of Eq. (6.19b), $Z''_{hk}(s) = -2X'_{hk}(s) + W'_h(s) W'_k(s) + W''_h(s) W_k(s)$ is obtained. Then, by taking into account that (i) $2X'_{hk}(s) + W'_h(s) W'_k(s) = 0$ from Eq. (6.14b), and (ii) $W_h(s)$ is a piece-wise linear function (i.e., $W''_h(s) = 0$), $Z''_{hk}(s) = 0$ follows, from which the statement.

Similarly to planar components, passive fields $W_{hk}(s)$, $Z_{hk}(s)$ are *shear fields* in a different meaning from what is meant in the linear approach. They induce non-constant out-of-plane

displacement which ensure unshearability up to the second-order. In other words, they produce second-order shear strain able to compensate the second-order effects caused by the conventional linear fields.

Second-order displacement field

In conclusion, the NGBT (second-order) displacement field is given by:

$$u(s, z) = \sum_{k=1}^K U_k(s) \varphi_k(z) + \sum_{h=1}^K \sum_{k=1}^K \left[U_{hk}(s) \varphi_h(z) \varphi_k(z) + X_{hk}(s) \varphi'_h(z) \varphi'_k(z) \right] \quad (6.21a)$$

$$v(s, z) = \sum_{k=1}^K V_k(s) \varphi_k(z) + \sum_{h=1}^K \sum_{k=1}^K \left[V_{hk}(s) \varphi_h(z) \varphi_k(z) + Y_{hk}(s) \varphi'_h(z) \varphi'_k(z) \right] \quad (6.21b)$$

$$w(s, z) = \sum_{k=1}^K W_k(s) \varphi'_k(z) + \sum_{h=1}^K \sum_{k=1}^K \left[W_{hk}(s) \varphi_h(z) \varphi'_k(z) + Z_{hk}(s) \varphi'_h(z) \varphi''_k(z) \right] \quad (6.21c)$$

Once linear conventional (active) fields are obtained (Section 6.1.1), Eqs. (6.15) and (6.20) allow to determine nonlinear passive fields that are slaves of the linear ones. In particular, two sets of passive fields (with both in-plane and out-of-plane components) are derived from both planar conventional displacements, U_k , V_k , and warping functions W_k : from the former the set of second-order fields U_{hk} , V_{hk} , W_{hk} arises whereas from the latter the set X_{hk} , Y_{hk} , Z_{hk} follows. Therefore, from K conventional first-order fields, 2 sets of $K \times K$ second-order fields derive; overall they are in number of $2K^2$.

Nonlinear (passive) trial functions include nonlinear effects induced by corresponding linear ones. As a consequence, if the linear response is governed by a subset of linear fields (as it usually is), the corresponding nonlinear response can be completely described by the same set of linear fields together with all passive ones generated by the linear subset itself. Therefore, once relevant linear fields have been identified, nonlinear analysis can be performed by just supplying nonlinear trial functions corresponding to relevant linear ones, without the need to include further linear fields, as conversely required by the classic nonlinear GBT approaches (e.g., Silvestre and Camotim, 2003b). For these reasons, the proposed NGBT approach complies with the spirit of GBT as a reduction method, since it allows to fully describe the TWM behavior by using the smallest number of trial functions. Moreover, it is also computationally efficient, since nonlinear fields are associated with linear coordinates (i.e., the problem dimension does not increase).

6.2 A formal analogy for the calculation of nonlinear fields

Passive fields can in principle be deduced via integration (Eqs. (6.15) and (6.20)). The procedure, which is in principle simple, may however become quite laborious as regards the planar problem, due to the need to enforce compatibility conditions at cross-section nodes. This is, in particular, the case of multi-connected cross-sections. As a matter of facts, in case of closed cells, the problem governing in-plane extension of cross-section elements and related to nonlinear fields U_{hk} , V_{hk} and X_{hk} , Y_{hk} is hyperstatic, thus profile elements may exhibit flexural

deformation involving their own elasticity. A simple and automated procedure can be obtained by noting the following analogy. Differential equations (6.14), leading to the evaluation of passive transverse shortening fields $U_{hk}(s)$, $X_{hk}(s)$, are formally analogous to:

$$U'(s) = \bar{\varepsilon}(s) \quad (6.22)$$

Similarly, differential equations (6.19), related to the evaluation of passive warping fields $W_{hk}(s)$, $Z_{hk}(s)$, are formally analogous to:

$$W'(s) = \bar{\gamma}(s) \quad (6.23)$$

where $U(s)$, $W(s)$ are unknown in-plane tangential and out-of-plane (warping) displacements, respectively, while $\bar{\varepsilon}(s)$, $\bar{\gamma}(s)$ are known terms. Consequently, Eqs. (6.22) and (6.23) are formally equivalent to those of a planar frame subjected to *nonuniform thermal variations*. In particular, these thermal loads are producing in-plane elongation $\bar{\varepsilon}(s)$ (i.e., *planar* problem, see Fig. 6.1a) and out-of-plane elongation $\bar{\gamma}(s)$ (i.e., *warping* problem, see Fig. 6.1b). Nonlinear trial functions can therefore be deduced as the *linear* solution of an *equivalent thermal problem* involving a planar frame having the shape of the cross-section. This approach is simple and straightforward and can be applied to TWMs with arbitrary open, closed or partially-closed cross-section. Moreover, it is also computationally efficient; in fact, since the solution of interest is the linear one, the equivalent thermal problem always has the same operator for any h, k , with the only known term to be updated.

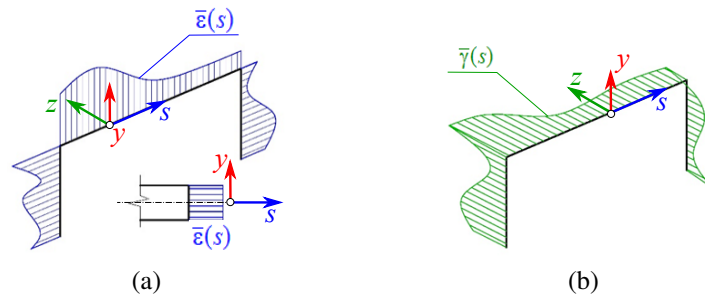


Figure 6.1: Equivalent thermal problem: (a) planar problem, and (b) warping problem.

6.2.1 Equivalent thermal problem for arbitrary TWM cross-sections

An infinitesimal segment of TWM with length dz is considered to be free in space (i.e., unconstrained), weightless (see Section 3.1) and subject to in-plane and out-of-plane thermal elongations $\bar{\varepsilon}(s)$, $\bar{\gamma}(s)$ uniformly distributed along the beam axis z . Since dz is infinitesimal, in-plane and out-of-plane (warping) displacements are not dependent on z and they are governed by two independent sets of uncoupled differential equations, which will be referred to in the following as Planar Thermal Problem (PTP) and Warping Thermal Problem (WTP).

Planar Thermal Problem (PTP)

The PTP is governed by the well-known equations for the behavior of an Euler-Bernoulli beam subjected to nonuniform thermal elongations along its axis:

$$U'(s) - \bar{\varepsilon}(s) = 0 \quad (6.24a)$$

$$V^{IV}(s) = 0 \quad (6.24b)$$

The continuous problem can be solved analytically by integrating Eq. (6.24) and enforcing compatibility conditions at connections between elements forming the frame. However, this procedure may become burdensome in case of closed cross-sections, where the problem governing the in-plane extension is hyperstatic. For these reason and coherently to as commonly performed in the Literature for the GBT cross-section analysis, the discrete version of the PTP is adopted. After discretizing the planar frame representative of the TWM cross-section into M finite elements by interposing possible additional nodes between the natural ones, the problem is reduced to N DOF. Following standard steps of the FE procedure (e.g., Ranzi and Gilbert, 2015), polynomial shape functions are adopted to approximate fields $U(s)$, $V(s)$. The local stiffness matrix and load vector \mathbf{K}_p^e and \mathbf{f}_p^e (with $e = 1, 2, \dots, M$ and subscript p identifying the *planar* problem) are evaluated for each element and then suitably assembled. The following algebraic problem is thus obtained:

$$\mathbf{K}_p \mathbf{q}_p = \mathbf{f}_p \quad (6.25)$$

where \mathbf{q}_p is a $N \times 1$ vector collecting nodal values of fields $U(s)$, $V(s)$. A set of constraint conditions must be introduced to solve Eq. (6.25). They can be conveniently chosen in order to make fields $U(s)$, $V(s)$ orthogonal to the three in-plane rigid-body motions (i.e., two translations and one rotation around the shear center). This can be achieved by prescribing fields $U(s)$, $V(s)$ and $V'(s)$ to have nil average on the cross-section mid-line \mathcal{C} .

The choice of polynomial shape functions to be adopted in PTP is worth of discussion. In fact, while classic cubic Hermite polynomials are perfectly suitable in approximating $V(s)$ (i.e., $V_{hk}(s)$ and $Y_{hk}(s)$), the approximation of tangential fields $U(s)$ must be consistent with the one adopted for active (linear) trial functions, as a direct consequence of the nonlinear Galerkin approach. Passive fields $X_{hk}(s)$, stemming from conventional active warping fields $W_k(s)$, are piece-wise linear functions as a consequence of the Vlasov hypothesis V2 (Bredt's condition). Therefore, they can be suitably approximate with linear Lagrangian polynomials. The classic six DOF FE can then be suited for the discrete description of the PTP. Corresponding stiffness matrix \mathbf{K}_p^e is reported in Appendix A.1.1, while the (equivalent thermic) load vector \mathbf{f}_p^e is defined as:

$$\mathbf{f}_p^e = EA \int_0^{l_e} [L_1(s, l_e) \ 0 \ 0 \ L_2(s, l_e) \ 0 \ 0]^T \bar{\varepsilon}(s) ds \quad (6.26)$$

where $L_1(s, l_e)$, $L_2(s, l_e)$ are linear Lagrange polynomial shape functions defined in Appendix A.1.1, E and A are the longitudinal elastic modulus and transverse area, while l_e being the length of the e -th cross-section FE ($e = 1, \dots, M$). Conversely, approximation of passive fields $U_{hk}(s)$ must be related to the one adopted for active functions $V_k(s)$. In case the latter have been described by cubic Hermite polynomials (see, e.g., elements FE₁ and FE₂ in Appendix A), $U_{hk}(s)$ must be 4th order continuous, which implies $U_{hk}(s)$ to be interpolated by 5th order

continuous polynomials with continuous first derivative. Corresponding FE to be adopted in the PTP, referred to in the following as FE_4 , is the ten DOF element illustrated in Fig. 6.2. Adopted interpolating functions, stiffness matrix and load vector are reported in Appendix A.2.1.

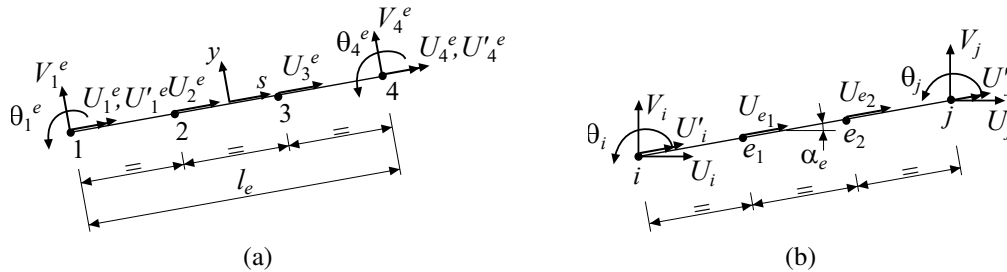


Figure 6.2: In-plane 10 DOF FE: nodal displacements in (a) local, and (b) global coordinates.

An illustrative example is proposed to clarify the procedure. It consists on a rectangular cross-section whose dimensions are illustrated in Fig. 6.3a. The cross-section is discretized with $n = 12$ nodes, then $M=12$ elements, as depicted in Fig. 6.3b. Conventional linear trial

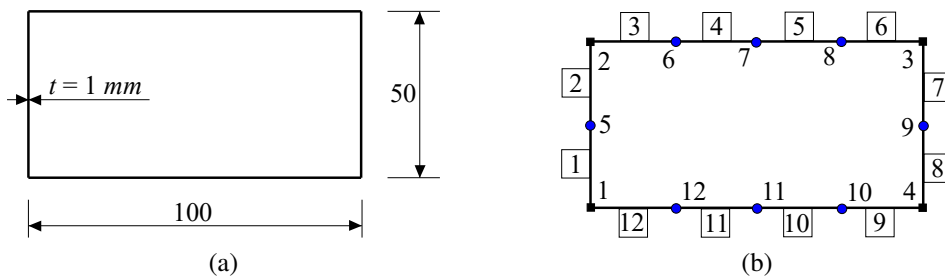


Figure 6.3: Illustrative example of nonlinear cross-section analysis: (a) geometry, (b) cross-section discretization.

functions $U_k(s), V_k(s), W_k(s)$ are obtained with the dynamic procedure (GBT-D) proposed in Section 3.1.1. Fig. 6.4 shows the first 8 fields, with the first three ones describing in-plane rigid-body motions and the fourth function depicting the global longitudinal shortening effect. Corresponding in-plane passive fields $U_{hk}(s), V_{hk}(s)$ are illustrated in Fig. 6.5, while functions

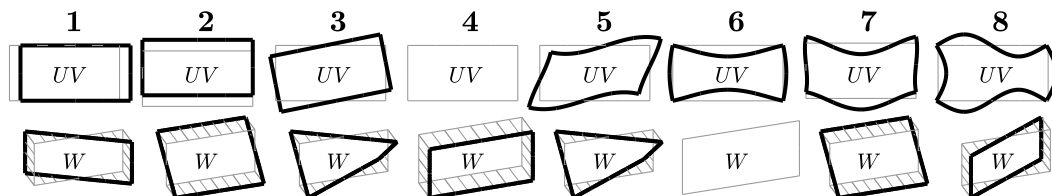


Figure 6.4: Illustrative example of nonlinear cross-section analysis: active conventional planar and warping trial functions.

$X_{hk}(s), Y_{hk}(s)$ are shown in Fig. 6.6, where both the full in-plane cross-section displacement UV and the sole transverse displacement U have been reported, the latter using the y -axis convention. Passive fields are obtained by solving a sequence of $2K^2$ PTP (6.25), being K

the number of active conventional fields. Despite the procedure might appear very demanding computationally and time consuming, it is in reality very efficient and straightforward. As a matter of facts, the PTP is a linear problem, thus the stiffness operator is always the same for any couple h, k , with the sole known terms to be updated at each step. The inverse of the stiffness operator, which is the most time consuming operation, needs to be performed only two times: the first for the problem governing fields $U_{hk}(s), V_{hk}(s)$ and described adopting elements FE_4 , the second for the one governing fields $X_{hk}(s), Y_{hk}(s)$ described by 6 DOF FE. As expected, nonlinear trial functions are extension fields, describing in-plane elongation of cross-section elements. Due to the presence of closed loops, elements forming the cross-section depict bending in case of non-symmetric elongations. Planar passive tangential fields $U_{hk}(s), X_{hk}(s)$ are, as expected, symmetric with respect to index permutation. Some of them are nil, since generating active fields (i.e., $V_k(s), W_k(s)$ for $U_{hk}(s), X_{hk}(s)$, respectively) depict constant distributions on the cross-section. Finally, fields $X_{hk}(s)$ are, as expected, step-wise linear on plates forming the cross-section.

Warping Thermal Problem (WTP)

In perfect analogy to the WEP (Section 3.1.2), the infinitesimal segment is assumed to behave in the WTP as a pure shear beam in the $s - z$ plane. This is an internally constrained Timoshenko beam, in which cross-section rotations are prevented, so that elements are only permitted to slide orthogonally to the axis. Therefore, the shear γ is the only strain, and the shear force T the only active stress. Equation governing its behavior under nonuniform thermal elongations along its longitudinal axis is:

$$W'(s) - \bar{\gamma}(s) = 0 \quad (6.27)$$

The WTP problem can easily be solved by integration along the cross-section mid-line \mathcal{C} , because of the continuity of the $W(s)$ function. Arbitrary integration constant stemming from the integration and describing the uniform (longitudinal) extension of the member can be suitably determined in order to make the warping orthogonal to the extension. This can be achieved by requiring the average warping function to be zero. The discrete version of the WTP is obtained by using the same discretization adopted for the previous PTP. Following standard steps of the FE procedure (e.g., Ranzi and Gilbert, 2015), polynomial shape functions are adopted to approximate fields $W(s)$, and the local stiffness matrix and load vector \mathbf{K}_w^e and \mathbf{f}_w^e (with $e = 1, 2, \dots, M$ and subscript w identifying the *warping* problem) are evaluated for each element and then suitably assembled. The following algebraic problem is thus obtained:

$$\mathbf{K}_w \mathbf{q}_w = \mathbf{f}_w \quad (6.28)$$

where \mathbf{q}_w is a vector collecting nodal values of fields $W(s)$.

Analogously to the PTP, the choice of shape functions for approximating fields $W(s)$ must be consistent with the one adopted for active (linear) trial functions. As previously demonstrated, passive fields $Z_{hk}(s)$ are piece-wise linear functions on the cross-section mid-line. Therefore, they can be approximated using the two DOF FE which calls for linear Lagrange polynomial shape functions $L_1(s, l_e), L_2(s, l_e)$ (see Appendix A.1.1). Corresponding stiffness matrix \mathbf{K}_w^e is reported in Appendix A.1.1, while the (equivalent thermic) load vector \mathbf{f}_w^e is de-

$k \backslash h$	1	2	3	4	5	6	7	8
1	UV	UV	UV	UV	UV	UV	UV	UV
	U	U	U	U	U	U	U	U
2	UV	UV	UV	UV	UV	UV	UV	UV
	U	U	U	U	U	U	U	U
3	UV	UV	UV	UV	UV	UV	UV	UV
	U	U	U	U	U	U	U	U
4	UV	UV	UV	UV	UV	UV	UV	UV
	U	U	U	U	U	U	U	U
5	UV	UV	UV	UV	UV	UV	UV	UV
	U	U	U	U	U	U	U	U
6	UV	UV	UV	UV	UV	UV	UV	UV
	U	U	U	U	U	U	U	U
7	UV	UV	UV	UV	UV	UV	UV	UV
	U	U	U	U	U	U	U	U
8	UV	UV	UV	UV	UV	UV	UV	UV
	U	U	U	U	U	U	U	U

Figure 6.5: Illustrative example of nonlinear cross-section analysis: passive in-plane trial functions $U_{hk}(s), V_{hk}(s)$.

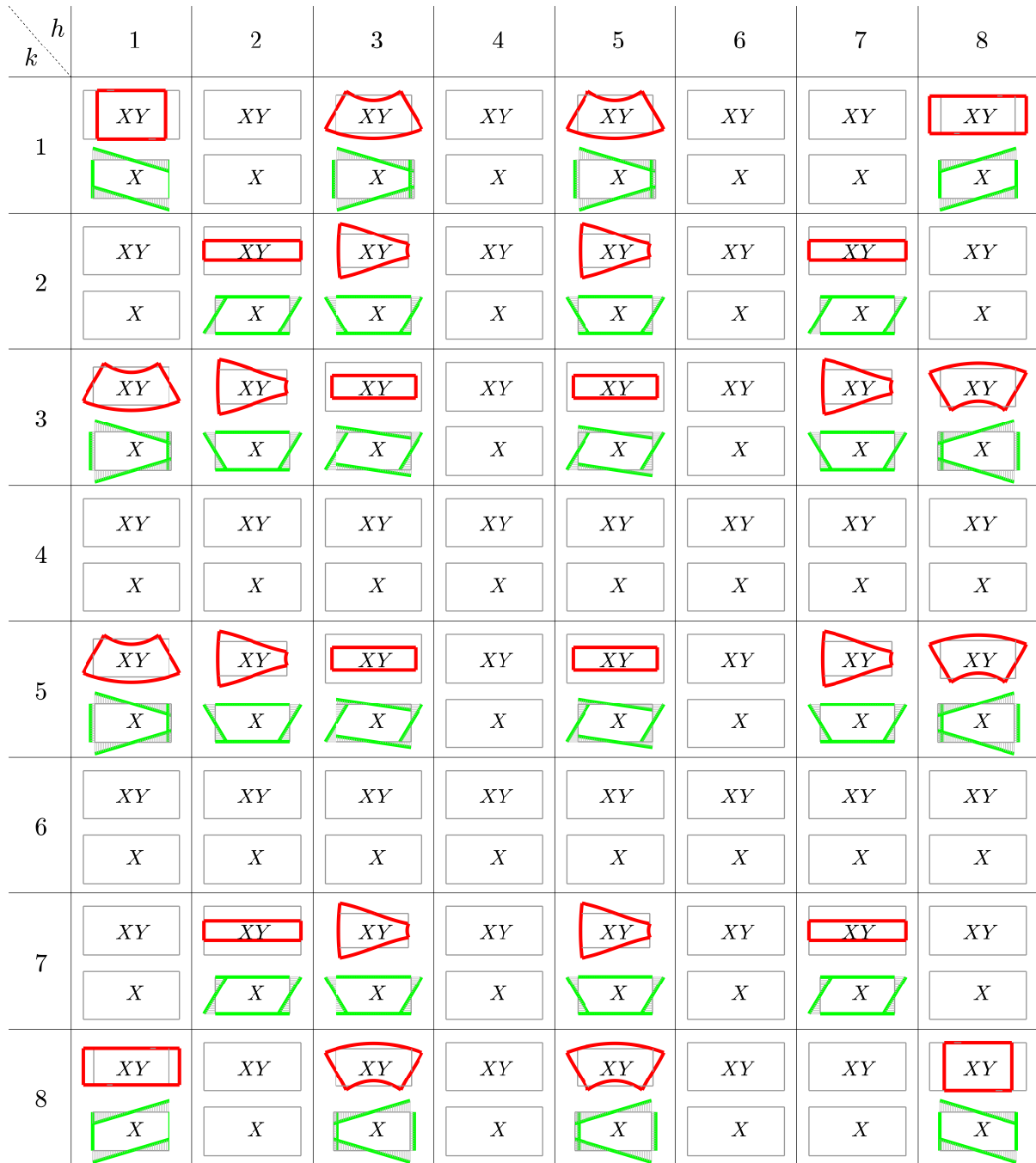


Figure 6.6: Illustrative example of nonlinear cross-section analysis: passive in-plane trial functions $X_{hk}(s), Y_{hk}(s)$.

defined as:

$$\mathbf{f}_w^e = G t \int_0^{l_e} [L_1(s, l_e) L_2(s, l_e)]^T \bar{\gamma}(s) ds \quad (6.29)$$

where G and t are, respectively, the tangential elastic modulus and thickness of the e -th cross-section FE ($e = 1, \dots, M$). Regarding fields $W_{hk}(s)$, a different choice must be performed. In case, in fact, active functions $V_k(s)$ have been described by cubic Hermite polynomials (see, e.g., elements FE₁ and FE₂ in Appendix A), $W'_{hk}(s)$ must be 5th order continuous, which implies $W_{hk}(s)$ to be interpolated by 6th order continuous polynomials with continuous first derivative. Corresponding FE to be adopted in the WTP, referred to in the following as FE₄, is the seven DOF element illustrated in Fig. 6.7. Adopted interpolating functions and corresponding stiffness matrix and equivalent thermal load vector are reported in Appendix A.2.1. Passive

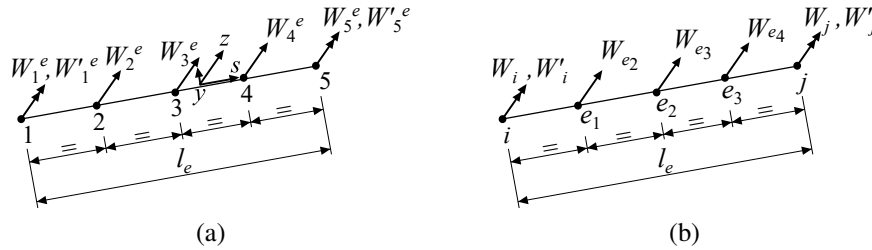


Figure 6.7: Out-of-plane 7 DOF FE: nodal displacements in (a) local, and (b) global coordinates.

fields $W_{hk}(s)$, $Z_{hk}(s)$ for the illustrative example are shown in Figs. 6.8 and 6.9, respectively. Analogously to planar passive fields, some of the warping ones are nil, depending on the values of generating active and passive trial functions. As expected, they are not symmetric with respect to index permutations, while fields $Z_{hk}(s)$ are piece-wise linear on plates forming the cross-section. Finally, same conclusion of PTP can be established regarding the computational efficiency of the procedure. Indeed, despite $2K^2$ problems need to be solved, i.e. one for each passive warping fields, the stiffness operator of Eq. (6.28) needs to be inverted only two time, one for the problem governing fields $W_{hk}(s)$ and described adopting elements FE₄, the second for the one governing fields $Z_{hk}(s)$ described by 2 DOF FE.

6.2.2 Kinematic procedure for open TWM cross-sections

Differently from the case of multi-connected cross-sections, the problem governing the in-plane extension is, in case of open cross-sections, isostatic. The elongation of one cross-section element causes in fact pure rigid-body translation of adjacent elements, in order to satisfy compatibility conditions on displacement and rotations. Consequently, transverse displacements $V(s)$ are piece-wise linear, while all elements composing the cross-section depict the same rotation. Therefore, the PTP can be suitably solved by means of the following *kinematic procedure*. A generic open cross-section is considered, formed by n_e flat elements delimited by $n_n = n_e + 1$ natural nodes (Fig. 6.10a). Local displacements U_i^e , V_i^e of natural nodes (Fig. 6.10b) are assumed as free parameters, while nil rotations are assumed for all cross-section elements (i.e.,

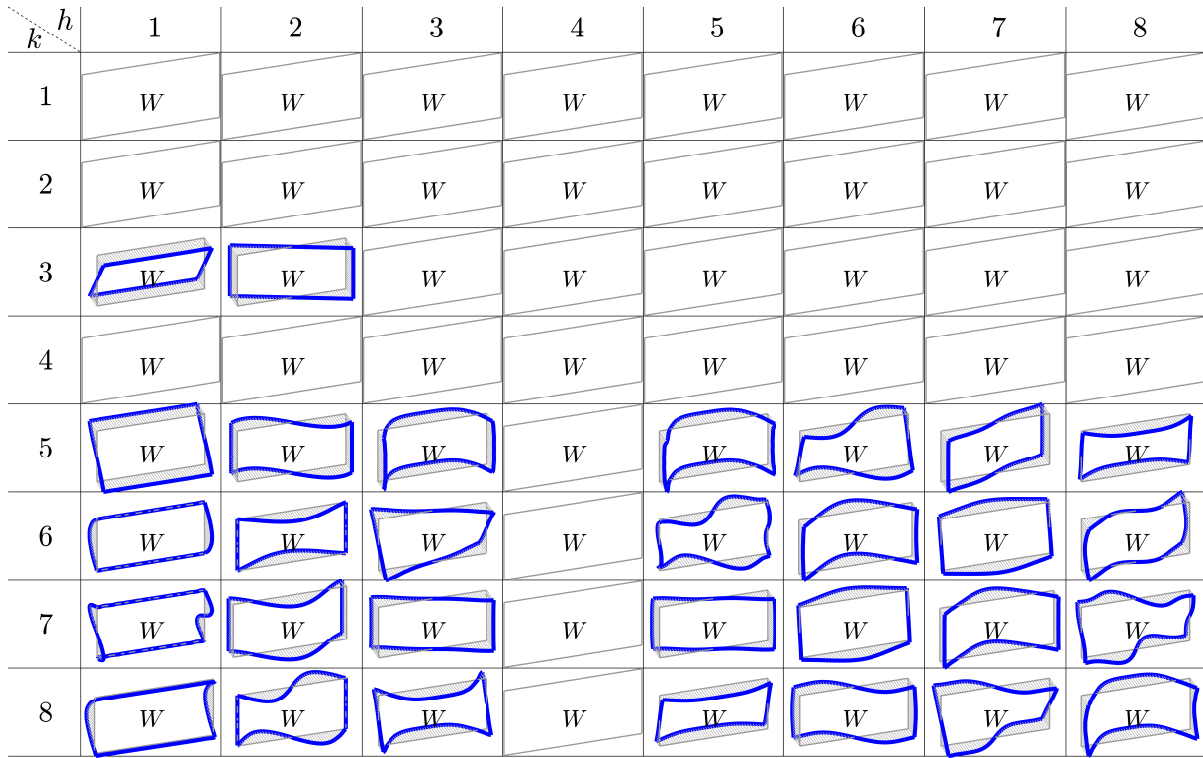


Figure 6.8: Illustrative example of nonlinear cross-section analysis: passive warping trial functions $W_{hk}(s)$.

$\theta_i^e = \theta_i = 0, i = 1, \dots, n_n$). Conditions prescribing (i) global elongation, and (ii) nil rotation, are imposed on each element. They can be rewritten in local coordinates as (Fig. 6.10b):

$$U_{i+1}^e - U_i^e = \int_i^{i+1} \bar{\varepsilon}(s) ds \tag{6.30a}$$

$$V_{i+1}^e - V_i^e = 0 \tag{6.30b}$$

or in global coordinates as (Fig. 6.10c):

$$(U_{i+1} - U_i) \cos \alpha_e + (V_{i+1} - V_i) \sin \alpha_e = \int_i^{i+1} \bar{\varepsilon}(s) ds \tag{6.31a}$$

$$(U_{i+1} - U_i) \sin \alpha_e - (V_{i+1} - V_i) \cos \alpha_e = 0 \tag{6.31b}$$

Eqs. (6.31) are in number $2n_e$ in front of $2(n_e + 1) = 2n_n$ unknowns. Remaining arbitrary ones are related to rigid-body translations in both tangential and transverse in-plane directions. They can be suitably chosen in such a way $U(s)$ and $V(s)$ depict nil average on the mid-line profile

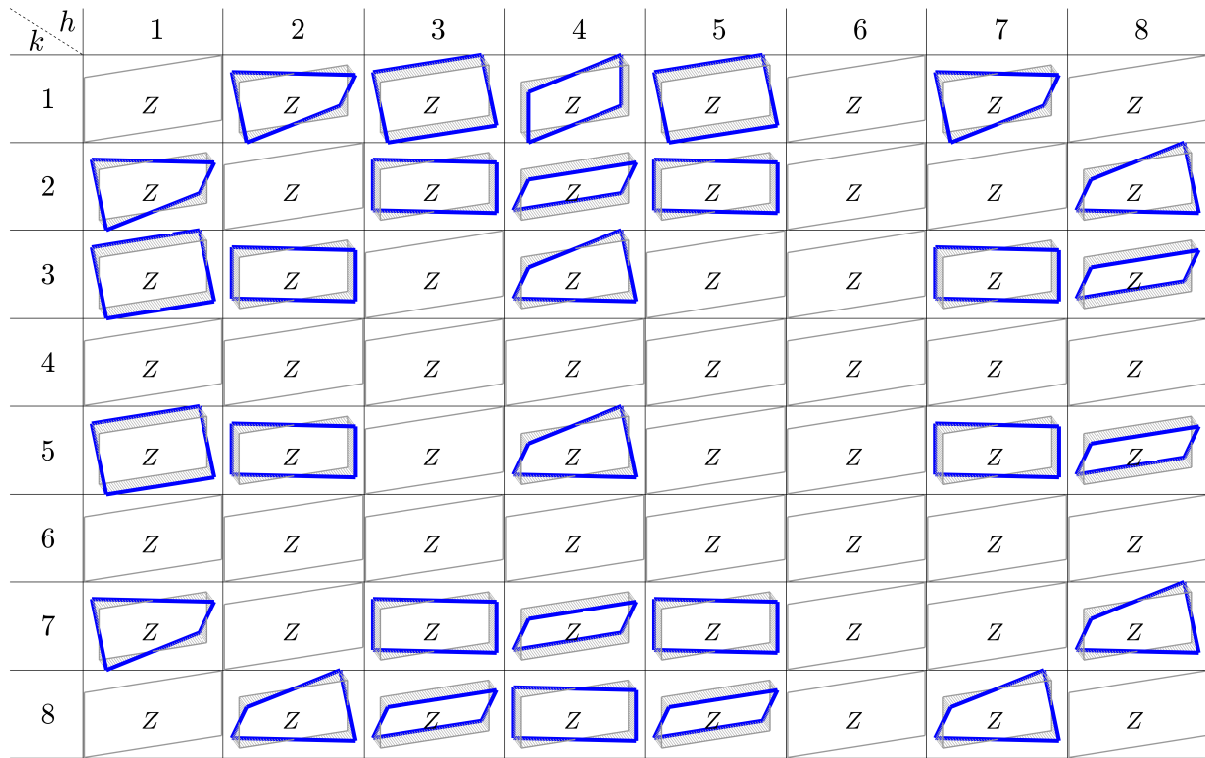


Figure 6.9: Illustrative example of nonlinear cross-section analysis: passive warping trial functions $Z_{hk}(s)$.

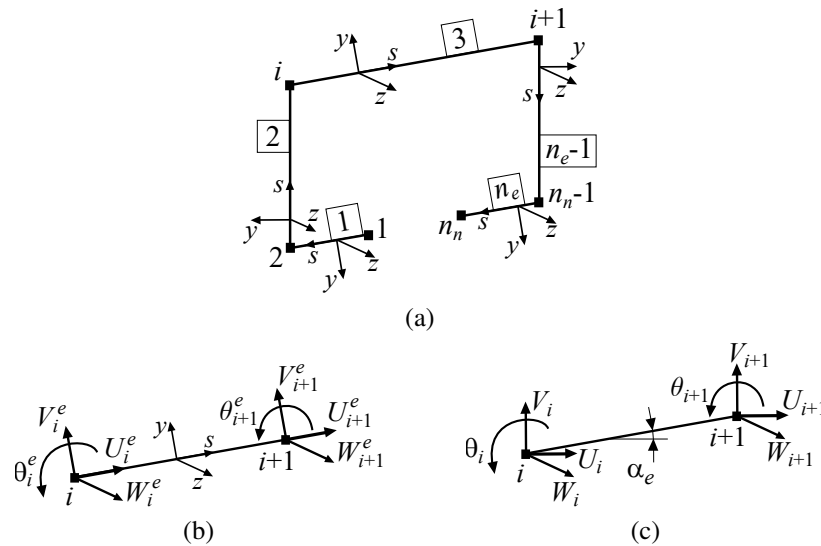


Figure 6.10: (a) TWM open cross-section, natural nodes and element nomenclature; natural nodes DOF in (b) local coordinates, and (c) global coordinates.

\mathcal{C} , i.e.:

$$\sum_{i=1}^{n_n} U_i = 0 \tag{6.32a}$$

$$\sum_{i=1}^{n_n} V_i = 0 \tag{6.32b}$$

Eqs. (6.31) and (6.32) can be rewritten in compact form as (subscript p identifying the *planar* problem):

$$\mathbf{A}_p \mathbf{q}_p = \bar{\boldsymbol{\varepsilon}} \tag{6.33}$$

where \mathbf{A}_p is a $2n_n \times 2n_n$ non-singular matrix, \mathbf{q}_p is a $2n_n \times 1$ vector collecting the unknown in-plane displacements of natural nodes, while $\bar{\boldsymbol{\varepsilon}}$ is a $2n_n \times 1$ vector collecting known terms. Once U_i, V_i are identified from Eq. (6.33), the distribution of the tangential in-plane displacement can be obtained for each element composing the cross-section as:

$$U(\bar{s}) = U_i^e + \int_i^{\bar{s}} \bar{\boldsymbol{\varepsilon}}(s) ds; \quad \bar{s} \in (i, i + 1), i = 1, \dots, n_e \tag{6.34}$$

The proposed kinematic procedure is illustrated by means of its application on the open cross-section shown in Fig. 6.11a. In order to identify linear conventional fields, the cross-section is discretized with $n = 11$ nodes, then $M=10$ elements, as depicted in Fig. 6.11b. The standard 6 DOF Euler-Bernoulli FE is adopted for this purpose. The first 8 conventional

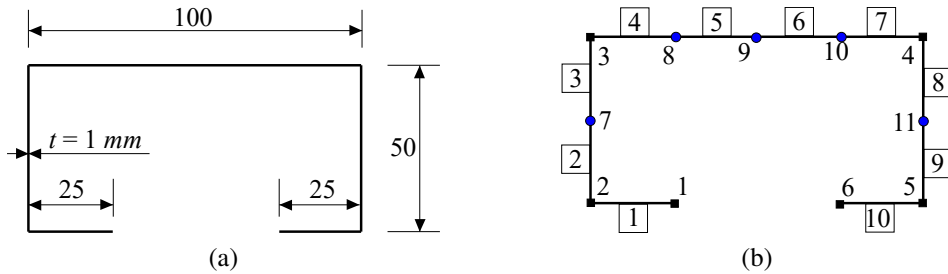


Figure 6.11: Illustrative example of nonlinear cross-section analysis on open cross-section: (a) geometry, (b) cross-section discretization.

trial functions $U_k(s), V_k(s), W_k(s)$ are reported in Fig. 6.12, where the first four fields describe rigid-body motions, including the global longitudinal shortening effect. Corresponding in-plane passive fields $U_{hk}(s), V_{hk}(s)$ and $X_{hk}(s), Y_{hk}(s)$ are illustrated in Figs. 6.13 and 6.14, respectively, where both the full in-plane cross-section displacement UV and the sole transverse displacement U have been reported, the latter using the y -axis convention. Nodal values of passive fields are first evaluated by solving a sequence of $2K^2$ linear systems (6.33). From them, functions $V_{hk}(s), X_{hk}(s)$ and $Y_{hk}(s)$ can be immediately identified, since they are piece-wise linear between two consecutive natural nodes. Conversely, distributions $U_{hk}(s)$, which are 5th polynomials in case the 6 DOF FE is adopted in linear cross-section analysis, need to be further evaluated by means of Eq. (6.34). The procedure is even more efficient than the corresponding

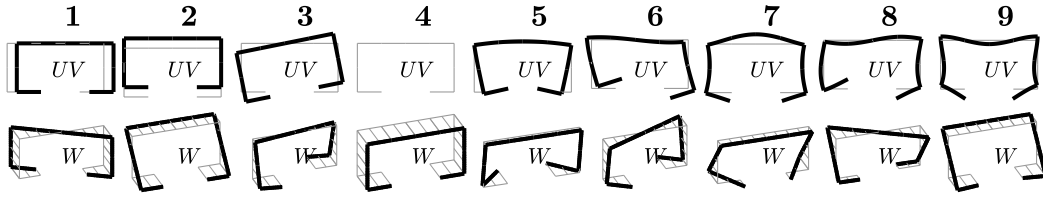


Figure 6.12: Illustrative example of nonlinear cross-section analysis on open cross-section: active conventional planar and warping trial functions.

thermal problem. In fact, the kinematic operator \mathbf{A}_p is the same for any couple h, k for both fields $U_{hk}(s)$ and $X_{hk}(s)$, and needs to be inverted only one time. The sole known term must be updated at each step. As expected, nonlinear trial functions describe pure in-plane elongation of cross-section elements, without bending. Planar passive tangential fields $U_{hk}(s)$, $X_{hk}(s)$ are, as expected, symmetric with respect to index permutation, while fields $X_{hk}(s)$ are step-wise linear on plates forming the cross-section.

In perfect analogy, a kinematic procedure can be developed in order to solve the WTP. After assuming local displacements $W_i^e = W_i$ of natural nodes (Figs. 6.10b and 6.10c) as free parameters, conditions on the global longitudinal elongations can be expressed as:

$$W_{i+1}^e - W_i^e = W_{i+1} - W_i = \int_i^{i+1} \bar{\gamma}(s) ds \quad (6.35)$$

while condition prescribing orthogonality of warping field with respect to uniform longitudinal elongation can be written as:

$$\sum_{i=1}^{n_n} W_i^e = \sum_{i=1}^{n_n} W_i = 0 \quad (6.36)$$

The n_n Eqs. (6.35) and (6.36) constitute a linear system which can be expressed in compact form as (subscript w identifying the *warping* problem):

$$\mathbf{A}_w \mathbf{q}_w = \bar{\gamma} \quad (6.37)$$

where \mathbf{A}_w is a $n_n \times n_n$ non-singular matrix, \mathbf{q}_w is a $n_n \times 1$ vector collecting the unknown warping displacements of natural nodes, while $\bar{\gamma}$ is a $n_n \times 1$ vector collecting known terms. After identifying W_i from Eq. (6.37), the distribution of the warping displacement can be obtained for each element composing the cross-section as:

$$W(\bar{s}) = W_i^e + \int_i^{\bar{s}} \bar{\gamma}(s) ds; \quad \bar{s} \in (i, i+1), i = 1, \dots, n_e \quad (6.38)$$

Warping passive fields $W_{hk}(s)$, $Z_{hk}(s)$ for the proposed open cross-section example are illustrated in Figs. 6.15 and 6.16, respectively. They have been obtained by solving a sequence of $2K^2$ linear system (6.37) where, analogously to the planar problem, the kinematic operator \mathbf{A}_w is the same for any couple h, k and needs to be inverted only one time. From the aforementioned systems, functions $Z_{hk}(s)$ can be immediately identified, since they are piece-wise

$k \backslash h$	1	2	3	4	5	6	7	8	9
1	UV	UV	UV	UV	UV	UV	UV	UV	UV
	U	U	U	U	U	U	U	U	U
2	UV	UV	UV	UV	UV	UV	UV	UV	UV
	U	U	U	U	U	U	U	U	U
3	UV	UV	UV	UV	UV	UV	UV	UV	UV
	U	U	U	U	U	U	U	U	U
4	UV	UV	UV	UV	UV	UV	UV	UV	UV
	U	U	U	U	U	U	U	U	U
5	UV	UV	UV	UV	UV	UV	UV	UV	UV
	U	U	U	U	U	U	U	U	U
6	UV	UV	UV	UV	UV	UV	UV	UV	UV
	U	U	U	U	U	U	U	U	U
7	UV	UV	UV	UV	UV	UV	UV	UV	UV
	U	U	U	U	U	U	U	U	U
8	UV	UV	UV	UV	UV	UV	UV	UV	UV
	U	U	U	U	U	U	U	U	U
9	UV	UV	UV	UV	UV	UV	UV	UV	UV
	U	U	U	U	U	U	U	U	U

Figure 6.13: Illustrative example of nonlinear cross-section analysis on open cross-section: passive in-plane trial functions $U_{hk}(s)$, $V_{hk}(s)$.

$h \backslash k$	1	2	3	4	5	6	7	8	9
1									
2									
3									
4									
5									
6									
7									
8									
9									

Figure 6.14: Illustrative example of nonlinear cross-section analysis on open cross-section: passive in-plane trial functions $X_{hk}(s)$, $Y_{hk}(s)$.

linear between two consecutive natural nodes. Conversely, distributions $W_{hk}(s)$, which are 6th polynomials in case the 6 DOF FE is adopted in linear cross-section analysis, need to be further evaluated by means of Eq. (6.38). As expected, passive warping fields are not symmetric with respect to index permutations, while fields $Z_{hk}(s)$ are piece-wise linear on plates forming the cross-section.

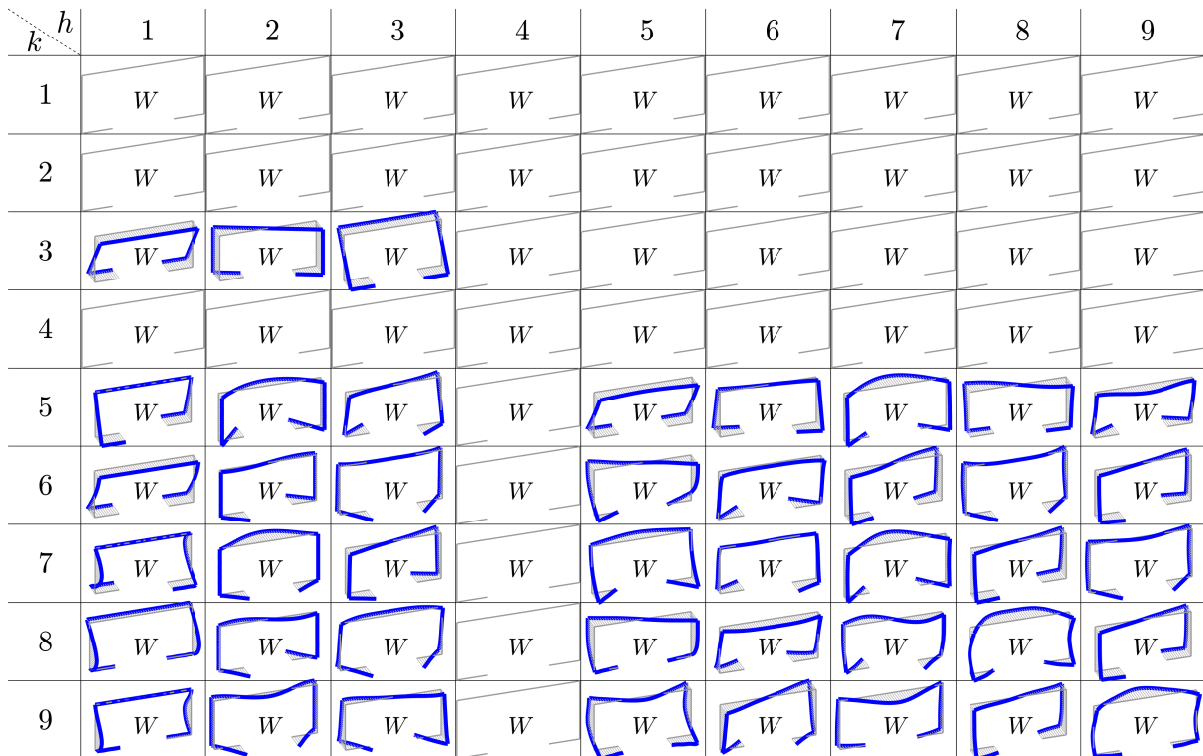


Figure 6.15: Illustrative example of nonlinear cross-section analysis on open cross-section: passive warping trial functions $W_{hk}(s)$.

6.3 Member analysis

The total potential energy principle is used to obtain the weak formulation of the elasticity problem. To this end, the Kirchhoff model is adopted to express the displacement field within the plate thickness, and a linear elastic constitutive law is assumed. By adopting the complete Green-Lagrange strain expression and neglecting nonlinear terms inherent to flexural strain terms, then considering that the NGBT (second-order) displacement field in Eq. (6.21) identically satisfies the Vlasov (Bredt) hypothesis depicted in Eq. (6.4), the following is ob-

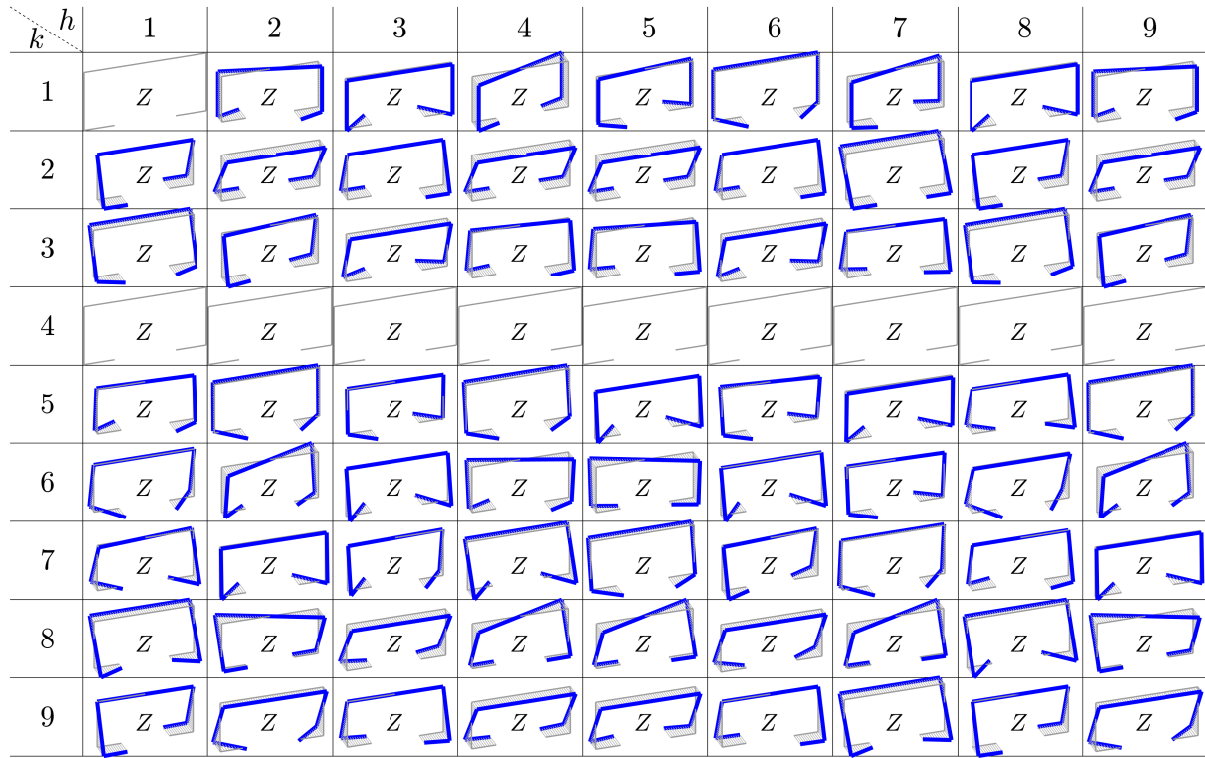


Figure 6.16: Illustrative example of nonlinear cross-section analysis on open cross-section: passive warping trial functions $Z_{hk}(s)$.

tained:

$$\begin{aligned}
 & \int_{\mathcal{L}} \int_{\mathcal{C}} \left\{ \frac{Et}{1-\nu^2} \left[w_{,z} + \frac{1}{2} (u_{,z}^2 + v_{,z}^2 + w_{,z}^2) \right] [u_{,z} \delta u_{,z} + v_{,z} \delta v_{,z} + (1 + w_{,z}) \delta w_{,z}] + \right. \\
 & \quad \left. + \frac{Et^3}{12(1-\nu^2)} [(v_{,ss} + \nu v_{,zz}) \delta v_{,ss} + (\nu v_{,ss} + v_{,zz}) \delta v_{,zz}] + \frac{Gt^3}{3} v_{,sz} \delta v_{,sz} \right\} ds dz = \\
 & \quad = \mu \int_{\mathcal{L}} \int_{\mathcal{C}} (f_s \delta u + f_y \delta v + f_z \delta w) ds dz \quad (6.39)
 \end{aligned}$$

where \mathcal{L} and \mathcal{C} are the beam length and the cross-section mid-line, respectively; E , G and ν are the longitudinal, tangential and Poisson moduli, respectively; f_s , f_y and f_z are surface loads applied at the middle surface of the member \mathcal{S} , respectively, μ is a load multiplier; the ‘‘comma’’ denotes differentiation with respect to the following variable, while the δ -operator denotes virtual quantities. By making use of the NGBT displacement field, Eq. (6.21), the variational equation is recast in the form:

$$\begin{aligned}
 & \int_{\mathcal{L}} \sum_{i=1}^K \sum_{j=1}^K \sum_{h=1}^K \sum_{k=1}^K \left\{ \mathcal{F}(\varphi_h, \delta\varphi_k; \mu) + \mathcal{N}_2(\varphi_j, \varphi_h, \delta\varphi_k; \mu) + \right. \\
 & \quad \left. + \mathcal{N}_3(\varphi_i, \varphi_j, \varphi_h, \delta\varphi_k) \right\} dz = 0 \quad \forall \delta\varphi_k(z) \quad (6.40)
 \end{aligned}$$

where \mathcal{F} , \mathcal{N}_2 and \mathcal{N}_3 are differential operators which are linear, bi- and three-linear, respectively, in the coordinates $\varphi_k(z)$. In particular, the linear operator \mathcal{F} describe the elastic behavior of the TWM in the geometrically linear regime and can be expressed as:

$$\begin{aligned} \mathcal{F}(\varphi_h, \delta\varphi_k; \mu) = & \left(B_{hk}^f \varphi_h + F_{kh}^f \varphi_h'' - \mu \int_C q_{1k} ds \right) \delta\varphi_k + \\ & + \left(D_{hk}^t \varphi_h' - \mu \int_C q_{2k} ds \right) \delta\varphi_k' + \left[F_{hk}^f \varphi_h + \left(C_{hk}^a + C_{hk}^f \right) \varphi_h'' \right] \delta\varphi_k'' \end{aligned} \quad (6.41)$$

where relevant structural matrices and load vectors are defined in Section 2.3. Concerning multi-linear operators \mathcal{N}_2 and \mathcal{N}_3 , they are related to nonlinear effects and can be expressed in the following form:

$$\begin{aligned} \mathcal{N}_2(\varphi_j, \varphi_h, \delta\varphi_k; \mu) = & \sum_{\beta=0}^3 \sum_{\eta=0}^3 \sum_{\zeta=0}^3 C_{j h k}^{\beta \eta \zeta} \partial_{\beta}(\varphi_j) \partial_{\eta}(\varphi_h) \partial_{\zeta}(\delta\varphi_k) + \\ & - \mu \sum_{\eta=0}^3 \sum_{\zeta=0}^3 P_{h k}^{\eta \zeta} \partial_{\eta}(\varphi_h) \partial_{\zeta}(\delta\varphi_k) \end{aligned} \quad (6.42a)$$

$$\mathcal{N}_3(\varphi_i, \varphi_j, \varphi_h, \delta\varphi_k) = \sum_{\alpha=0}^3 \sum_{\beta=0}^3 \sum_{\eta=0}^3 \sum_{\zeta=0}^3 C_{i j h k}^{\alpha \beta \eta \zeta} \partial_{\alpha}(\varphi_i) \partial_{\beta}(\varphi_j) \partial_{\eta}(\varphi_h) \partial_{\zeta}(\delta\varphi_k) \quad (6.42b)$$

where notation $\partial_{\lambda}(\cdot)$ denotes the λ -th derivative with respect to z , while constants $C_{j h k}^{\beta \eta \zeta}$, $C_{i j h k}^{\alpha \beta \eta \zeta}$ and functions $P_{h k}^{\eta \zeta}(z)$ are known terms related linear and passive trial functions and external surface loads. Since their formulation is burdensome, they won't be reported in full in the present thesis, and only one of them for each typology is briefly illustrated in the following as example:

$$C_{j h k}^{220} = \frac{Et}{(1-\nu^2)} \int_C \left[\frac{t^2}{6} V_j(s) V_{hk}(s) + \frac{\nu t^2}{3} Y_{jh}(s) V_k''(s) + W_j(s) W_{kh}(s) \right] ds \quad (6.43a)$$

$$C_{i j h k}^{1313} = \frac{Et}{(1-\nu^2)} \int_C \left[Z_{ij}(s) Z_{hk}(s) + \frac{t^2}{3} Y_{ij}(s) Y_{hk}(s) \right] ds \quad (6.43b)$$

$$P_{h k}^{10}(z) = \int_C f_z(s, z) W_{kh}(s) ds \quad (6.43c)$$

Starting from Eq. (6.41) and consistently with the spirit of GBT, a set of coupled nonlinear ordinary differential equations, referred to as *nonlinear GBT (NGBT) equations*, and corresponding boundary conditions could be obtained by performing the standard steps of variational calculus (e.g., Berdichevsky, 2009). Some outlines on this topic will be briefly addressed in the following. It is worth to be noted that GBT equations are in number K , i.e. the size of the nonlinear problem remains the same as the linear one. Nonlinear GBT equations are solved numerically by means of a FE procedure (e.g., Bathe, 2014). When linear coordinates $\varphi_k(z)$ are interpolated

in the domain $z \in [0, \mathcal{L}]$, usually by means of cubic Hermite polynomial shape functions (see Section 2.3), a nonlinear algebraic system in the nodal value vectors \mathbf{q} is derived in the form:

$$\mathbf{K}\mathbf{q} + \mathbf{n}_2(\mathbf{q}, \mathbf{q}; \mu) + \mathbf{n}_3(\mathbf{q}, \mathbf{q}, \mathbf{q}; \mu) = \mu(\mathbf{p} + \mathbf{P}\mathbf{q}) \quad (6.44)$$

where the column vectors \mathbf{n}_i are quadratic and cubic homogeneous forms of displacements, and \mathbf{P} is the second-order effect loading matrix. It is stressed, once again, that the size of the nonlinear problem remains the same as the linear one. Its solution can be addressed by standard incremental-iterative techniques such as those described in Silvestre and Camotim (2003b) using the tangent stiffness matrix that can be deduced from the depicted multi-linear forms.

Nonlinear GBT equations and boundary conditions

It is easy to prove that nonlinear GBT equations are 6th order in $\varphi_k(z)$, due in particular to terms related to passive modes $Y_{hk}(s)$ and $Z_{hk}(s)$ (see, e.g., Eq. (6.43b)) participating into the definition of $v_{,zz}$ and $w_{,z}$, respectively, in Eq. (6.39). Referring in particular to Eq. (6.43b), its associated factor is $\varphi'_i \varphi''_j \varphi'_h \delta \varphi'''_k$. After integration by parts, it leads to terms proportional to $\varphi'_i \varphi''_j \varphi_h^{IV}$, $\varphi'_i \varphi_j^V \varphi_h''$ and $\varphi'_i \varphi'_j \varphi_h^{VI}$.

Boundary conditions, of course, determine the values of the Lagrangian parameters \mathbf{q} at the ends $z = 0, \mathcal{L}$ of a single-span beam. Their imposition, however, is not a trivial task, since they should be consistently formulated in a nonlinear kinematic context. Indeed, Eq. (6.21) point out that it is impossible to impose arbitrary boundary conditions. For instance, the classic constraint of “simply-supported beam with free warping” requires the geometric conditions $u = 0, v = 0$ at $z = 0, \mathcal{L}$, as well as the mechanical conditions $\varepsilon_z = 0 \Rightarrow w_{,z} = 0$ (free warping) and $v_{,zz} = 0$ (i.e., plate bending moment equal to zero). In the linear field they are all fulfilled by $\varphi_k = 0, \varphi''_k = 0$, for any k , but in the nonlinear regime it is no longer valid. This depends on the fact that this constraint is incompatible with the hypothesis of transverse inextensibility. If, in fact, it was $w \neq 0$ and $u = 0$, with $v = 0$ to the beam edge, the center line of the profile would lengthen of $\varepsilon_s = w_{,z}^2/2$, in violation of the inextensibility constraint. Therefore, it needs to release some conditions. If u is left free, allowing the shortening of the mid-line to the edge, it can still impose $\varphi_k = 0, \varphi''_k = 0$ that, however, cancel only the linear part of u and ε_z . Non-linearities will produce $u \neq 0$, consistently with the internal constraint, but they involve an error on the mechanical condition $\varepsilon_z = 0$. In the spirit of FE technique, however, this will be satisfied “on average” thanks to the weak formulation.

From these arguments, it can be argued that the most non-linear effect occurs when the end sections of the beam can not approach, i.e. when the warping is zero at both the extremes. These conditions, indeed, produce axial elongation, generally negligible at the first order. To constrain warping $\varphi_k = 0, \varphi'_k = 0$ have to be imposed at the edges. These conditions imply that plates are also clamped at the edges.

6.4 Applications

Two examples are presented in order to validate and illustrate the application and capabilities of the proposed method. The first application concerns a beam of length $\mathcal{L} = 1$ m having

the C-lipped cross-section illustrated in Fig. 6.11a. The material properties adopted in the calculation specify an elastic modulus $E = 200$ GPa and Poisson's ratio $\nu = 0.3$. The beam is not pre-stressed, and it is assumed to be fully clamped and fully warping restrained at both end sections ($\varphi_k(0) = \varphi_k'(0) = 0$ and $\varphi_k(\mathcal{L}) = \varphi_k'(\mathcal{L}) = 0$, $k = 1, \dots, K$), while the external load consists of a vertical uniform pressure load $p_{sy}(s, z)$ applied to the upper side of the entire web panel (Fig. 6.17). The discretization adopted in the cross-section analysis is shown by Fig. 6.11b. The one adopted in the member analysis (i.e., along the beam axis z) involves 10 finite elements. In order to validate and verify the numerical accuracy of the proposed method,

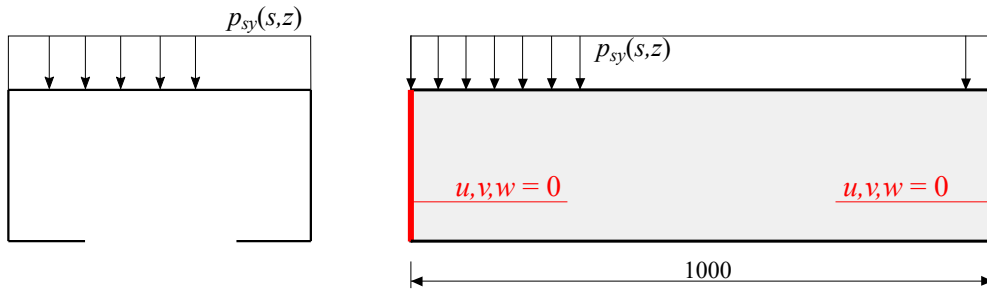


Figure 6.17: Illustrative application on lipped channel member: load arrangement and restraints conditions.

the FE software ABAQUS/Standard (Simulia, 2010) has been used. The beam is modeled by the S4 shell finite element available in the standard ABAQUS library. This general-purpose conventional shell element is based on the general plate theory which automatically turns into the Kirchhoff model as the thickness decreases. Moreover, these elements account for finite membrane strains and arbitrary large rotations; therefore, it is suitable for large-strain (geometrically nonlinear) analysis. The whole beam is discretized through quadrangular shell elements with about 5 mm width, altogether 10,000 finite elements. Together with the non-linear numerical analysis, a standard linear buckling analysis has been performed. The first linear buckling mode (corresponding to the first positive eigenvalue) showed by the beam subjected to the load described above is a local-plate buckling mode (see Fig. 6.18) that mainly involves the web of the C-lipped section at the mid-span of the beam. The associated linear buckling critical load is equal to $p_{sy,cr} = 0.114$ MPa. A subset of active and passive trial functions for the C-lipped cross-section has been shown in Figs. 6.12 to 6.16. Figs. 6.20 and 6.21 show a comparison between the solution obtained using the proposed approach and the ABAQUS solution at specific locations of the structure, which will be specified hereinafter. In the following, the term “L” refers to the solution of the linear problem obtained by using the subset of conventional linear fields listed in brackets. Label “NL” refers to the solution obtained by the proposed model using the specified subset of conventional linear fields together with all the corresponding passive fields provided by the nonlinear cross-section analysis methodology. The importance of each linear field in describing the overall response of the beam may be represented by the so-called *participation factors* (e.g., Taig et al., 2016) defined based on the contribution of each field to the total (internal) work done to deform the TWM, as:

$$p_k = \frac{\mathcal{W}_k}{\sum_{k=1}^K |\mathcal{W}_k|} \quad (6.45)$$

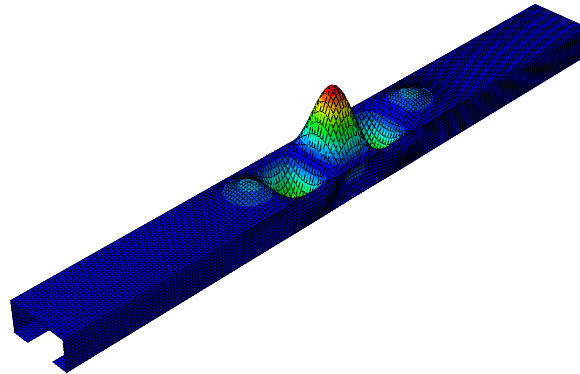


Figure 6.18: Illustrative application on lipped channel member: first mode of buckling.

being \mathcal{W}_k the elastic work done by the k -th linear trial function. Participation factors for the considered applications are reported in Fig. 6.19. Because of the geometry properties and load arrangement, significant linear fields are the only ones that are symmetrical with respect to the vertical axis of cross-section symmetry. In particular, the first four symmetric fields (**2,5,7,9**) are the most participating in describing the response of the TWM. Furthermore, the conventional longitudinal shortening field (**4**) can be completely neglected in the linear analysis because of the orthogonality between the load direction and the z axis.

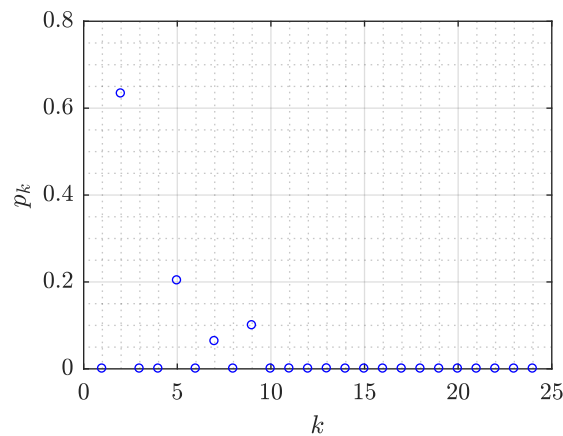


Figure 6.19: Illustrative application on lipped channel member: participation factor.

Fig. 6.20 shows the vertical displacement of the mid-web node 9 (Fig. 6.11b) at mid-span of the beam, for the specified subsets of linear fields. From a qualitative point of view, the proposed NL solution provides a good approximation of the numerical solution using the first 3 (linear) fields only (**2,5,7**-Fig. 6.20a). The non-linear curve shows an initial softening behavior, then it becomes progressively hardening when the first critical linear buckling load is exceeded (i.e., p_{sy} approximately greater than 0.114 MPa). The NL solution is able to catch the initial softening behavior and it shows an inflection point just in the neighborhood of the first critical

linear buckling load. From a quantitative point of view, differences between the 3-field GBT and ABAQUS solution is about 10% in both linear and nonlinear results. By the addition of the the longitudinal shortening field (**4** - Fig. 6.20a), which allows to include the uniform axial (longitudinal) elongation of the TWM, an improvement of the NL solution is obtained. When increasing the load, in fact, the catenary action provided by external restraints becomes progressively more important. Therefore, the inclusion of the beam capability to extend uniformly along its axis plays an important role in getting accurate results. In order to reach a global refinement, other vertical symmetrical conventional fields may be added. Fig. 6.20b shows the same graph with the supplement of conventional field **9** (i.e., the fourth vertical symmetric conventional field). The global behavior of the proposed solution is maintained but quantitative differences with respect to the ABAQUS solution are now limited and reduced to about half.

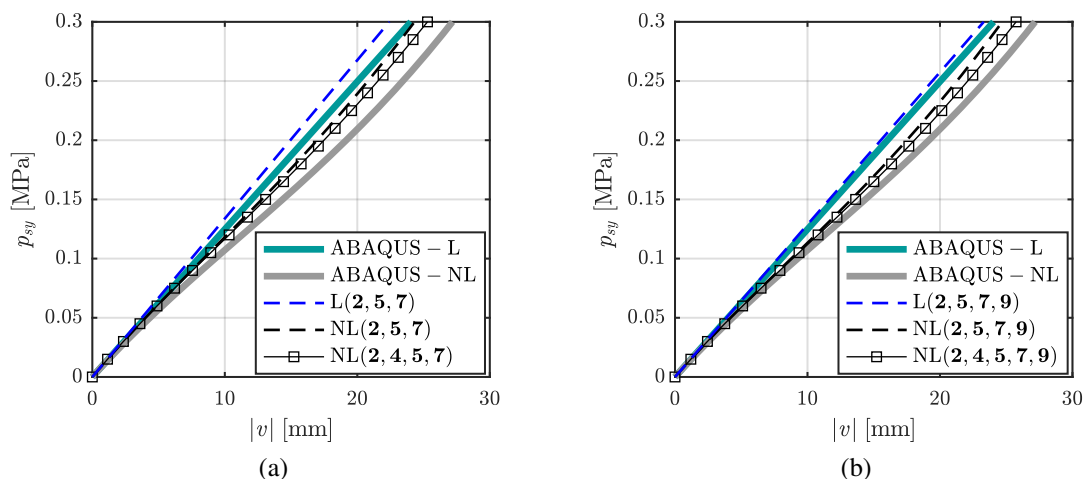


Figure 6.20: Illustrative application on lipped channel member. Vertical displacement of the mid-web node ad mid-span of the beam: comparison between proposed NGBT solution obtained using (a) 3 or (b) 4 linear fields and ABAQUS solution.

Fig. 6.21 shows the horizontal displacement of the top-edge node 3 (Fig. 6.11b) at mid-span of the beam. Similarly to the previous case, the qualitative non-linear behavior is fully reached by the proposed NL approach using the first 3 significant conventional (linear) fields only (**2,5,7** - Fig. 6.21a). Quantitatively, differences between the 3-field NL model and the ABAQUS solution is still about 10%. The addition of the the conventional longitudinal shortening field **4** (Fig. 6.21a) allows to further improve the NL solution (similarly to first, differences with respect to the ABAQUS solution are reduced to about half). The addition of one conventional vertical symmetric (linear) field (**9**) makes the solution obtained by the proposed NL approach practically coincident with the ABAQUS solution (Fig. 6.21b). In this case linear solutions are not relevant since they do not allow the transverse displacement of the cross-section nodes.

The second application concerns a TWM having the closed rectangular cross-section illustrated in Fig. 6.3a. The material properties adopted in the calculation specify an elastic modulus $E = 200 \text{ GPa}$ and Poisson’s ratio $\nu = 0.3$. The beam possess length $\mathcal{L} = 1 \text{ m}$ and it is assumed to be simply supported (i.e. warping free) at both end sections, while it is restrained from warping at mid-span (Fig. 6.22). The external load consists of a vertical uniform pressure

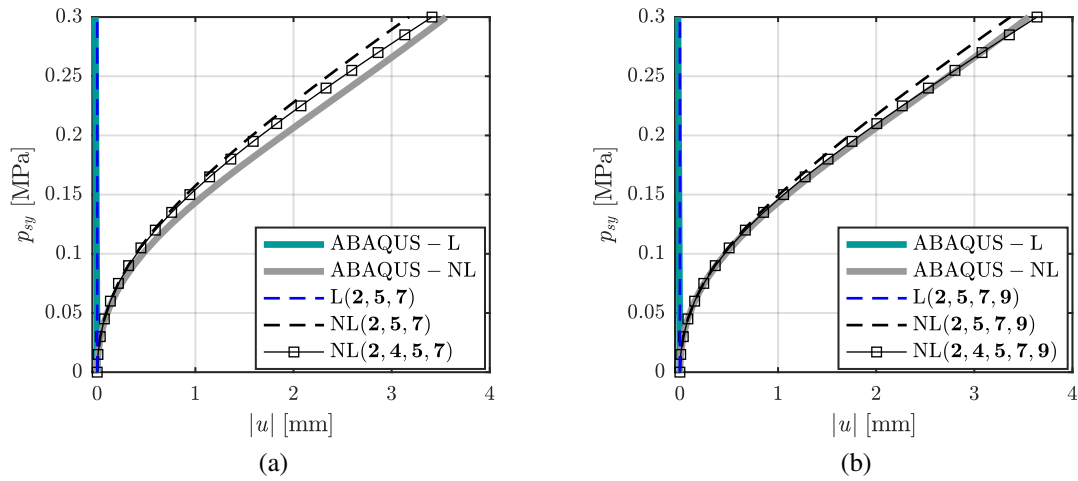


Figure 6.21: Illustrative application on lipped channel member. Horizontal displacement of the top-edge node at mid-span of the beam: comparison between proposed NGBT solution obtained using (a) 3 or (b) 4 linear fields and ABAQUS solution.

load $p_{sy}(s, z)$ applied to the upper side of the entire web panel (Fig. 6.22). The discretization adopted in the cross-section analysis is shown by Fig. 6.3b. The one adopted in the member analysis (i.e., along the beam axis z) involves 10 finite elements.

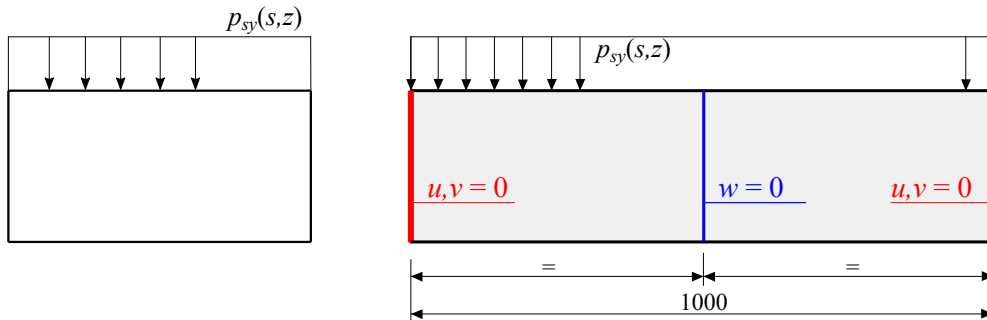


Figure 6.22: Illustrative application on closed TWM: load arrangement and restraints conditions.

A refined shell-FE model has been developed for validation purposes using the software ABAQUS/Standard (Simulia, 2010). Similarly to as done for the previous application, the whole beam is discretized through quadrangular shell elements of type S4 with about 2 mm width, altogether 75,000 finite elements. Together with the non-linear numerical analysis, a standard linear buckling analysis has been performed. The first linear buckling mode (corresponding to the first positive eigenvalue) showed by the beam subjected to the load described above is a local-plate buckling mode (see Fig. 6.23) that mainly involves the superior flange at the mid-span of the beam. The associated linear buckling critical load is equal to $p_{sy,cr} = 0.052$ MPa.

A subset of active and passive trial functions has been shown in Figs. 6.4 to 6.6, 6.8 and 6.9. The linear analysis has been first performed, in order to evaluate participation factors. They are shown in Fig. 6.24. As expected and analogously to the previous application, significant linear

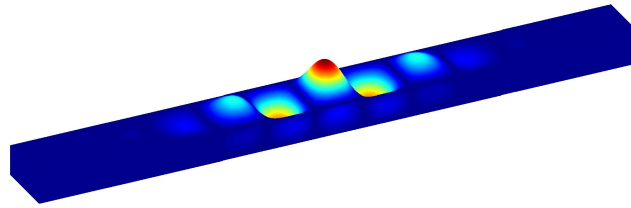


Figure 6.23: Illustrative application on closed TWM: first mode of buckling.

fields are the only ones that are symmetrical with respect to the vertical axis of cross-section symmetry, with in particular the first three symmetric fields (2,6,7) describing almost the entire response of the beam in the geometrically linear regime. The conventional longitudinal shortening field (4) can be completely neglected in the linear analysis because of the orthogonality between the load direction and the z axis. Nevertheless, it plays a fundamental role when modeling the nonlinear regime, modeling approaching of the beam end-sections induced by the beam transverse deflection. This effect would not be described by passive fields since the latter are able to model nonlinear effects limited to as regard the cross-section.

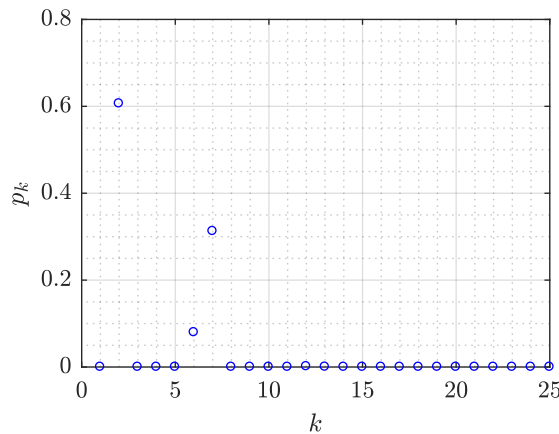


Figure 6.24: Illustrative application on closed TWM: participation factor.

Fig. 6.25 depict displacements u , v , w at selected points of the cross-section. In particular, displacements are plotted in correspondence of the beam coordinate z in which they reach their maximum value, that is mid-span (i.e., $z = \mathcal{L}/2$) as regards tangential and transverse in-plane displacements u , v and the beam end-section (i.e., $z = 0, \mathcal{L}$) concerning warping displacements w . As regards the proposed NGBT model, the solution obtained by including the subset of the sole relevant fields (2,4,6,7), together with all the corresponding passive fields provided by the nonlinear cross-section analysis methodology, is compared with both the reference FE solution and the corresponding NGBT solution obtained by using the whole set of (linear and nonlinear) fields, the latter referred to as in figures with the nomenclature *full*. From a qualitative point of view, the proposed NL solution provides an excellent approximation of the numerical solution using the sole relevant fields (2,4,6,7). The non-linear curve describes a softening behavior, becoming progressively more evident when the first critical linear buckling load is exceeded

(i.e., p_{sy} approximately greater than 0.052 MPa). From a quantitative point of view, the 4-field GBT and ABAQUS solution are practically coincident up to a load equal to about $p_{sy} = 0.20$ MPa. When the latter is exceeded, some difference between the two models begin to appear. They are however very limited (about 10% when $p_{sy} = 0.30$ MPa). As expected, the addition of further trial functions does not improve the NGBT result. In fact, the 4-field NGBT solution is coincident with the corresponding one obtained by using the full set of linear and nonlinear fields. This aspect is the key-feature of the proposed NGBT approach, where nonlinear effects are fully described by passive fields associated to the subset of relevant linear functions. As a consequence, the proposed approach is very efficient from a computational viewpoint, since the use of a (commonly very limited) subset of trial functions reduces exponentially the required computational effort with respect to the case where the full set of functions is adopted.

Finally, displacements of the whole cross-section are shown in Fig. 6.26 for a reference load of 0.25 MPa. In particular, Fig. 6.26a shows the in-plane displacements at the beam mid-span, while Fig. 6.26b depicts warping distribution at the beam end section. For clarity, the plotted variables have been suitably scaled, and scale coefficient is reported for each plot. The evident softening behavior depicted by the analyzed TWM can be explained thanks to the significant inward deflection of both superior and inferior flanges, which is responsible for the progressive reduction of the beam stiffness with respect to vertical loads. The proposed NGBT approach appears able to perfectly reproduce the numerical non-linear response of the beam. Transverse shortening of the superior flange points out the fundamental role of passive (transverse shortening) fields in the nonlinear analysis. Once again, it is stressed the fact that the 4-fields (reduced) NGBT solution is perfectly coincident with the NGBT ones obtained by using the full set of trial functions.

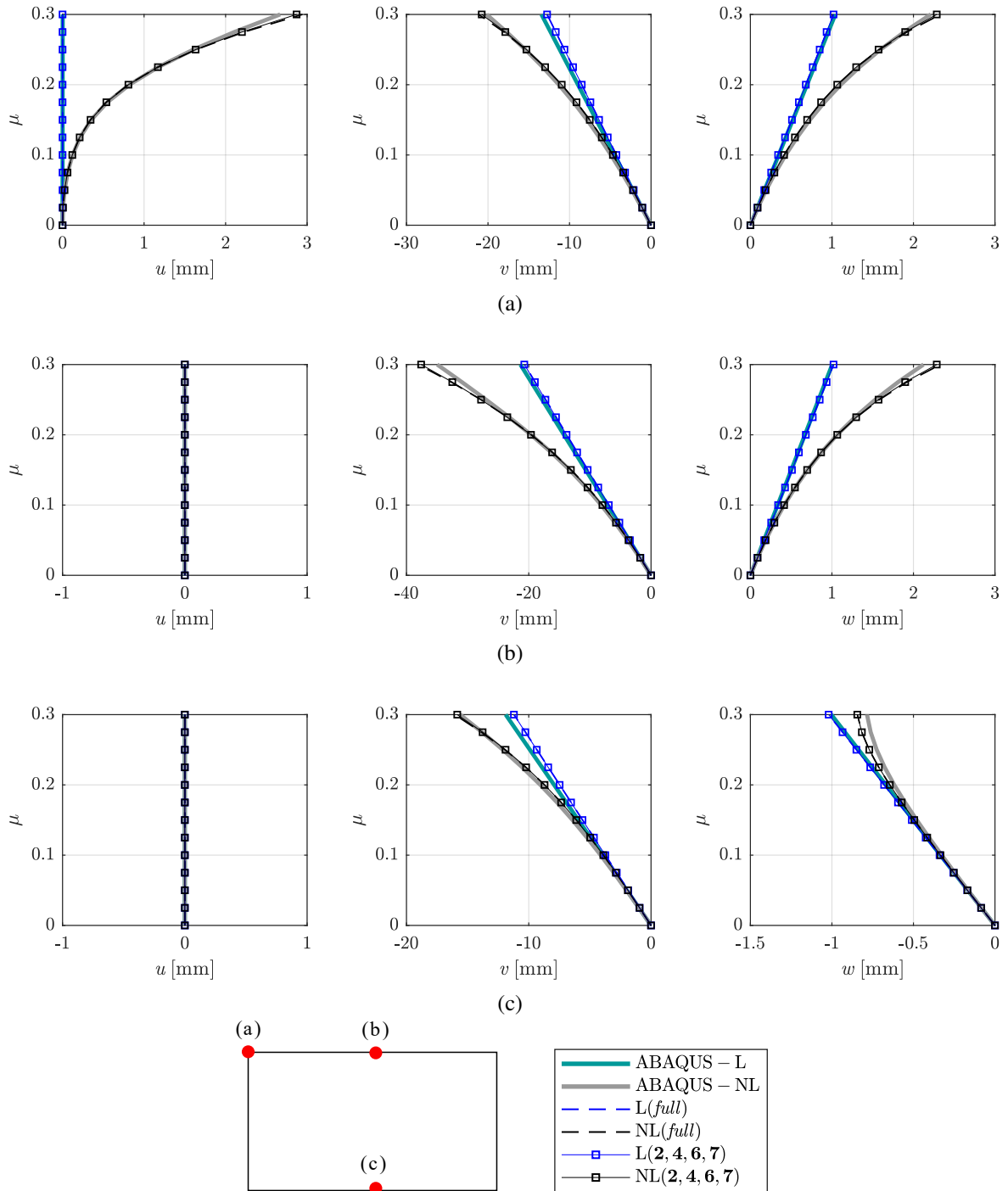


Figure 6.25: Illustrative application on closed TWM: Horizontal, vertical and warping displacement at selected points of the TWM.

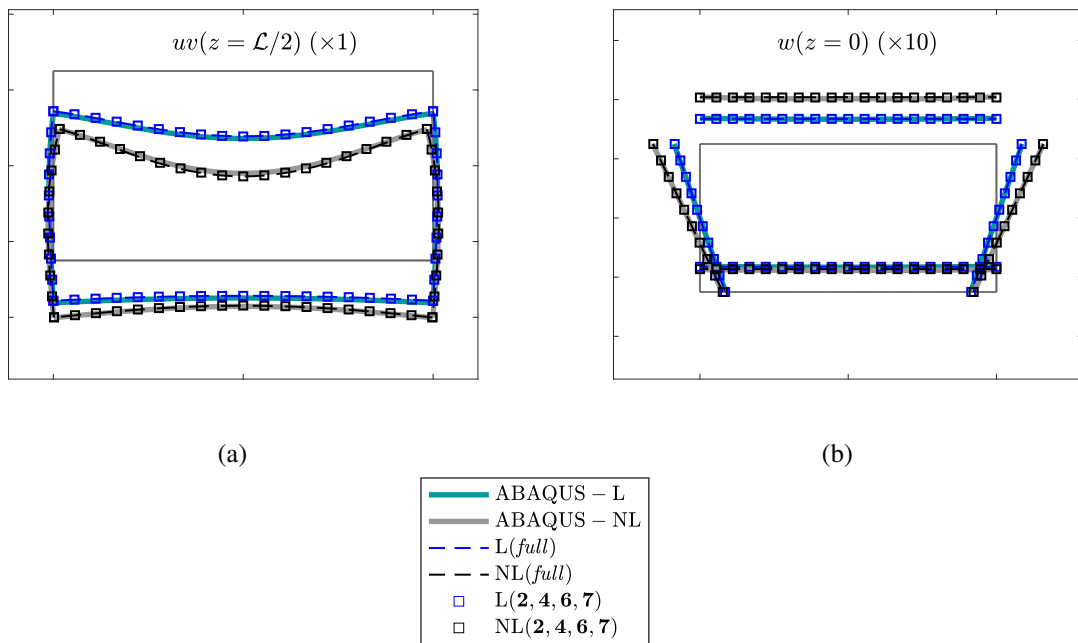


Figure 6.26: Illustrative application on closed TWM: (a) in-plane displacement at mid-span, (b) warping displacement at end-section.

Chapter 7

Conclusions and perspectives

7.1 Conclusions

The Generalized Beam Theory (GBT) is a very efficient and reliable tool for the linear and nonlinear analysis of thin-walled members TWMs. Its characteristic feature is the capability to give a clear physical interpretation to the mechanical behavior experienced by the TWM, as well as to reduce the the three-dimensional continuous elasticity problem to a vector-valued one-dimensional one.

In this Thesis, new approaches have been proposed for the linear and nonlinear analyses of TWMs in the framework of the GBT, aimed to improve its reliability and numerical efficiency. A novel straightforward dynamic procedure has been proposed for the cross-section analysis (Chapter 3), able to provide the full set of trial functions, included conventional and non-conventional ones, by means of a very limited number of eigenvalue problems, in particular three for mono-connected (i.e., open) cross-section and four for multi-connected (i.e. closed and partially closed) ones. Regarding the latter, they involve hybrid (i.e., mixed extension-flexural) fields for their intrinsic (hyperstatic) characteristics. The procedure maintains its simplicity in all conditions, in addition to provide very clean and precise deformation fields, having a clear physical interpretation without the need of further manipulation operations. The importance of selecting a consistent set of polynomial shape functions for the finite element representation specified for the cross-section analysis has also been discussed. Locking problems have been shown to occur when this consistency is not satisfied.

A GBT-based approach has been developed for the partial analysis of multi-component TWMs (Chapter 4). The approach relies on the identification of a suitable set of linear trial functions capable of describing both longitudinal and transverse partial interaction taking place at the interface plane between adjacent components. To this end, two dynamic procedures for the cross-section analysis have been proposed. The first one stems from the so-called unconstrained approach available in the Literature, while the second one is the generalization of the novel dynamic procedure previously introduced to multi-component TWMs. The latter is noteworthy for its capability in combining precision and cleanliness, in terms of obtained deformation fields, with a simple and straightforward (i.e., not recursive, conversely than the unconstrained approach) procedure. The proposed approach has been validated against the numerical values obtained by means of a shell finite element model developed in ABAQUS/Standard.

A displacement-based GBT formulation has been developed for the analysis of composite TWMs with large web penetrations (Chapter 5). The approach benefits of the partial interaction model described above, and allows to model composite TWMs with large squared web penetrations and localized longitudinal stiffeners with a systematic and straightforward fashion. In particular, it allows to transform GBT-based beam FEs into an assembly of flat quadrilateral GBT-based shell elements that benefits of assembly procedures commonly adopted in standard

FE models. As a consequence, continuity of displacement fields between adjacent members composing the structural system can be automatically enforced, with no need to introduce burdensome constraint equations. The accuracy and ease-to-use of the proposed approach has been shown by means of an application on a large-span composite beam with multiple web-perforations taken from the Literature, and results are compared with the ones obtained by means of a refined shell-based FE model for validation purposes.

Finally, a nonlinear GBT approach (NGBT) has been formulated, based on the nonlinear Galerkin method. The key feature is represented by a nonlinear cross-section analysis, able to provide a set of (passive) nonlinear trial functions, which are slave of conventional (active) linear ones and able to include geometrically nonlinear effects. To this end, the Vlasov hypothesis of (i) in-plane inextensibility, and (ii) undeformability against shear (the latter substituted by the Bredt's condition of constant shear stress flow on closed loops) have been enforced on the full (nonlinear) Green-Lagrange strain expressions. A direct and computationally efficient procedure for the evaluation of nonlinear fields has been proposed, based on a formal thermal analogy. The proposed model can be applied to general (i.e., open, closed and partially-closed) cross-sections and is able to well describe the TWM nonlinear behavior by means of a very limited number of (linear and nonlinear) fields. Moreover, since passive fields are slave of linear ones, the number of unknowns of the nonlinear problem (i.e., its dimension) remains the same as the linear one. Therefore, the approach complies the spirit of GBT as a reduction method, in addition to be very efficient from a computational viewpoint. Comparison between results obtained with the proposed approach and the ones obtained by means of refined shell-based FE analyses are very promising.

7.2 Further research

Concerning the GBT-based approaches proposed in this Thesis, the following suggestions for further researches can be addressed:

- the capability to model TWMs with arbitrary curved cross-section and longitudinal axis should be included in the GBT framework. To this end, the spline interpolation may be used for describing the TWM geometry;
- the model describing the linear-elastic behavior of multi-components members should be further developed to include contact and separation between the various components forming the TWM;
- a geometrically nonlinear GBT approach should be addressed for the buckling and post-buckling analysis of multi-components members; to this end, the capability to include contact and separation at various interfaces constitutes a fundamental feature;
- the displacement-based GBT approach should be extended to include arbitrary-shaped perforations; moreover, the inclusion of transverse stiffeners as well as the capability to model girders with discrete diaphragms may represent an interesting development which would make the proposed GBT formulation suitable for composite steel-concrete bridges analysis;

-
- the study of the influence of in-plane and membrane shear strains on the geometrically nonlinear behavior of TWMs (i.e., the validity of the Vlasov theory in the nonlinear field) is also of great interest. In this sense, the proposed NGBT approach should be extended to account, through passive fields, of small (i.e., second-order) in-plane and membrane shear strains;
 - based on the Koiter approach, passive fields should be suited for the introduction of passive buckling modes, to be adopted for the post-critical analysis of TWMs.

Appendix A

Stiffness and Mass Element Matrices for cross-section Finite Elements

A.1 Beam Finite Elements for linear cross-section analysis

A.1.1 In-plane 6 DOF, out-of-plane 2 DOF finite element (FE₁)

A classic six DOF (Euler-Bernoulli) beam FE is considered (Fig. A.1a), based on which displacement fields U, V are interpolated through linear Lagrangian and cubic Hermite polynomial functions, respectively, as follows:

$$U(s) \Big|_{s=0}^{l_e} = \sum_{n=1}^2 L_n(s, l_e) U_n^e; \quad V(s) \Big|_{s=0}^{l_e} = \sum_{n=1}^2 H_{2n-1}(s, l_e) V_n^e + H_{2n}(s, l_e) \theta_n^e \quad (\text{A.1a,b})$$

where:

$$L_1(s, l_e) = 1 - \frac{s}{l_e}; \quad L_2(s, l_e) = \frac{s}{l_e} \quad (\text{A.2a,b})$$

and

$$H_1(s, l_e) = 1 - 3 \left(\frac{s}{l_e} \right)^2 + 2 \left(\frac{s}{l_e} \right)^3; \quad H_2(s, l_e) = l_e \left[\frac{s}{l_e} - 2 \left(\frac{s}{l_e} \right)^2 + \left(\frac{s}{l_e} \right)^3 \right] \quad (\text{A.3a,b})$$

$$H_3(s, l_e) = 3 \left(\frac{s}{l_e} \right)^2 - 2 \left(\frac{s}{l_e} \right)^3; \quad H_4(s, l_e) = l_e \left[- \left(\frac{s}{l_e} \right)^2 + \left(\frac{s}{l_e} \right)^3 \right] \quad (\text{A.3c,d})$$

Referring to the consistent mass approach (e.g., Inman, 2013), the stiffness \mathbf{K}_p^e and the mass \mathbf{M}_p^e matrices for the generic e -th element in PEPs are defined as:

$$\mathbf{K}_p^e = \frac{EJ}{l_e} \begin{bmatrix} \frac{EA}{EJ} & 0 & 0 & -\frac{EA}{EJ} & 0 & 0 \\ 0 & \frac{12}{l_e^2} & \frac{6}{l_e} & 0 & -\frac{12}{l_e^2} & \frac{6}{l_e} \\ 0 & \frac{6}{l_e} & 4 & 0 & -\frac{6}{l_e} & 2 \\ -\frac{EA}{EJ} & 0 & 0 & \frac{EA}{EJ} & 0 & 0 \\ 0 & -\frac{12}{l_e^2} & -\frac{6}{l_e} & 0 & \frac{12}{l_e^2} & -\frac{6}{l_e} \\ 0 & \frac{6}{l_e} & 2 & 0 & -\frac{6}{l_e} & 4 \end{bmatrix} \quad (\text{A.4a})$$

$$\mathbf{M}_p^e = \frac{\rho l_e}{420} \begin{bmatrix} 140 & 0 & 0 & 70 & 0 & 0 \\ 0 & 156 & 22l_e & 0 & 54 & -13l_e \\ 0 & 22l_e & 4l_e^2 & 0 & 13l_e & -3l_e^2 \\ 70 & 0 & 0 & 140 & 0 & 0 \\ 0 & 54 & 13l_e & 0 & 156 & -22l_e \\ 0 & -13l_e & -3l_e^2 & 0 & -22l_e & 4l_e^2 \end{bmatrix} \quad (\text{A.4b})$$

where E and ρ are the longitudinal elastic modulus and mass density, respectively, A and J are the transverse area and the moment of inertia, respectively, referred to a unitary-length beam segment, and l_e is the length of the FE.

Based on a two DOF beam FE (Fig. A.1b), linear Lagrangian interpolating polynomial functions (Eq. (A.2)) have been adopted for out-of-plane displacements, i.e.,

$$W(s)\Big|_{s=0}^{l_e} = \sum_{n=1}^2 L_n(s, l_e) W_n^e \quad (\text{A.5})$$

Referring to the consistent mass approach, the stiffness \mathbf{K}_w^e and the mass \mathbf{M}_w^e matrices for the generic e -th element in WEP are defined as:

$$\mathbf{K}_w^e = \frac{Gt}{l_e} \begin{bmatrix} 1 & -1 \\ -1 & 1 \end{bmatrix}; \quad \mathbf{M}_w^e = \frac{\rho l_e}{6} \begin{bmatrix} 2 & 1 \\ 1 & 2 \end{bmatrix} \quad (\text{A.6a,b})$$

where G and t are, respectively, the tangential elastic modulus and thickness.

A.1.2 In-plane 7 DOF, out-of-plane 3 DOF finite element (FE₂)

The seven DOF (Euler-Bernoulli) beam FE is considered (Fig. A.1c), based on which displacement fields U, V are interpolated through parabolic Lagrangian and cubic Hermite polynomial functions, respectively, as follows:

$$U(s)\Big|_{s=0}^{l_e} = \sum_{n=1}^3 L_n(s, l_e) U_n^e \quad (\text{A.7a})$$

$$V(s)\Big|_{s=0}^{l_e} = \sum_{n=1}^2 H_{2n-1}(s, l_e) V_{2n-1}^e + H_{2n}(s, l_e) \theta_{2n-1}^e \quad (\text{A.7b})$$

where:

$$L_1(s, l_e) = 1 - 3\frac{s}{l_e} + 2\left(\frac{s}{l_e}\right)^2; \quad L_2(s, l_e) = 4\frac{s}{l_e} - 4\left(\frac{s}{l_e}\right)^2 \quad (\text{A.8a,b})$$

$$L_3(s, l_e) = -\frac{s}{l_e} + 2\left(\frac{s}{l_e}\right)^2 \quad (\text{A.8c})$$

and Hermite polynomials $H_n(s, l_e)$ are defined in Eq. (A.3). Referring to the consistent mass approach (e.g., Inman, 2013), the stiffness \mathbf{K}_p^e and the mass \mathbf{M}_p^e matrices for the generic e -th

element in PEPs are defined as:

$$\mathbf{K}_p^e = \frac{EJ}{l_e} \begin{bmatrix} \frac{7EA}{3EJ} & 0 & 0 & \frac{-8EA}{3EJ} & \frac{EA}{EJ} & 0 & 0 \\ 0 & \frac{12}{l_e^2} & \frac{6}{l_e} & 0 & 0 & -\frac{12}{l_e^2} & \frac{6}{l_e} \\ 0 & \frac{6}{l_e} & 4 & 0 & 0 & -\frac{6}{l_e} & 2 \\ \frac{-8EA}{3EJ} & 0 & 0 & \frac{16EA}{3EJ} & \frac{-8EA}{EJ} & 0 & 0 \\ \frac{EA}{EJ} & 0 & 0 & \frac{-8EA}{3EJ} & \frac{7EA}{3EJ} & 0 & 0 \\ 0 & -\frac{12}{l_e^2} & -\frac{6}{l_e} & 0 & 0 & \frac{12}{l_e^2} & -\frac{6}{l_e} \\ 0 & \frac{6}{l_e} & 2 & 0 & 0 & -\frac{6}{l_e} & 4 \end{bmatrix} \quad (\text{A.9a})$$

$$\mathbf{M}_p^e = \frac{\rho l_e}{420} \begin{bmatrix} 56 & 0 & 0 & 28 & -14 & 0 & 0 \\ 0 & 156 & 22l_e & 0 & 0 & 54 & -13l_e \\ 0 & 22l_e & 4l_e^2 & 0 & 0 & 13l_e & -3l_e^2 \\ 28 & 0 & 0 & 224 & 28 & 0 & 0 \\ -14 & 0 & 0 & 28 & 56 & 0 & 0 \\ 0 & 54 & 13l_e & 0 & 0 & 156 & -22l_e \\ 0 & -13l_e & -3l_e^2 & 0 & 0 & -22l_e & 4l_e^2 \end{bmatrix} \quad (\text{A.9b})$$

where E and ρ are the longitudinal elastic modulus and mass density, respectively, A and J are the transverse area and the moment of inertia, respectively, referred to a unitary-length beam segment, and l_e is the length of the FE.

Based on a three DOF beam FE (Fig. A.1d), parabolic Lagrangian interpolating polynomial functions (Eq. (A.8)) have been adopted for out-of-plane displacements, i.e.,

$$W(s) \Big|_{s=0}^{l_e} = \sum_{n=1}^3 L_n(s, l_e) W_n^e \quad (\text{A.10})$$

Referring to the consistent mass approach, the stiffness \mathbf{K}_w^e and the mass \mathbf{M}_w^e matrices for the generic e -th element in WEP are defined as:

$$\mathbf{K}_w^e = \frac{Gt}{6l_e} \begin{bmatrix} 14 & -16 & 2 \\ -16 & 32 & -16 \\ 2 & -16 & 14 \end{bmatrix}; \quad \mathbf{M}_w^e = \frac{\rho l_e}{30} \begin{bmatrix} 4 & 2 & -1 \\ 2 & 16 & 2 \\ -1 & 2 & 4 \end{bmatrix} \quad (\text{A.11a,b})$$

where G and t are, respectively, the tangential elastic modulus and thickness.

A.1.3 In-plane 11 DOF, out-of-plane 5 DOF finite element (FE₃)

The eleven DOF (Euler-Bernoulli) beam FE is considered (Fig. A.1e), based on which displacement fields U, V are interpolated through 4th order Lagrangian and 5th order Hermite polynomial functions, respectively, as follows:

$$U(s) \Big|_{s=0}^{l_e} = \sum_{n=1}^5 L_n(s, l_e) U_n^e \quad (\text{A.12a})$$

$$V(s) \Big|_{s=0}^{l_e} = \sum_{n=1}^3 H_{2n-1}(s, l_e) V_{2n+1}^e + H_{2n}(s, l_e) \theta_{2n+1}^e \quad (\text{A.12b})$$

where:

$$L_1(s, l_e) = 1 - \frac{25}{3} \frac{s}{l_e} + \frac{70}{3} \left(\frac{s}{l_e}\right)^2 - \frac{80}{3} \left(\frac{s}{l_e}\right)^3 + \frac{32}{3} \left(\frac{s}{l_e}\right)^4 \quad (\text{A.13a})$$

$$L_2(s, l_e) = 16 \frac{s}{l_e} - \frac{208}{3} \left(\frac{s}{l_e}\right)^2 + 96 \left(\frac{s}{l_e}\right)^3 - \frac{128}{3} \left(\frac{s}{l_e}\right)^4 \quad (\text{A.13b})$$

$$L_3(s, l_e) = -12 \frac{s}{l_e} + 76 \left(\frac{s}{l_e}\right)^2 - 128 \left(\frac{s}{l_e}\right)^3 + 64 \left(\frac{s}{l_e}\right)^4 \quad (\text{A.13c})$$

$$L_4(s, l_e) = \frac{16}{3} \frac{s}{l_e} - \frac{112}{3} \left(\frac{s}{l_e}\right)^2 + \frac{224}{3} \left(\frac{s}{l_e}\right)^3 - \frac{128}{3} \left(\frac{s}{l_e}\right)^4 \quad (\text{A.13d})$$

$$L_5(s, l_e) = -\frac{s}{l_e} + \frac{22}{3} \left(\frac{s}{l_e}\right)^2 - 16 \left(\frac{s}{l_e}\right)^3 + \frac{32}{3} \left(\frac{s}{l_e}\right)^4 \quad (\text{A.13e})$$

and

$$H_1(s, l_e) = 1 - 23 \left(\frac{s}{l_e}\right)^2 + 66 \left(\frac{s}{l_e}\right)^3 - 68 \left(\frac{s}{l_e}\right)^4 + 24 \left(\frac{s}{l_e}\right)^5 \quad (\text{A.14a})$$

$$H_2(s, l_e) = l_e \left[\frac{s}{l_e} - 6 \left(\frac{s}{l_e}\right)^2 + 13 \left(\frac{s}{l_e}\right)^3 - 12 \left(\frac{s}{l_e}\right)^4 + 4 \left(\frac{s}{l_e}\right)^5 \right] \quad (\text{A.14b})$$

$$H_3(s, l_e) = 16 \left(\frac{s}{l_e}\right)^2 - 32 \left(\frac{s}{l_e}\right)^3 + 16 \left(\frac{s}{l_e}\right)^4 \quad (\text{A.14c})$$

$$H_4(s, l_e) = l_e \left[-8 \left(\frac{s}{l_e}\right)^2 + 32 \left(\frac{s}{l_e}\right)^3 - 40 \left(\frac{s}{l_e}\right)^4 + 16 \left(\frac{s}{l_e}\right)^5 \right] \quad (\text{A.14d})$$

$$H_5(s, l_e) = 7 \left(\frac{s}{l_e}\right)^2 - 34 \left(\frac{s}{l_e}\right)^3 + 52 \left(\frac{s}{l_e}\right)^4 - 24 \left(\frac{s}{l_e}\right)^5 \quad (\text{A.14e})$$

$$H_6(s, l_e) = l_e \left[-\left(\frac{s}{l_e}\right)^2 + 5 \left(\frac{s}{l_e}\right)^3 - 8 \left(\frac{s}{l_e}\right)^4 + 4 \left(\frac{s}{l_e}\right)^5 \right] \quad (\text{A.14f})$$

Referring to the consistent mass approach (e.g., Inman, 2013), the stiffness \mathbf{K}_p^e and the mass \mathbf{M}_p^e matrices for the generic e -th element in PEPs are defined as:

$$\mathbf{K}_p^e = \frac{EJ}{l_e} \begin{bmatrix}
 \frac{985 EA}{189 EJ} & 0 & 0 & \frac{-6848 EA}{945 EJ} & \frac{1016 EA}{315 EJ} & 0 & 0 & \frac{-1472 EA}{945 EJ} & \frac{347 EA}{945 EJ} & 0 & 0 \\
 0 & \frac{5092}{35 l_e^2} & \frac{1138}{35 l_e} & 0 & 0 & \frac{-512}{5 l_e^2} & \frac{384}{7 l_e} & 0 & 0 & \frac{-1508}{35 l_e^2} & \frac{242}{35 l_e} \\
 0 & \frac{1138}{35 l_e} & \frac{332}{35} & 0 & 0 & \frac{-128}{5 l_e} & \frac{64}{7} & 0 & 0 & \frac{-242}{35 l_e} & \frac{38}{35} \\
 \frac{-6848 EA}{945 EJ} & 0 & 0 & \frac{3328 EA}{189 EJ} & \frac{-4736 EA}{315 EJ} & 0 & 0 & \frac{5888 EA}{945 EJ} & \frac{-1472 EA}{945 EJ} & 0 & 0 \\
 \frac{1016 EA}{315 EJ} & 0 & 0 & \frac{-4736 EA}{315 EJ} & \frac{496 EA}{21 EJ} & 0 & 0 & \frac{-4736 EA}{315 EJ} & \frac{1016 EA}{315 EJ} & 0 & 0 \\
 0 & \frac{-512}{5 l_e^2} & \frac{-128}{5 l_e} & 0 & 0 & \frac{1024}{5 l_e^2} & 0 & 0 & 0 & \frac{-512}{5 l_e^2} & \frac{384}{7 l_e} \\
 0 & \frac{384}{7 l_e} & \frac{64}{7} & 0 & 0 & 0 & \frac{256}{7} & 0 & 0 & \frac{-128}{5 l_e} & \frac{64}{7} \\
 \frac{-1472 EA}{945 EJ} & 0 & 0 & \frac{5888 EA}{945 EJ} & \frac{-4736 EA}{315 EJ} & 0 & 0 & \frac{3328 EA}{945 EJ} & \frac{-6848 EA}{945 EJ} & 0 & 0 \\
 \frac{347 EA}{945 EJ} & 0 & 0 & \frac{-1472 EA}{945 EJ} & \frac{1016 EA}{315 EJ} & 0 & 0 & \frac{-6848 EA}{945 EJ} & \frac{985 EA}{189 EJ} & 0 & 0 \\
 0 & \frac{-1508}{35 l_e^2} & \frac{-242}{35 l_e} & 0 & 0 & \frac{-512}{5 l_e^2} & \frac{-128}{5 l_e} & 0 & 0 & \frac{5092}{35 l_e^2} & \frac{1138}{35 l_e} \\
 0 & \frac{242}{35 l_e} & \frac{38}{35} & 0 & 0 & \frac{384}{7 l_e} & \frac{64}{7} & 0 & 0 & \frac{1138}{35 l_e} & \frac{332}{35}
 \end{bmatrix} \quad (\text{A.15a})$$

$$\mathbf{M}_p^e = \frac{\rho l_e}{124740} \begin{bmatrix}
 6424 & 0 & 0 & 6512 & -3828 & 0 & 0 & 1232 & -638 & 0 & 0 \\
 0 & 18828 & 1026 l_e & 0 & 0 & 7942 & -1440 l_e & 0 & 0 & 2358 & -261 l_e \\
 0 & 1026 l_e & 72 l_e^2 & 0 & 0 & 792 l_e & -108 l_e^2 & 0 & 0 & 261 l_e & -27 l_e^2 \\
 6512 & 0 & 0 & 39424 & -8448 & 0 & 0 & 5632 & 1232 & 0 & 0 \\
 -3828 & 0 & 0 & -8448 & 41184 & 0 & 0 & -8448 & -3828 & 0 & 0 \\
 0 & 7920 & 792 l_e & 0 & 0 & 50688 & 0 & 0 & 0 & 7920 & -792 l_e \\
 0 & -1440 l_e & -108 l_e^2 & 0 & 0 & 0 & 1152 l_e^2 & 0 & 0 & 1440 l_e & -108 l_e^2 \\
 1232 & 0 & 0 & 5632 & -8448 & 0 & 0 & 39424 & 6512 & 0 & 0 \\
 -638 & 0 & 0 & 1232 & -3828 & 0 & 0 & 6512 & 6424 & 0 & 0 \\
 0 & 2358 & 261 l_e & 0 & 0 & 7920 & 1440 l_e & 0 & 0 & 18828 & -1026 l_e \\
 0 & -261 l_e & -27 l_e^2 & 0 & 0 & -792 l_e & -108 l_e^2 & 0 & 0 & -1026 l_e & 72 l_e^2
 \end{bmatrix} \quad (\text{A.15b})$$

where E and ρ are the longitudinal elastic modulus and mass density, respectively, A and J are the transverse area and the moment of inertia, respectively, referred to a unitary-length beam segment, and l_e is the length of the FE.

Based on the five DOF beam FE (Fig. A.1f), 4th order Lagrangian interpolating polynomial functions (Eq. (A.19)) have been adopted for out-of-plane displacements, i.e.,

$$W(s)\Big|_{s=0}^{l_e} = \sum_{n=1}^5 L_n(s, l_e) W_n^e \quad (\text{A.16})$$

Referring to the consistent mass approach, the stiffness \mathbf{K}_w^e and the mass \mathbf{M}_w^e matrices for the generic e -th element in WEP are defined as:

$$\mathbf{K}_w^e = \frac{Gt}{1890l_e} \begin{bmatrix} 9850 & -13696 & 6069 & -2944 & 694 \\ -13696 & 33280 & -28416 & 11776 & -2944 \\ 6069 & -28416 & 44640 & -28416 & 6069 \\ -2944 & 11776 & -28416 & 33280 & -13696 \\ 694 & -2944 & 6069 & -13696 & 9850 \end{bmatrix} \quad (\text{A.17a})$$

$$\mathbf{M}_w^e = \frac{\rho l_e}{5670} \begin{bmatrix} 6424 & 6512 & -3828 & 1232 & -638 \\ 6512 & 39424 & -8448 & 5632 & 1232 \\ -3828 & -8448 & 41184 & -8448 & -3828 \\ 1232 & 5632 & -8448 & 39424 & 6512 \\ -638 & 1232 & -3828 & 6512 & 6424 \end{bmatrix} \quad (\text{A.17b})$$

where G and t are, respectively, the tangential elastic modulus and thickness.

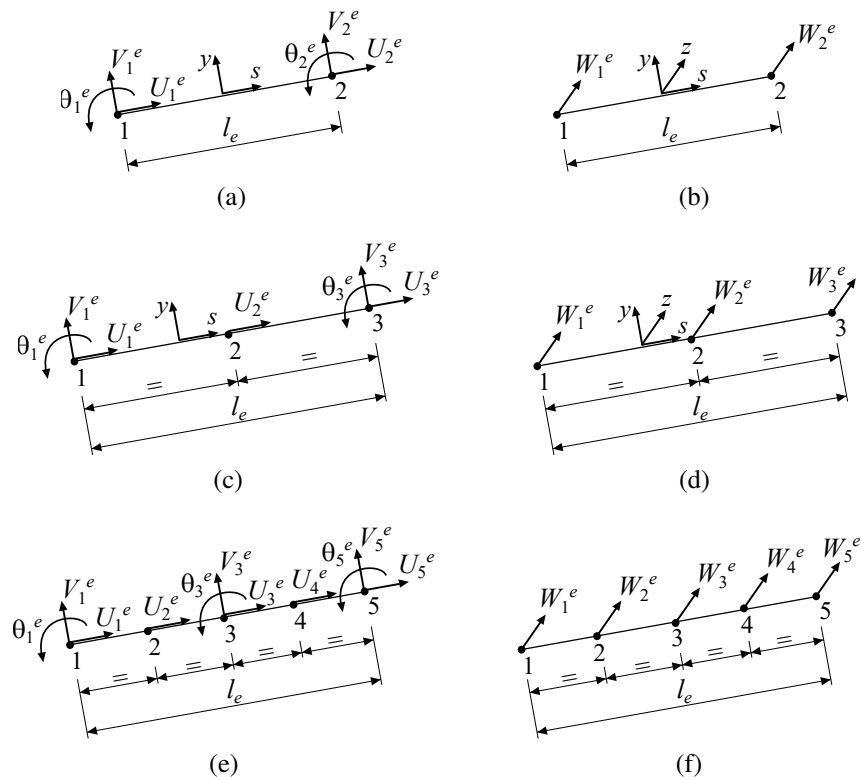


Figure A.1: Beam Finite Elements for linear cross-section analysis: (a) in-plane 6 DOF FE, (b) out-of-plane 2 DOF FE, (c) in-plane 11 DOF FE, (d) out-of-plane 3 DOF FE, (e) in-plane 11 DOF FE, (f) out-of-plane 5 DOF FE.

A.2 Beam Finite Elements for nonlinear cross-section analysis

A.2.1 In-plane 10 DOF, out-of-plane 7 DOF finite element (FE₄)

The ten DOF (Euler-Bernoulli) beam FE is considered (Fig. A.2a), based on which displacement fields U, V are interpolated through 5th order and 3rd order Hermite polynomial functions, respectively, as follows:

$$U(s) \Big|_{s=0}^{l_e} = \sum_{n=1}^4 F_n(s, l_e) U_n^e + F_5(s) U_1'^e + F_6(s) U_4'^e \quad (\text{A.18a})$$

$$V(s) \Big|_{s=0}^{l_e} = \sum_{n=1}^3 H_{2n-1}(s, l_e) V_n^e + H_{2n}(s, l_e) \theta_n^e \quad (\text{A.18b})$$

where:

$$F_1(s, l_e) = \frac{(3s - 2l_e)(s - l_e)^2(3s - l_e)(2l_e + 13s)}{4l_e^5} \quad (\text{A.19a})$$

$$F_2(s, l_e) = -\frac{81s^2(3s - 2l_e)(s - l_e)^2}{4l_e^5} \quad (\text{A.19b})$$

$$F_3(s, l_e) = \frac{81s^2(s - l_e)^2(3s - l_e)}{4l_e^5} \quad (\text{A.19c})$$

$$F_4(s, l_e) = -\frac{s^2(13s - 15l_e)(3s - 2l_e)(3s - l_e)}{4l_e^5} \quad (\text{A.19d})$$

$$F_5(s, l_e) = \frac{s(s - l_e)^2(-9sl_e + 2l_e^2 + 9s^2)}{2l_e^4} \quad (\text{A.19e})$$

$$F_6(s, l_e) = \frac{s^2(3s - 2l_e)(s - l_e)(3s - l_e)}{2l_e^4} \quad (\text{A.19f})$$

while Hermite polynomials $H_n(s, l_e)$ are defined in Eq. (A.3).

The seven DOF beam FE is considered (Fig. A.2b), based on which 6th order Hermite interpolating polynomial functions have been adopted for out-of-plane displacements, as follows:

$$W(s) \Big|_{s=0}^{l_e} = \sum_{n=1}^5 N_n(s, l_e) W_n^e + N_6(s, l_e) W_1'^e + N_7(s, l_e) W_5'^e \quad (\text{A.20})$$

where:

$$N_1(s, l_e) = -\frac{(4s - 3l_e)(s - l_e)^2(2s - l_e)(4s - l_e)(3l_e + 28s)}{9l_e^6} \quad (\text{A.21a})$$

$$N_2(s, l_e) = \frac{256s^2(4s - 3l_e)(s - l_e)^2(2s - l_e)}{9l_e^6} \quad (\text{A.21b})$$

$$N_3(s, l_e) = -\frac{16s^2(4s - 3l_e)(s - l_e)^2(4s - l_e)}{l_e^6} \quad (\text{A.21c})$$

$$N_4(s, l_e) = \frac{256s^2(s - l_e)^2(-6sl_e + l_e^2 + 8s^2)}{9l_e^6} \quad (\text{A.21d})$$

$$N_5(s, l_e) = -\frac{s^2(28s - 31l_e)(4s - 3l_e)(2s - l_e)(4s - l_e)}{9l_e^6} \quad (\text{A.21e})$$

$$N_6(s, l_e) = -\frac{s(4s - 3l_e)(s - l_e)^2(2s - l_e)(4s - l_e)}{3l_e^5} \quad (\text{A.21f})$$

$$N_7(s, l_e) = \frac{s^2(4s - 3l_e)(s - l_e)(2s - l_e)(4s - l_e)}{3l_e^5} \quad (\text{A.21g})$$

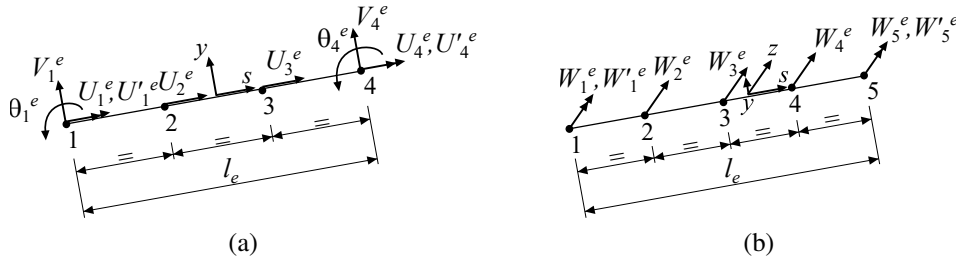


Figure A.2: Beam Finite Elements for nonlinear cross-section analysis: (a) in-plane 10 DOF FE, (b) out-of-plane 7 DOF FE.

Being E and G the longitudinal and transverse elastic modulus, respectively, A and J the transverse area and the moment of inertia, respectively, referred to a unitary-length beam segment, t the thickness and l_e the length of the FE, the stiffness matrix and equivalent load vector to be used in the PTP, \mathbf{K}_p^e and \mathbf{f}_p^e , respectively, and the stiffness matrix and load vector to be used in the WTP, \mathbf{K}_w^e and \mathbf{f}_w^e , respectively, are defined for the generic e -th element as:

$$\mathbf{K}_p^e = \begin{bmatrix} \frac{147AE}{40l_e} & \frac{37AE}{280} & 0 & 0 & -\frac{2187AE}{560l_e} & 0 & \frac{129AE}{17AE} & -\frac{17AE}{280} & 0 & 0 \\ \frac{37AE}{280} & \frac{AE l_e}{21} & 0 & 0 & -\frac{27AE}{280} & -\frac{27AE}{280} & \frac{560l_e}{17AE} & -\frac{AE l_e}{84} & 0 & 0 \\ 0 & 0 & \frac{12EJ}{l_e^3} & \frac{6EJ}{l_e^2} & 0 & 0 & 0 & 0 & -\frac{12EJ}{l_e^3} & \frac{6EJ}{l_e^2} \\ 0 & 0 & \frac{6EJ}{l_e^2} & \frac{4EJ}{l_e} & 0 & 0 & 0 & 0 & -\frac{6EJ}{l_e^2} & \frac{2EJ}{l_e} \\ -\frac{2187AE}{560l_e} & -\frac{27AE}{280} & 0 & 0 & \frac{2187AE}{280l_e} & -\frac{2187AE}{2187AE} & 0 & \frac{27AE}{280} & 0 & 0 \\ 0 & -\frac{27AE}{280} & 0 & 0 & -\frac{2187AE}{560l_e} & \frac{560l_e}{2187AE} & -\frac{2187AE}{560l_e} & \frac{27AE}{280} & 0 & 0 \\ \frac{129AE}{560l_e} & \frac{17AE}{280} & 0 & 0 & 0 & -\frac{2187AE}{560l_e} & \frac{147AE}{40l_e} & -\frac{37AE}{280} & 0 & 0 \\ -\frac{17AE}{280} & -\frac{1}{84}AE l_e & 0 & 0 & \frac{27AE}{280} & \frac{27AE}{280} & -\frac{37AE}{280} & \frac{AE l_e}{21} & 0 & 0 \\ 0 & 0 & -\frac{12EJ}{l_e^3} & -\frac{6EJ}{l_e^2} & 0 & 0 & 0 & 0 & \frac{12EJ}{l_e^3} & -\frac{6EJ}{l_e^2} \\ 0 & 0 & \frac{6EJ}{l_e^2} & \frac{2EJ}{l_e} & 0 & 0 & 0 & 0 & -\frac{6EJ}{l_e^2} & \frac{4EJ}{l_e} \end{bmatrix} \quad (\text{A.22a})$$

$$\mathbf{f}_p^e = AE \int_0^{l_e} [F_1(s, l_e) \ F_5(s, l_e) \ 0 \ 0 \ F_2(s, l_e) \ F_3(s, l_e) \ F_4(s, l_e) \ F_6(s, l_e) \ 0 \ 0]^T \bar{\varepsilon}(s) ds \quad (\text{A.22b})$$

$$\mathbf{K}_w^e = \frac{Gt}{l_e} \begin{bmatrix} 4.8023 & 0.110048l_e & -5.17081 & 0.320154 & 0.267251 & -0.218902 & 0.04104l_e \\ 0.110048l_e & 0.0320667l_e^2 & -0.0670408l_e & -0.0854257l_e & 0.0834589l_e & -0.04104l_e & 0.00585217l_e^2 \\ -5.17081 & -0.0670408l_e & 10.7411 & -6.30457 & 0.467005 & 0.267251 & -0.0834589l_e \\ 0.320154 & -0.0854257l_e & -6.30457 & 11.9688 & -6.30457 & 0.320154 & 0.0854257l_e \\ 0.267251 & 0.0834589l_e & 0.467005 & -6.30457 & 10.7411 & -5.17081 & 0.0670408l_e \\ -0.218902 & -0.04104l_e & 0.267251 & 0.320154 & -5.17081 & 4.8023 & -0.110048l_e \\ 0.04104l_e & 0.00585217l_e^2 & -0.0834589l_e & 0.0854257l_e & 0.0670408l_e & -0.110048l_e & 0.0320667l_e^2 \end{bmatrix} \quad (\text{A.22c})$$

$$\mathbf{f}_w^e = Gt \int_0^{l_e} [N_1(s, l_e) \ N_6(s, l_e) \ N_2(s, l_e) \ N_3(s, l_e) \ N_4(s, l_e) \ N_5(s, l_e) \ N_7(s, l_e)]^T \bar{\gamma}(s) ds \quad (\text{A.22d})$$

Appendix B

The planar Euler-Bernoulli beam as an equivalent Generalized Spring

A mono-dimensional deformable member is considered, whose configuration can be uniquely identified through the position field of its two orientated end-nodes (Fig. B.1a). It is assumed that the member can be subjected to forces and couples applied at the end-nodes only (Fig. B.1b). In this context, the *local strain-displacement relationships* can be expressed as Luongo and Paolone (1997):

$$\boldsymbol{\varepsilon} = \mathbf{u}_B - \mathbf{u}_A - \boldsymbol{\theta}_A \times \mathbf{AB} \quad (\text{B.1a})$$

$$\boldsymbol{\kappa} = \boldsymbol{\theta}_B - \boldsymbol{\theta}_A \quad (\text{B.1b})$$

where $\boldsymbol{\varepsilon}$ and $\boldsymbol{\kappa}$ are referred to as *linear deformation* and *curvature* vectors, respectively. The

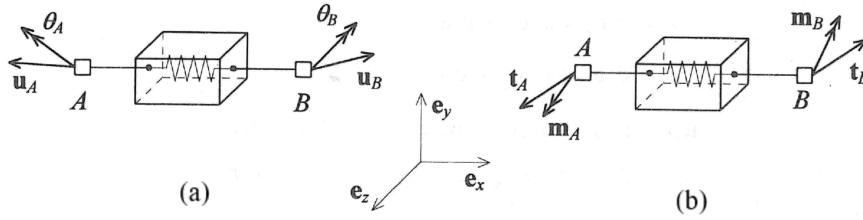


Figure B.1: Mono-dimensional deformable member: (a) displacements, and (b) internal forces.

local equilibrium equations can be obtained by resorting to the balance principles:

$$\mathbf{t}_A + \mathbf{t}_B = \mathbf{0} \quad (\text{B.2a})$$

$$\mathbf{m}_A + \mathbf{m}_B + \mathbf{AB} \times \mathbf{t}_B = \mathbf{0} \quad (\text{B.2b})$$

in which the vertex A has been chosen as pole. Since internal forces have to satisfy Eqs. (B.2), they are not independent. By assuming, $\mathbf{t}_B = \boldsymbol{\sigma}$ and $\mathbf{m}_B = \boldsymbol{\mu}$, where $\boldsymbol{\sigma}$ and $\boldsymbol{\mu}$ are arbitrary vector, it is obtained:

$$\mathbf{t}_A = -\boldsymbol{\sigma}; \quad \mathbf{m}_A = -\boldsymbol{\mu} - \mathbf{AB} \times \boldsymbol{\sigma}; \quad \mathbf{t}_B = \boldsymbol{\sigma}, \quad \mathbf{m}_B = \boldsymbol{\mu} \quad (\text{B.3a-c})$$

where $\boldsymbol{\sigma}$ and $\boldsymbol{\mu}$ are referred to as *force-stress* and *couple-stress* vectors.

Since the member can only exhibit in-plane deformations (e.g., plane strain regime), then \mathbf{u}_A and \mathbf{u}_B are parallel to the plane $x - y$, while $\boldsymbol{\theta}_A$ and $\boldsymbol{\theta}_B$ are orthogonal to the same plane. The only non-null deformations are ε_x , ε_y and κ_z . By naming:

$$\varepsilon_x = \varepsilon; \quad \varepsilon_y = \gamma; \quad \kappa_z = \kappa \quad (\text{B.4a-c})$$

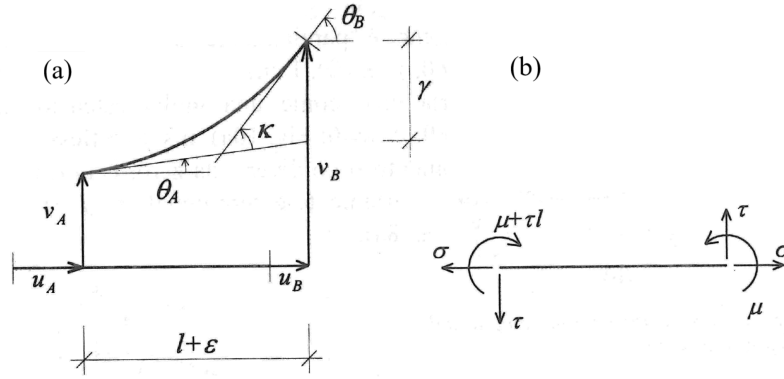


Figure B.2: Mono-dimensional deformable member under plane strain/stress regime: (a) geometrical interpretation of strains and (b) stresses

the local strain-displacement relationships (Eq. (B.1)) can be rewritten as follows:

$$\varepsilon = u_B - u_A \quad (\text{B.5a})$$

$$\gamma = v_B - v_A - \theta_A l \quad (\text{B.5b})$$

$$\kappa = \theta_B - \theta_A \quad (\text{B.5c})$$

in which ε , γ and κ are referred to as *axial deformation*, *shear deformation* and *bending*, respectively. By interpreting the mono-dimensional deformable member as a planar Euler-Bernoulli beam, Eqs. (B.5) can be viewed as *global* deformations of the beam, whose geometrical meaning is clearly shown by Fig. B.2a. The corresponding plane stress regime is characterized by \mathbf{t}_A and \mathbf{t}_B vectors parallel to the plane $x - y$, whereas $\boldsymbol{\mu}_A$ and $\boldsymbol{\mu}_B$ are orthogonal to the same plane. The non-zero stresses are σ_x , σ_y and μ_z , which are referred to as:

$$\sigma_x = \sigma; \quad \sigma_y = \tau; \quad \mu_z = \mu \quad (\text{B.6a-c})$$

whose components in the balanced conditions are shown in Fig. B.2b.

Constitutive equations are given by Luongo and Paolone (1997):

$$\begin{Bmatrix} \sigma \\ \tau \\ \mu \end{Bmatrix} = \begin{bmatrix} C^a & 0 & 0 \\ 0 & C^s & -\frac{C^s l}{2} \\ 0 & -\frac{C^s l}{2} & C^f \end{bmatrix} \begin{Bmatrix} \varepsilon \\ \gamma \\ \kappa \end{Bmatrix} \quad (\text{B.7})$$

where l is the length of the member, and C_a , C_s and C_f are the axial, shear and flexural stiffness, respectively. They can be interpreted as the global stiffness of a generalized spring, whose global behavior is identical to an (homogeneous) planar Euler-Bernoulli beam in terms of both global deformations and internal forces. They can be determined by solving the classic elastic problem relating to a conventional Euler-Bernoulli beam. The following stiffness are then obtained:

$$C^a = \frac{EA}{l}; \quad C^s = \frac{12EI}{l^3}; \quad C^f = \frac{4EJ}{l} \quad (\text{B.8a-c})$$

where E , A and J are, respectively, the elastic module, the transverse area and the moment of inertia of the beam. Finally, the elastic potential energy \mathcal{U} of the planar Euler-Bernoulli

interpreted as an equivalent generalized spring can be expressed as:

$$\mathcal{U} = \frac{1}{2}(C^a \varepsilon^2 + C^s \gamma^2 + C^f \kappa^2 - l C^s \gamma \kappa) \quad (\text{B.9})$$

Appendix C

Constrained algebraic eigenvalue problems

A constrained dynamic eigenvalue problem can be expressed as:

$$\delta \mathbf{q}^T (\mathbf{K} - \lambda \mathbf{M}) \mathbf{q} = 0 \quad (\text{C.1a})$$

$$\mathbf{A} \mathbf{q} = \mathbf{0} \quad (\text{C.1b})$$

where the first equations represents the Virtual Work Principle for a N -DOF free undamped system, while the latter expresses a system of M linear constraints for the nodal displacements collected in the vector \mathbf{q} . The system (C.1) admits non-trivial solutions $\mathbf{q} \neq \mathbf{0}$ if, and only if, matrices \mathbf{K} and \mathbf{M} are Hermitian (i.e. symmetric in case of real matrices) and at least one of them is positive definite. Constraint conditions can be used to reduce the problem by expressing the M slave DOF \mathbf{q}_s in terms of the $(N - M)$ master DOF \mathbf{q}_m . By partitioning Eq. (C.1b)) as:

$$\begin{bmatrix} \mathbf{A}_m & \mathbf{A}_s \end{bmatrix} \begin{bmatrix} \mathbf{q}_m \\ \mathbf{q}_s \end{bmatrix} = \mathbf{0} \quad (\text{C.2})$$

and assuming \mathbf{A}_s to be a non-singular matrix, the vector \mathbf{q} can be expressed as a function of the sole master DOF \mathbf{q}_m based on

$$\mathbf{q} = \mathbf{R} \mathbf{q}_m \quad (\text{C.3})$$

where:

$$\mathbf{q} = \begin{bmatrix} \mathbf{q}_m \\ \mathbf{q}_s \end{bmatrix}; \quad \mathbf{R} = \begin{bmatrix} \mathbf{I} \\ -\mathbf{A}_s^{-1} \mathbf{A}_m \end{bmatrix} \quad (\text{C.4a,b})$$

By substituting Eq. (C.3)) and $\delta \mathbf{q} = \mathbf{R} \delta \mathbf{q}_m$ into Eq. (C.1a), the following constrained algebraic eigenvalue problem is then obtained:

$$(\mathbf{K}_R - \lambda \mathbf{M}_R) \mathbf{q}_m = \mathbf{0} \quad (\text{C.5})$$

where :

$$\mathbf{K}_R = \mathbf{R}^T \mathbf{K} \mathbf{R}; \quad \mathbf{M}_R = \mathbf{R}^T \mathbf{M} \mathbf{R} \quad (\text{C.6a,b})$$

Appendix D

Displacement-based GBT equations and relevant boundary conditions

Based on the following variable change outlined in Section 5.1, the weak formulation of the elasticity problem can be rewritten as follows:

$$\begin{aligned}
& \int_{\mathcal{L}} \left\{ \delta \mathbf{u}'^T [\mathbf{T}_p^T \quad \mathbf{T}_{wp}^T] \left(\mathbf{F}^T \mathbf{T}_p \mathbf{u} + \mathbf{C} \begin{bmatrix} \mathbf{T}_p \\ \mathbf{T}_{wp} \end{bmatrix} \mathbf{u}'' + \begin{bmatrix} \mathbf{C}^{\Omega W} \\ \mathbf{C}^{WW} \end{bmatrix} \mathbf{T}_w \mathbf{w}' \right) + \right. \\
& \quad + \delta \mathbf{u}^T [\mathbf{T}_p^T \quad \mathbf{T}_{wp}^T] \left(\mathbf{D} \begin{bmatrix} \mathbf{T}_p \\ \mathbf{T}_{wp} \end{bmatrix} \mathbf{u}' + \begin{bmatrix} \mathbf{D}^{\Omega W} \\ \mathbf{D}^{WW} \end{bmatrix} \mathbf{T}_w \mathbf{w} - \mathbf{q}_2 \right) + \\
& \quad + \delta \mathbf{u}^T \mathbf{T}_p^T \left(\mathbf{B} \mathbf{T}_p \mathbf{u} + \mathbf{F} \begin{bmatrix} \mathbf{T}_p \\ \mathbf{T}_{wp} \end{bmatrix} \mathbf{u}'' + \mathbf{F}^W \mathbf{T}_w \mathbf{w}' - \mathbf{q}_1 \right) + \\
& \quad + \delta \mathbf{w}'^T \mathbf{T}_w^T \left(\mathbf{F}^{W T} \mathbf{T}_w \mathbf{u} + [\mathbf{C}^{W\Omega} \quad \mathbf{C}^{WW}] \begin{bmatrix} \mathbf{T}_p \\ \mathbf{T}_{wp} \end{bmatrix} \mathbf{u}'' + \mathbf{C}^{WW} \mathbf{T}_w \mathbf{w}' \right) \\
& \quad \left. + \delta \mathbf{w}^T \mathbf{T}_w^T \left([\mathbf{D}^{W\Omega} \quad \mathbf{D}^{WW}] \begin{bmatrix} \mathbf{T}_p \\ \mathbf{T}_{wp} \end{bmatrix} \mathbf{u}' + \mathbf{D}^{WW} \mathbf{T}_w \mathbf{w} - \mathbf{q}_W \right) \right\} dz + \\
& \quad - \sum_B \{ \delta \mathbf{u}^T \mathbf{T}_p^T \mathbf{P}_1 + \delta \mathbf{u}'^T [\mathbf{T}_p^T \quad \mathbf{T}_{wp}^T] \mathbf{P}_2 + \delta \mathbf{w}^T \mathbf{T}_w^T \mathbf{P}_W \} = 0 \quad (\text{D.1})
\end{aligned}$$

Relevant structural matrices \mathbf{B} , \mathbf{C} , \mathbf{D} , \mathbf{F} in Eq. (D.1) are defined as follows:

$$\mathbf{B} = \mathbf{B}^e + \mathbf{B}^f; \quad \mathbf{C} = \begin{bmatrix} (\mathbf{C}^{\Omega\Omega} + \mathbf{C}^f) & \mathbf{C}^{\Omega W} \\ \mathbf{C}^{W\Omega} & \mathbf{C}^{WW} \end{bmatrix} \quad (\text{D.2a,b})$$

$$\mathbf{F} = [(\mathbf{F}^{\Omega} + \mathbf{F}^f) \quad \mathbf{F}^W]; \quad \mathbf{D} = \begin{bmatrix} (\mathbf{D}^{\Omega\Omega} + \mathbf{D}^t) & \mathbf{D}^{\Omega W} \\ \mathbf{D}^{W\Omega} & \mathbf{D}^{WW} \end{bmatrix} \quad (\text{D.2c,d})$$

being:

$$B_{hk}^e = \frac{Et}{1-\nu^2} \int_c U'_h(s) U'_k(s) ds; \quad B_{hk}^f = \frac{Et^3}{12(1-\nu^2)} \int_c V''_h(s) V''_k(s) ds \quad (\text{D.3a,b})$$

$$C_{hk}^{\Omega\Omega} = \frac{Et}{1-\nu^2} \int_c \Omega_h(s) \Omega_k(s) ds; \quad C_{hk}^{\Omega W} = \frac{Et}{1-\nu^2} \int_c \Omega_h(s) W_k(s) ds \quad (\text{D.3c,d})$$

$$C_{hk}^{WW} = \frac{Et}{1-\nu^2} \int_c W_h(s) W_k(s) ds; \quad C_{hk}^f = \frac{Et^3}{12(1-\nu^2)} \int_c V_h(s) V_k(s) ds \quad (\text{D.3e,f})$$

$$F_{hk}^{\Omega} = \frac{\nu Et}{1-\nu^2} \int_c U'_h(s) \Omega_k(s) ds; \quad F_{hk}^W = \frac{\nu Et}{1-\nu^2} \int_c U'_h(s) W_k(s) ds \quad (\text{D.3g,h})$$

$$F_{hk}^f = \frac{\nu Et^3}{12(1-\nu^2)} \int_c V''_h(s) V_k(s) ds; \quad C_{hk}^{W\Omega} = C_{kh}^{\Omega W} \quad (\text{D.3i,j})$$

$$D_{hk}^{\Omega\Omega} = Gt \int_c [U_h(s) + \Omega'_h(s)] [U_k(s) + \Omega'_k(s)] ds \quad (\text{D.3k})$$

$$D_{hk}^{\Omega W} = Gt \int_c [U_h(s) + \Omega'_h(s)] W'_k(s) ds; \quad D_{hk}^{W\Omega} = D_{kh}^{\Omega W} \quad (\text{D.3l,m})$$

$$D_{hk}^{WW} = Gt \int_c W'_h(s) W'_k(s) ds; \quad D_{hk}^f = \frac{Gt^3}{3} \int_c V'_h(s) V'_k(s) ds \quad (\text{D.3n,o})$$

where superscripts f , t , and e refer to the flexural, torsional and (transverse) extensional nature of the underlying energy terms, respectively, superscripts Ω and W identifies axial (longitudinal) terms and refer on the typology of warping distributions involved, while while E , G , ν and t are the longitudinal, tangential, Poisson moduli and thickness, respectively, of each cross-section element. The relevant loading vectors included in Eq. (D.1) can be expressed as:

$$q_{1k} = \int_c [f_s(s, z) U_k(s) + f_y(s, z) V_k(s)] ds$$

$$P_{1k} = \int_c \sum_B [F_{Bs}(s) U_k(s) + F_{By}(s) V_k(s)] d$$

and

$$\mathbf{q}_2 = \begin{bmatrix} \mathbf{q}_\Omega \\ \mathbf{q}_W \end{bmatrix}; \quad \mathbf{P}_2 = \begin{bmatrix} \mathbf{P}_\Omega \\ \mathbf{P}_W \end{bmatrix} \quad (\text{D.5a,b})$$

being

$$q_{\Omega k} = \int_{\mathcal{C}} f_z(s, z) \Omega_k(s) ds; \quad q_{Wk} = \int_{\mathcal{C}} f_z(s, z) W_k(s) ds \quad (\text{D.6a,b})$$

$$P_{\Omega k} = \int_{\mathcal{C}} F_{Bz}(s, z) \Omega_k(s) ds; \quad P_{Wk} = \int_{\mathcal{C}} F_{Bz}(s, z) W_k(s) ds \quad (\text{D.6c,d})$$

with $\mathbf{f}(s, z) = f_s(s, z)\mathbf{e}_s(s) + f_y(s, z)\mathbf{e}_y(s) + f_z(s, z)\mathbf{e}_z(s)$ being forces per unit area acting on the middle surface \mathcal{S} and $\mathbf{F}_B(s) = F_{Bs}(s)\mathbf{e}_s(s) + F_{By}(s)\mathbf{e}_y(s) + F_{Bz}(s)\mathbf{e}_z(s)$ being forces per unit length applied on the boundaries $B = 0, L$ (i.e., on the mid-line \mathcal{C} of the end cross-sections at $z = 0, L$, respectively). Based on Eq. (D.1), the *displacement-based GBT equations* can be obtained by performing the standard steps of calculus of variations (e.g., Berdichevsky, 2009), obtaining:

$$\begin{aligned} & \left[\mathbf{T}_p^T \quad \mathbf{T}_{wp}^T \right] \left\{ \mathbf{C} \begin{bmatrix} \mathbf{T}_p \\ \mathbf{T}_{wp} \end{bmatrix} \mathbf{u}^{IV} + \begin{bmatrix} \mathbf{C}^{\Omega W} \\ \mathbf{C}^{WW} \end{bmatrix} \mathbf{T}_w \mathbf{w}''' + \right. \\ & \quad \left. + \left(\mathbf{F}^T \mathbf{T}_p - \mathbf{D} \begin{bmatrix} \mathbf{T}_p \\ \mathbf{T}_{wp} \end{bmatrix} \right) \mathbf{u}'' - \begin{bmatrix} \mathbf{D}^{\Omega W} \\ \mathbf{D}^{WW} \end{bmatrix} \mathbf{T}_w \mathbf{w}' + \mathbf{q}'_2 \right\} + \\ & \quad \left. + \mathbf{T}_p^T \left\{ \mathbf{F} \begin{bmatrix} \mathbf{T}_p \\ \mathbf{T}_{wp} \end{bmatrix} \mathbf{u}'' - \mathbf{F}^w \mathbf{T}_w \mathbf{w}' + \mathbf{B} \mathbf{T}_p \mathbf{u} - \mathbf{q}_1 \right\} = 0 \quad (\text{D.7a}) \end{aligned}$$

$$\begin{aligned} & - \mathbf{T}_w^T \left\{ \begin{bmatrix} \mathbf{C}^{W\Omega} & \mathbf{C}^{WW} \end{bmatrix} \begin{bmatrix} \mathbf{T}_p \\ \mathbf{T}_{wp} \end{bmatrix} \mathbf{u}''' + \mathbf{C}^{WW} \mathbf{T}_w \mathbf{w}'' + \right. \\ & \quad \left. + \left(\mathbf{F}^T \mathbf{T}_p - \begin{bmatrix} \mathbf{D}^{W\Omega} & \mathbf{D}^{WW} \end{bmatrix} \begin{bmatrix} \mathbf{T}_p \\ \mathbf{T}_{wp} \end{bmatrix} \right) \mathbf{u}' - \mathbf{D}^{WW} \mathbf{T}_w \mathbf{w} + \mathbf{q}_W \right\} = 0 \quad (\text{D.7b}) \end{aligned}$$

with corresponding boundary conditions terms to be applied at $z = 0, L$:

$$\delta \mathbf{u}'^T \left(\left[\mathbf{T}_p^T \quad \mathbf{T}_{wp}^T \right] \left\{ \mathbf{C} \begin{bmatrix} \mathbf{T}_p \\ \mathbf{T}_{wp} \end{bmatrix} \mathbf{u}'' + \begin{bmatrix} \mathbf{C}^{\Omega W} \\ \mathbf{C}^{WW} \end{bmatrix} \mathbf{T}_w \mathbf{w}' + \mathbf{F}^T \mathbf{T}_p \mathbf{u} - \mathbf{P}_2 \right\} \right) = 0 \quad (\text{D.8a})$$

$$\begin{aligned} & \delta \mathbf{u}^T \left(- \left[\mathbf{T}_p^T \quad \mathbf{T}_{wp}^T \right] \left\{ \mathbf{C} \begin{bmatrix} \mathbf{T}_p \\ \mathbf{T}_{wp} \end{bmatrix} \mathbf{u}''' + \begin{bmatrix} \mathbf{C}^{\Omega W} \\ \mathbf{C}^{WW} \end{bmatrix} \mathbf{T}_w \mathbf{w}'' + \right. \right. \\ & \quad \left. \left. + \left(\mathbf{F}^T \mathbf{T}_p - \mathbf{D} \begin{bmatrix} \mathbf{T}_p \\ \mathbf{T}_{wp} \end{bmatrix} \right) \mathbf{u}' - \begin{bmatrix} \mathbf{D}^{\Omega W} \\ \mathbf{D}^{WW} \end{bmatrix} \mathbf{T}_w \mathbf{w} \right\} - \mathbf{T}_p^T \mathbf{P}_1 \right) = 0 \quad (\text{D.8b}) \end{aligned}$$

$$\delta \mathbf{w}^T \left(\mathbf{T}_w^T \left\{ \begin{bmatrix} \mathbf{C}^{W\Omega} & \mathbf{C}^{WW} \end{bmatrix} \begin{bmatrix} \mathbf{T}_p \\ \mathbf{T}_{wp} \end{bmatrix} \mathbf{u}'' + \mathbf{C}^{WW} \mathbf{T}_w \mathbf{w}' + \mathbf{F}^T \mathbf{T}_p \mathbf{u} - \mathbf{P}_W \right\} \right) = 0 \quad (\text{D.8c})$$

In case of multi-component TWM, the partial shear interaction in both longitudinal and transverse directions can be included by adopting the procedure outlined in Section 5.2. The multi-component cross-section is assumed to be formed by N_m components linked together by means of N_{sc} shear-deformable connectors. By denoting with E_α , G_α , ν_α and t_α the longitudinal, tangential, Poisson moduli and thickness, respectively, of the α -th component ($\alpha = 1, \dots, N_m$) and being k_L^n and k_T^n the longitudinal and transverse shear elastic stiffens of the n -th connector ($n = 1, \dots, N_{sc}$), structural matrices defined in Eq. Eq. (D.2) can be rewritten as:

$$B_{hk}^e = \sum_{\alpha=1}^{N_m} \frac{E_\alpha t_\alpha}{1 - \nu_\alpha^2} \int_{\mathcal{C}_\alpha} U_h'(s) U_k'(s) ds + \sum_{n=1}^{N_{sc}} k_T^n \bar{V}_h^n \bar{V}_k^n \quad (\text{D.9a})$$

$$B_{hk}^f = \sum_{\alpha=1}^{N_m} \frac{E_\alpha t_\alpha^3}{12(1 - \nu_\alpha^2)} \int_{\mathcal{C}_\alpha} V_h''(s) V_k''(s) ds \quad (\text{D.9b})$$

$$D_{hk}^{\Omega\Omega} = \sum_{\alpha=1}^{N_m} G_\alpha t_\alpha \int_{\mathcal{C}_\alpha} [U_h(s) + \Omega_h'(s)] [U_k(s) + \Omega_k'(s)] ds + \sum_{n=1}^{N_{sc}} k_L^n \bar{W}_h^n \bar{W}_k^n \quad (\text{D.9c})$$

$$D_{hk}^{\Omega W} = \sum_{\alpha=1}^{N_m} G_\alpha t_\alpha \int_{\mathcal{C}_\alpha} [U_h(s) + \Omega_h'(s)] W_k(s) ds \quad (\text{D.9d})$$

$$C_{hk}^{\Omega\Omega} = \sum_{\alpha=1}^{N_m} \frac{E_\alpha t_\alpha}{1 - \nu_\alpha^2} \int_{\mathcal{C}_\alpha} \Omega_h(s) \Omega_k(s) ds; \quad C_{hk}^{\Omega W} = \sum_{\alpha=1}^{N_m} \frac{E_\alpha t_\alpha}{1 - \nu_\alpha^2} \int_{\mathcal{C}_\alpha} \Omega_h(s) W_k(s) ds \quad (\text{D.9e,f})$$

$$C_{hk}^{WW} = \sum_{\alpha=1}^{N_m} \frac{E_\alpha t_\alpha}{1 - \nu_\alpha^2} \int_{\mathcal{C}_\alpha} W_h(s) W_k(s) ds; \quad C_{hk}^{W\Omega} = C_{kh}^{\Omega W} \quad (\text{D.9g,h})$$

$$C_{hk}^f = \sum_{\alpha=1}^{N_m} \frac{E_\alpha t_\alpha^3}{12(1 - \nu_\alpha^2)} \int_{\mathcal{C}_\alpha} V_h(s) V_k(s) ds; \quad D_{hk}^{W\Omega} = D_{kh}^{\Omega W} \quad (\text{D.9i,j})$$

$$D_{hk}^{WW} = \sum_{\alpha=1}^{N_m} G_\alpha t_\alpha \int_{\mathcal{C}_\alpha} W_h(s) W_k(s) ds; \quad D_{hk}^t = \sum_{\alpha=1}^{N_m} \frac{G_\alpha t_\alpha^3}{3} \int_{\mathcal{C}_\alpha} V_h'(s) V_k'(s) ds \quad (\text{D.9k,l})$$

$$F_{hk}^\Omega = \sum_{\alpha=1}^{N_m} \frac{\nu_\alpha E_\alpha t_\alpha}{1 - \nu_\alpha^2} \int_{\mathcal{C}_\alpha} U_h'(s) \Omega_k(s) ds; \quad F_{hk}^W = \sum_{\alpha=1}^{N_m} \frac{\nu_\alpha E_\alpha t_\alpha}{1 - \nu_\alpha^2} \int_{\mathcal{C}_\alpha} U_h'(s) W_k(s) ds \quad (\text{D.9m,n})$$

$$F_{hk}^f = \sum_{\alpha=1}^{N_m} \frac{\nu_\alpha E_\alpha t_\alpha}{12(1 - \nu_\alpha^2)} \int_{\mathcal{C}_\alpha} V_h''(s) V_k(s) ds \quad (\text{D.9o})$$

while load vectors can be expressed as:

$$q_{1k} = \sum_{\alpha=1}^{N_m} \int_{\mathcal{C}_\alpha} [f_s(s, z)U_k(s) + f_y(s, z)V_k(s)] ds \quad (\text{D.10a})$$

$$q_{\Omega k} = \sum_{\alpha=1}^{N_m} \int_{\mathcal{C}_\alpha} f_z(s, z)\Omega_k(s) ds \quad (\text{D.10b})$$

$$q_{Wk} = \sum_{\alpha=1}^{N_m} \int_{\mathcal{C}_\alpha} f_z(s, z)W_k(s) ds \quad (\text{D.10c})$$

$$P_{1k} = \sum_{\alpha=1}^{N_m} \int_{\mathcal{C}_\alpha} \sum_B [F_{Bs}(s)U_k(s) + F_{By}V_k(s)] ds \quad (\text{D.10d})$$

$$P_{\Omega k} = \sum_{\alpha=1}^{N_m} \int_{\mathcal{C}_\alpha} \sum_B [F_{Bz}(s, z)\Omega_k(s)] ds \quad (\text{D.10e})$$

$$P_{Wk} = \sum_{\alpha=1}^{N_m} \int_{\mathcal{C}_\alpha} \sum_B [F_{Bz}(s, z)W_k(s)] ds \quad (\text{D.10f})$$

REFERENCES

- Abambres, M., Camotim, D. and Silvestre, N. (2013). Physically non-linear GBT analysis of thin-walled members, *Computers & Structures* **129**: 148–165. doi: 10.1016/j.compstruc.2013.04.022.
- Abambres, M., Camotim, D. and Silvestre, N. (2014). GBT-based elastic–plastic post-buckling analysis of stainless steel thin-walled members, *Thin-Walled Structures* **83**: 85–102. doi: 10.1016/j.tws.2014.01.004.
- Abambres, M., Camotim, D., Silvestre, N. and Rasmussen, K. J. R. (2014). GBT-based structural analysis of elastic–plastic thin-walled members, *Computers & Structures* **136**: 1–23. doi: 10.1016/j.compstruc.2014.01.001.
- Ádány, S. (2017). Constrained shell finite element method for thin-walled members, part 1: constraints for a single band of finite elements, *Thin-Walled Structures* . in press. doi: 10.1016/j.tws.2017.01.015.
- Ádány, S. and Schafer, B. W. (2006a). Buckling mode decomposition of single-branched open cross-section members via finite strip method: Application and examples, *Thin-Walled Structures* **44**(5): 585–600. doi: 10.1016/j.tws.2006.03.014.
- Ádány, S. and Schafer, B. W. (2006b). Buckling mode decomposition of single-branched open cross-section members via finite strip method: Derivation, *Thin-Walled Structures* **44**(5): 563–584. doi: 10.1016/j.tws.2006.03.013.
- Ádány, S. and Schafer, B. W. (2008). A full modal decomposition of thin-walled, single-branched open cross-section members via the constrained finite strip method, *Journal of Constructional Steel Research* **64**(1): 12–29. doi: 10.1016/j.jcsr.2007.04.004.
- Ádány, S., Silvestre, N., Schafer, B. W. and Camotim, D. (2009). GBT and cFSM: two modal approaches to the buckling analysis of unbranched thin-walled members, *Advanced Steel Construction* **5**(2): 195–223. doi: 10.18057/ijasc.2009.5.2.8.
- Ádány, S., Visy, D. and Nagy, R. (2017). Constrained shell finite element method, part 2: application to linear buckling analysis of thin-walled members, *Thin-Walled Structures* . in press. doi: 10.1016/j.tws.2017.01.022.
- Basaglia, C. and Camotim, D. (2013). Enhanced generalised beam theory buckling formulation to handle transverse load application effects, *International Journal of Solids and Structures* **50**(3-4): 531–547. doi: 10.1016/j.ijsolstr.2012.10.010.
- Basaglia, C. and Camotim, D. (2015). Buckling analysis of thin-walled steel structural systems using generalized beam theory (GBT), *International Journal of Structural Stability and Dynamics* **15**(1): 1540004. doi: 10.1142/s0219455415400040.
- Basaglia, C., Camotim, D., Gonçalves, R. and Graça, A. (2013). GBT-based assessment of the buckling behaviour of cold-formed steel purlins restrained by sheeting, *Thin-Walled Structures* **72**: 217–229. doi: 10.1016/j.tws.2013.06.005.

- Basaglia, C., Camotim, D. and Silvestre, N. (2008). Global buckling analysis of plane and space thin-walled frames in the context of GBT, *Thin-Walled Structures* **46**(1): 79–101. doi: 10.1016/j.tws.2007.07.007.
- Basaglia, C., Camotim, D. and Silvestre, N. (2009). GBT-based local, distortional and global buckling analysis of thin-walled steel frames, *Thin-Walled Structures* **47**(11): 1246–1264. doi: 10.1016/j.tws.2009.04.003.
- Basaglia, C., Camotim, D. and Silvestre, N. (2010). GBT-based buckling analysis of thin-walled steel frames with arbitrary loading and support conditions, *International Journal of Structural Stability and Dynamics* **10**(03): 363–385. doi: 10.1142/s0219455410003531.
- Basaglia, C., Camotim, D. and Silvestre, N. (2011). Non-linear GBT formulation for open-section thin-walled members with arbitrary support conditions, *Computers & Structures* **89**(21-22): 1906–1919. doi: 10.1016/j.compstruc.2011.07.001.
- Basaglia, C., Camotim, D. and Silvestre, N. (2013). Post-buckling analysis of thin-walled steel frames using generalised beam theory (GBT), *Thin-Walled Structures* **62**: 229–242. doi: 10.1016/j.tws.2012.07.003.
- Bathe, K. J. (2014). *Finite Element Procedures*, K.J. Bathe, Watertown, MA.
- Bauld, N. R. and Tzeng, L. (1984). A vlasov theory for fiber-reinforced beams with thin-walled open cross sections, *International Journal of Solids and Structures* **20**(3): 277–297. doi: 10.1016/0020-7683(84)90039-8.
- Bebiano, R., Calçada, R., Camotim, D. and Silvestre, N. (2017). Dynamic analysis of high-speed railway bridge decks using generalised beam theory, *Thin-Walled Structures* **114**: 22–31. doi: 10.1016/j.tws.2017.01.027.
- Bebiano, R., Camotim, D. and Gonçalves, R. (2013). GBTUL 2.0 – a second-generation code for GBT-based buckling and vibration analysis of thin-walled members, *Proceedings of the 10th Pacific Structural Steel Conference (PSSC 2013)*, Research Publishing Services.
- Bebiano, R., Camotim, D. and Silvestre, N. (2013). Dynamic analysis of thin-walled members using generalised beam theory (GBT), *Thin-Walled Structures* **72**: 188–205. doi: 10.1016/j.tws.2013.07.004.
- Bebiano, R., Gonçalves, R. and Camotim, D. (2015). A cross-section analysis procedure to rationalise and automate the performance of GBT-based structural analyses, *Thin-Walled Structures* **92**: 29–47. doi: 10.1016/j.tws.2015.02.017.
- Bebiano, R., Silvestre, N. and Camotim, D. (2007). GBT formulation to analyze the buckling behavior of thin-walled members subjected to non-uniform bending, *International Journal of Structural Stability and Dynamics* **07**(01): 23–54. doi: 10.1142/s0219455407002216.
- Bebiano, R., Silvestre, N. and Camotim, D. (2008a). GBTUL - a code for the buckling analysis of cold-formed steel members, *Proceedings of the 19th International Speciality Conference*

- on Cold-Formed Steel Structures, St. Louis, Missouri, USA, October 14-15*, Missouri University of Science and Technology, pp. 61–79.
- Bebiano, R., Silvestre, N. and Camotim, D. (2008b). Local and global vibration of thin-walled members subjected to compression and non-uniform bending, *Journal of Sound and Vibration* **315**(3): 509–535. doi: 10.1016/j.jsv.2008.02.036.
- Berdichevsky, V. (2009). *Variational Principles of Continuum Mechanics*, Springer Berlin Heidelberg.
- Bernstein, D. S. (2005). *Matrix Mathematics: Theory, Facts, and Formulas with Application to Linear Systems Theory*, Princeton University Press.
- Budiansky, B. (1974). Theory of buckling and post-buckling behavior of elastic structures, *Advances in applied mechanics* **14**: 1–65. doi: 10.1016/S0065-2156(08)70030-9.
- Cai, J. and Moen, C. D. (2015). Generalized beam theory buckling analysis for members with holes, *Proceedings of the Eighth International Conference on Advances in Steel Structures, Lisbon, Portugal, July 22-24*.
- Cai, J. and Moen, C. D. (2016). Elastic buckling analysis of thin-walled structural members with rectangular holes using generalized beam theory, *Thin-Walled Structures* **107**: 274–286. doi: 10.1016/j.tws.2016.06.014.
- Camotim, D., Basaglia, C. and Silvestre, N. (2010). GBT buckling analysis of thin-walled steel frames: A state-of-the-art report, *Thin-Walled Structures* **48**(10-11): 726–743. doi: 10.1016/j.tws.2009.12.003.
- Camotim, D., Silvestre, N., Basaglia, C. and Bebiano, R. (2008). GBT-based buckling analysis of thin-walled members with non-standard support conditions, *Thin-Walled Structures* **46**(7-9): 800–815. doi: 10.1016/j.tws.2008.01.019.
- Casafont, M., Bonada, J., Pastor, M. M. and Roure, F. (2015). GBT calculation of distortional and global buckling loads of cold-formed steel channels columns with multiple perforations, *Proceedings of the Eighth International Conference on Advances in Steel Structures, Lisbon, Portugal, July 22-24*.
- Casafont, M., Bonada, J., Pastor, M. M., Roure, F. and Susín, A. (2018). Linear buckling analysis of perforated cold-formed steel storage rack columns by means of the generalised beam theory, *International Journal of Structural Stability and Dynamics* **18**(1): 1850004. doi: 10.1142/s0219455418500049.
- Casafont, M., Marimon, F., Pastor, M. and Ferrer, M. (2011). Linear buckling analysis of thin-walled members combining the generalised beam theory and the finite element method, *Computers & Structures* **89**(21-22): 1982–2000. doi: 10.1016/j.compstruc.2011.05.016.
- Casafont, M., Marimon, F. and Pastor, M. M. (2009). Calculation of pure distortional elastic buckling loads of members subjected to compression via the finite element method, *Thin-Walled Structures* **47**(6-7): 701–729. doi: 10.1016/j.tws.2008.12.001.

- Cava, D., Camotim, D., Dinis, P. B. and Madeo, A. (2016). Numerical investigation and direct strength design of cold-formed steel lipped channel columns experiencing local–distortional–global interaction, *Thin-Walled Structures* **105**: 231–247. doi: 10.1016/j.tws.2016.03.025.
- Cheung, Y. K. (1976). *Finite Strip Method in Structural Analysis*, Elsevier Science.
- Davies, J. M. and Leach, P. (1992). Some applications of generalized beam theory, *Proceedings of the 11th International Specialty Conference on Cold-Formed Steel Structures*. Paper 2.
- Davies, J. M. and Leach, P. (1994). First-order generalised beam theory, *Journal of Constructional Steel Research* **31**(2-3): 187–220. doi: 10.1016/0143-974X(94)90010-8.
- Davies, J. M., Leach, P. and Heinz, D. (1994). Second-order generalised beam theory, *Journal of Constructional Steel Research* **31**(2-3): 221–241. doi: 10.1016/0143-974X(94)90011-6.
- Davies, J. M., Leach, P. and Taylor, A. (1997). The design of perforated cold-formed steel sections subject to axial load and bending, *Thin-Walled Structures* **29**(1-4): 141–157. doi: 10.1016/S0263-8231(97)00024-4.
- de Miranda, S., Gutiérrez, A., Mileta, R. and Ubertini, F. (2013). A generalized beam theory with shear deformation, *Thin-Walled Structures* **67**: 88–100. doi: 10.1016/j.tws.2013.02.012.
- de Miranda, S., Madeo, A., Melchionda, D., Patruno, L. and Ruggerini, A. W. (2017). A corotational based geometrically nonlinear generalized beam theory: buckling FE analysis, *International Journal of Solids and Structures* **121**: 212–227. doi: 10.1016/j.ijsolstr.2017.05.030.
- Dezi, L., Gara, F. and Leoni, G. (2003). Shear-lag effect in twin-girder composite decks, *Steel and Composite Structures* **3**(2): 111–122. doi: 10.12989/scs.2003.3.2.111.
- Dezi, L., Gara, F., Leoni, G. and Tarantino, A. M. (2001). Time-dependent analysis of shear-lag effect in composite beams, *Journal of Engineering Mechanics* **127**(1): 71–79. doi: 10.1061/(ASCE)0733-9399(2001)127:1(71).
- Dinis, P. B. and Camotim, D. (2011). Local/distortional/global mode interaction in simply supported cold-formed steel lipped channel columns, *International Journal of Structural Stability and Dynamics* **11**(05): 877–902. doi: 10.1142/s0219455411004385.
- Dinis, P. B., Camotim, D. and Silvestre, N. (2006). GBT formulation to analyse the buckling behaviour of thin-walled members with arbitrarily ‘branched’ open cross-sections, *Thin-Walled Structures* **44**(1): 20–38. doi: 10.1016/j.tws.2005.09.005.
- Dinis, P. B., Camotim, D. and Silvestre, N. (2010). On the local and global buckling behaviour of angle, t-section and cruciform thin-walled members, *Thin-Walled Structures* **48**(10-11): 786–797. doi: 10.1016/j.tws.2010.04.012.
- Dinis, P. B., Camotim, D. and Silvestre, N. (2012). On the mechanics of thin-walled angle column instability, *Thin-Walled Structures* **52**: 80–89. doi: 10.1016/j.tws.2011.12.007.

- Eccher, G., Rasmussen, K. J. R. and Zandonini, R. (2009). Geometric nonlinear isoparametric spline finite strip analysis of perforated thin-walled structures, *Thin-Walled Structures* **47**(2): 219–232. doi: 10.1016/j.tws.2008.05.013.
- Fletcher, C. A. J. (1984). *Computational Galerkin Methods*, Springer-Verlag GmbH.
- Gara, F., Ranzi, G. and Leoni, G. (2010). Short- and long-term analytical solutions for composite beams with partial interaction and shear-lag effects, *International Journal of Steel Structures* **10**(4): 359–372. doi: 10.1007/BF03215844.
- Garcea, G., Gonçalves, R., Bilotta, A., Manta, D., Bebiano, R., Leonetti, L., Magisano, D. and Camotim, D. (2016). Deformation modes of thin-walled members: A comparison between the method of generalized eigenvectors and generalized beam theory, *Thin-Walled Structures* **100**: 192–212. doi: 10.1016/j.tws.2015.11.013.
- Genoese, A., Genoese, A., Bilotta, A. and Garcea, G. (2014a). Buckling analysis through a generalized beam model including section distortions, *Thin-Walled Structures* **85**: 125–141. doi: 10.1016/j.tws.2014.08.012.
- Genoese, A., Genoese, A., Bilotta, A. and Garcea, G. (2014b). A generalized model for heterogeneous and anisotropic beams including section distortions, *Thin-Walled Structures* **74**: 85–103. doi: 10.1016/j.tws.2013.09.019.
- Georgieva, I., Schueremans, L., Vandewalle, L. and Pyl, L. (2012). Design of built-up cold-formed steel columns according to the direct strength method, *Procedia Engineering* **40**: 119–124. doi: 10.1016/j.proeng.2012.07.066.
- Girhammar, U. A. and Gopu, V. K. A. (1993). Composite beam-columns with inter-layer slip—exact analysis, *Journal of Structural Engineering* **119**(4): 1265–1282. doi: 10.1061/(asce)0733-9445(1993)119:4(1265).
- Gonçalves, R., Bebiano, R. and Camotim, D. (2014). On the shear deformation modes in the framework of generalized beam theory, *Thin-Walled Structures* **84**: 325–334. doi: 10.1016/j.tws.2014.07.012.
- Gonçalves, R. and Camotim, D. (2004). GBT local and global buckling analysis of aluminium and stainless steel columns, *Computers & Structures* **82**(17-19): 1473–1484. doi: 10.1016/j.compstruc.2004.03.043.
- Gonçalves, R. and Camotim, D. (2007). Thin-walled member plastic bifurcation analysis using generalised beam theory, *Advances in Engineering Software* **38**(8-9): 637–646. doi: 10.1016/j.advengsoft.2006.08.027.
- Gonçalves, R. and Camotim, D. (2010). Steel-concrete composite bridge analysis using generalised beam theory, *Steel and Composite Structures* **10**(3): 223–243. doi: 10.12989/scs.2010.10.3.223.

- Gonçalves, R. and Camotim, D. (2011). Generalised beam theory-based finite elements for elastoplastic thin-walled metal members, *Thin-Walled Structures* **49**(10): 1237–1245. doi: 10.1016/j.tws.2011.05.011.
- Gonçalves, R. and Camotim, D. (2012). Geometrically non-linear generalised beam theory for elastoplastic thin-walled metal members, *Thin-Walled Structures* **51**: 121–129. doi: 10.1016/j.tws.2011.10.006.
- Gonçalves, R. and Camotim, D. (2013a). Buckling behaviour of thin-walled regular polygonal tubes subjected to bending or torsion, *Thin-Walled Structures* **73**: 185–197. doi: 10.1016/j.tws.2013.08.006.
- Gonçalves, R. and Camotim, D. (2013b). Elastic buckling of uniformly compressed thin-walled regular polygonal tubes, *Thin-Walled Structures* **71**: 35–45. doi: 10.1016/j.tws.2013.04.016.
- Gonçalves, R. and Camotim, D. (2013c). On the behaviour of thin-walled steel regular polygonal tubular members, *Thin-Walled Structures* **62**: 191–205. doi: 10.1016/j.tws.2012.08.006.
- Gonçalves, R. and Camotim, D. (2016). GBT deformation modes for curved thin-walled cross-sections based on a mid-line polygonal approximation, *Thin-Walled Structures* **103**: 231–243. doi: 10.1016/j.tws.2015.12.025.
- Gonçalves, R. and Camotim, D. (2017a). Efficient gbt displacement-based finite elements for non-linear problems, *Proceedings of the Annual Stability Conference Structural Stability Research Council San Antonio, Texas, March 21-24*.
- Gonçalves, R. and Camotim, D. (2017b). Improving the efficiency of GBT displacement-based finite elements, *Thin-Walled Structures* **111**: 165–175. doi: 10.1016/j.tws.2016.10.020.
- Gonçalves, R., Dinis, P. B. and Camotim, D. (2009). GBT formulation to analyse the first-order and buckling behaviour of thin-walled members with arbitrary cross-sections, *Thin-Walled Structures* **47**(5): 583–600. doi: 10.1016/j.tws.2008.09.007.
- Gonçalves, R., Henriques, D. and Camotim, D. (2016). Recent developments in the gbt-based numerical modeling of steel-concrete composite beams, *Proceedings of the Annual Stability Conference, Structural Stability Research Council, Orlando, Florida, April 12-15*, pp. 471–486.
- Gonçalves, R., Peres, N., Bebiano, R. and Camotim, D. (2015). Global–local–distortional vibration of thin-walled rectangular multi-cell beams, *International Journal of Structural Stability and Dynamics* **15**(08): 1540022. doi: 10.1142/s0219455415400222.
- Gonçalves, R., Ritto-Corrêa, M. and Camotim, D. (2010). A new approach to the calculation of cross-section deformation modes in the framework of generalized beam theory, *Computational Mechanics* **46**(5): 759–781. doi: 10.1007/s00466-010-0512-2.
- Hanaor, A. (2000). Tests of composite beams with cold-formed sections, *Journal of Constructional Steel Research* **54**(2): 245–264. doi: 10.1016/s0143-974x(99)00046-2.

- Henriques, D., Gonçalves, R. and Camotim, D. (2014). Non-linear analysis of steel-concrete beams using generalized beam theory, *Proceedings of the 11th World Congress on Computational Mechanics (WCCM XI), Barcelona, Spain, July, 20-25*.
- Henriques, D., Gonçalves, R. and Camotim, D. (2015). A physically non-linear GBT-based finite element for steel and steel-concrete beams including shear lag effects, *Thin-Walled Structures* **90**: 202–215. doi: 10.1016/j.tws.2015.01.010.
- Henriques, D., Gonçalves, R. and Camotim, D. (2016). GBT-based finite element to assess the buckling behaviour of steel–concrete composite beams, *Thin-Walled Structures* **107**: 207–220. doi: 10.1016/j.tws.2016.06.005.
- Hutchinson, J. W. (1974). Plastic buckling, *Advances in Applied Mechanics*, Elsevier, pp. 67–144. doi: 10.1016/s0065-2156(08)70031-0.
- Inman, D. J. (2013). *Engineering Vibration*, Pearson.
- Jiang, C. and Davies, J. M. (1997). Design of thin-walled purlins for distortional buckling, *Thin-Walled Structures* **29**(1-4): 189–202. doi: 10.1016/S0263-8231(97)00022-0.
- Kantorovich, L. V. (1933). A direct method of solving the problem of the minimum of a double integral, *Izv. AN SSSR OMEN* **5**: 647–652. (in Russian).
- Kantorovich, L. V. (1942). A utilisation of the idea of the method of Acad. B. G. Galerkin in the method of reduction to ordinary differential equations, *Priklad. Matem. i Mekh.* **6**: 31–40. (in Russian).
- Kantorovich, L. V. and Krylov, V. I. (1958). *Approximate methods of higher analysis*, P. Noordhoff Ltd, Groningen, The Netherlands.
- Landesmann, A., Camotim, D. and Garcia, R. (2016). On the strength and DSM design of cold-formed steel web/flange-stiffened lipped channel columns buckling and failing in distortional modes, *Thin-Walled Structures* **105**: 248–265. doi: 10.1016/j.tws.2016.03.023.
- Lau, S. and Hancock, G. (1986). Buckling of thin flat-walled structures by a spline finite strip method, *Thin-Walled Structures* **4**(4): 269–294. doi: 10.1016/0263-8231(86)90034-0.
- Leach, P. (1994). The calculation of modal cross-section properties for use in the generalized beam theory, *Thin-Walled Structures* **19**(1): 61–79. doi: 10.1016/0263-8231(94)90005-1.
- Leach, P. and Davies, J. M. (1996). An experimental verification of the generalized beam theory applied to interactive buckling problems, *Thin-Walled Structures* **25**(1): 61–79. doi: 10.1016/0263-8231(95)00031-3.
- Li, Z. and Schafer, B. W. (2010). Buckling analysis of cold-formed steel members with general boundary conditions using cufsm: conventional and constrained finite strip method, *Proceedings of the 20th International Speciality Conference on Cold-Formed Steel Structures, Saint Louis, Missouri, USA, November 3-4*.

- Luongo, A. and Paolone, A. (1997). *Meccanica delle Strutture. Sistemi rigidi ad elasticità concentrata*, CEA, Milano, Italy. (in Italian).
- Luongo, A. and Pignataro, M. (1988). Multiple interaction and localization phenomena in the postbuckling of compressed thin-walled members, *AIAA journal* **26**(11): 1395–1402. doi: 10.2514/3.10053.
- Luongo, A. and Zulli, D. (2013). *Mathematical Models of Beams and Cables*, ISTE LTD.
- Luongo, A. and Zulli, D. (2014). A non-linear one-dimensional model of cross-deformable tubular beam, *International Journal of Non-Linear Mechanics* **66**: 33–42. doi: 10.1016/j.ijnonlinmec.2014.03.008.
- Martins, A. D., Camotim, D. and Dinis, P. B. (2017a). Behaviour and DSM design of stiffened lipped channel columns undergoing local-distortional interaction, *Journal of Constructional Steel Research* **128**: 99–118. doi: 10.1016/j.jcsr.2016.07.030.
- Martins, A. D., Camotim, D. and Dinis, P. B. (2017b). Local-distortional interaction in cold-formed steel beams: Behaviour, strength and DSM design, *Thin-Walled Structures* **119**: 879–901. doi: 10.1016/j.tws.2017.06.011.
- Martins, A. D., Camotim, D. and Dinis, P. B. (2017c). On the direct strength design of cold-formed steel columns failing in local-distortional interactive modes, *Thin-Walled Structures* **120**: 432–445. doi: 10.1016/j.tws.2017.06.027.
- Martins, A. D., Camotim, D., Gonçalves, R. and Dinis, P. B. (2016). On the mechanics of local-distortional interaction in thin-walled lipped channel beams, *Proceedings of the 7th International Conference on Coupled Instabilities in Metal Structures, Baltimore, Maryland, Novembre 7-8*.
- Martins, A. D., Dinis, P. B. and Camotim, D. (2016). On the influence of local-distortional interaction in the behaviour and design of cold-formed steel web-stiffened lipped channel columns, *Thin-Walled Structures* **101**: 181–204. doi: 10.1016/j.tws.2015.11.021.
- Martins, A. D., Dinis, P. B., Camotim, D. and Providência, P. (2015). On the relevance of local-distortional interaction effects in the behaviour and design of cold-formed steel columns, *Computers & Structures* **160**: 57–89. doi: 10.1016/j.compstruc.2015.08.003.
- Martins, A. D., Landesmann, A., Camotim, D. and Dinis, P. B. (2017). Distortional failure of cold-formed steel beams under uniform bending: Behaviour, strength and DSM design, *Thin-Walled Structures* **118**: 196–213. doi: 10.1016/j.tws.2017.04.009.
- Mesacasa, E., Dinis, P. B., Camotim, D. and Malite, M. (2014). Mode interaction in thin-walled equal-leg angle columns, *Thin-Walled Structures* **81**: 138–149. doi: 10.1016/j.tws.2013.06.021.
- Mills, O. M. (2001). *Design of Simply-Supported Composite Beams with Large Web Penetrations*, 2.0 edn, Composite Structures Design Manual DB1.3.

- Natário, P., Silvestre, N. and Camotim, D. (2012). Localized web buckling analysis of beams subjected to concentrated loads using GBT, *Thin-Walled Structures* **61**: 27–41. doi: 10.1016/j.tws.2012.05.014.
- Nedelcu, M. (2010). GBT formulation to analyse the behaviour of thin-walled members with variable cross-section, *Thin-Walled Structures* **48**(8): 629–638. doi: 10.1016/j.tws.2010.03.001.
- Nedelcu, M. (2011). GBT formulation to analyse the buckling behaviour of isotropic conical shells, *Thin-Walled Structures* **49**(7): 812–818. doi: 10.1016/j.tws.2011.02.006.
- Nedelcu, M. (2012). GBT-based buckling mode decomposition from finite element analysis of thin-walled members, *Thin-Walled Structures* **54**: 156–163. doi: 10.1016/j.tws.2012.02.009.
- Nedelcu, M. (2014). Buckling mode identification of perforated thin-walled members by using GBT and shell FEA, *Thin-Walled Structures* **82**: 67–81. doi: 10.1016/j.tws.2014.04.005.
- Nedelcu, M. and Cucu, H. L. (2014). Buckling modes identification from FEA of thin-walled members using only GBT cross-sectional deformation modes, *Thin-Walled Structures* **81**: 150–158. doi: 10.1016/j.tws.2013.06.007.
- Newmark, N. M., Siess, C. P. and Viest, I. M. (1951). Test and analysis of composite beams with incomplete interaction, *Proceedings of the Society for Experimental Stress Analysis* **9**(1): 75–92.
- Nguyen, N. T., Oehlers, D. J. and Bradford, M. A. (2001). An analytical model for reinforced concrete beams with bolted side plates accounting for longitudinal and transverse partial interaction, *International Journal of Solids and Structures* **38**: 6985–6996. doi: 10.1016/s0020-7683(01)00036-1.
- Oden, J. T. and Ripperger, E. A. (1981). *Mechanics of Elastic Structures*, McGraw-Hill Inc., US.
- Peres, N., Gonçalves, R. and Camotim, D. (2016). First-order generalised beam theory for curved thin-walled members with circular axis, *Thin-Walled Structures* **107**: 345–361. doi: 10.1016/j.tws.2016.06.016.
- Pham, C. H. (2017). Shear buckling of plates and thin-walled channel sections with holes, *Journal of Constructional Steel Research* **128**: 800–811. doi: 10.1016/j.jcsr.2016.10.013.
- Piccardo, G., Ranzi, G. and Luongo, A. (2014a). A complete dynamic approach to the generalised beam theory cross-section analysis including extension and shear modes, *Mathematics and Mechanics of Solids* **19**(8): 900–924. doi: 10.1177/1081286513493107.
- Piccardo, G., Ranzi, G. and Luongo, A. (2014b). A direct approach for the evaluation of the conventional modes within the GBT formulation, *Thin-Walled Structures* **74**: 133–145. doi: 10.1016/j.tws.2013.09.008.

- Prokopov, V. G., Bepalova, E. I. and Sherenkovskii, Y. V. (1982). Method of reduction to the ordinary differential equations of I. v. Kantorovich and a general method for the solution of multidimensional heat-transfer equations, *Journal of engineering physics* **42**(6): 687–692. doi: 10.1007/BF00835105.
- Ranzi, G. and Bradford, M. A. (2009). Nonlinear analysis of composite beams with partial shear interaction by means of the direct stiffness method, *Steel and Composite structures* **9**(2): 131–158. doi: 10.12989/scs.2009.9.2.131.
- Ranzi, G., Dall'Asta, A., Ragni, L. and Zona, A. (2010). A geometric nonlinear model for composite beams with partial interaction, *Engineering Structures* **32**(5): 1384–1396. doi: 10.1016/j.engstruct.2010.01.017.
- Ranzi, G., Gara, F. and Ansourian, P. (2006). General method of analysis for composite beams with longitudinal and transverse partial interaction, *Computers & Structures* **84**: 2373–2384. doi: 10.1016/j.compstruc.2006.07.002.
- Ranzi, G. and Gilbert, R. I. (2015). *Structural Analysis - Principles, Methods and Modelling*, CRC Press, Boca Raton, FL.
- Ranzi, G. and Luongo, A. (2011). A new approach for thin-walled member analysis in the framework of gbt, *Thin-Walled Structures* **49**(11): 1404–1414. doi: 10.1016/j.tws.2011.06.008.
- Ranzi, G. and Luongo, A. (2014). An analytical approach for the cross-sectional analysis of generalised beam theory, *Proceedings of the Institution of Civil Engineers - Structures and Buildings* **167**(7): 414–425. doi: 10.1680/stbu.12.00057.
- Reddy, J. N. (2005). *An Introduction to the Finite Element Method*, McGraw-Hill Education (ISE Editions).
- Rizzi, N. and Tatone, A. (1996). Nonstandard models for thin-walled beams with a view to applications, *Journal of Applied Mechanics* **63**(2): 399. doi: 10.1115/1.2788878.
- Ruta, G., Pignataro, M. and Rizzi, N. (2006). A direct one-dimensional beam model for the flexural-torsional buckling of thin-walled beams, *Journal of Mechanics of Materials and Structures* **1**(8): 1479–1496. doi: 10.2140/jomms.2006.1.1479.
- Schafer, B. W. and Ádány, S. (2006). Buckling analysis of cold-formed steel members using cufsm: conventional and constrained finite strip methods, *Proceedings of the 18th International Speciality Conference on Cold-Formed Steel Structures, Orlando, Florida, October 26-27*.
- Schardt, R. (1983). The generalised beam theory, instability and plastic collapse of steel structures, *Proceedings of the M.R. Horne conference, University of Manchester, Granada, London*, pp. 469–475.
- Schardt, R. (1989). *Verallgemeinerte Technische Biegetheorie*, Springer, Berlin, Heidelberg. (in German).

- Schardt, R. (1994). Generalized beam theory - an adequate method for coupled stability problems, *Thin-Walled Structures* **19**(2-4): 161–180. doi: 10.1016/0263-8231(94)90027-2.
- Silva, N. F., Silvestre, N. and Camotim, D. (2006). GBT formulation to analyse the buckling behaviour of FRP composite branched thin-walled members, *Proceedings of the III European Conference on Computational Mechanics, Solids, Structures and Coupled Problems in Engineering, Lisbon, Portugal, 5-8 June*, Springer Netherlands, pp. 705–705.
- Silva, N. M. F., Camotim, D. and Silvestre, N. (2010). On the use of generalized beam theory to assess the buckling and postbuckling behavior of laminated CFRP cylindrical stiffened panels, *International Journal of Structural Stability and Dynamics* **10**(04): 737–760. doi: 10.1142/s0219455410003713.
- Silva, N. M. F., Camotim, D., Silvestre, N., Correia, J. and Branco, F. A. (2011). First-order, buckling and post-buckling behaviour of GFRP pultruded beams. part 2: Numerical simulation, *Computers & Structures* **89**(21-22): 2065–2078. doi: 10.1016/j.compstruc.2011.07.006.
- Silva, N., Silvestre, N. and Camotim, D. (2010). GBT formulation to analyse the buckling behaviour of FRP composite open-section thin-walled columns, *Composite Structures* **93**(1): 79–92. doi: 10.1016/j.compstruct.2010.06.013.
- Silvestre, N. (2007). Generalised beam theory to analyse the buckling behaviour of circular cylindrical shells and tubes, *Thin-Walled Structures* **45**(2): 185–198. doi: 10.1016/j.tws.2007.02.001.
- Silvestre, N. (2008). Buckling behaviour of elliptical cylindrical shells and tubes under compression, *International Journal of Solids and Structures* **45**(16): 4427–4447. doi: 10.1016/j.ijsolstr.2008.03.019.
- Silvestre, N., Abambres, M. and Camotim, D. (2017). Influence of the deformation mode nature on the 1st order post-yielding strength of thin-walled beams, *Thin-Walled Structures* . doi: 10.1016/j.tws.2017.09.027.
- Silvestre, N. and Camotim, D. (2002a). First-order generalised beam theory for arbitrary orthotropic materials, *Thin-Walled Structures* **40**(9): 755–789. doi: 10.1016/S0263-8231(02)00025-3.
- Silvestre, N. and Camotim, D. (2002b). Second-order generalised beam theory for arbitrary orthotropic materials, *Thin-Walled Structures* **40**(9): 791–820. doi: 10.1016/s0263-8231(02)00026-5.
- Silvestre, N. and Camotim, D. (2003a). GBT buckling analysis of pultruded FRP lipped channel members, *Computers & Structures* **81**(18-19): 1889–1904. doi: 10.1016/s0045-7949(03)00209-8.
- Silvestre, N. and Camotim, D. (2003b). Nonlinear generalized beam theory for cold-formed steel members, *International Journal of Structural Stability and Dynamics* **03**(04): 461–490. doi: 10.1142/s0219455403001002.

- Silvestre, N. and Camotim, D. (2004a). Distortional buckling formulae for cold-formed steel C- and Z-section members: Part i-derivation, *Thin-Walled Structures* **42**(11): 1567–1597. doi: 10.1016/j.tws.2004.05.001.
- Silvestre, N. and Camotim, D. (2004b). Distortional buckling formulae for cold-formed steel C- and Z-section members: Part II-validation and application, *Thin-Walled Structures* **42**(11): 1599–1629. doi: 10.1016/j.tws.2004.05.002.
- Silvestre, N. and Camotim, D. (2006a). Gbt-based local and global vibration analysis of loaded composite open-section thin-walled members, *International Journal of Structural Stability and Dynamics* **06**(01): 1–29. doi: 10.1142/s0219455406001800.
- Silvestre, N. and Camotim, D. (2006b). Local-plate and distortional postbuckling behavior of cold-formed steel lipped channel columns with intermediate stiffeners, *Journal of Structural Engineering* **132**(4): 529–540. doi: 10.1061/(asce)0733-9445(2006)132:4(529).
- Silvestre, N. and Camotim, D. (2006c). Vibration behaviour of axially compressed cold-formed steel members, *Steel and Composite Structures* **6**(3): 221–236. doi: 10.12989/scs.2006.6.3.221.
- Silvestre, N. and Camotim, D. (2013a). Generalized beam theory to analyze the vibration of open-section thin-walled composite members, *Journal of Engineering Mechanics* **139**(8): 992–1009. doi: 10.1061/(asce)em.1943-7889.0000507.
- Silvestre, N. and Camotim, D. (2013b). Shear deformable generalized beam theory for the analysis of thin-walled composite members, *Journal of Engineering Mechanics* **139**(8): 1010–1024. doi: 10.1061/(asce)em.1943-7889.0000506.
- Silvestre, N., Camotim, D. and Silva, N. F. (2011). Generalized beam theory revisited: from the kinematical assumptions to the deformation mode determination, *International Journal of Structural Stability and Dynamics* **11**(05): 969–997. doi: 10.1142/s0219455411004427.
- Simão, P. and Simões da Silva, L. (2004). A unified energy formulation for the stability analysis of open and closed thin-walled members in the framework of the generalized beam theory, *Thin-Walled Structures* **42**(10): 1495–1517. doi: 10.1016/j.tws.2004.03.021.
- Simulia, D. S. (2010). *ABAQUS Analysis User's Manual, version 6.10*, Dassault Systèmes Simulia Corp., Providence, RI, USA.
- Steindl, A. and Troger, H. (2001). Methods for dimension reduction and their application in nonlinear dynamics, *International Journal of Solids and Structures* **38**(10-13): 2131–2147. doi: 10.1016/S0020-7683(00)00157-8.
- Taig, G. and Ranzi, G. (2014). Generalised beam theory (GBT) for stiffened sections, *International Journal of Steel Structures* **14**(2): 381–397. doi: 10.1007/s13296-014-2017-x.
- Taig, G. and Ranzi, G. (2015). Generalised beam theory (GBT) for composite beams with partial shear interaction, *Engineering Structures* **99**: 582–602. doi: 10.1016/j.engstruct.2015.05.025.

- Taig, G. and Ranzi, G. (2016). Generalised beam theory for composite beams with longitudinal and transverse partial interaction, *Mathematics and Mechanics of Solids* **22**(10): 2011–2039. doi: 10.1177/1081286516653799.
- Taig, G., Ranzi, G. and D'Annibale, F. (2015). An unconstrained dynamic approach for the generalised beam theory, *Continuum Mechanics and Thermodynamics* **27**(4-5): 879–904. doi: 10.1007/s00161-014-0358-5.
- Taig, G., Ranzi, G. and Luongo, A. (2016). GBT pre-buckling and buckling analyses of thin-walled members under axial and transverse loads, *Continuum Mechanics and Thermodynamics* **28**(1-2): 41–66. doi: 10.1007/s00161-014-0399-9.
- Troger, H. and Steindl, A. (1991). *Nonlinear Stability and Bifurcation Theory*, Springer Vienna. doi: 10.1007/978-3-7091-9168-2.
- Vlasov, V. Z. (1932). A new practical method for the engineering calculation of claddings and shells, *Stroit. Prom-st.* **11**: 33–38. (in Russian).
- Vlasov, V. Z. (1961). *Thin-walled elastic beams*, Israel Program for Scientific Translations Ltd.
- Vrcelj, Z. and Bradford, M. A. (2008). A simple method for the inclusion of external and internal supports in the spline finite strip method (SFSM) of buckling analysis, *Computers & Structures* **86**(6): 529–544. doi: 10.1016/j.compstruc.2007.05.001.
- Xu, R. and Wang, G. (2013). Bending solutions of the timoshenko partial-interaction composite beams using euler-bernoulli solutions, *Journal of Engineering Mechanics* **139**(12): 1881–1885. doi: 10.1061/(ASCE)EM.1943-7889.0000614.
- Zona, A. and Ranzi, R. (2011). Finite element models for nonlinear analysis of steel-concrete composite beams with partial interaction in combined bending and shear, *Finite Elements in Analysis and Design* **47**(2): 98–118. doi: 10.1016/j.finel.2010.09.006.